

Solid drug dispersions and
mucoadhesive formulations with
poly(2-oxazolines), poly(*N*-(2-
hydroxylpropyl)methacrylamide)
and their derivatives

Xiaoning Shan

Submitted for the degree of Doctor of Philosophy

School of Pharmacy

September 2021

Declaration of original authorship

‘Declaration: I confirm that this is my own work and the use of all material from other sources has been properly and fully acknowledged.’

Xiaoning Shan

September 2021

This thesis is dedicated to my family and grandparents for their encouragement, to myself for my own efforts.

Acknowledgment

First and foremost, I would like to express my deep and sincere gratitude to my supervisors, Professor Vitaliy Khutoryanskiy and Professor Adrian Williams for their invaluable support and guidance throughout my research. Their immense knowledge and plentiful experience have encouraged me in all the time of my academic research. They have allowed me the freedom to explore my theories but were always able to bring fresh ideas to my thoughts and make me passionate again about the process of research. Their patience and care always make me feel that I have another two “fathers” in a foreign country.

The University of Reading, the Chemical Analysis Facility are acknowledged for providing access to proton nuclear magnetic resonance, Fourier transform infrared spectroscopy, differential scanning calorimetry, powder X-ray diffractometry and USP Apparatus II. I would also like to thank China Scholarship Council for nomination for the scholarship.

My heartfelt thanks go to the pleasant people that helped with various analyses, Dr. Daulet Kaldybekov, Dr. Ellen Hackle, Prof. Kenneth Shankland, Dr. Pedro Rivas Ruiz and other wonderful people that I cannot afford to express all their names. I would like to thank my lab mates (Jamila, Twana, Ibrahim, Roman, Sam, Manfei, Yuehuai, Pong, Fhata and all those who left and who joined the group recently) for a cherished time spent together in the lab, and in social settings.

Finally, I would like to express my thanks to all of my friends, my family and my grandparents for their encouragement and support during the ups and downs of this journey.

Xiaoning Shan

September 2021

Abstract

The first chapter provides an overview on intermolecular interactions in solid dispersions of amide-containing nonionic water-soluble polymers including polyvinyl pyrrolidone (PVP), polyvinylpyrrolidone-co-vinyl acetate (PVP/VA), poly(N-vinyl caprolactam)-polyvinyl acetate-polyethylene glycol graft copolymer (Soluplus) and poly(2-oxazolines). Chapters 2 and 3 focus on the effects of structure and properties of PVP and poly(2-oxazolines) on solid dispersions. A series of poly(2-oxazolines) with equivalent degrees of polymerization were synthesized and these polymers and PVP were used to prepare solid dispersions with haloperidol or ibuprofen. Chapter 2 demonstrated that increasing the number of hydrophobic groups (-CH₂- and -CH₃) in the polymer resulted in greater inhibition of crystallinity of haloperidol. Interestingly, drug crystallization inhibition by poly(2-isopropyl-2-oxazoline) was lower than with its isomeric poly(2-propyl-2-oxazoline) because of the semi-crystalline nature of the former polymer. In order to explore the impacts of both polymer hydrophobicity and drug-polymer hydrogen bonding, in chapter 3, ibuprofen, a hydrophobic crystalline drug and strong hydrogen bond donor (because of its carboxylic group), was selected to prepare solid dispersions with poly(2-oxazolines) and PVP. Chapter 3 indicates the crystallinity disruption is predominantly due to hydrogen bonding between the drug molecule (ibuprofen) and the polymer. Both chapters show the crystallization inhibition was consistent with drug dissolution studies using these solid dispersions, with the exception of poly(2-propyl-2-oxazoline), which exhibited lower critical solution temperature that affected the release of haloperidol and ibuprofen.

Chapter 4 and 5 investigate the mucoadhesion properties of modified poly(2-ethyl-2-oxazoline) and poly(N-(2-hydroxypropyl)methacrylamide) (PHPMA), respectively. In chapter 4, the presence of methacryloyl groups and residual amines in methacrylated poly(2-ethyl-2-oxazoline) had a strong synergistic effect on the mucoadhesive properties of these polymers. In chapter 5, the presence of maleimide

groups was shown to positively affect the mucoadhesive properties of PHPMA. These poly(2-ethyl-2-oxazoline) derivatives and PHPMA derivatives have significant potential as mucoadhesive materials for formulation of dosage forms for nasal drug delivery.

The final chapter discusses the general conclusions and possible future work. The poly(2-oxazolines) and functionalized derivatives appear to offer great potential in pharmaceutical applications.

List of publications

1. **Shan, X.**; Williams, A. C.; Khutoryanskiy, V. V., Polymer structure and property effects on solid dispersions with haloperidol: Poly(N-vinyl pyrrolidone) and poly(2-oxazolines) studies. *International Journal of Pharmaceutics* 2020, 590, 119884.
2. **Shan, X.**; Moghul, M. A.; Williams, A. C.; Khutoryanskiy, V. V., Mutual Effects of Hydrogen Bonding and Polymer Hydrophobicity on Ibuprofen Crystal Inhibition in Solid Dispersions with Poly(N-vinyl pyrrolidone) and Poly(2-oxazolines). *Pharmaceutics* 2021, 13, 659.
3. **Shan, X.**; Aspinall, S.; Kaldybekov, D.B.; Buang, F.; Williams, A.C.; Khutoryanskiy, V.V., Synthesis and Evaluation of Methacrylated Poly(2-ethyl-2-oxazoline) as a Mucoadhesive Polymer for Nasal Drug Delivery. *ACS Applied Polymer Materials* 2021, 3, 5882-5992.

List of conferences

Pharmacy PhD showcase, University of Reading, April 2018 - Poster

4th London Polymer Group Symposium, United Kingdom, November 2018 - Poster

Biomaterials Symposium in Lancaster, United Kingdom, February 2019 - Poster

Pharmacy PhD showcase, University of Reading, April 2019 - Speaker

1st British-Kazakh-Russian Online Conference on Drug Delivery, May 2020 -
Speaker

Pharmacy PhD showcase, University of Reading, July 2020 - Speaker

United Kingdom and Ireland Controlled Release Society (UKICRS) online
symposium 2020, October 2020 - Speaker

List of contents

Declaration of original authorship	i
Acknowledgment	iii
Abstract	iv
List of publications	vi
List of conferences	vii
List of figures	ix
List of tables	xvi
Abbreviations	xviii
Chapter 1: Overview of intermolecular interactions in solid dispersions with amide-containing nonionic water-soluble polymers	1
Chapter 2: Polymer structure and property effects on solid dispersions with haloperidol: Poly(N-vinyl pyrrolidone) and poly(2-oxazolines) studies	77
Chapter 3: Mutual Effects of Hydrogen Bonding and Polymer Hydrophobicity on Ibuprofen Crystal Inhibition in Solid Dispersions with Poly(N-vinyl pyrrolidone) and Poly(2-oxazolines)	106
Chapter 4: Synthesis and Evaluation of Methacrylated Poly(2-ethyl-2-oxazoline) as a Mucoadhesive Polymer for Nasal Drug Delivery	132
Chapter 5: Mucoadhesive formulations with maleimide modified poly(N-(2-hydroxylpropyl)methacrylamide) copolymer for nasal drug delivery	151
Chapter 6: General discussion and future work	183
Appendix	190

List of figures

Chapter 1

Figure 1	PVP synthesis and structure.	4
Figure 2	PVP/VA synthesis and structure.	24
Figure 3	Soluplus® structure.	34
Figure 4	POZ synthesis and structure.	44
Figure 5	POZ with hydrocarbon side-chains with increasing hydrophobicity (from left to right) and consequently decreasing cloud point temperature.	45
Figure 6	Solubility of POZ with hydrocarbon side-chains in water and various organic solvents.	47
Figure 7	Glass transition and melting temperatures of poly(2-n-alkyl- 2-oxazoline)s with varying side-chain length obtained from DSC.	47
Figure 8	Drug delivery applications of POZ.	48
Figure 9	Amide-containing water-soluble polymers which have not yet been studied in solid dispersions.	52

Chapter 2

Figure 1	Synthesis of high molar weight PMOZ, PnPOZ and PiPOZ by hydrolysis of PEOZ and subsequent acylation of linear PEI.	81
Figure 2	DSC thermograms (second scan) of PVP, PEOZ and synthesized PEI, PMOZ, PnPOZ and PiPOZ showing decreasing glass transition temperatures with increasing numbers of carbon atoms in the side chain.	81
Figure 3	X-ray diffraction diffractograms of PVP, PEOZ and synthesized PEI, PMOZ, PnPOZ and PiPOZ.	82
Figure 4	X-ray diffraction diagrams of PVP-HP SDs (a) and PEOZ-HP SDs (b).	82
Figure 5	FTIR spectra of HP, PVP and PVP-HP solid dispersions in the range of 1750–1550 cm^{-1} .	82
Figure 6	DSC thermograms of PVP-HP (a) and PEOZ-HP (b) solid dispersions. Dashed curve shows the trend in the endothermic events.	83
Figure 7	DSC thermograms of solid dispersions formed by PMOZ, PiPOZ, PEOZ and PnPOZ at [polymer]/[drug] = 15:1 M ratio.	84
Figure 8	Crystallinity of polymer-HP solid dispersions as a function of polymer molar fraction.	84
Figure 9	Structures of solid dispersions formed by fully amorphous (a) and semi-crystalline (b) polymers. Red tetragonal symbols represent drug molecules and curved lines represent polymer chains.	85
Figure 10	Temperature-composition phase diagrams of polymer-haloperidol solid dispersions showing the experimental and predicted melting temperatures T_m (liquid-solid phase transition curve) as well as experimental and predicted glass transition temperatures. Error bars reflect one standard deviation ($n = 3$) but are within the symbols for the experimental results.	86
Figure 11	Dissolution profiles of pure haloperidol and from different polymerhaloperidol solid dispersions. Cumulative % drug release with standard error of mean has been plotted against time.	86
Figure S1	$^1\text{H-NMR}$ spectra of synthesized PMOZ, PnPOZ and PiPOZ in CD_3OD .	90
Figure S2	DSC trace of PiPOZ, at a heating rate of 10 $^\circ\text{C}/\text{min}$. The first run started from 25 $^\circ\text{C}$ to 220 $^\circ\text{C}$, the second run after quenching started from -50 $^\circ\text{C}$ to 220 $^\circ\text{C}$.	91
Figure S3	FTIR spectra of PVP, PEOZ and synthesized PEI, PMOZ, PnPOZ and PiPOZ. Spectra are offset for clarity.	92

Figure S4	X-ray diffraction patterns of PMOZ-HP SDs (a), PnPOZ-HP SDs (b) and PiPOZ-HP SDs (c). Patterns are offset for clarity.	94
Figure S5	FTIR spectra of PVP-HP SDs (a), PEOZ-HP SDs (b), PMOZ-HP SDs (c), PnPOZ-HP SDs (d) and PiPOZ-HP SDs (e). Spectra are offset for clarity.	97
Figure S6	FTIR spectra of individual PEOZ and HP as well as PEOZ-HP 15:1 mol as physical mixtures (PM) and solid dispersions (SD).	98
Figure S7	DSC thermograms of PMOZ-HP SDs (a), PiPOZ-HP SDs (b), PnPOZ-HP SDs (c) analyzed using Method 1 and PnPOZ-HP SDs (d) analyzed using Method 2. Traces are offset for clarity.	100
Figure S8	Crystallinity of PiPOZ in SDs calculated by DSC and PXRD and (insert) enlarged DSC traces of PiPOZ-HP SDs	102
Figure S9	The A~B plots for PVP-HP (a), PEOZ-HP (b), PnPOZ-HP (c), PMOZ-HP (d) and PiPOZ-HP (e) solid dispersions. Error bars show standard deviation (n=3).	105

Chapter 3

Figure 1	X-ray diffraction diagrams of PVP-IB SDs (a), PEOZ-IB SDs (b), PnPOZ-IB SDs (c), PiPOZ-IB SDs (d), and PMOZ-IB SDs (e).	112
Figure 2	FTIR spectra of PVP-IB SDs (a), PEOZ-IB SDs (b), PnPOZ-IB SDs (c), PiPOZ-IB SDs (d), and PMOZ-IB SDs (e) in the range of 1800–1550 cm^{-1} .	115
Figure 3	DSC thermograms of PVP-IB SDs (a), PEOZ-IB SDs (b), PnPOZ-IB SDs (c), PiPOZ-IB SDs (d), and PMOZ-IB SDs (e).	119
Figure 4	Crystallinity of polymer-IB solid dispersions as a function of polymer molar fraction.	119
Figure 5	Dissolution profiles of pure IB and from different polymer-IB solid dispersions ((polymer repeat unit)/(drug) = 1:1 mol/mol). Cumulative % drug release with standard error of mean has been plotted against time.	122
Figure S1	FTIR of ibuprofen.	126
Figure S2	FTIR full spectra of PVP-IB SDs (a), PEOZ-IB SDs (b), PnPOZ-IB SDs (c), PiPOZ-IB SDs (d) and PMOZ-IB SDs (e).	129
Figure S3	FTIR spectra of PVP-IB SDs and POZ-IB SDs in the range of 1400~900 cm^{-1} . The peaks (marked with an arrow) are attributed to C-N mode.	130

Chapter 4

Figure 1	Synthesis of methacrylated poly(2-ethyl-2-oxazoline) (MAPEOZ).	135
Figure 2	¹ H NMR spectra of MAPEOZ recorded in D ₂ O.	136
Figure 3	FTIR spectra of PEOZ and MAPEOZ in the range of 2100-600 cm ⁻¹ .	137
Figure 4	DSC thermograms (second scan) of PEOZ and MAPEOZ samples showing increasing glass transition temperatures with increasing methacrylation.	137
Figure 5	(a) Turbidity measurements of aqueous solutions of PEOZ and MAPEOZ samples (1 mg/mL). (b) T _{cp} as a function of MA mol % in MAPEOZ polymers.	137
Figure 6	(a) Fluorescence images showing retention of 1 mg/mL glycol chitosan, PEOZ, MA ₁₀ PEOZ, MA ₂₅ PEOZ, MA ₃₅ PEOZ solutions using 0.05 mg/mL sodium fluorescein as the solvent, and pure 0.05 mg/mL sodium fluorescein solution on sheep nasal mucosa and washed with ANF. Scale bar is 2 mm. (b) Retention of 1 mg/mL glycol chitosan, PEOZ, MA ₁₀ PEOZ, MA ₂₅ PEOZ, MA ₃₅ PEOZ solutions using 0.05 mg/mL sodium fluorescein as the solvent and pure 0.05 mg/mL sodium fluorescein solution on sheep nasal mucosa as washed with different volumes of ANF (pH=5.7, n=3, mean ± SD, “*” represents p < 0.05).	138
Figure 7	Proposed mechanism of interaction between MAPEOZ polymers and mucosal surfaces.	139
Figure 8	Viability of HEK 293 cells determined after treatment with PEOZ, P(EOZ-co-EI ₁₅), P(EOZ-co-EI ₂₈), P(EOZ-co-EI ₅₃), MA ₁₀ PEOZ, MA ₂₅ PEOZ and MA ₃₅ PEOZ for 72 h. The untreated cells served as the control. Values are expressed as means ± SD (n = 3).	140
Figure 9	Mucus production by Arion lusitanicus slugs in response to 60 min exposure to PEOZ and its methacrylated derivatives as well as positive (BAC) and negative (PBS) controls. Statistically significant differences are given as follows: ****p < 0.0001; ns: no significance.	140
Figure S1	¹ H-NMR spectra of PEOZ and hydrolysed PEOZ in D ₂ O.	145
Figure S2	First order kinetic plot for the hydrolysis of PEOZ 500 kDa at 100 °C, [HCl]=18 wt%.	146
Figure S3	¹ H-NMR spectrum of MA ₅₅ PEOZ in DMSO-d ₆ .	147
Figure S4	FTIR full spectra of PEOZ and MAPEOZ.	147
Figure S5	Photographs of mucus production by Arion lusitanicus slugs in contact with positive (1% solution of BAC in PBS) and negative	150

(PBS solution) controls as well as PEOZ and its methacrylated derivatives (1 mg/mL each) after 60 min exposure.

Chapter 5

Figure 1	Synthesis of PHPMA-Mi conjugates.	162
Figure 2	¹ H NMR spectra of PHPMA and PHPMA-Mi in D ₂ O.	163
Figure 3	FTIR spectra of PHPMA and PHPMA-Mi in the range of 3800-600 cm ⁻¹ .	165
Figure 4	(a) Fluorescence images showing retention of 1 mg/mL glycol chitosan, PHPMA, PHPMA-Mi ₂₅ , PHPMA-Mi ₁₁ solutions using 0.05 mg/mL sodium fluorescein as the solvent, and pure 0.05 mg/mL sodium fluorescein solution on sheep nasal mucosa and washed with ANF. Scale bar is 2 mm. (b) Retention of 1 mg/mL glycol chitosan, PHPMA, PHPMA-Mi ₁₁ , PHPMA-Mi ₂₅ solutions using 0.05 mg/mL sodium fluorescein as the solvent and pure 0.05 mg/mL sodium fluorescein solution on sheep nasal mucosa as washed with different volumes of ANF (pH=5.7, n=3, mean ± SD, “*” represents p < 0.05).	167
Figure 5	(a) Force of detachment and (b) work of adhesion of dextran, PHPMA, PHPMA-Mi ₁₁ and PHPMA-Mi ₂₅ to sheep nasal mucosa measured using tensile test (n=3, mean ± SD, “*” represents p < 0.05).	168
Figure 6	Viability of HEK 293 cells determined after treatment with different concentrations (25, 50, 75, 100, 125 and 150 µg/mL) of PHPMA, PHPMA-Mi ₁₁ and PHPMA-Mi ₂₅ for 72 h. The untreated cells served as the control. Values were expressed as means ± SD (n = 3), “*” represents p < 0.05, “**” represents p < 0.005, “***” represents p < 0.001.	170
Figure 7	Mucus production by <i>Arion lusitanicus</i> slugs in response to 60 min exposure to PHPMA, PHPMA-Mi ₁₁ and PHPMA-Mi ₂₅ as well as positive and negative controls. Statistically significant differences are given as: “*****” represents p < 0.0001; “**” represents p < 0.05; “ns” represents no significance.	171
Figure S1	(a) at 0 h (UV detector at 220 nm), the first peak was attributed to DMA, the second peak (2.8 min) was attributed to PHPMA-TT which showed two UV maximum absorption wavelength at 272 nm and 306 nm; (b) at 3 h (UV detector at 220 nm), the first peak was attributed to DMA and released TT groups, the second peak (2.4 min) was attributed to PHPMA-Mi which showed one UV maximum absorption wavelength at 275 nm.	179
Figure S2	SEC profiles of polymers (UV detector at 220 nm).	180

Figure S3 Mucus production by *Arion lusitanicus* slugs in contact with positive (1% solution of BAC in PBS) and negative (PBS solution) controls as well as test materials after 60 min exposure. 182

Appendix

Figure 1 Synthesis of poly(2-ethyl-2oxazoline) macromonomers and hydrogels. 191

Figure 2 ¹H NMR spectra of APEOZ and bis-APEOZ. The degree of functionality was calculated from the integrals of the peaks of the vinylic protons of the acrylate (labeled as f) in comparison with the end methyl protons of the polymer backbone (labeled as a). 192

List of tables

Chapter 1

Table 1	Drugs employed in solid dispersions with PVP. “N” represents no references about the interactions (September 2021).	10
Table 2	Commercial solid dispersion products produced with PVP. *Withdrawn in 2000 due to adverse drug reactions.	23
Table 3	Drugs employed in solid dispersions with PVP/VA. “N” represents no references about the interactions. (September 2021)	28
Table 4	Commercial solid dispersion products produced with PVP/VA.	34
Table 5	Drugs employed in solid dispersions with Soluplus®. “N” represents no references about the interactions. (September 2021)	37
Table 6	Drugs employed in solid dispersions with POZ. “N” represents no references about the interactions. (September 2021)	49

Chapter 2

Table 1	Solubility parameters of drug and polymers.	85
Table S1	Melting temperatures of haloperidol in solid dispersions with PnPOZ analysed by two methods.	101
Table S2	Crystallinity (%) of PiPOZ calculated from DSC and PXRD data.	102

Chapter 3

Table 1	The red shift of the carbonyl stretching mode from the carboxylic acid of IB at 1710 cm^{-1} in (polymer)/(IB) = 0.3 mol and 1:1 mol solid dispersions.	116
Table 2	Solubility parameters of drug and polymers.	120
Table 3	Flory–Huggins interaction parameters of polymer–IB solid dispersion systems at the molar ratio of 0.3:1.	121
Table S1	FTIR spectral data of ibuprofen (s- strong; w- weak; symmetrical; asym-asymmetrical; str-stretching; m-medium; vs-very strong; vw – very weak.).	130

Chapter 4

Table 1	Composition of MAPEOZ calculated from the ¹ H NMR spectra.	136
Table S1	Composition of P(EOZ- <i>co</i> -EI) calculated from the standard curve in Fig. S2.	146
Table S2	Retention values of 1 mg/mL glycol chitosan, PEOZ, MA ₁₀ PEOZ, MA ₂₅ PEOZ, MA ₃₅ PEOZ solutions using 0.05 mg/mL sodium fluorescein as the solvent and pure 0.05 mg/mL sodium fluorescein solution on sheep nasal mucosa as washed with different volumes of ANF (pH=5.7). Values were expressed as means (n = 3).	148
Table S3	Values of viability of HEK 293 cells determined after treatment with different concentrations (25, 50, 75, 100, 125 and 150 µg/mL) of PEOZ, P(EOZ- <i>co</i> -EI ₁₅), P(EOZ- <i>co</i> -EI ₂₈), P(EOZ- <i>co</i> -EI ₅₃), MA ₁₀ PEOZ, MA ₂₅ PEOZ and MA ₃₅ PEOZ for 72 h. The untreated cells served as the control. Values were expressed as means (n = 3).	149

Chapter 5

Table 1	Characterization of polymers.	164
Table S1	Retention values of 1 mg/mL glycol chitosan, PHPMA, PHPMA-Mi ₁₁ and PHPMA-Mi ₂₅ solutions using 0.05 mg/mL sodium fluorescein as the solvent and pure 0.05 mg/mL sodium fluorescein solution on sheep nasal mucosa as washed with different volumes of ANF (pH=5.7). Values were expressed as means (n = 3).	180
Table S2	Values of viability of HEK 293 cells determined after treatment with different concentrations (25, 50, 75, 100, 125 and 150 µg/mL) of PHPMA, PHPMA-Mi ₁₁ and PHPMA-Mi ₂₅ for 72 h. The untreated cells served as the control. Values were expressed as means (n = 3).	181

Appendix

Table 1	Characterization of polymers.	193
---------	-------------------------------	-----

Abbreviations

AEMI	2-aminoethyl maleimide trifluoroacetate
AIBN	Azobisisobutyronitrile
ANF	Artificial nasal fluid
APEOZ	Acrylated poly(2-ethyl-2-oxazoline)
APIs	Active pharmaceutical ingredients
BAC	Benzalkonium chloride
CA	Cefuroxime axetil
CED	Cohesive energy density
CEL	Celecoxib
CROP	Cationic ring-opening polymerization
CTA	(1-cyano-1-methyl-ethyl) benzenecarbodithioate
CUR	Curcumin
DDS	Drug delivery systems
DIPEA	N,N-diisopropylethylamine
DMA	N, N-dimethylacetamide
DMSO	Dimethyl sulfoxide
DMSO-d ₆	Deuterated DMSO
D ₂ O	Deuterium oxide
DSC	Differential scanning calorimetry
FDA	Food and Drug Administration
FEL	Felodipine
FTIR	Fourier transform infrared
HHB	Hydrophobic–hydrophilic balance
HME	Hot melt extrusion
¹ H NMR	Proton nuclear magnetic resonance
HP	Haloperidol
HPMA	N-(2-hydroxypropyl)methacrylamide
IBP; IB	Ibuprofen
LCST	Lower critical solution temperature

Ma- β -Ala-TT	3-(3-methacrylamidopropanoyl)thiazolidine-2-thione
MAPEOZ	Methacrylated poly(2-ethyl-2-oxazoline)
PBS	Phosphate buffered saline
PDI	Polydispersity
PEI	Poly (ethylene imine)
PEOZ	Poly(2-ethyl-2-oxazoline)
P(EOZ-co-EI)	Poly[(2-ethyl-2-oxazoline)- <i>co</i> -ethylenimine]
PHPMA	Poly(N-(2-hydroxylpropyl)methacrylamide)
PHPMA-Mi	PHPMA functionalised with maleimide groups
PHPMA-TT	Poly(HPMA-co-Ma- β -Ala-TT)
PiPOZ	Poly(2-isopropyl-2-oxazoline)
PMOZ	Poly(2-methyl-oxazoline)
PnPOZ	Poly(2-propyl-2-oxazoline)
POZ	Poly(2-oxazolines); poly(2-alkyl-oxazoline)
PsecBuOZ	Poly(2-sec-butyl-2-oxazoline)
PVP	Poly(N-vinyl pyrrolidone); polyvinyl pyrrolidone
PVP/VA	Polyvinylpyrrolidone-co-vinyl acetate
PXRD	Powder X-Ray Diffractometry
RAFT	Reversible addition–fragmentation chain transfer
ROS	Reactive oxygen species
SDs	solid dispersions
SEC	Size exclusion chromatography
SGF	Simulated gastric fluid
SMI	Slug mucosal irritation
Soluplus [®]	Poly(N-vinyl caprolactam)–polyvinyl acetate–polyethylene glycol graft copolymer
T _{cp}	Cloud point temperature
TDP	Nitrendipine
TEA	Triethylamine
TEGDMA	Triethylene glycol dimethacrylate
T _g	Glass transition temperature

T _m	Melting temperature
TSD	Ternary solid dispersion
V70	2,2'-Azobis(4-methoxy-2,4-dimethylvaleronitrile)
VP	Vinylpyrrolidone

Chapter 1

Overview of intermolecular interactions in solid dispersions with amide-containing nonionic water-soluble polymers

This chapter illustrates the typical intermolecular interactions between amide-containing nonionic water-soluble polymers and drugs in solid dispersions, and the influence of the interactions on drug crystallinity, drug stability and dissolution rate. In addition, the amide-containing water-soluble polymers which have not yet been studied in solid dispersions will also be described.

This manuscript is under review before submission.

Overview of intermolecular interactions in solid dispersions with amide-containing nonionic water-soluble polymers

*Xiaoning Shan, Adrian C. Williams, Vitaliy V. Khutoryanskiy**

Reading School of Pharmacy, University of Reading, Whiteknights, PO Box 224,
Reading RG6 6AD, United Kingdom

KEYWORDS: solid dispersions, polymers, intermolecular interactions,
crystallinity, stability, dissolution

Abstract:

It is well known that the solid dispersion approach has been widely and successfully applied to improve the solubility, dissolution rate and, consequently, the bioavailability of poorly water-soluble drugs. Various reviews on solid dispersions and carriers used for solubility enhancement of poorly water-soluble drugs have been recently reported. However, there the intermolecular interactions in solid dispersions of amide-containing nonionic water-soluble polymers, which could act as hydrogen bond acceptors and donors in intermolecular interactions between the carrier and drugs, have not been previously reviewed. Here, we explore typical intermolecular interactions between amide-containing nonionic water-soluble polymers and drugs, and the influence of these interactions on drug crystallinity, drug stability and dissolution rate. In addition, other amide-containing water-soluble polymers which may be useful in solid dispersions are described.

1. Introduction

Solid dispersion technology using various pharmaceutically acceptable polymer excipients has successfully improved dissolution rates and thereby absorption of poorly water-soluble drugs [1]. Drugs can potentially co-exist in both an amorphous form and in a crystalline state in solid dispersions. The crystalline state has a long-range order molecular packing, with a characteristic melting point (T_m), and

generally excellent stability whereas the amorphous state is characterized by disorganised or the complete loss of lattice packing which provides good drug solubility and enhanced bioavailability. A disadvantage of the high free energy amorphous state is physical instability [2, 3]. Therefore, due to the higher free energy of the amorphous form of drug, these dispersions are not thermodynamically stable with the drug tending to re-crystallize upon storage to its more thermodynamically stable, crystalline form [4].

The presence of a hydrophilic polymer in the solid dispersion tends to maintain the drug in the amorphous form for extended periods, while the mixing of the drug at the molecular level with the hydrophilic polymer serves to improve its dissolution rate [5, 6]. A polymer with a high glass transition temperature (T_g) will increase the T_g of the system which corresponds to the deceleration of molecular mobility controlling the cold crystallization process at a certain temperature. In contrast to the above, a polymer with a low T_g will decrease the T_g of the system which corresponds to the acceleration of molecular mobility [7]. The molecular interactions between the drug and the hydrophilic polymer are therefore key drivers for the drug to remain in its amorphous form when stored or during the dissolution process itself [8].

Intermolecular interactions such as hydrogen bonding, ionic interactions, van der Waals forces, dipole-dipole interactions and hydrophobic effects (effect of polymer hydrophobicity on solid dispersions) commonly occur between components in solid dispersions [9]. These molecular interactions crucially affect drug crystallinity, drug release and the stability of the solid dispersion system. Generally, these interactions may inhibit drug crystallinity (to some extent), maintain physical stability during storage and improve drug dissolution rate [10, 11]. For solid dispersions using nonionic amide-containing water-soluble polymers as carriers, the primary interactions are typically hydrogen bonding, van der Waals interactions, dipole-dipole interactions, and hydrophobic interactions. Of these, hydrogen bonding

usually plays a pivotal role in determining the overall interaction strength between the drug and polymer components [12-15]. This review considers various amide-containing nonionic water-soluble polymers used to prepare solid dispersions and explores the influence of drug-polymer interactions on drug crystallinity, drug stability and dissolution rate. In addition, amide-containing water-soluble polymers which have not yet been studied in solid dispersions are described.

2. Amide-containing nonionic water-soluble polymers in solid dispersion studies.

Numerous amide-containing nonionic water-soluble polymers have been used as solid dispersion carriers, notably polyvinyl pyrrolidone (PVP), polyvinylpyrrolidone-co-vinyl acetate (PVP/VA), poly(N-vinyl caprolactam)-polyvinyl acetate-polyethylene glycol graft copolymer (Soluplus®) and poly(2-oxazolines). Amide-containing water-soluble polymers as potential future carriers are discussed in Section 3.

2.1 Polyvinyl pyrrolidone (PVP)

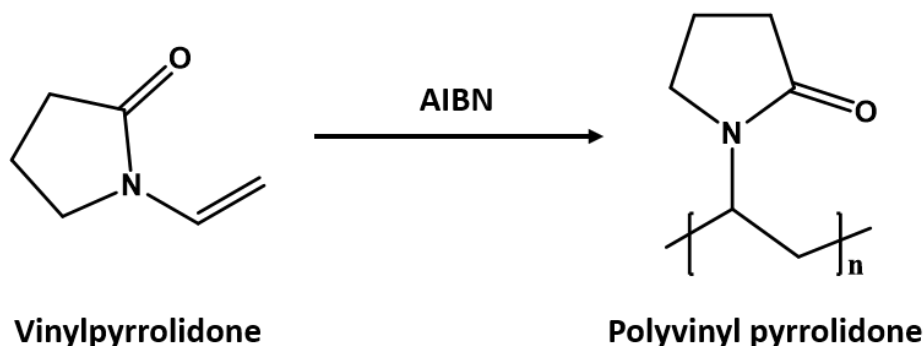


Figure 1. PVP synthesis and structure.

2.1.1 PVP synthesis, general properties and applications in solid dispersions

PVP is a water-soluble polymer that also dissolves in other polar solvents. It is synthesized via free radical polymerization starting from the vinylpyrrolidone (VP) monomer, using a free radical initiator such as azobisisobutyronitrile (AIBN). The synthesis and structure of PVP are given in Figure 1. There are different grades of PVP which are grouped according to their molecular weight by K values, e.g., K12

(2600–5500 Da), K17 (7100–11,000 Da), K25 (19,300–31,100 Da), K30 (31,700–51,400 Da), and K90 (790,000–1,350,000 Da) [16]. Cross-linked PVP is also available as a swellable excipient used in tablet formulations and has also been used as a carrier for solid dispersions [17, 18].

PVP possesses many pharmaceutically useful properties including excellent solubility in water and other conventional solvents, adhesive and binding properties, film-forming ability, affinity to hydrophilic and hydrophobic surfaces, ability to form complexes with numerous drugs and is a thickening agent. Thus, PVP is a widely used excipient in various drug delivery systems for oral, topical, transdermal, and ocular administration [19].

PVP is a biocompatible and non-toxic polymer; it was recognized as safe by the Food and Drug Administration (FDA). However, PVP is highly hygroscopic due to the electronegative groups of the carbonyl moiety in the pyrrolidone structure which can form hydrogen bond with water [20]. This may worsen physical stability and lead to drug recrystallization in the polymer carrier caused by the plasticizing effect of absorbed water. Therefore, moisture adsorption must be controlled during storage. The influence of hygroscopicity on the thickness of PVP films can be avoided by adding acetylated monoglycerides to the coating mixture [21].

PVP is extensively used to formulate solid dispersions; a Scopus database search (September 2021) yielded 939 records of PVP based solid dispersions since 1978. Some 122 drugs have been incorporated with PVP into solid dispersions, summarised in Table 1. Owing to its solubility in a wide variety of organic solvents, PVP is particularly suitable for the preparation of solid dispersions by the solvent method, which can be scaled-up by spray drying. Therefore, a large number of studies attempted to formulate PVP-based dispersions through solvent and spray drying methods [22-28]. PVP is an amorphous polymer so doesn't melt into a liquid at high temperatures, which makes it unsuitable for producing solid dispersion via the fusion method, particularly for low melting point and thermo-labile drugs.

Nevertheless, reports describe the use of hot melt extrusion (HME) for preparation of solid drug dispersions [29-32]. Furthermore, the rate of dissolution of PVP-based solid dispersions is highly dependent on the molecular weight of PVP employed to prepare the dispersions; an increase in the molecular weight correlated negatively with the rate of dissolution, due to an increase in the viscosity and swelling of PVP within the solution phase. This consequently decreases the diffusion of drug molecules from the surface boundaries of the viscous material into the bulk of the solution, leading to retarded dissolution [33]. The optimum balance between dissolution rate and polymer grade has led to the prolific utility of PVP 30 K grade, among others, to prepare PVP-based dispersions. Moreover, PVP has been used for the dissolution enhancement of very slightly soluble drugs by its high hydrophilicity and strong interaction with some drug molecules [34]. The commercial solid dispersion products produced with PVP are summarised in Table 2.

2.1.2 Influence of drug-PVP interactions in solid dispersions on drug crystallinity, drug stability and dissolution rate

It can be seen from Table 1 that, of the 122 drugs dispersed into PVP, approximately 65% were reported to hydrogen bond with the carrier whilst dipole-dipole interactions were reported in four studies, hydrophobic interactions were reported in three studies and Van der Waals interactions were described in three publications; approximately 30% of the studies reported no interactions between the drug and carrier. PVP can form a hydrogen bond either through the nitrogen or carbonyl group on the pyrrole ring. However, steric hindrance constrains the involvement of the nitrogen atom in intermolecular interactions, thus making the carbonyl group more favorable for hydrogen bonding [35].

Intermolecular interactions are largely responsible for drug crystallinity reduction and consequent improvements in dissolution rate. Our recent study [36] described solid dispersions of haloperidol prepared using PVP and poly(2-oxazolines) and showed that hydrogen bonding interactions and hydrophobic effects influenced the

crystallinity of the drug and its release from solid dispersions. PVP was superior to the poly(2-oxazolines) in reducing crystallinity of haloperidol and gave rapid drug release from solid dispersions. This was attributed to not only its relative high hydrophobicity but also its ability to form hydrogen bonds with the drug molecules. Kanaze et al. [37] found that dissolution enhancement of flavonoid aglycone drugs naringenin and hesperetin was achieved by the solid dispersion technique; drug dissolution was 100% after 2 h using PVP as the carrier whereas using a PEG carrier resulted in lower dissolution at 2 h (<70%). This difference was attributed to the amorphous form and nano-dispersions of the flavanoid drugs into the PVP matrix, whereas with PEG the compounds were partially crystalline with particle sizes > 1 μm . FTIR spectra showed the presence of hydrogen bonds between PVP carbonyl groups and hydroxyl groups of both flavanone aglycones. These interactions prevent crystallization of naringenin and hesperetin aglycones in the PVP matrix. On the other hand, the ability of PEG carrier to form hydrogen bonds with flavanone glycosides or aglycones was limited, thus both flavanone glycosides and their aglycones remained predominantly crystalline.

Li et al. [38] found that the hydrogen bonds were formed between PEG and nitrendipine (TDP) and that these interactions were stronger than the hydrogen bonds formed between PVP and TDP. 3D molecular docking results of TDP with PEG or PVP showed that TDP-PEG had only hydrogen bond energy while TDP-PVP had both hydrogen bond energy and hydrophobic energy, resulting in higher overall binding energy of TDP-PVP. The higher binding energy of TDP-PVP can sufficiently explain why the involvement of TDP had stronger impact on PVP and the better amorphous state of TDP in TDP-PVP. The faster drug release of TDP-PVP was attributed to stronger binding energy (between drug and excipient) than TDP-PEG. The higher binding energy contributed to better amorphous state of TDP in TDP-PVP, reflecting that the intermolecular forces had significant influence on drug dissolution.

Karavas et al. [39] found that the hydrogen bonding interactions are the cause for the dissolution enhancement of felodipine (FEL) from FEL: PVP binary systems for high polymer concentrations where the hydrogen bonding intensity is high. The mechanism of such enhancement could be attributed to the effect of the interactions on the solubility and the specific surface of FEL particles in the system.

Jun et al. [40] reported a higher dissolution rate of cefuroxime axetil (CA) from solid dispersions, which was probably attributed to the formation of amorphous or non-crystalline forms due to intermolecular hydrogen bonds, resulting from the crystallization inhibition facilitated by PVP K-30, the increased wettability and reduction in particle size, resulting in an increased surface area available for dissolution.

Ghobashy et al. [41] found the *in vitro* rate of amlodipine dissolution depends on the drug–polymer intermolecular H bond. The rate of amlodipine dissolution is increased due to the drug–drug intramolecular hydrogen bonding replaced with the drug–polymer intermolecular hydrogen bonding, which reduces the crystal packing. The presence of hydrogen bonds between amlodipine and the hydrophilic polymers (PVP) in the solid dispersions is the primary cause of the rise in its solubility and dissolution.

Guedes et al. [42] established that the rise in the rate of dissolution of LPSF/FZ4 in binary solid dispersion systems is directly related to the presence and intensity of intermolecular interactions formed with the hydrophilic polymers, especially the hydrogen bonds identified. These interactions at molecular level appear to control the changes in the physical (crystalline or amorphous) state and to have an influence on particle size. For the LPSF/FZ4–PVP 1:9 system, which provided better results in terms of a dissolution profile, various characterization techniques showed the existence of relatively stronger interactions than those with the PEG polymer, and this was confirmed by a theoretical study of molecular modeling. This suggests that PVP is the preferred polymer for use in formulations developed for LPSF/FZ4 to

improve its solubility, dissolution, and gastrointestinal absorption.

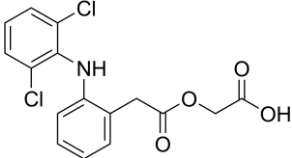
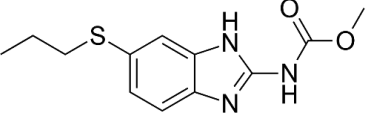
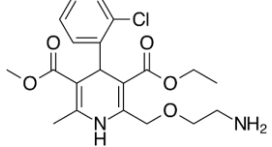
In addition, the intermolecular interactions are also responsible for physical stability, particularly carbonyl functionality of PVP usually forms hydrogen bonds with the drugs containing -NH_2 and -OH functionalities. For example, Obaidat et al. [43] found that a specific molecular interaction between the -NH_2 group of celecoxib (CEL) and the -C=O group of PVP was the major reason behind the formation and performance of a stable CEL-PVP amorphous system. By specifically interacting with CEL, PVP arrested drug molecular motions, and prevented the rearrangement of CEL molecules from a disordered molecular state into a thermodynamically stable, ordered crystalline form. Thus, the interaction with PVP provided enhanced physical stability to the amorphous form of CEL.

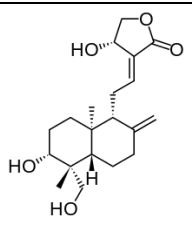
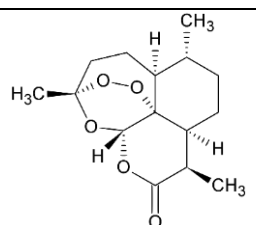
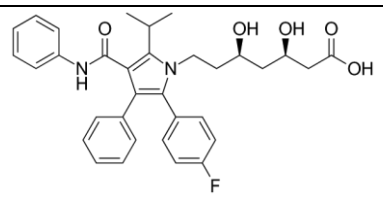
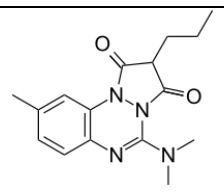
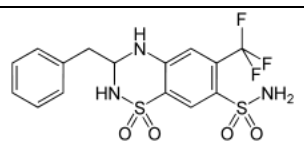
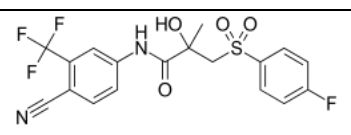
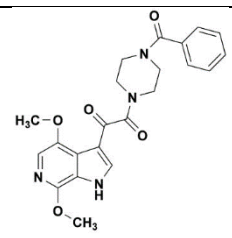
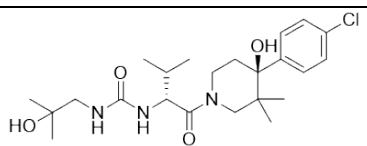
Kakran et al. [44] reported that curcumin (CUR) dispersions in PVP maintained their amorphous nature better than the CUR dispersion in PEG after storage for 9 months. This can be explained not only by the higher glass transition temperature (T_g) for PVP (155 °C) than that of PEG (−22 °C), which resulted in more stable formulations with PVP, but also by the presence of functional groups that are either donors or acceptors for hydrogen bonds, since specific interactions increase the solubility of the drug in its carrier and also seem to play an important role in inhibiting phase separation and crystallization of a drug. The CUR interactions were greater with PVP than with PEG (as confirmed by FTIR study), which also contributed to improved stability of the CUR dispersion in PVP. Greater drug-PVP interactions also increased the solubility of the drug in its carrier and thus inhibited phase separation and crystallization of the drug.

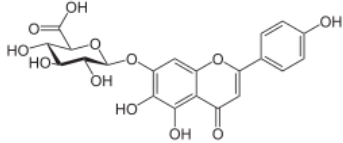
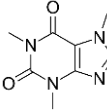
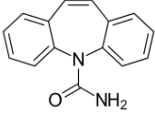
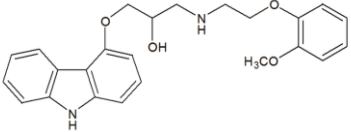
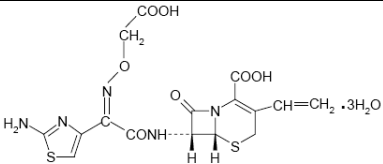
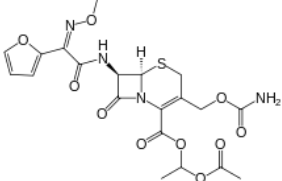
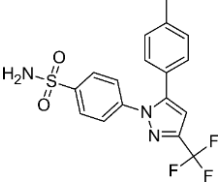
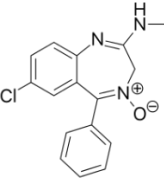
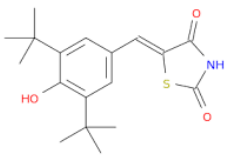
Due to the potential for electron sharing in COOH hydrogen bond donor moieties, the bond between the O and the H is relatively weaker for the OH group compared to the bond between the N and H in NH hydrogen bond donor moieties. Thus, the hydrogen atom in the COOH moiety is a better hydrogen-bond donor compared to the hydrogen atom in the NH moiety. This in turn leads to stronger hydrogen bonds

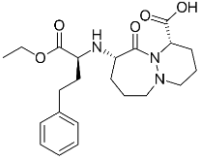
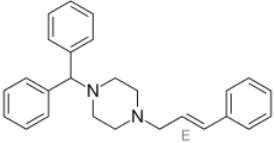
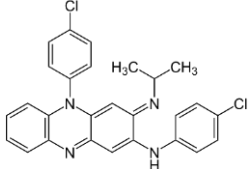
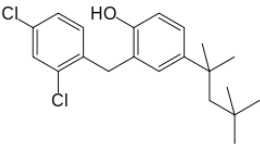
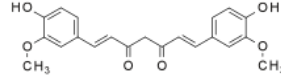
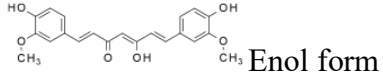
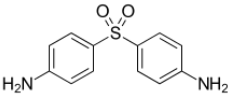
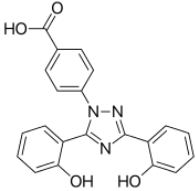
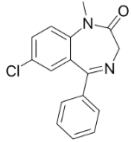
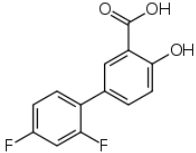
between $\text{COOH}_{\text{drug}}-\text{CO}_{\text{PVP}}$ compared to the hydrogen bonds between $\text{NH}_{\text{drug}}-\text{CO}_{\text{PVP}}$. It is speculated that the strength of the drug-polymer interactions, which in turn will influence the mixing enthalpy, it is important to determine which system will be susceptible to moisture induced immiscibility. Thus, model drugs with NH moieties were sensitive to moisture induced immiscibility while those containing COOH functions did not undergo this phenomenon. For example, Rumondor et al. [45] found that in the case of nifedipine, felodipine, droperidol and pimozide, drug-polymer hydrogen bonds are formed between the NH moiety of the drug and the carbonyl moiety of PVP (susceptible to moisture-induced phase separation); for ketoprofen and indomethacin, hydrogen bonds were formed between the COOH moiety of the drug and the carbonyl moiety of PVP (no experimental evidence of moisture-induced phase separation).

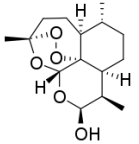
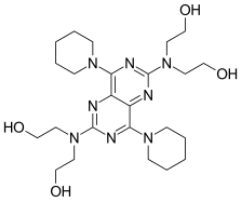
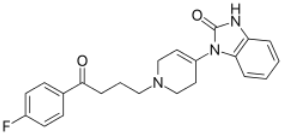
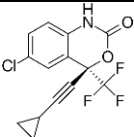
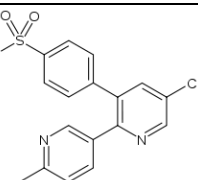
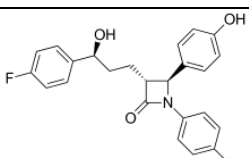
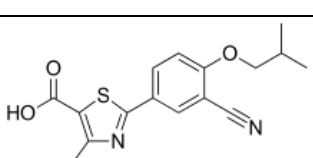
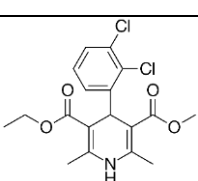
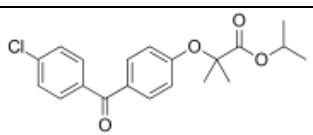
Table 1. Drugs employed in solid dispersions with PVP. “N” represents “no interactions reported” (September 2021).

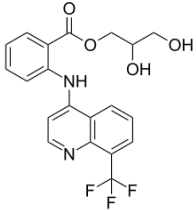
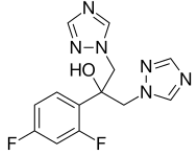
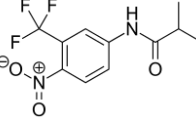
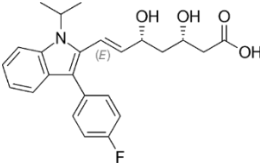
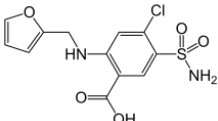
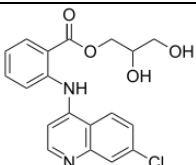
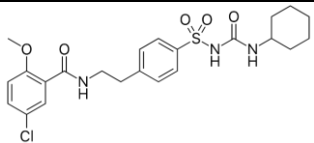
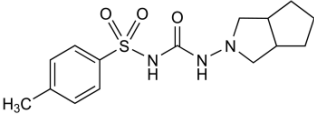
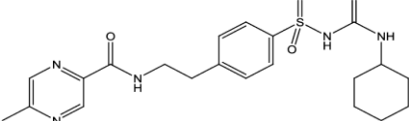
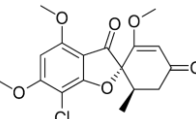
No.	Drug	Chemical Structure	Drug-PVP interactions			
			Hydrogen bonding	Dipole-dipole	Hydrophobicity	Van der Waals
1	Aceclofenac		[22]	N	N	N
2	Albendazole		[46]	N	N	N
3	Amlodipine		[41]	N	N	N

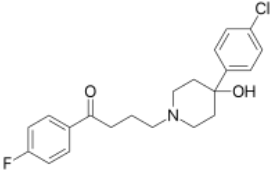
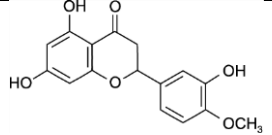
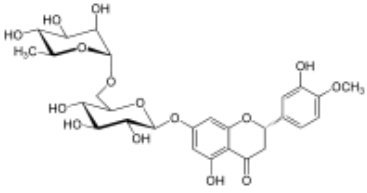
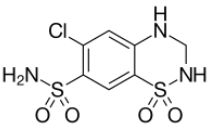
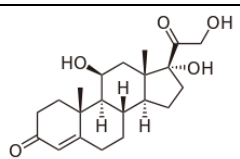
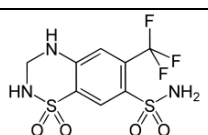
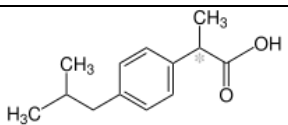
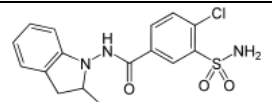
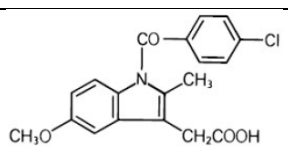
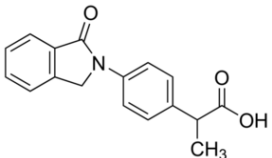
4	Andrographolide		[23, 47]	N	N	N
5	Artemisinin		N	N	N	N
6	Atorvastatin		[48]	N	N	N
7	Azapropazone		N	N	N	N
8	Bendroflumethiazide		N	N	N	N
9	Bicalutamide		[24, 30, 49]	N	N	N
10	BMS-488043		[50]	N	N	N
11	BMS-817399		[51]	N	N	N

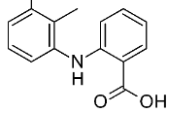
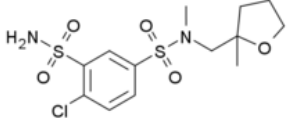
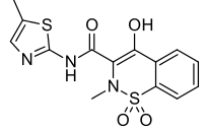
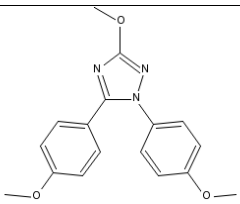
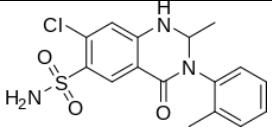
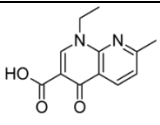
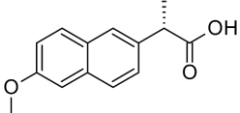
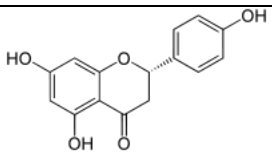
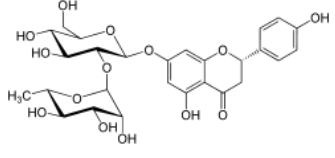
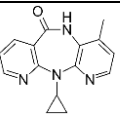
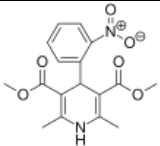
12	Breviscapine		[52]	N	N	N
13	Caffeine		N	N	N	N
14	Carbamazepine		[25]	N	N	N
15	Carvedilol		[53]	N	N	N
16	Cefixime		[26]	N	N	N
17	Cefuroxime axetil		[40]	N	N	N
18	Celecoxib		[43]	N	N	N
19	Chlordiazepoxide		N	N	N	N
20	CI-987		N	N	N	N

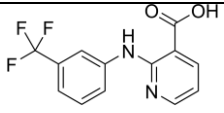
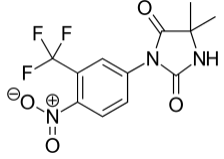
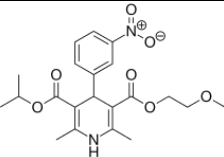
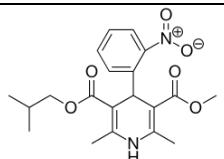
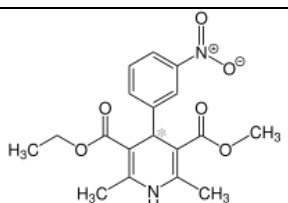
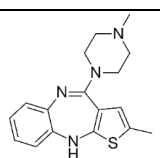
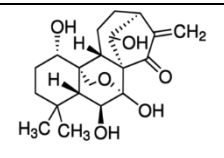
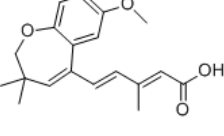
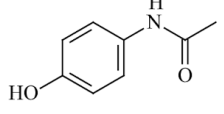
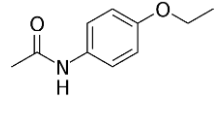
21	Cilazapril		[54]	N	N	N
22	Cinnarizine		N	N	N	N
23	Clofazimine		[55]	N	N	N
24	Clofoctol		[56]	N	N	N
25	Curcumin	<p> Keto form</p> <p> Enol form</p>	[44, 57]	N	N	N
26	Dapsone		[58]	N	N	N
27	Deferasirox		[59]	N	N	N
28	Diazepam		N	N	N	N
29	Diflunisal		[60]	N	N	N

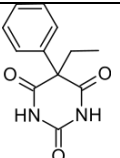
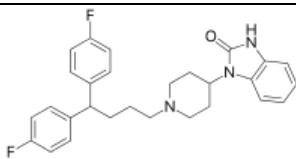
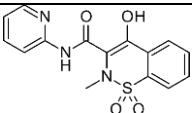
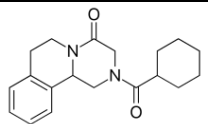
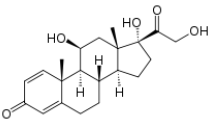
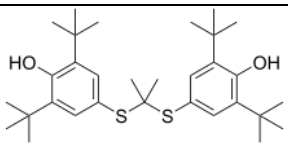
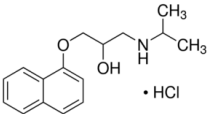
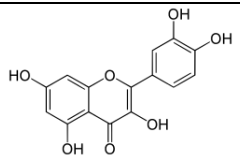
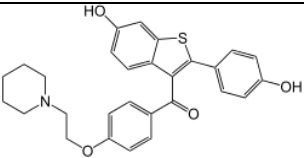
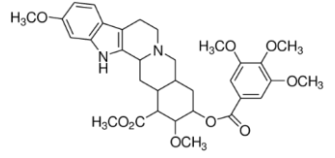
30	Dihydroartemisinin		[61]	N	N	N
31	Dipyridamole		[62]	N	N	N
32	Droperidol		[45]	N	N	N
33	Efavirenz		[27, 28]	N	N	N
34	Etoricoxib		N	N	N	N
35	Ezetimibe		[63]	N	N	N
36	Febuxostat		[64]	N	N	[64]
37	Felodipine		[39, 65-68]	N	N	[65]
38	Fenofibrate		N	N	N	N

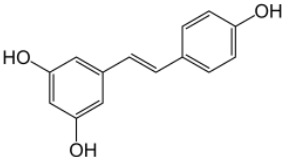
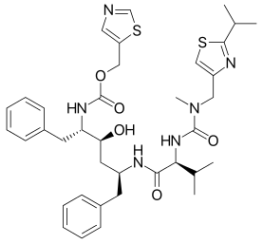
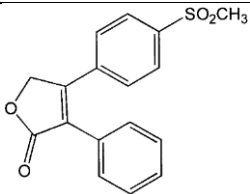
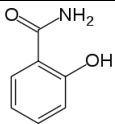
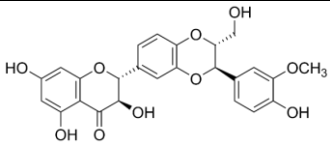
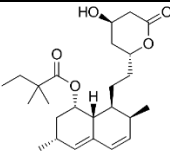
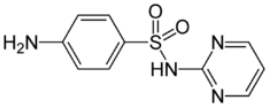
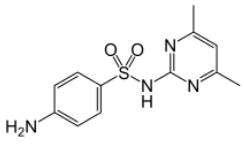
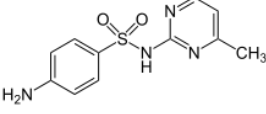
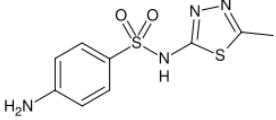
39	Floctafenine		N	N	N	N
40	Fluconazole		[69]	N	N	N
41	Flutamide		[70]	N	N	N
42	Fluvastatin		N	N	N	N
43	Furosemide		[71]	N	N	N
44	Glafenine		N	N	N	N
45	Glibenclamide		N	N	N	N
46	Gliclazide		[72]	N	N	N
47	Glipizide		[73]	N	N	N
48	Griseofulvin		N	N	N	N

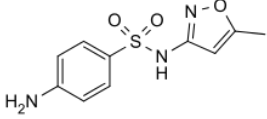
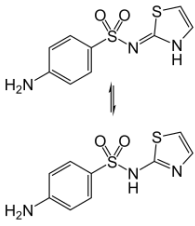
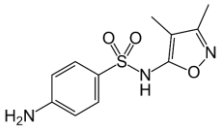
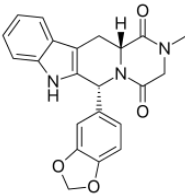
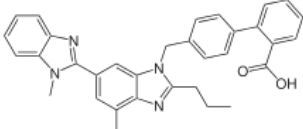
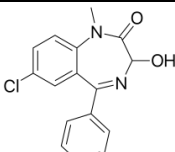
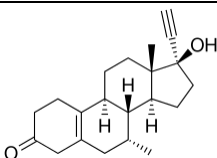
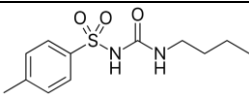
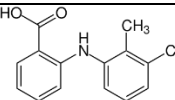
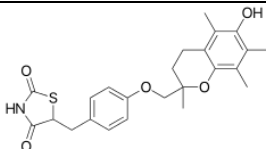
49	Haloperidol		[74]	N	[36]	N
50	Hesperetin		[37, 65]	N	N	N
51	Hesperidin		[37]	N	N	N
52	Hydrochlorothiazide		N	N	N	N
53	Hydrocortisone		[75]	N	N	N
54	Hydroflumethiazide		N	N	N	N
55	Ibuprofen		[35, 76-78]	N	N	N
56	Indapamide		N	N	N	N
57	Indomethacin		[31, 45, 79-81]	N	N	N
58	Indoprofen		[56]	N	N	N

69	Mefenamic acid		[89]	N	N	N
70	Mefruside		N	N	N	N
71	Meloxicam		N	N	N	N
72	3-Methoxy-1,5-bis(4-methoxyphenyl)-1H-1,2,4-triazole		N	N	N	N
73	Metolazone		N	N	N	N
74	Nalidixic acid		N	[90]	N	[90]
75	Naproxen		[91, 92]	N	N	N
76	Naringenin		[37]	N	N	N
77	Naringin		[37]	N	N	N
78	Nevirapine		N	N	N	N
79	Nifedipine		[45, 93, 94]	N	N	N

80	Niflumic acid		N	N	N	N
81	Nilutamide		[56]	N	N	N
82	Nimodipine		[95]	N	N	N
83	Nisoldipine		[96, 97]	N	N	N
84	Nitrendipine		[38]	N	[38]	N
85	Olanzapine		[98]	N	N	N
86	Oridonin		N	N	N	N
87	Oxeglitazar		[99]	N	N	N
88	Paracetamol		[100]	N	N	N
89	Phenacetin		[101]	N	N	N

90	Phenobarbital		[93]	N	N	N
91	Pimozide		[45]	N	N	N
92	Piroxicam		[102, 103]	N	N	N
93	Praziquantel		N	N	N	N
94	Prednisolone		N	N	N	N
95	Probucol		[56]	N	N	N
96	Propranolol hydrochloride		[92]	N	N	N
97	Quercetin		[104]	N	N	N
98	Raloxifene		[105]	N	N	N
99	Reserpine		N	N	N	N

100	Resveratrol		[106]	N	N	N
101	Ritonavir		N	N	[107]	N
102	Rofecoxib		N	N	N	N
103	Salicylamide		[92]	N	N	N
104	Silymarin		N	N	N	N
105	Simvastatin		[108, 109]	N	N	N
106	Sulfadiazine		[110]	N	N	N
107	Sulfadimidine					
108	Sulfamerazine					
109	Sulfamethizole		[111]	N	N	N

110	Sulfamethoxazole		[112]	N	N	N
111	Sulfathiazole		[110]	N	N	N
112	Sulfisoxazole		N	N	N	N
113	Tadalafil		[113]	N	N	N
114	Telmisartan		N	N	N	N
115	Temazepam		[114]	N	N	N
116	Tibolone		[115]	N	N	N
117	Tolbutamide		[31]	N	N	N
118	Tolfenamic Acid		[116]	N	N	N
119	Troglitazone		N	N	N	N

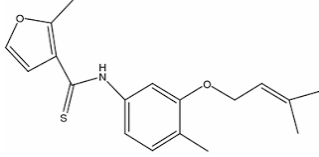
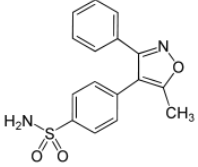
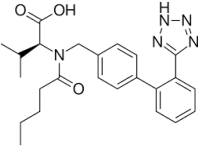
120	UC-781		[117]	N	N	N
121	Valdecoxib		N	N	N	N
122	Valsartan		[118]	N	N	N

Table 2. Commercial solid dispersion products produced with PVP. *Withdrawn in 2000 due to adverse drug reactions.

Product name	Drug	Indication	Company
Afeditab [®]	Nifedipine	Lower high blood pressure	Elan Corp, Ireland
Cesamet [®]	Nabilone	Treat nausea and vomiting caused by chemotherapy	Eli Lilly and Company, USA; Valeant Pharmaceuticals, Canada; Meda Pharmaceuticals
Ibuprofen [®]	Ibuprofen	Anti-inflammatory	Soliqs, Germany
Isoptin SRE-240 [®]	Verapamil	Lower high blood pressure	Soliqs, Germany
Rezulin ^{®*}	Troglitazone	Antidiabetic	Pfizer, USA

2.2 Polyvinylpyrrolidone-co-vinyl acetate (PVP/VA)

2.2.1 PVP/VA synthesis, general properties and applications in solid dispersions

PVP/VA is an amorphous and water-soluble polymer. It is a copolymer of vinyl pyrrolidone and vinyl acetate in a 6:4 ratio, which is also popularly known by the trade names Kollidon VA64 (BASF, Germany) and Plasdone S-630 (Ashland, USA).

The synthesis and structure of PVP/VA are given in Figure 2.

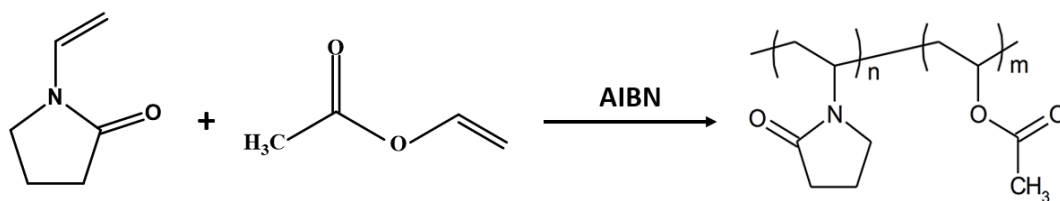


Figure 2. PVP/VA synthesis and structure.

PVP/VA has traditionally been used as a binder and film-forming agent in the pharmaceutical industry [119]. PVP/VA has a significant advantage over PVP in terms of processability. First, owing to the relatively less hydrophilic vinyl acetate substituent, PVP/VA exhibits phase solubility with a wide range of active pharmaceutical ingredients (APIs) with varied polarity [34]. Furthermore, a recent study demonstrated that the physical stability of the PVP/VA copolymer may be better than that of pure PVP due to an overall decrease in the hygroscopicity of the polymer [120]. This means that replacing the hydrophilic VP repeat units with hydrophobic VA repeat units will not only significantly inhibit the crystallization upon dissolution of the amorphous solid dispersion, but may also improve the physical stability of the formulation during storage [121, 122]. For example, Chen et al. [62] found the moisture uptake into PVP/VA SDs was lower than that for PVP SDs at the same weight ratio of dipyridamole and carriers, attributed to the difference between the chemical structures of PVP and PVP/VA. Second, it was also found that the tensile strengths of tablets composed of PVP/VA SDs at various ratios were greater than those of tablets of PVP SDs at the same compression pressure [62]. This result could be explained by the lower T_g of PVP/VA copolymer compared to PVP which made it an excellent direct compression binder aid and allowed it to undergo plastic deformation during compression. Also, the lower T_g and higher degradation temperature presents an opportunity to employ the polymer to formulate solid dispersions of low as well as high melting temperature APIs [119]. Therefore, when the drug is sensitive to moisture, or when the compressibility of the drug powder is poor, PVP/VA may be a better material than PVP. There are 49

drugs reportedly incorporated into PVP/VA as solid dispersions, summarised in Table 3. The commercial solid dispersion products produced with PVP/VA are presented in Table 4.

2.2.2 Influence of drug-PVP/VA interactions in solid dispersions on drug crystallinity, drug stability and dissolution rate

It could be seen from Table 3 that hydrogen bonding interactions between drug and PVP/VA are much more often reported than the other intermolecular interactions. Therefore, the influence of hydrogen bonding interactions between drug and PVP/VA on drug crystallinity, drug stability and dissolution are considered below.

It has been demonstrated that the replacement of about 40% of vinyl pyrrolidone units with vinyl acetate (as in PVP/VA) results in reduced inhibition of crystallization and the PVP homopolymer is more effective in crystallization inhibition than the copolymer at a comparable molecular weight [123] because the higher VP content leads to higher propensity to hydrogen bonding with the API [83]. Chan et al. reported that the intensity of ketoprofen-polymer interaction follows the trend $PVP > PVP/VA > PVA$ and the degree of drug-polymer interaction does interfere with the degree of amorphousness in the solid dispersion during the manufacturing process [124]. In similar studies but with ibuprofen (IBP), the interaction parameters $\chi_{IBP-polymer}$ are negative and vary in the order $PVP < PVP/VA < PVA$ which means that the order of IBP-polymer miscibility is $PVP > PVP/VA > PVA$ [78]; the “dissolving powers” of the polymers tested for indomethacin and nifedipine also follow the order $PVP > PVP/VA > PVA$ [125]. In another study, out of 10 APIs (celecoxib, clotrimazole, cinnarizine, felodipine, indomethacin, itraconazole, ketoconazole, ketoprofen, loratadine, miconazole), only celecoxib, clotrimazole, felodipine, indomethacin, and ketoconazole resulted in the formation of single-phase homogenous amorphous solids with no crystalline content. A possible explanation of these occurrences was presented, based on the interaction between API and PVP/VA, which can lead to their complete miscibility

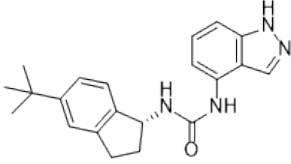
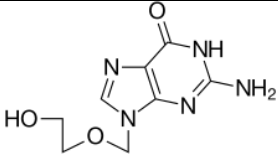
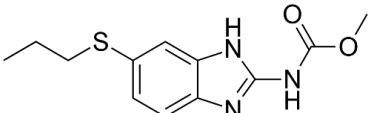
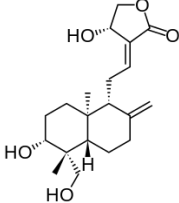
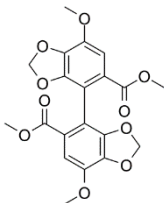
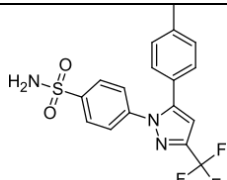
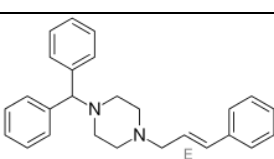
in the amorphous solid dispersion [126].

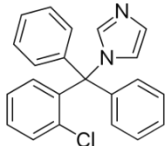
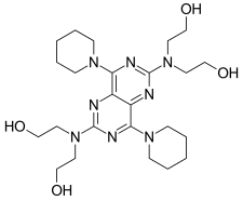
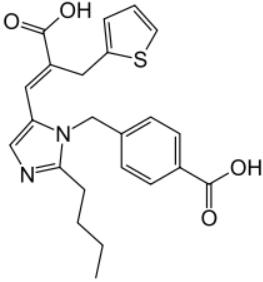
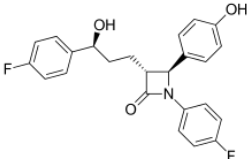
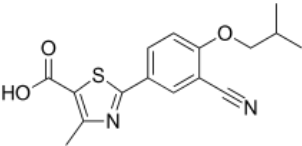
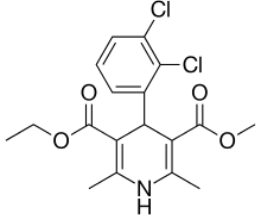
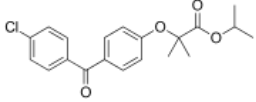
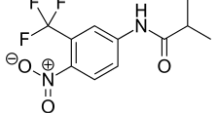
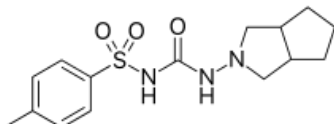
Different degrees of hydrogen bonding between drug and polymer determines the amount of moisture that is taken up by the sample and thus the physical stability. For example, a significant physicochemical interaction between the drug (indomethacin, lacidipine, nifedipine and tolbutamide) and polymer (PVP and PVP/VA) was found for all extrudates. This interaction was caused by hydrogen bonding between the carbonyl group of the polymer and a H-donor group of the drug. The lacidipine-PVP/VA extrudate showed some crystallinity after 4 weeks storage at 25°C/75% RH. In comparison, indomethacin-PVP/VA extrudate was stable for 8 weeks under the same conditions [31]. In another study [127], felodipine, pimozone, indomethacin and quinidine were used as model drugs with PVP and PVP/VA used as carriers; favorable drug-polymer interactions in the form of hydrogen bonding were found in all drug-polymer systems. For PVP/VA-containing systems, evidence for stronger drug-polymer interactions can be found with indomethacin when compared to those formed with felodipine, quinidine, and pimozone. This was supported by analyzing the red shift experienced by the carbonyl peak of the vinylpyrrolidone moiety of PVP/VA when hydrogen bonded to the different drugs. In indomethacin-PVP/VA, 42~44 cm⁻¹ shifts to lower wavenumbers were observed, greater than the 19~22 cm⁻¹ shifts observed for the other PVP/VA-containing solid dispersions investigated. Chemically, indomethacin contains a COOH hydrogen bond donor group. This group is a better hydrogen bond donor compared to the NH group in felodipine and pimozone and the OH group in quinidine, resulting in stronger drug-polymer interactions. This analysis supports experimental evidence whereby no evidence for moisture-induced drug-polymer immiscibility was observed for indomethacin-PVP/VA, in contrast to the three other systems. This study also showed that the hygroscopicity of the polymer must be considered in addition to considering the strength of the drug-polymer interactions. For felodipine- and quinidine-containing systems, the extent of amorphous-amorphous phase separation following exposure to moisture was more severe for

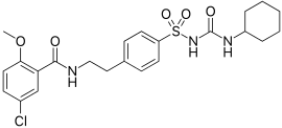
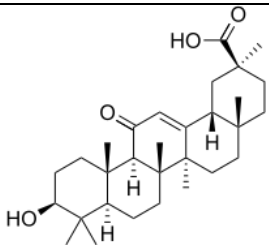
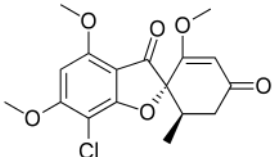
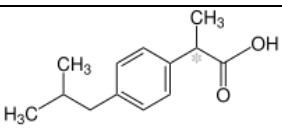
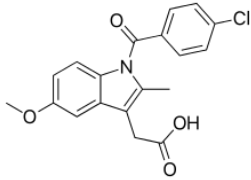
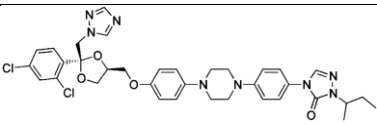
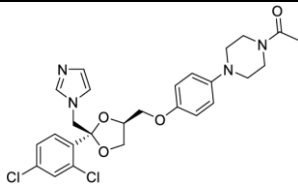
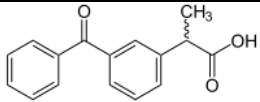
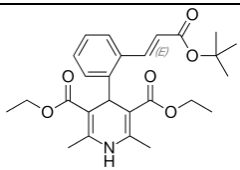
PVP-containing solid dispersions than for the corresponding PVP/VA-containing solid dispersions. For example, for felodipine-PVP samples containing 50% (w/w) polymer, storage at 84% RH resulted in a 50% reduction in the intensity of the peak assigned to drug-polymer hydrogen bonding relative to the peak assigned to drug-drug hydrogen bonding. For the comparable PVP/VA system, only a 17% reduction in the relative intensity was observed. For the quinidine-PVP sample containing 50% polymer, storage at 84% RH resulted in a 47% reduction in the intensity of the peak assigned to drug-polymer hydrogen bonding relative to the free vinylpyrrolidone carbonyl moiety. For the comparable PVP/VA system, the reduction was only 11%. For both felodipine- and quinidine-containing model systems, the strength of drug-polymer hydrogen bonding for PVP/VA-containing systems is approximately equal to that of their PVP-containing counterparts, as evidenced by similar red shifts observed from the IR spectra. Thus, the smaller extent of drug-polymer de-mixing for PVP/VA-containing systems is most likely explained by the reduction in the amount of water absorbed than by the strength of drug-polymer interactions.

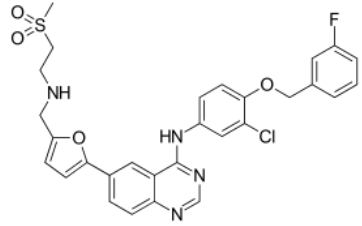
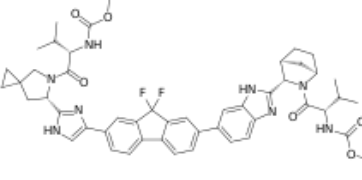
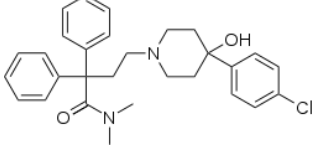
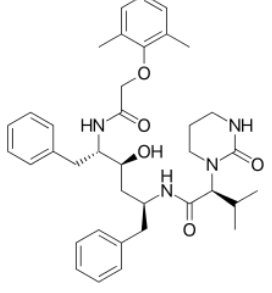
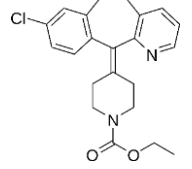
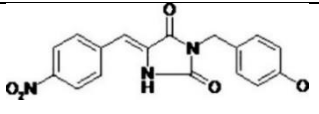
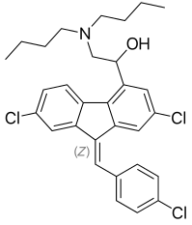
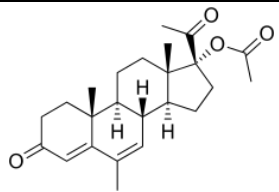
A study has also shown that the solubility of glycyrrhetic acid can be improved by ternary solid dispersion (TSD) systems that incorporate alkalizers. PVP/VA relies on hydrogen bonds to interact with alkalizers, and glycyrrhetic acid interacts with alkalizers to form ion-pair complexes through strong electrostatic attraction. This may be an important reason for the increase in the dissolution of glycyrrhetic acid [128].

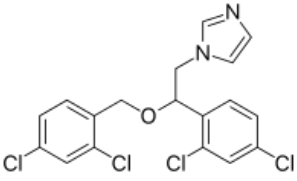
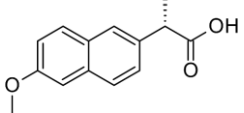
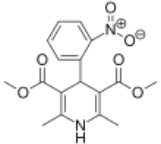
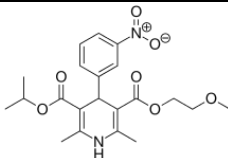
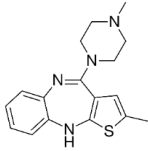
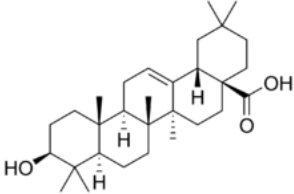
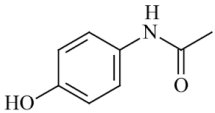
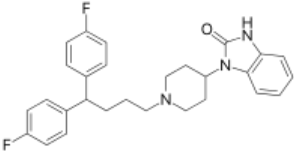
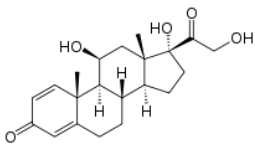
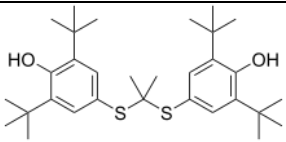
Table 3. Drugs employed in solid dispersions with PVP/VA. “N” represents “no interactions reported” (September 2021).

No.	Drug	Chemical structure	Drug-polymer interactions			
			Hydrogen bonding	Dipole-dipole	Hydrophobicity	Van der Waals
1	ABT-102		N	N	N	N
2	Acyclovir		N	N	N	N
3	Albendazole		[123]	N	N	N
4	Andrographolid e		[129]	N	N	N
5	Bifendate		N	N	N	N
6	Celecoxib		[126]	N	N	N
7	Cinnarizine		N	N	N	N

8	Clotrimazole		[126]	N	N	N
9	Dipyridamole		[62]	N	N	N
10	Eprosartan		N	N	N	N
11	Ezetimibe		[130]	N	N	N
12	Febuxostat		[64]	N	N	[64]
13	Felodipine		[126, 127, 131]	N	N	N
14	Fenofibrate		N	N	N	N
15	Flutamide		N	N	N	N
16	Gliclazide		N	N	N	N

17	Glyburide		[132]	N	N	N
18	Glycyrrhetic Acid		N	N	N	N
19	Griseofulvin		N	N	N	N
20	Ibuprofen		[78]	N	N	N
21	Indomethacin		[31, 81, 125-127]	N	[81]	N
22	Itraconazole		N	N	N	N
23	Ketoconazole		N	[131]	N	N
24	Ketoprofen		[83, 124]	N	N	N
25	Lacidipine		[31]	N	N	N

26	Lapatinib		N	N	N	N
27	Ledipasvir		[133]	N	N	N
28	Loperamide		N	N	N	N
29	Lopinavir		[134]	N	N	N
30	Loratadine		N	N	N	N
31	LPSF/FZ4		N	N	N	N
32	Lumefantrine		N	N	N	N
33	Megestrol acetate		N	N	N	N

34	Miconazole		N	N	N	N
35	Naproxen		[100]	N	N	N
36	Nifedipine		N	N	N	N
37	Nimodipine		[135]	N	N	N
38	Olanzapine		N	N	N	N
39	Oleanolic acid		[136]	N	N	N
40	Paracetamol		[137]	N	N	N
41	Pimozide		[127]	N	N	N
42	Prednisolone		[138]	N	N	N
43	Probucol		N	N	N	N

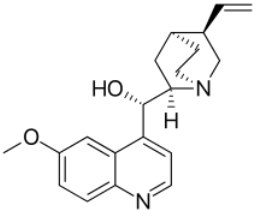
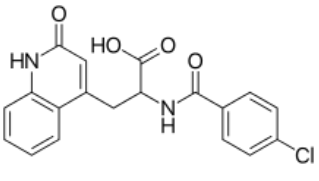
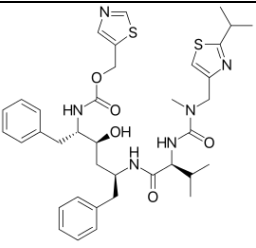
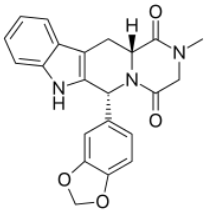
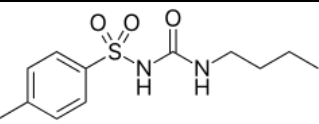
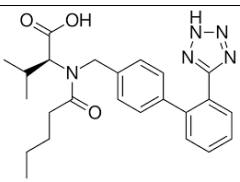
44	Quinidine		[127]	N	N	N
45	Rebamipide		[139]	N	N	N
46	Ritonavir		[140]	N	N	N
47	Tadalafil		[113, 141]	N	N	N
48	Tolbutamide		N	N	N	N
49	Valsartan		N	N	N	N

Table 4. Commercial solid dispersion products produced with PVP/VA.

Product name	Drug	Indication	Company
Kaletra [®]	Lopinavir/Ritonavir	Anti-viral (HIV)	Abbott Laboratories, USA
Novir [®]	Ritonavir	Anti-viral (HIV)	Abbott Laboratories, USA
Belsomra [®]	Suvorexant	Insomnia	Merck
Viekira [™]	Ombitasavir etc.	Chronic hepatitis C virus (HCV)	AbbVie
Harvoni [®]	Ledipasvir/Sofosbuvir	Chronic hepatitis C virus (HCV)	Gilead Sciences

2.3 Poly(N-vinyl caprolactam)–polyvinyl acetate–polyethylene glycol graft copolymer (Soluplus[®])

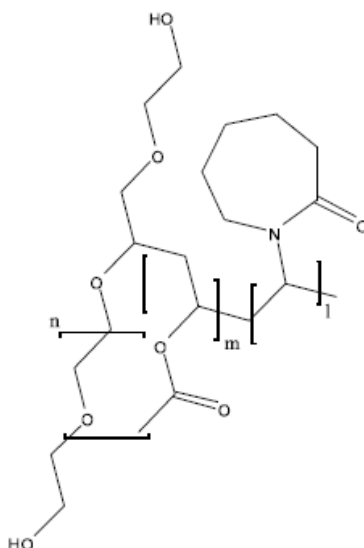


Figure 3. Soluplus[®] structure.

2.3.1 Soluplus[®] general properties and applications in solid dispersions

Soluplus[®] is a triblock graft copolymer consisting of polyethylene glycol (13% PEG 6000), poly(N-vinyl caprolactam) (57%), and polyvinyl acetate (30%). It is an amphiphilic polymer, wherein PEG provides hydrophilicity, vinyl caprolactam is water soluble with a lower critical solution temperature, while vinyl acetate domains are lipophilic within the polymer matrix. The molecular weight of

Soluplus® usually ranges from 90,000 to 1,40,000 g/mol. It is an amorphous polymer with a relatively low glass transition temperature (T_g) of 70°C [113, 142]. Developed specifically for solid solutions, Soluplus® is free flowing and can be easily extruded for processing by, for example, hot melt extrusion (HME). Soluplus® can also be used as a matrix former in spray drying and as a binder in wet granulation or dry granulation and in drug layering. However, to date, only one commercial solid dispersion product produced with Soluplus® has been marketed- Febuxostat/Zentiva.

For Soluplus®-based dispersions, the API is generally dispersed molecularly within the polymer matrix [143]. Upon exposure to the solvent or dissolution media, the API can form a supersaturated solution as it dissolves along with the polymer [144]. There are very few reports describing the crystallization or precipitation inhibition properties of Soluplus®. Guan et al. [145] reported that Soluplus® synergistically inhibited crystal nucleation and growth of lacidipine, leading to prolonged supersaturation. Soluplus® also exhibits swelling property, which may offset potential dissolution rate improvements due to limited diffusion through the swelled polymer. Slamova et al. [146] reported that tadalafil release from a Soluplus® dispersion was retarded due to swelling of the polymer during dissolution. Nevertheless, the swelling property of Soluplus® can be leveraged to formulate delayed release solid dispersions.

2.3.2 Influence of drug-Soluplus® interactions in solid dispersions on drug crystallinity, drug stability and dissolution rate

It could be seen from Table 5 that hydrogen bonding interactions remain the most commonly reported intermolecular interaction between drugs and Soluplus®. Song et al. demonstrated that hydrogen bonding interactions between andrographolide and Soluplus® led to enhanced interface wetting, consequently leading to an improved dissolution rate [129]. Griseofulvin showed remarkable supersaturation from Soluplus®-based dispersion due to inhibition of API recrystallization through

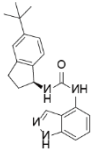
stronger intermolecular interactions [147]. The improved lopinavir solubility and bioavailability was attributed to the stronger hydrogen bonding interactions between lopinavir and Soluplus[®] in the HME process [134]. Hydrogen bonds between the thioacetyl group of spironolactone and the donor hydroxyl groups of Soluplus[®] played a decisive role in the formation of a molecular solution and drug micellization, resulting in improved solubility and dissolution efficiency which was greatest at a drug/Soluplus[®] ratio 1:4 [148].

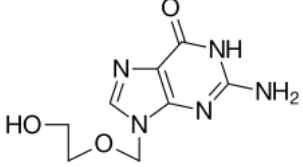
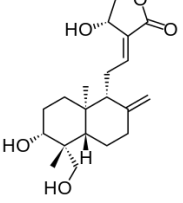
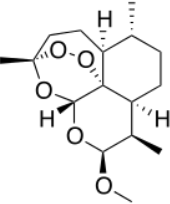
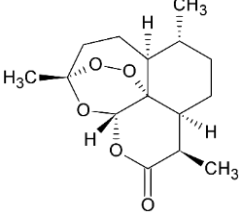
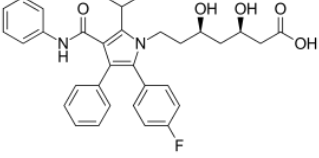
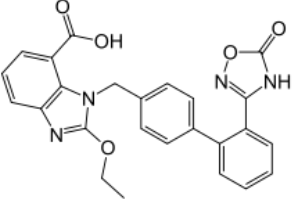
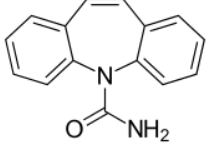
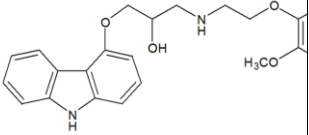
In addition, physical stability is always a challenging issue regarding amorphous drugs. A 20:80 simvastatin /Soluplus SD showed that little change took place in the dissolution profiles after 3 months storage (40°C, RH 75%), indicating good physicochemical stability, which was expected to be enhanced by the combined effect of the enhanced T_g value by Soluplus (the T_g of the solid dispersion system was increased by Soluplus) and the intermolecular hydrogen bonding between the amorphous simvastatin and Soluplus [149]. In an efavirenz-Soluplus solid dispersion study, a long-term stability experiment indicated that efavirenz remained amorphous under the storage conditions since Soluplus can engage in hydrogen bonding with efavirenz, resulting in reduced molecular mobility and retarded crystallization during storage under the studied conditions [150]. The improved stability of artemisinin during storage is attributed to strong intermolecular interaction between the drug and Soluplus which reduces molecular mobility and recrystallization [151]. LPSF/FZ4 not only forms hydrogen bonding through its N-H groups with C=O groups on Soluplus, but also by its C=O with O-H groups on Soluplus. Due to this additional formation of hydrogen bonds, Soluplus[®]-based SD systems might exhibit a greater degree of intermolecular interactions than those with PVP which would be expected because the O-H groups in Soluplus[®] are stronger hydrogen bond donors than the N-H group of LPSF/FZ4, allowing them to form hydrogen bonds more easily with this drug, corroborated by the results of in vitro stability and dissolution studies [152]. The hydrogen bonding interactions

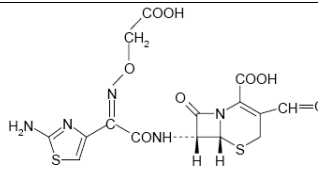
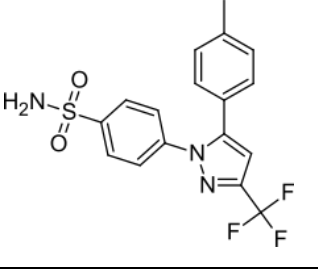
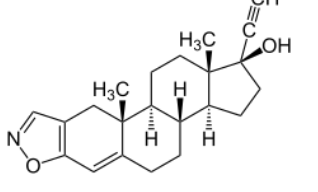
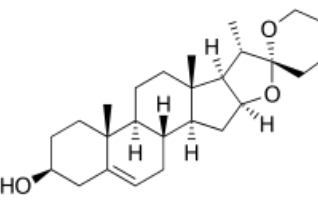
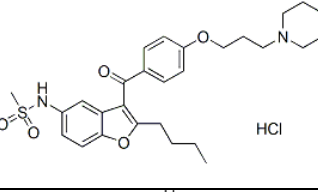
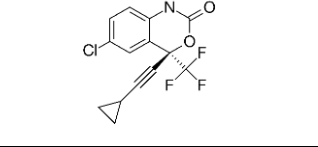
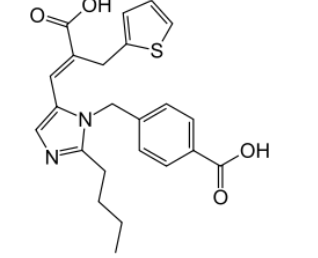
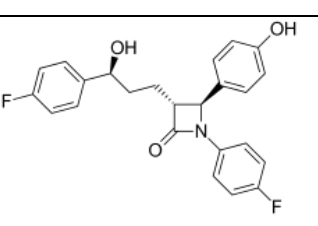
between the hydroxyl group of diosgenin and the carbonyl group (hydrogen bond acceptor) of Soluplus have been confirmed and not only inhibited drug crystallization but also enhanced the solid solubility of the drug [153]. Jog et al. demonstrated the physical stability of an ABT-102/Soluplus[®] dispersion as a consequence of strong hydrogen bonding between –C=O function of Soluplus[®] and –N-H moiety of the drug [154].

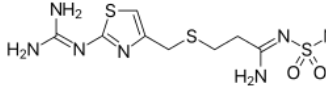
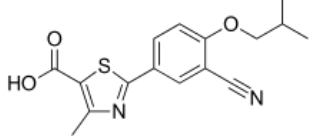
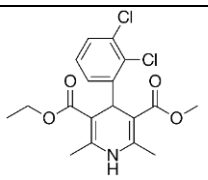
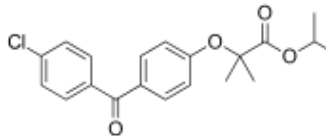
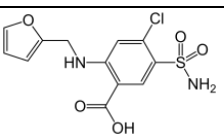
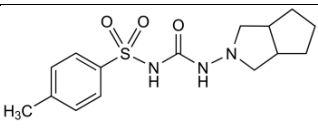
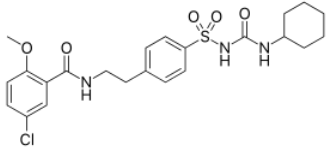
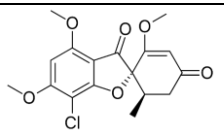
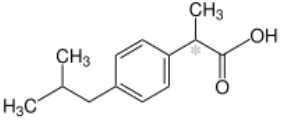
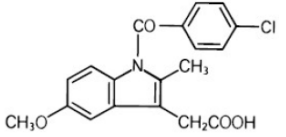
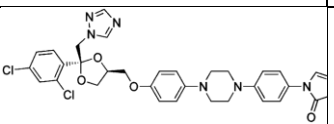
However, structured intermolecular bonding between API and polymer can have adverse effects on stabilization of the disordered phase as the disruption of these bonding patterns may result in phase separation (polymer-rich regions were formed). Singh et al. prepared itraconazole/Soluplus[®] solid dispersion through hot-melt extrusion. The dispersion was stabilized due to hydrogen bonding between API and polymer. However, while attempting to formulate tablets from the prepared dispersion, Soluplus[®]-rich regions were formed during compression. It was indicated that the disruption of hydrogen bonding leads to phase separation [155]. Often, the hydrogen bonding interactions are complemented by API-polymer solubility/miscibility.

Table 5. Drugs employed in solid dispersions with Soluplus[®]. “N” represents “no interactions reported” (September 2021).

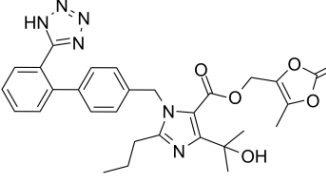
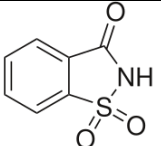
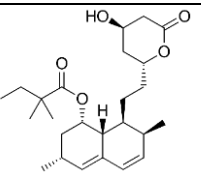
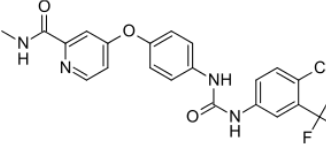
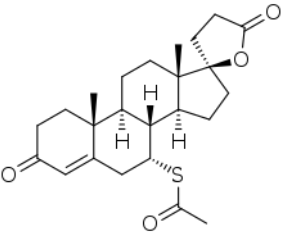
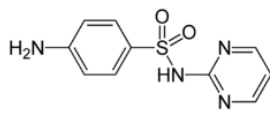
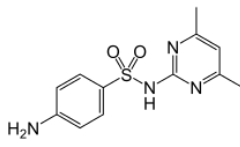
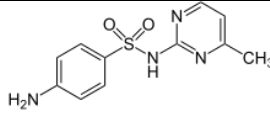
No.	Drug	Chemical structure	Drug-polymer interactions			
			Hydrogen bonding	Dipole-dipole	Hydrophobicity	Van der Waals
1	ABT-102		[154]	N	N	N

2	Acyclovir		N	N	N	N
3	Andrographolide		[129]	N	N	N
4	Artemether		[156]	N	N	N
5	Artemisinin		N	N	N	N
6	Atorvastatin		[157]	N	N	N
7	Azilsartan		N	N	N	N
8	Carbamazepine		[158]	N	N	N
9	Carvedilol		[159]	N	N	N

10	Cefixime		N	N	N	N
11	Celecoxib		[43]	N	N	N
12	Danazol		N	N	N	N
13	Diosgenin		[153]	N	N	N
14	Dronedarone hydrochloride		N	N	N	N
15	Efavirenz		[150]	N	N	N
16	Eprosartan		N	N	N	N
17	Ezetimibe		[150]	N	N	N

18	Famotidine		[160]	N	N	N
19	Febuxostat		[64]	N	N	[64]
20	Felodipine		[161]	N	N	N
21	Fenofibrate		N	N	N	N
22	Furosemide		[162]	N	N	N
23	Gliclazide		N	N	N	N
24	Glyburide		[132]	N	N	N
25	Griseofulvin		[147, 163]	N	N	N
26	Ibuprofen		[164]	N	N	N
27	Indomethacin		N	N	N	N
28	Itraconazole		[155]	N	N	N

29	Lacidipine		N	N	N	N
30	Lapatinib		N	N	N	N
31	Lansoprazole		[165]	N	N	N
32	Lopinavir		[134]	N	N	N
33	LPSF/FZ4		[152]	N	N	N
34	Naproxen		[164]	N	N	N
35	Nimodipine		[166]	N	N	N
36	Nisoldipine		[167]	N	N	N
37	Olanzapine		N	N	N	N

38	Olmesartan medoxomil		N	N	N	N
39	Saccharin		[168]	N	N	N
40	Simvastatin		[149]	N	N	N
41	Sorafenib		N	N	N	N
42	Spirolactone		[148]	N	N	N
43	Sulfadiazine					
44	Sulfadimidine		[110]	N	N	N
45	Sulfamerazine					

46	Sulfathiazole					
47	Tadalafil		[113]	N	N	N
48	Tamoxifen citrate		[169]	N	N	N
49	Telmisartan		N	N	N	N
50	Valsartan		N	N	N	N

2.4 Poly(2-oxazolines) (POZ)

2.4.1 POZ synthesis, general properties and applications in solid dispersions

Firstly reported in 1966–1997, independently by four research groups [170-173], poly(2-oxazolines) (POZ) have been of great interest due to their narrow molecular weight distribution, tunable properties, and excellent biocompatibility [174]. POZ are potential candidates to overcome some of the limitations reported with pharmaceutical applications of PEG while retaining the required features—

biocompatibility, low dispersity, responsiveness, high functionalization potential, and high versatility attainable by copolymerization —providing a polymeric platform for novel biomedical applications [175-179].

POZ are readily obtained via the cationic ring-opening polymerization (CROP) of 2-oxazolines [180], as depicted in Fig. 4.

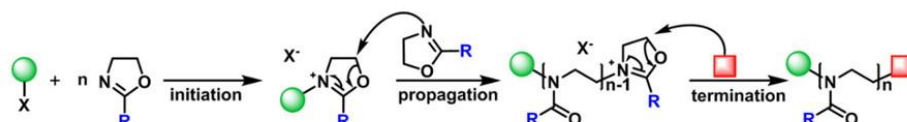


Figure 4. POZ synthesis and structure.

Functional polymers are accessible by selection of the initiator and terminating agent in a one pot synthesis [181-183], while the side chains are tunable by modification of the 2-substituent of the 2-oxazoline monomer, allowing control over the hydrophilicity and lower critical solution temperature (LCST) transition of the polymer (Fig. 5). Poly(2-methyl-oxazoline) (PMeOx or PMOZ), which has been reported to be even more hydrophilic than polyethylene glycol [184], is fully water soluble from 0 to 100°C; POZ with longer alkyl side-chains exhibit LCST behavior. Figure 5 shows the cloud point temperatures (T_{CP} , the temperature where the transmittance rapidly decreases due to agglomeration of the polymer chains) of POZ with increasing hydrophobicity. It should be noted that the T_{CP} depends on the molar mass, the concentration, the polymer end-groups and the conditions of the measurement [185] and therefore comparisons of T_{CP} values reported in the literature should be used cautiously.

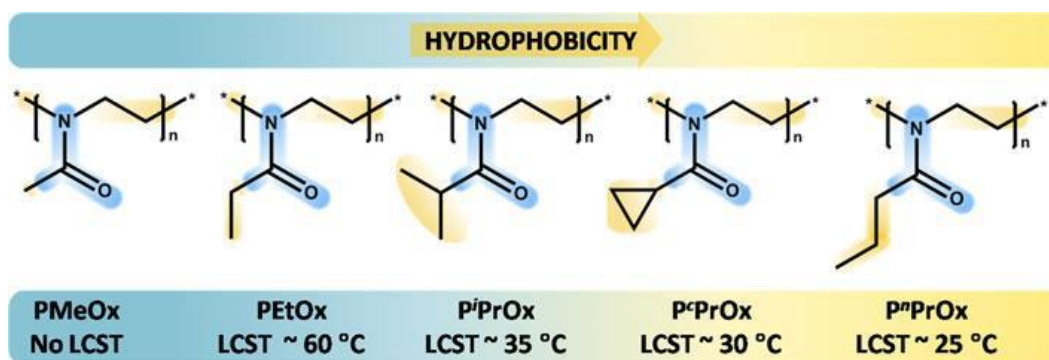


Figure 5. POZ with hydrocarbon side-chains with increasing hydrophobicity (from left to right) and consequently decreasing cloud point temperature [186].

The variation of the side-chain structure of POZ allows tuning of the properties from very hydrophilic (PMOZ) to very hydrophobic (long alkyl side-chains) polymers. Consequently, the solution behavior of POZ strongly depends on the side-chain structure [187]. Figure 6 gives an overview of the solubility of various POZ with hydrocarbon side-chains in water and common organic solvents.

Figure 7 shows the glass transition temperatures (T_g) and melting temperatures (T_m) obtained from DSC of poly(2-oxazolines) with 1–17 carbon atoms in the side-chain. Polymers with 1–5 carbon atoms in the side-chain show a T_g that decreases linearly with increasing side-chain length which can be explained by the increasing flexibility of the side-chains. For PMOZ, PEOZ and PnPOZ, no melting peaks were observed by DSC, while polymers with four or more carbon atoms in the side-chain were found to be semicrystalline with a T_m around 150°C [187].

POZ constitute a polymer class with exceptional properties for their use in a plethora of different biomedical applications and are proposed as a versatile platform for the development of new medicines (Fig. 8). However, use of POZ as a carrier in solid dispersions is reported in few studies. Fael et al. [187] found that a lower molecular weight of PEOZ (5000 g/mol) was superior to a higher molecular weight polymer (50,000 g/mol) in improving the dissolution behavior of glipizide.

Boel et al. [188] showed that PEOZ maintained supersaturation of itraconazole and fenofibrate to a similar extent as PVP, PVP/VA and HPMC. Everaerts et al. [189] selected PEOZ, PnPOZ, poly(2-sec-butyl-2-oxazoline) (PsecBuOZ) and a combination of PEOZ with either PnPOZ or PsecBuOZ as carriers for amorphous solid dispersions with six drugs and highlighted the potential of POZ as a novel polymer carrier to form amorphous solid dispersions. In our studies [36, 190], PVP and a series of water-soluble poly(2-oxazolines) including PMOZ, PEOZ, PnPOZ and PiPOZ were used to prepare solid dispersions with haloperidol and ibuprofen, and the effects of polymer structure and properties on drug crystallinity were demonstrated. Claeys et al. [191] demonstrated that PEOZ is a potentially interesting matrix for controlled release formulations produced by hot melt extrusion followed by injection molding. They found that both a highly water-soluble drug (metoprolol tartrate) as well as a poorly water-soluble drug (fenofibrate) could be solubilized within the polymeric matrix upon hot melt extrusion. Whereas formulation of a highly water-soluble drug led to a slower dissolution and drug release profile, due to a slower dissolution rate of the polymeric matrix compared to the pure drug, a dramatic increase in dissolution rate was observed when a poorly water-soluble drug was formulated. Furthermore, they also showed that the release rate could be tailored by varying the molecular weight of the PEOZ.

However, POZ is still not approved by the FDA for medical purposes (currently, only PEOZ is approved by the FDA as an indirect food additive) due to the shortage of pre-clinical evaluations on effectiveness and toxicokinetics *in vivo*.

	Water	MeOH	CHCl ₃	MeCN	DMF	PhCl	DMAc
PMeOx	+	+	-	+/- ^a		-	+
PEtOx	LCST	+	+	+	+	+	+
P <i>n</i> -PrOx	LCST	+	+	+		+	+
P <i>n</i> -NonOx	-		+	-	-		+
PPhOx	-		+	+	+		+
Pc-BuOx	-	-		+/- ^b		+/- ^b	+/- ^b
Pc-PentOx	-	-		-		-	-
Pc-HexOx	-	-		-		+/- ^c	+/- ^c

MeOH, methanol; CHCl₃, chloroform; MeCN, acetonitrile; DMF, *N,N'*-dimethylformamide; PhCl, chlorobenzene; DMAc, *N,N'*-dimethylacetamide; +, soluble; -, insoluble; +/-, partially soluble; LCST, lower critical solution temperature.

^a Poor solubility for molar mass > ca 20 kDa.

^b Soluble after heating, precipitated on cooling.

^c Soluble after heating.

Figure 6. Solubility of POZ with hydrocarbon side-chains in water and various organic solvents [192].

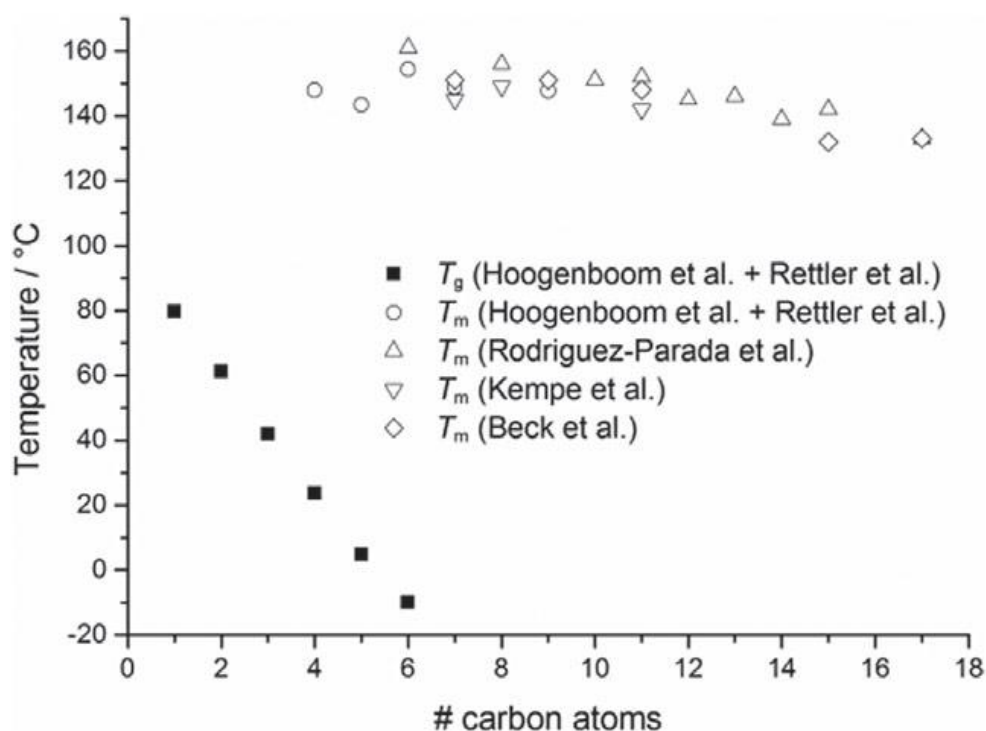


Figure 7. Glass transition and melting temperatures of poly(2-*n*-alkyl- 2-oxazoline)s with varying side-chain length obtained from DSC [192].

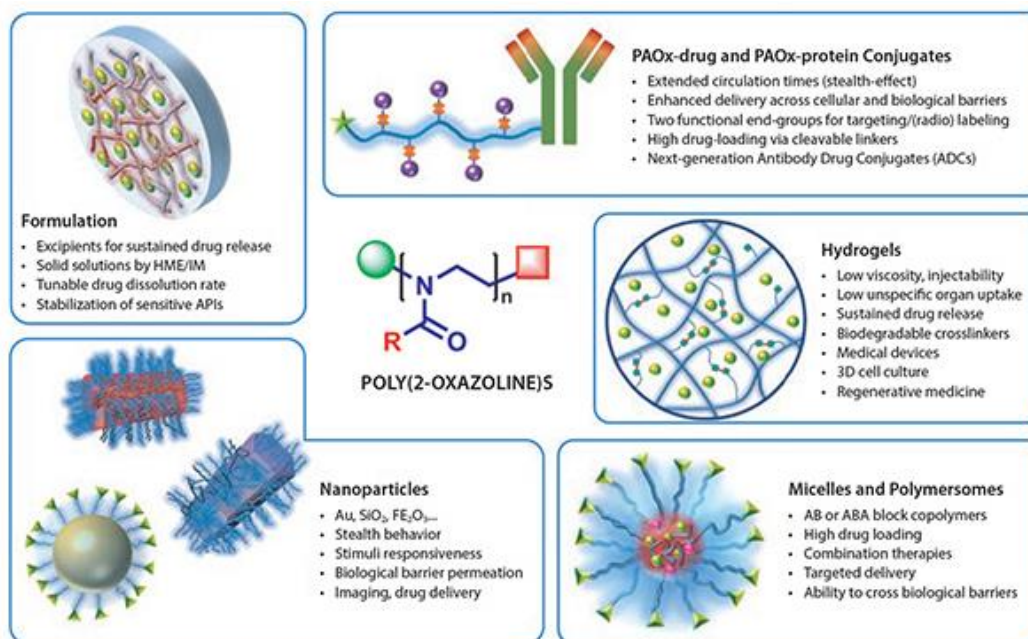


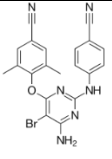
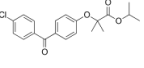
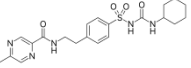
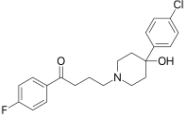
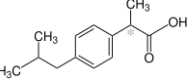
Figure 8. Drug delivery applications of POZ. (AVROXA BV, a company from Ghent University, Belgium.)

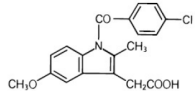
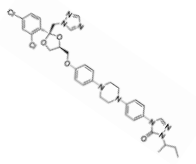
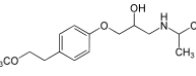
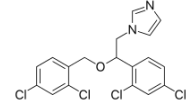
2.4.2 Influence of drug-POZ interactions in solid dispersions on drug crystallinity, drug stability and dissolution rate

It can be seen from Table 6 that only nine drugs have been studied in solid dispersions with POZ to date. In one of our previous studies on the effects of polymer structure and property on haloperidol crystallinity, it has been demonstrated that an increase in the hydrophobicity in a series of POZ also favored drug crystallinity reduction. However, poly(2-isopropyl-2-oxazoline) had poor ability to reduce crystallinity of haloperidol, which was related to the semi-crystalline nature of this polymer. Dissolution studies gave good agreement with the levels of drug crystallinity measured in the solid dispersions. However, solid dispersions with poly(n-propyl-2-oxazoline) released the drug very slowly due to its lower critical solution temperature and hence insolubility of this polymer in the dissolution medium [36]. The mutual effects of hydrogen bonding and polymer

hydrophobicity on ibuprofen crystal inhibition in solid dispersions with PVP and POZ was studied [190]; PMOZ, the most hydrophilic polymer, showed the poorest ability to reduce or inhibit the crystallinity of IB. In contrast, the more hydrophobic polymers PVP, PEOZ, PnPOZ and PiPOZ provided greater but similar abilities to reduce IB crystallinity, despite the differing polymer hydrophobicity's and that PiPOZ is semi-crystalline. These results indicate that crystallinity disruption is predominately due to hydrogen bonding between the drug molecules and the polymer.

Table 6. Drugs employed in solid dispersions with POZ. “N” represents “no interactions reported” (September 2021).

No.	Drug	Chemical structure	Polymer	Drug-polymer interactions			
				Hydrogen bonding	Dipole-dipole	Hydrophobicity	Van der Waals
1	Etravirine		PEOZ/PnPOZ blend	N	N	N	N
2	Fenofibrate		PEOZ PEOZ/PnPOZ blend	N	N	N	N
3	Glipizide		PEOZ	N	N	N	N
4	Haloperidol		PMOZ PEOZ PnPOZ PiPOZ	N	N	[36]	N
5	Ibuprofen		PMOZ PEOZ PnPOZ PiPOZ PEOZ/PnPOZ blend	[190]	N	N	N

6	Indomethacin		PEOZ PnPOZ PsecBuOx PEOZ/PnPOZ blend PEOZ/ PsecBuOx blend	N	N	N	N
7	Itraconazole		PEOZ PnPOZ PsecBuOx PEOZ/PnPOZ blend PEOZ/ PsecBuOx blend	N	N	N	N
8	Metoprolol tartrate		PEOZ	N	N	N	N
9	Miconazole		PEOZ/PnPOZ blend	N	N	N	N

3. Amide-containing water-soluble polymers which have not yet been studied in solid dispersions

Amide-containing water-soluble polymers which have not yet been studied in solid dispersions are summarized in Figure 9.

Poly(N-vinyl acetamide) is a polymer with affinity for both water and alcohol made primarily from N-vinylacetamide monomer. Expected applications include as a hydrophilic agent, thickening agent and dispersing agent [193].

Polyacrylamides including polyacrylamide, poly(N-isopropylacrylamide), poly(N, N-dimethylacrylamide) and poly(N, N-diethylacrylamide) are high molecular weight water soluble or swellable polymers formed from acrylamide or its derivatives. Their glass transition temperatures are well above room temperature (> 400 K). The only commercially important polyacrylamide is polyacrylamide. It is a non-ionic, water-soluble, and biocompatible polymer that can be tailored to meet

a broad range of applications. The polymer can be synthesized as a simple linear chain or as a cross-linked structure. The cross-linked polymer can absorb and retain extremely large amounts of water because the amide groups form strong hydrogen bonds with water molecules. Hydrated polyacrylamide is a soft gel that is used in gel electrophoresis and as a super water-absorbing polymer. The biomedical and pharmaceuticals applications of polyacrylamide have been described by Jain [194] and Yang [195].

Poly(N-isopropylacrylamide), poly(N, N-diethylacrylamide) and poly(N-vinyl caprolactam) are temperature-responsive polymers. Poly(N-vinyl caprolactam) is a well-studied temperature-responsive polymer, second to poly(N-isopropylacrylamide) which is the most popular temperature-responsive polymer. The polymers show similar LCST behavior in water between 30 and 32°C [196, 197], which thus limits their applications in solid dispersions.

Given these polymers have amide groups which, as H-bond acceptors, could form hydrogen bonding interactions with APIs having H-bond donors, there is potential for those which do not show LCST to be carriers in solid dispersions.

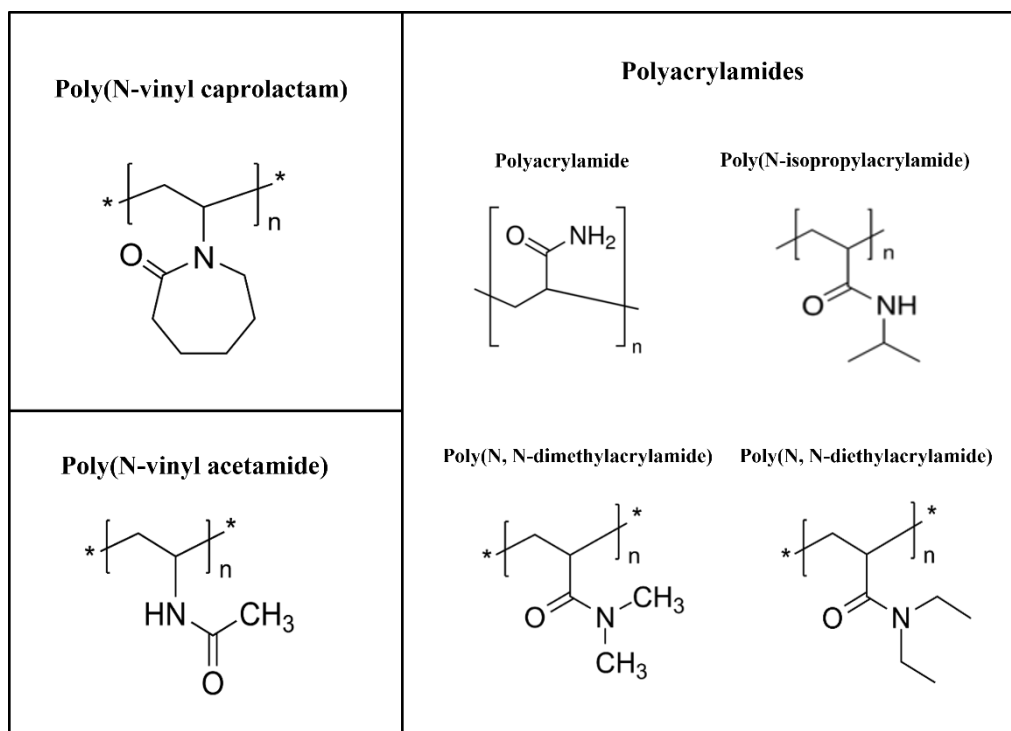


Figure 9. Amide-containing water-soluble polymers which have not yet been studied in solid dispersions.

4. Conclusions

Intermolecular interactions, in particular hydrogen bonding, in solid dispersions using amide-containing nonionic water-soluble polymers as carriers are key factors highly influencing drug crystallinity, stability and dissolution rate following oral administration. Many of the amide-containing nonionic water-soluble carriers such as PVP, PVP/VA and Soluplus that can be applied are already extensively studied as excipients. The possibility of exploring other amide-containing nonionic water-soluble carriers such as poly(N-vinyl acetamide) and polyacrylamide to produce an optimized product further extends the range of possibilities for formulation.

References

- [1] S. Janssens, G. Van den Mooter, Review: physical chemistry of solid dispersions, *J. Pharm. Pharmacol.*, 61 (2009) 1571-1586.
- [2] D. Jelic, Thermal Stability of Amorphous Solid Dispersions, *Molecules*, 26 (2021).
- [3] G.V.d. Mooter., The use of amorphous solid dispersions: A formulation strategy to overcome poor solubility and dissolution rate, *Drug discovery today. Technologies*, 9 (2012) e71-e174.
- [4] C. Leuner, J. Dressman, Improving drug solubility for oral delivery using solid dispersions., *Eur J Pharm Biopharm.*, 50 (2000) 47-60.
- [5] G. Verreck, K. Six, G. Van den Mooter, L. Baert, J. Peeters, M.E. Brewster, Characterization of solid dispersions of itraconazole and hydroxypropylmethylcellulose prepared by melt extrusion-Part I., *Int J Pharm.*, 251 (2003) 165-174.

- [6] H. Valizadeh, P. Zakeri-Milani, M. Barzegar-Jalali, G. Mohammadi, M.A. Danesh-Bahreini, K. Adibkia, A. Nokhodchi, Preparation and characterization of solid dispersions of piroxicam with hydrophilic carriers, *Drug Dev. Ind. Pharm.*, 33 (2007) 45-56.
- [7] J. Knapik-Kowalczyk, K. Chmiel, J. Pacult, K. Bialek, L. Tajber, M. Paluch, Enhancement of the Physical Stability of Amorphous Sildenafil in a Binary Mixture, with either a Plasticizing or Antiplasticizing Compound, *Pharmaceutics*, 12 (2020).
- [8] H. Al-Obaidi, S. Brocchini, G. Buckton, Anomalous properties of spray dried solid dispersions, *J Pharm Sci*, 98 (2009) 4724-4737.
- [9] T.T.D. Tran, P.H.L. Tran, Molecular Interactions in Solid Dispersions of Poorly Water-Soluble Drugs, *Pharmaceutics*, 12 (2020).
- [10] H. Al-Obaidi, G. Buckton, Evaluation of griseofulvin binary and ternary solid dispersions with HPMCAS, *AAPS PharmSciTech*, 10 (2009) 1172-1177.
- [11] H. Al-Obaidi, M.J. Lawrence, S. Shah, H. Moghul, N. Al-Saden, F. Bari, Effect of drug-polymer interactions on the aqueous solubility of milled solid dispersions, *Int. J. Pharm.*, 446 (2013) 100-105.
- [12] J. Guan, L. Jin, Q. Liu, H. Xu, H. Wu, X. Zhang, S. Mao, Exploration of supersaturable lacidipine ternary amorphous solid dispersion for enhanced dissolution and in vivo absorption, *Eur. J. Pharm. Sci.*, 139 (2019) 105043.
- [13] S. Sarabu, V.R. Kallakunta, S. Bandari, A. Batra, V. Bi, T. Durig, F. Zhang, M.A. Repka, Hypromellose acetate succinate based amorphous solid dispersions via hot melt extrusion: Effect of drug physicochemical properties, *Carbohydr. Polym.*, 233 (2020) 115828.
- [14] B. Tian, X. Ju, D. Yang, Y. Kong, X. Tang, Effect of the third component on the aging and crystallization of cinnarizine-soluplus(R) binary solid dispersion, *Int. J. Pharm.*, 580 (2020) 119240.

- [15] Y. Tian, E. Jacobs, D.S. Jones, C.P. McCoy, H. Wu, G.P. Andrews, The design and development of high drug loading amorphous solid dispersion for hot-melt extrusion platform, *Int. J. Pharm.*, 586 (2020) 119545.
- [16] R.C. Rowe, P.J. Sheskey, M.E. Quinn, *Handbook of pharmaceutical excipients*. Sixth Edition, London and Chicago: Pharmaceutical Press, (2009).
- [17] C.F. Rawlinson, A.C. Williams, P. Timmins, I. Grimsey, Polymer-mediated disruption of drug crystallinity, *Int. J. Pharm.*, 336 (2007) 42-48.
- [18] A.C. Williams, P. Timmins, M. Lu, R.T. Forbes, Disorder and dissolution enhancement: deposition of ibuprofen on to insoluble polymers, *Eur. J. Pharm. Sci.*, 26 (2005) 288-294.
- [19] V. Bühler., *Polyvinylpyrrolidone-excipients for pharmaceuticals*, Springer, (2005).
- [20] C.S. Yee., *The Development of PVP-based Solid Dispersions using Hot Melt Extrusion for the Preparation of Immediate Release Formulations*, Doctoral thesis, University of East Anglia, (2013).
- [21] A.S. Alam., E.L. Parrott., Effect of adjuvants on tackiness of polyvinylpyrrolidone film coating, *J. Pharm. Sci.*, 61 (1972) 265-268.
- [22] M.J. Kim, J.H. Lee, H. Yoon, S.J. Kim, D.Y. Jeon, J.E. Jang, D. Lee, G. Khang, Preparation, characterization and in vitro dissolution of aceclofenac-loaded PVP solid dispersions prepared by spray drying or rotary evaporation method, *J. Pharm. Investig.*, 43 (2013) 107-113.
- [23] C. Bothiraja, M.B. Shinde, S. Rajalakshmi, A.P. Pawar, Evaluation of molecular pharmaceutical and in-vivo properties of spray-dried isolated andrographolide-PVP, *J. Pharm. Pharmacol.*, 61 (2009) 1465-1472.
- [24] J. Szafraniec, A. Antosik, J. Knapik-Kowalczyk, K. Gawlak, M. Kurek, J. Szlek, W. Jamroz, M. Paluch, R. Jachowicz, Molecular Disorder of Bicalutamide-

Amorphous Solid Dispersions Obtained by Solvent Methods, *Pharmaceutics*, 10 (2018).

[25] S. Sethia, E. Squillante, Solid dispersion of carbamazepine in PVP K30 by conventional solvent evaporation and supercritical methods, *Int. J. Pharm.*, 272 (2004) 1-10.

[26] P. Desai, Y. Pore, Physicochemical characterization of spray dried cefixime polymeric nanoparticles using factorial design approach, *J. Appl. Pharm. Sci.*, (2016) 124-132.

[27] L.D. Alves, M.F. de La Roca Soares, C.T. de Albuquerque, E.R. da Silva, A.C. Vieira, D.A. Fontes, C.B. Figueiredo, J.L. Soares Sobrinho, P.J. Rolim Neto, Solid dispersion of efavirenz in PVP K-30 by conventional solvent and kneading methods, *Carbohydr. Polym.*, 104 (2014) 166-174.

[28] L. Fitriani., M. Fadhila., E. Zaini., Preparation of Efavirenz - PVP K-30 Solid Dispersion by Spray Drying Technique, *Res. J. Pharm. Biol. Chem. Sci.*, 6 (2015) 925-930.

[29] L. Martinez-Marcos, D.A. Lamprou, R.T. McBurney, G.W. Halbert, A novel hot-melt extrusion formulation of albendazole for increasing dissolution properties, *Int. J. Pharm.*, 499 (2016) 175-185.

[30] G.P. Andrews, O.A. AbuDiak, D.S. Jones, Physicochemical characterization of hot melt extruded bicalutamide-polyvinylpyrrolidone solid dispersions, *J Pharm Sci*, 99 (2010) 1322-1335.

[31] A. Forster., J. Hempenstall., T. Rades., Characterization of glass solutions of poorly watersoluble drugs produced by melt extrusion with hydrophilic amorphous polymers, *J. Pharm. Pharmacol.*, 53 (2001) 303-315.

[32] M.F. Pina, M. Zhao, J.F. Pinto, J.J. Sousa, D.Q. Craig, The influence of drug physical state on the dissolution enhancement of solid dispersions prepared via hot-

melt extrusion: a case study using olanzapine, *J Pharm Sci*, 103 (2014) 1214-1223.

[33] H. Nogami, T. Nagai, A. Kondo, Dissolution Kinetics of Polyvinylpyrrolidone of Various Molecular Weights., *Chem. Pharm. Bull.*, 18 (1970) 2290-2296.

[34] A.R. Nair, Y.D. Lakshman, V.S.K. Anand, K.S.N. Sree, K. Bhat, S.J. Dengale, Overview of Extensively Employed Polymeric Carriers in Solid Dispersion Technology, *AAPS PharmSciTech*, 21 (2020) 309.

[35] H. Sekizaki, K. Danjo, H. Eguchi, Y. Yonezawa, H. Sunada, A. Otsuka, Solid-State Interaction of Ibuprofen with Polyvinylpyrrolidone., *Chem. Pharm. Bull.*, 43 (1995) 988-993.

[36] X. Shan, A.C. Williams, V.V. Khutoryanskiy, Polymer structure and property effects on solid dispersions with haloperidol: Poly(N-vinyl pyrrolidone) and poly(2-oxazolines) studies, *Int. J. Pharm.*, 590 (2020) 119884.

[37] F.I. Kanaze, E. Kokkalou, I. Niopas, M. Georgarakis, A. Stergiou, D. Bikiaris, Dissolution enhancement of flavonoids by solid dispersion in PVP and PEG matrixes: A comparative study, *J. Appl. Polym. Sci.*, 102 (2006) 460-471.

[38] J. Li, N. Fan, C. Li, J. Wang, S. Li, Z. He, The tracking of interfacial interaction of amorphous solid dispersions formed by water-soluble polymer and nitrendipine, *Appl. Surf. Sci.*, 420 (2017) 136-144.

[39] E. Karavas, G. Ktistis, A. Xenakis, E. Georgarakis, Effect of hydrogen bonding interactions on the release mechanism of felodipine from nanodispersions with polyvinylpyrrolidone, *Eur. J. Pharm. Biopharm*, 63 (2006) 103-114.

[40] S.W. Jun, M.-S. Kim, G.H. Jo, S. Lee, J.S. Woo, J.-S. Park, S.-J. Hwang, Cefuroxime axetil solid dispersions prepared using solution enhanced dispersion by supercritical fluids, *J. Pharm. Pharmacol.*, 57 (2005) 1529-1537.

[41] M.M. Ghobashy, D.M. Alshangiti, S.A. Alkhursani, S.A. Al-Gahtany, F.S. Shokr, M. Madani, Improvement of In Vitro Dissolution of the Poor Water-Soluble

Amlodipine Drug by Solid Dispersion with Irradiated Polyvinylpyrrolidone, ACS omega, 5 (2020) 21476-21487.

[42] F.L. Guedes, B.G. de Oliveira, M.Z. Hernandez, C.A. De Simone, F.J. Veiga, C. de Lima Mdo, I.R. Pitta, S.L. Galdino, P.J. Neto, Solid dispersions of imidazolidinedione by PEG and PVP polymers with potential antischistosomal activities, AAPS PharmSciTech, 12 (2011) 401-410.

[43] R.M. Obaidat, B. AlTaani, A. Ailabouni, Effect of different polymeric dispersions on In-vitro dissolution rate and stability of celecoxib class II drug, J. Polym. Res., 24 (2017).

[44] M. Kakran, N.G. Sahoo, Y.W. Tan, L. Li, Ternary dispersions to enhance solubility of poorly water soluble antioxidants, Colloids Surf, A Physicochem Eng Asp, 433 (2013) 111-121.

[45] A.C.F. Rumondor., Patrick J. Marsac, Lindsay A. Stanford, L.S. Taylor., Phase Behavior of Poly(vinylpyrrolidone) Containing Amorphous Solid Dispersions in the Presence of Moisture, Mol. Pharm., 6 (2009) 1492-1505.

[46] R. Kalaiselvan., G.P. Mohanta., P.K. Manna., R. Manavalan., Inhibition of albendazole crystallization in poly(vinylpyrrolidone) solid molecular dispersions, Pharmazie, 61 (2006) 618-624.

[47] C.C. Yen, Y.K. Liang, C.P. Cheng, M.C. Hsu, Y.T. Wu, Oral Bioavailability Enhancement and Anti-Fatigue Assessment of the Andrographolide Loaded Solid Dispersion, Int. J. Mol. Sci., 21 (2020).

[48] A. Jahangiri, M. Barzegar-Jalali, Y. Javadzadeh, H. Hamishehkar, K. Adibkia, Physicochemical characterization of atorvastatin calcium/ezetimibe amorphous nano-solid dispersions prepared by electrospraying method, Artif. Cells Nanomed. Biotechnol., 45 (2017) 1-8.

[49] F. Ren, Q. Jing, Y. Tang, Y. Shen, J. Chen, F. Gao, J. Cui, Characteristics of

bicalutamide solid dispersions and improvement of the dissolution, *Drug Dev. Ind. Pharm.*, 32 (2006) 967-972.

[50] M. Tobbyn, J. Brown, A.B. Dennis, M. Fakes, Q. Gao, J. Gamble, Y.Z. Khimyak, G. McGeorge, C. Patel, W. Sinclair, P. Timmins, S. Yin, Amorphous drug-PVP dispersions: application of theoretical, thermal and spectroscopic analytical techniques to the study of a molecule with intermolecular bonds in both the crystalline and pure amorphous state, *J Pharm Sci*, 98 (2009) 3456-3468.

[51] H. Chen, Y. Pui, C. Liu, Z. Chen, C.-C. Su, M. Hageman, M. Hussain, R. Haskell, K. Stefanski, K. Foster, O. Gudmundsson, F. Qian, Moisture-Induced Amorphous Phase Separation of Amorphous Solid Dispersions: Molecular Mechanism, Microstructure, and Its Impact on Dissolution Performance, *J. Pharm. Sci.*, 107 (2018) 317-326.

[52] W. Cong, L. Shen, D. Xu, L. Zhao, K. Ruan, Y. Feng, Solid dispersion tablets of breviscapine with polyvinylpyrrolidone K30 for improved dissolution and bioavailability to commercial breviscapine tablets in beagle dogs, *Eur. J. Drug Metab. Pharmacokinet.*, 39 (2014) 203-210.

[53] A. Sharma., C.P. Jain., Preparation and characterization of solid dispersions of carvedilol with PVP K30, *Res. Pharm. Sci*, 5 (2010) 49-56.

[54] K. Regulska, M. Regulski, A. Wzgarda, A. Kotowska, A. Ignasiak, B. Cwiertnia, B. Stanisiz, Does Polyvinylpyrrolidone Improve the Chemical Stability of Cilazapril in Solid State?, *Iran. J. Pharm. Res*, 18 (2019) 579-595.

[55] A.S. Narang, A.K. Srivastava, Evaluation of solid dispersions of Clofazimine, *Drug Dev. Ind. Pharm.*, 28 (2002) 1001-1013.

[56] A.C. Rumondor, H. Wikstrom, B. Van Eerdenbrugh, L.S. Taylor, Understanding the tendency of amorphous solid dispersions to undergo amorphous-amorphous phase separation in the presence of absorbed moisture, *AAPS PharmSciTech*, 12 (2011) 1209-1219.

- [57] Y. He, H. Liu, W. Bian, Y. Liu, X. Liu, S. Ma, X. Zheng, Z. Du, K. Zhang, D. Ouyang, Molecular Interactions for the Curcumin-Polymer Complex with Enhanced Anti-Inflammatory Effects, *Pharmaceutics*, 11 (2019).
- [58] L.L. Chaves, A.C. Vieira, D. Ferreira, B. Sarmiento, S. Reis, Rational and precise development of amorphous polymeric systems with dapsona by response surface methodology, *Int. J. Biol. Macromol.*, 81 (2015) 662-671.
- [59] A. Farmoudeh, A. Rezaeirosan, M. Abbaspour, A. Nokhodchi, P. Ebrahimnejad, Solid Dispersion Pellets: An Efficient Pharmaceutical Approach to Enrich the Solubility and Dissolution Rate of Deferasirox, *Biomed Res. Int.*, 2020 (2020) 8583540.
- [60] M.C. Martı́nez-Oha'rriz, C. Rodrı́guez-Espinosa, C. Martı́n, M.M.G. i, M.C. Tros-Ilduya, M. Sa'nchez, Solid Dispersions of Diflunisal - PVP: Polymorphic and Amorphous States of the Drug, *Drug Dev. Ind. Pharm.*, 28 (2002) 717-725.
- [61] M.T. Ansari, V.B. Sunderland, Solid dispersions of dihydroartemisinin in polyvinylpyrrolidone, *Arch. Pharm. Res.*, 31 (2008) 390-398.
- [62] S. Chen, J. Zhu, F. Ma, Q. Fang, Y. Li, Preparation and characterization of solid dispersions of dipyridamole with a carrier "copolyvidonum Plasdone S-630", *Drug Dev. Ind. Pharm.*, 33 (2007) 888-899.
- [63] A. Jahangiri, M. Barzegar-Jalali, A. Garjani, Y. Javadzadeh, H. Hamishehkar, M. Rameshrad, K. Adibkia, Physicochemical characterization and pharmacological evaluation of ezetimibe-PVP K30 solid dispersions in hyperlipidemic rats, *Colloids Surf. B*, 134 (2015) 423-430.
- [64] A. Kini, S.B. Patel, Phase behavior, intermolecular interaction, and solid state characterization of amorphous solid dispersion of Febuxostat, *Pharm Dev Technol.*, 22 (2017) 45-57.
- [65] D. Bikiaris, G.Z. Papageorgiou, A. Stergiou, E. Pavlidou, E. Karavas, F.

Kanaze, M. Georgarakis, Physicochemical studies on solid dispersions of poorly water-soluble drugs, *Thermochim. Acta*, 439 (2005) 58-67.

[66] H. Konno, L.S. Taylor, Influence of different polymers on the crystallization tendency of molecularly dispersed amorphous felodipine, *J Pharm Sci*, 95 (2006) 2692-2705.

[67] A.C. Rumondor, I. Ivanisevic, S. Bates, D.E. Alonzo, L.S. Taylor, Evaluation of drug-polymer miscibility in amorphous solid dispersion systems, *Pharm. Res.*, 26 (2009) 2523-2534.

[68] K. Suknuntha, D. S. Jones, V. Tantishaiyakul, Properties of felodipine-poly(vinylpyrrolidone) solid dispersion films and the impact of solvents, *Sci.*, 38 (2012) 188.

[69] S.S. S., P.M. V., A.S. S., D. Ji., A. Pranit., Solid Dispersions of Poorly Water Soluble Drug Using Spray Drying Technique, *Int. J. Drug Deliv.*, 5 (2013) 323-330.

[70] A. Trivino, A. Gumireddy, F. Meng, D. Prasad, H. Chauhan, Drug-polymer miscibility, interactions, and precipitation inhibition studies for the development of amorphous solid dispersions for the poorly soluble anticancer drug flutamide, *Drug Dev. Ind. Pharm.*, 45 (2019) 1277-1291.

[71] C. Doherty., P. York., Evidence for Solid- and Liquid-State Interactions in a Furosemide-Polyvinylpyrrolidone Solid Dispersion, *J. Pharm. Sci.*, 76 (1987) 731-737.

[72] S. Biswal, J. Sahoo, P.N. Murthy, Physicochemical properties of solid dispersions of gliclazide in polyvinylpyrrolidone K90, *AAPS PharmSciTech*, 10 (2009) 329-334.

[73] A. Mehramizi, B. Alijani, M. Pourfarzib, F.A. Dorkoosh, M. Rafiee -Tehrani, Solid carriers for improved solubility of glipizide in osmotically controlled oral drug delivery system, *Drug Dev. Ind. Pharm.*, 33 (2007) 812-823.

- [74] H. Saluja, A. Mehanna, R. Panicucci, E. Atef, Hydrogen Bonding: Between Strengthening the Crystal Packing and Improving Solubility of Three Haloperidol Derivatives, *Molecules*, 21 (2016).
- [75] R. Dontireddy, A.M. Crean, A comparative study of spray-dried and freeze-dried hydrocortisone/polyvinyl pyrrolidone solid dispersions, *Drug Dev. Ind. Pharm.*, 37 (2011) 1141-1149.
- [76] S. Bogdanova, I. Pajeva, P. Nikolova, I. Tsakovska, B. Muller, Interactions of poly(vinylpyrrolidone) with ibuprofen and naproxen: experimental and modeling studies, *Pharm. Res.*, 22 (2005) 806-815.
- [77] N.M. Najib., M. Suleiman., A. Malakh., Characteristics of the in vitro release of ibuprofen from polyvinylpyrrolidone solid dispersions, *Int. J. Pharm.*, 32 (1986) 229-236.
- [78] T.X. Xiang, B.D. Anderson, Effects of Molecular Interactions on Miscibility and Mobility of Ibuprofen in Amorphous Solid Dispersions With Various Polymers, *J Pharm Sci*, 108 (2019) 178-186.
- [79] E. Khodaverdi., N. Khalili., F. Zangiabadi., A. Homayouni., Preparation, characterization and stability studies of glassy solid dispersions of indomethacin using PVP and isomalt as carriers, *Iran. J. Basic Med. Sci.*, 15 (2012) 820-832.
- [80] M.M. Knopp, N.E. Olesen, P. Holm, P. Langguth, R. Holm, T. Rades, Influence of Polymer Molecular Weight on Drug-Polymer Solubility: A Comparison between Experimentally Determined Solubility in PVP and Prediction Derived from Solubility in Monomer, *J Pharm Sci*, 104 (2015) 2905-2912.
- [81] H. Ueda, S. Aikawa, Y. Kashima, J. Kikuchi, Y. Ida, T. Tanino, K. Kadota, Y. Tozuka, Anti-plasticizing effect of amorphous indomethacin induced by specific intermolecular interactions with PVA copolymer, *J Pharm Sci*, 103 (2014) 2829-2838.

- [82] P. Mistry, S. Mohapatra, T. Gopinath, F.G. Vogt, R. Suryanarayanan, Role of the Strength of Drug-Polymer Interactions on the Molecular Mobility and Crystallization Inhibition in Ketoconazole Solid Dispersions, *Mol Pharm*, 12 (2015) 3339-3350.
- [83] E. Browne, Z.A. Worku, A.M. Healy, Physicochemical Properties of Poly-Vinyl Polymers and Their Influence on Ketoprofen Amorphous Solid Dispersion Performance: A Polymer Selection Case Study, *Pharmaceutics*, 12 (2020).
- [84] A. Mukharya, S. Chaudhary, N. Mansuri, A.K. Misra, Solid-state characterization of lacidipine/PVP K(29/32) solid dispersion primed by solvent co-evaporation, *Int. J. Pharm. Investig.*, 2 (2012) 90-96.
- [85] M. Yu, L. Sun, W. Li, Z. Lan, B. Li, L. Tan, M. Li, X. Yang, Investigation of structure and dissolution properties of a solid dispersion of lansoprazole in polyvinylpyrrolidone, *J. Mol. Struct.*, 1005 (2011) 70-77.
- [86] X. Zhang, N. Sun, B. Wu, Y. Lu, T. Guan, W. Wu, Physical characterization of lansoprazole/PVP solid dispersion prepared by fluid-bed coating technique, *Powder Technol.*, 182 (2008) 480-485.
- [87] R.P. Patel, M.M. Patel, Physicochemical characterization and dissolution study of solid dispersions of Lovastatin with polyethylene glycol 4000 and polyvinylpyrrolidone K30, *Pharm Dev Technol.*, 12 (2007) 21-33.
- [88] B.R. Sharannavar., A.P. Gadad., Physicochemical characterization and dissolution study of spray dried amorphous Lovastatin with Polyvinylpyrrolidone K30, *J. Pharm. Innov.*, 7 (2018) 498-502.
- [89] N. Kang, J. Lee, J.N. Choi, C. Mao, E.H. Lee, Cryomilling-induced solid dispersion of poor glass forming/poorly water-soluble mefenamic acid with polyvinylpyrrolidone K12, *Drug Dev. Ind. Pharm.*, 41 (2015) 978-988.
- [90] S. Mallick., A. Sahu., K. Pal., Dissolution behavior of nalidixic acid solid

dispersions using water soluble dispersion carriers, *Acta Pol Pharm.*, 61 (2004) 21-30.

[91] Z. Ayenew, A. Paudel, G. Van den Mooter, Can compression induce demixing in amorphous solid dispersions? A case study of naproxen-PVP K25, *Eur. J. Pharm. Biopharm.*, 81 (2012) 207-213.

[92] R. Nair., N. Nyamweya., S. Goñen., L.J. Martí'nez-Miranda., S.W. Hoag., Influence of various drugs on the glass transition temperature of poly(vinylpyrrolidone): a thermodynamic and spectroscopic investigation, *Int. J. Pharm.*, 225 (2001) 83-96.

[93] Y. Aso, S. Yoshioka, Molecular mobility of nifedipine-PVP and phenobarbital-PVP solid dispersions as measured by ¹³C-NMR spin-lattice relaxation time, *J Pharm Sci*, 95 (2006) 318-325.

[94] K. Kothari, V. Ragoonanan, R. Suryanarayanan, The role of drug-polymer hydrogen bonding interactions on the molecular mobility and physical stability of nifedipine solid dispersions, *Mol Pharm*, 12 (2015) 162-170.

[95] Z. Sun, H. Zhang, H. He, L. Sun, X. Zhang, Q. Wang, K. Li, Z. He, Cooperative effect of polyvinylpyrrolidone and HPMC E5 on dissolution and bioavailability of nimodipine solid dispersions and tablets, *Asian J. Pharm. Sci.*, 14 (2019) 668-676.

[96] R.B. Chavan, A. Lodagekar, B. Yadav, N.R. Shastri, Amorphous solid dispersion of nisoldipine by solvent evaporation technique: preparation, characterization, in vitro, in vivo evaluation, and scale up feasibility study, *Drug Deliv. Transl. Res.*, 10 (2020) 903-918.

[97] F.u. Hassnain., S. Bashir., M. Asad., I. Nazir., S. Qamar., M. Imran., H.M.M. Asjad., Formulation and characterization of solid dispersion of Nisoldipine by solvent evaporation method, *Journal of Pharmacy and Alternative Medicine*, 2 (2012) 21-28.

- [98] M. Paisana, M. Wahl, J. Pinto, Role of Polymeric Excipients in the Stabilization of Olanzapine when Exposed to Aqueous Environments, *Molecules*, 20 (2015) 22364-22382.
- [99] V. Majerik., G. Horvath., G. Charbit., E. Badens., L. Szokonya., N. Bosc., E. Teillaud., Solid dispersions of oxeglitazar in PVP K17 and poloxamer 407 by supercritical antisolvent and coevaporation methods, *Hung. j. ind. chem.*, 34 (2006) 41-49.
- [100] K. Lehmkemper, S.O. Kyeremateng, O. Heinzerling, M. Degenhardt, G. Sadowski, Long-Term Physical Stability of PVP- and PVPVA-Amorphous Solid Dispersions, *Mol Pharm*, 14 (2017) 157-171.
- [101] L.S. Usmanova, M.A. Ziganshin, I.T. Rakipov, N.M. Lyadov, A.E. Klimovitskii, T.A. Mukhametzyanov, A.V. Gerasimov, Microspherical Particles of Solid Dispersion of Polyvinylpyrrolidone K29-32 for Inhalation Administration, *Biomed Res. Int.*, 2018 (2018) 2412156.
- [102] V. Tantishaiyakul., N. Kaewnopparat., S. Ingkatawornwong., Properties of solid dispersions of piroxicam in polyvinylpyrrolidone, *Int. J. Pharm.*, 181 (1999) 143-151.
- [103] K. Wu, J. Li, W. Wang, D.A. Winstead, Formation and characterization of solid dispersions of piroxicam and polyvinylpyrrolidone using spray drying and precipitation with compressed antisolvent, *J Pharm Sci*, 98 (2009) 2422-2431.
- [104] A.R. de Mello Costa, F.S. Marquiáfavel, M.M. de Oliveira Lima Leite Vaz, B.A. Rocha, P.C. Pires Bueno, P.L.M. Amaral, H. da Silva Barud, A.A. Berreta-Silva, Quercetin-PVP K25 solid dispersions, *J. Therm. Anal. Calorim.*, 104 (2010) 273-278.
- [105] T.H. Tran, B.K. Poudel, N. Marasini, J.S. Woo, H.G. Choi, C.S. Yong, J.O. Kim, Development of raloxifene-solid dispersion with improved oral bioavailability via spray-drying technique, *Arch. Pharm. Res.*, 36 (2013) 86-93.

- [106] B. Wang, D. Wang, S. Zhao, X. Huang, J. Zhang, Y. Lv, X. Liu, G. Lv, X. Ma, Evaluate the ability of PVP to inhibit crystallization of amorphous solid dispersions by density functional theory and experimental verify, *Eur. J. Pharm. Sci.*, 96 (2017) 45-52.
- [107] G.A. Ilevbare, H. Liu, K.J. Edgar, L.S. Taylor, Understanding Polymer Properties Important for Crystal Growth Inhibition—Impact of Chemically Diverse Polymers on Solution Crystal Growth of Ritonavir, *Cryst. Growth Des.*, 12 (2012) 3133-3143.
- [108] A.A. Ambike, K.R. Mahadik, A. Paradkar, Spray-dried amorphous solid dispersions of simvastatin, a low tg drug: in vitro and in vivo evaluations, *Pharm. Res.*, 22 (2005) 990-998.
- [109] M. Rao., Y. Mandage., I. Khole., G. Munjapara., Characterization of Solid Dispersions of Simvastatin with PVP K30 and Poloxamer 188, *Ind J Pharm Edu Res*, 45 (2011) 145-152.
- [110] V. Caron, Y. Hu, L. Tajber, A. Erxleben, O.I. Corrigan, P. McArdle, A.M. Healy, Amorphous solid dispersions of sulfonamide/Soluplus(R) and sulfonamide/PVP prepared by ball milling, *AAPS PharmSciTech*, 14 (2013) 464-474.
- [111] H. Sekikawa., M. Nakano., T. Arita., Inhibitory effect of polyvinylpyrrolidone on the crystallization of drugs, *Chem. Pharm. Bull.*, 26 (1978) 118-126.
- [112] G. Pravin., V.S. Singh., J. Shubham., G. Amol., Solubility Enhancement of Sulfamethoxazole by Solid Dispersion using Spray Dryer Technique, *J. drug deliv. ther.*, 9 (2019) 76-79.
- [113] K. Wlodarski, W. Sawicki, K. Haber, J. Knapik, Z. Wojnarowska, M. Paluch, P. Lepek, L. Hawelek, L. Tajber, Physicochemical properties of tadalafil solid dispersions - Impact of polymer on the apparent solubility and dissolution rate of tadalafil, *Eur. J. Pharm. Biopharm*, 94 (2015) 106-115.

- [114] G.V.d. Mooter., P. Augustijns., N. Blaton., R. Kinget., Physico-chemical characterization of solid dispersions of temazepam with polyethylene glycol 6000 and PVP K30, *Int. J. Pharm.*, 164 (1998) 67-80.
- [115] S. Papadimitriou, D. Bikiaris, Dissolution rate enhancement of the poorly water-soluble drug Tibolone using PVP, SiO₂, and their nanocomposites as appropriate drug carriers, *Drug Dev. Ind. Pharm.*, 35 (2009) 1128-1138.
- [116] P. Thybo, J. Kristensen, L. Hovgaard, Characterization and physical stability of tolfenamic acid-PVP K30 solid dispersions, *Pharm Dev Technol.*, 12 (2007) 43-53.
- [117] F. Damian., N. Blaton., H. Desseyn., K. Clou., P. Augustijns., L. Naesens., J. Balzarini., R. Kinget., G.V.d. Mooter., Solid state properties of pure UC-781 and solid dispersions with polyvinylpyrrolidone (PVP K30), *J. Pharm. Pharmacol.*, 53 (2001) 1109-1116.
- [118] W.-J. Xu., Y. Liu., L.-L. Shi., J.-H. Cui., Q.-R. Cao., In vitro dissolution and physicochemical characterizations of novel PVP-based solid dispersions containing valsartan prepared by a freeze-drying method, *Pak. J. Pharm. Sci.*, 27 (2014) 1799-1804.
- [119] B. V., Polyvinylpyrrolidone excipients for pharmaceuticals: povidone, crospovidone and copovidone. 1st edition., Berlin: Springer-Verlag Berlin Heidelberg, (2005).
- [120] M.B. Rask, M.M. Knopp, N.E. Olesen, R. Holm, T. Rades, Influence of PVP/VA copolymer composition on drug-polymer solubility, *Eur. J. Pharm. Sci.*, 85 (2016) 10-17.
- [121] L.S. Taylor, F.W. Langkilde, G. Zografi, Fourier transform Raman spectroscopic study of the interaction of water vapor with amorphous polymers, *J Pharm Sci*, 90 (2001) 888-901.

- [122] A. Prudic, T. Kleetz, M. Korf, Y. Ji, G. Sadowski, Influence of copolymer composition on the phase behavior of solid dispersions, *Mol Pharm*, 11 (2014) 4189-4198.
- [123] R. Kalaiselvan, G.P. Mohanta, P.K. Manna, R. Manavalan, Inhibition of albendazole crystallization in poly(vinylpyrrolidone) solid molecular dispersions, *Pharmazie*, 61 (2006) 618-624.
- [124] S.-Y. Chan, Y.-Y. Chung, X.-Z. Cheah, E.Y.-L. Tan, J. Quah, The characterization and dissolution performances of spray dried solid dispersion of ketoprofen in hydrophilic carriers, *Asian J. Pharm. Sci.*, 10 (2015) 372-385.
- [125] Y. Sun, J. Tao, G.G. Zhang, L. Yu, Solubilities of crystalline drugs in polymers: an improved analytical method and comparison of solubilities of indomethacin and nifedipine in PVP, PVP/VA, and PVAc, *J Pharm Sci*, 99 (2010) 4023-4031.
- [126] P. Panini, M. Rampazzo, A. Singh, F. Vanhoutte, G. Van den Mooter, Myth or Truth: The Glass Forming Ability Class III Drugs Will Always Form Single-Phase Homogenous Amorphous Solid Dispersion Formulations, *Pharmaceutics*, 11 (2019).
- [127] A.C.F. Rumondor., L.S. Taylor., Effect of Polymer Hygroscopicity on the Phase Behavior of Amorphous Solid Dispersions in the Presence of Moisture, *Mol. Pharm.*, 7 (2009).
- [128] L. Dong, Y. Mai, Q. Liu, W. Zhang, J. Yang, Mechanism and Improved Dissolution of Glycyrrhetic Acid Solid Dispersion by Alkalizers, *Pharmaceutics*, 12 (2020).
- [129] B. Song., J. Wang., S.-J. Lu., L.-N. Shan., Andrographolide solid dispersions formulated by Soluplus to enhance interface wetting, dissolution, and absorption, *J. Appl. Polym. Sci.*, 48354 (2019).
- [130] M.K. Riekes, A. Engelen, B. Appeltans, P. Rombaut, H.K. Stulzer, G. Van den Mooter, New Perspectives for Fixed Dose Combinations of Poorly Water-Soluble

Compounds: a Case Study with Ezetimibe and Lovastatin, *Pharm. Res.*, 33 (2016) 1259-1275.

[131] Y. Chen, C. Liu, Z. Chen, C. Su, M. Hageman, M. Hussain, R. Haskell, K. Stefanski, F. Qian, Drug-polymer-water interaction and its implication for the dissolution performance of amorphous solid dispersions, *Mol Pharm*, 12 (2015) 576-589.

[132] M. Alshafiee, M.K. Aljammal, D. Markl, A. Ward, K. Walton, L. Blunt, S. Korde, S.K. Pagire, A.L. Kelly, A. Paradkar, B.R. Conway, K. Asare-Addo, Hot-melt extrusion process impact on polymer choice of glyburide solid dispersions: The effect of wettability and dissolution, *Int. J. Pharm.*, 559 (2019) 245-254.

[133] C. Que, X. Lou, D.Y. Zemlyanov, H. Mo, A.S. Indulkar, Y. Gao, G.G.Z. Zhang, L.S. Taylor, Insights into the Dissolution Behavior of Ledipasvir-Copovidone Amorphous Solid Dispersions: Role of Drug Loading and Intermolecular Interactions, *Mol Pharm*, 16 (2019) 5054-5067.

[134] P. Zi, C. Zhang, C. Ju, Z. Su, Y. Bao, J. Gao, J. Sun, J. Lu, C. Zhang, Solubility and bioavailability enhancement study of lopinavir solid dispersion matrixed with a polymeric surfactant - Soluplus, *Eur. J. Pharm. Sci.*, 134 (2019) 233-245.

[135] X. Zheng, R. Yang, X. Tang, L. Zheng, Part I: characterization of solid dispersions of nimodipine prepared by hot-melt extrusion, *Drug Dev. Ind. Pharm.*, 33 (2007) 791-802.

[136] N. Gao, M. Guo, Q. Fu, Z. He, Application of hot melt extrusion to enhance the dissolution and oral bioavailability of oleanolic acid, *Asian J. Pharm. Sci.*, 12 (2017) 66-72.

[137] C.S. Yee, The Development of PVP-based Solid Dispersions using Hot Melt Extrusion for the Preparation of Immediate Release Formulations, PhD thesis, (2013).

- [138] M. Palanisamy, J. Khanam, Solid dispersion of prednisolone: solid state characterization and improvement of dissolution profile, *Drug Dev. Ind. Pharm.*, 37 (2011) 373-386.
- [139] R. Tanaka, Y. Hattori, Y. Horie, H. Kamada, T. Nagato, M. Otsuka, Characterization of Amorphous Solid Dispersion of Pharmaceutical Compound with pH-Dependent Solubility Prepared by Continuous-Spray Granulator, *Pharmaceutics*, 11 (2019).
- [140] H.S. Purohit, L.S. Taylor, Phase Behavior of Ritonavir Amorphous Solid Dispersions during Hydration and Dissolution, *Pharm. Res.*, 34 (2017) 2842-2861.
- [141] K. Wlodarski, W. Sawicki, A. Kozyra, L. Tajber, Physical stability of solid dispersions with respect to thermodynamic solubility of tadalafil in PVP-VA, *Eur. J. Pharm. Biopharm.*, 96 (2015) 237-246.
- [142] J.F. Alopaeus, E. Hagesaether, I. Tho, Micellisation Mechanism and Behaviour of Soluplus(R)(-)Furosemide Micelles: Preformulation Studies of an Oral Nanocarrier-Based System, *Pharmaceutics*, 12 (2019).
- [143] E.S. Bochmann, D. Neumann, A. Gryczke, K.G. Wagner, Micro-scale prediction method for API-solubility in polymeric matrices and process model for forming amorphous solid dispersion by hot-melt extrusion, *Eur. J. Pharm. Biopharm.*, 107 (2016) 40-48.
- [144] T. O., T. K., A. S., Excipient update - soluplus®: An understanding of supersaturation from amorphous solid dispersions, *Drug Deliv Technol.*, 15 (2015).
- [145] J. Guan, X. Huan, Q. Liu, L. Jin, H. Wu, X. Zhang, S. Mao, Synergetic effect of nucleation and crystal growth inhibitor on in vitro-in vivo performance of supersaturable lacidipine solid dispersion, *Int. J. Pharm.*, 566 (2019) 594-603.
- [146] M. Slámová, T. Školáková, A. Školáková, J. Patera, P. Zámotný, Preparation of solid dispersions with respect to the dissolution rate of active substance, *J. Drug*

Deliv. Sci. Technol, 56 (2020) 101518.

[147] M. Rahman, S. Ahmad, J. Tarabokija, E. Bilgili, Roles of surfactant and polymer in drug release from spray-dried hybrid nanocrystal-amorphous solid dispersions (HyNASDs), Powder Technol., 361 (2020) 663-678.

[148] N. Al-Zoubi, F. Odah, W. Obeidat, A. Al-Jaberi, I. Partheniadis, I. Nikolakakis, Evaluation of Spironolactone Solid Dispersions Prepared by Co-Spray Drying With Soluplus((R)) and Polyvinylpyrrolidone and Influence of Tableting on Drug Release, J Pharm Sci, 107 (2018) 2385-2398.

[149] Y. Zhang, Y. Liu, Y. Luo, Q. Yao, Y. Zhong, B. Tian, X. Tang, Extruded Soluplus/SIM as an oral delivery system: characterization, interactions, in vitro and in vivo evaluations, Drug Deliv., 23 (2016) 1902-1911.

[150] Z.M. Lavra, D. Pereira de Santana, M.I. Re, Solubility and dissolution performances of spray-dried solid dispersion of Efavirenz in Soluplus, Drug Dev. Ind. Pharm., 43 (2017) 42-54.

[151] C. Kulkarni, A.L. Kelly, T. Gough, V. Jadhav, K.K. Singh, A. Paradkar, Application of hot melt extrusion for improving bioavailability of artemisinin a thermolabile drug, Drug Dev. Ind. Pharm., 44 (2018) 206-214.

[152] G. Schver, D.D. Sun, S.P.M. Costa, K.E.R. Silva, J.F. Oliveira, L.A. Rolim, M.C.P. de Azevedo Albuquerque, A. de Lima Aires, M. Lima, I.R. Pitta, P.I. Lee, P.J. Rolim-Neto, Solid dispersions to enhance the delivery of a potential drug candidate LPSF/FZ4 for the treatment of schistosomiasis, Eur. J. Pharm. Sci., 115 (2018) 270-285.

[153] P. Liu, J.Y. Zhou, J.H. Chang, X.G. Liu, H.F. Xue, R.X. Wang, Z.S. Li, C.S. Li, J. Wang, C.Z. Liu, Soluplus-Mediated Diosgenin Amorphous Solid Dispersion with High Solubility and High Stability: Development, Characterization and Oral Bioavailability, Drug Des. Dev. Ther, 14 (2020) 2959-2975.

- [154] R. Jog, R. Gokhale, D.J. Burgess, Solid state drug-polymer miscibility studies using the model drug ABT-102, *Int. J. Pharm.*, 509 (2016) 285-295.
- [155] A. Singh, A. Bharati, P. Frederiks, O. Verkinderen, B. Goderis, R. Cardinaels, P. Moldenaers, J. Van Humbeeck, G. Van den Mooter, Effect of Compression on the Molecular Arrangement of Itraconazole-Soluplus Solid Dispersions: Induction of Liquid Crystals or Exacerbation of Phase Separation?, *Mol Pharm*, 13 (2016) 1879-1893.
- [156] R.A. Fule, T.S. Meer, A.R. Sav, P.D. Amin, Artemether-Soluplus Hot-Melt Extrudate Solid Dispersion Systems for Solubility and Dissolution Rate Enhancement with Amorphous State Characteristics, *Journal of pharmaceutics*, 2013 (2013) 151432.
- [157] B. Altaani, R. Obaidat, W. Malkawi, Enhancement of dissolution of atorvastatin through preparation of polymeric solid dispersions using supercritical fluid technology, *Res Pharm Sci*, 15 (2020) 123-136.
- [158] J. Djuris, I. Nikolakakis, S. Ibric, Z. Djuric, K. Kachrimanis, Preparation of carbamazepine-Soluplus solid dispersions by hot-melt extrusion, and prediction of drug-polymer miscibility by thermodynamic model fitting, *Eur. J. Pharm. Biopharm*, 84 (2013) 228-237.
- [159] R.N. Shamma, M. Basha, Soluplus®: A novel polymeric solubilizer for optimization of Carvedilol solid dispersions: Formulation design and effect of method of preparation, *Powder Technol.*, 237 (2013) 406-414.
- [160] M. Basha, A. Salama, S.H. Noshi, Soluplus((R)) based solid dispersion as fast disintegrating tablets: a combined experimental approach for enhancing the dissolution and antiulcer efficacy of famotidine, *Drug Dev. Ind. Pharm.*, 46 (2020) 253-263.
- [161] J. Lu, K. Cuellar, N.I. Hammer, S. Jo, A. Gryczke, K. Kolter, N. Langley, M.A. Repka, Solid-state characterization of Felodipine-Soluplus amorphous solid

dispersions, *Drug Dev. Ind. Pharm.*, 42 (2016) 485-496.

[162] R. Prasad, P. Radhakrishnan, S.K. Singh, P.R.P. Verma, Furosemide - Soluplus(R) Solid Dispersion: Development and Characterization, *Recent Pat. Drug Deliv. Formul*, 11 (2017) 211-220.

[163] M. Rahman, S. Ahmad, J. Tarabokija, N. Parker, E. Bilgili, Spray-Dried Amorphous Solid Dispersions of Griseofulvin in HPC/Soluplus/SDS: Elucidating the Multifaceted Impact of SDS as a Minor Component, *Pharmaceutics*, 12 (2020).

[164] S.O. Kyeremateng, M. Pudlas, G.H. Woehrle, A fast and reliable empirical approach for estimating solubility of crystalline drugs in polymers for hot melt extrusion formulations, *J Pharm Sci*, 103 (2014) 2847-2858.

[165] C. Mendiratta., V. Kadam., V. Pokharkar., Lansoprazole solid dispersion using a novel amphiphilic polymer Soluplus®, *J. Chem. Pharm. Res.*, 3 (2011) 536-543.

[166] R.Y. AlSheyyab., R.M. Obaidat., Y.R. Altall., R.T. Abuhuwaij., R.R. Ghanma., A.S. Ailabouni., H.A. Mashaqbeh., S. Al-Haj., Solubility enhancement of nimodipine through preparation of Soluplus® dispersions, *J. Appl. Pharm. Sci.*, 9 (2019) 30-37.

[167] S.K. Vats, R.N. Gupta, K. Ramaraju, R. Singh, Design and Statistical Evaluation of a Multiunit Delivery System Containing Nisoldipine-Soluplus® Solid Dispersion for Hypertension Chronotherapy, *Int. j. pharm.*, 8 (2016) 170.

[168] S.-Y. Lin, H.-L. Lin, Y.-T. Chi, R.-Y. Hung, Y.-T. Huang, W.-H. Hsieh, C.-Y. Kao, Influence of Soluplus on Solid-State Properties and Physical Stability of Indomethacin-Saccharin Co-crystal Formation Prepared by Air-Drying Process, *J. Pharm. Innov.*, 11 (2016) 109-119.

[169] H.H. Abduljabbar, S.N. Abd Alhammid, Enhancement of the Solubility and the Dissolution Rate of Tamoxifen Citrate Solid Dispersion Using Soluplus by Solvent Evaporation Technique, *Asian J. Pharm. Clin. Res.*, 12 (2019) 216.

- [170] T.G. Bassiri., A. Levy., M. Litt., Polymerization of cyclic imino ethers. I. Oxazolines., *J Polym Sci C.*, 5 (1967) 871-879.
- [171] T. Kagiya., S. Narisawa., T. Maeda., K. Fukui., Ring - opening polymerization of 2 - substituted 2 - oxazolines., *J Polym Sci C.*, 4 (1966) 441-445.
- [172] W. Seeliger., E. Aufderhaar., W. Diepers., R. Feinauer., R. Nehring., W. Thier., H. Hellmann., Recent syntheses and reactions of cyclic imidic esters., *Angew Chem Int Ed Engl.*, 5 (1966).
- [173] D.A. Tomalia., D.P. Sheetz., Homopolymerization of 2 - alkyl - and 2 - aryl - 2 - oxazolines., *J Polym Sci A.*, 4 (1966) 2253-2265.
- [174] R. Hoogenboom, Poly(2-oxazoline)s: a polymer class with numerous potential applications, *Angewandte Chemie*, 48 (2009) 7978-7994.
- [175] N. Adams, U.S. Schubert, Poly(2-oxazolines) in biological and biomedical application contexts, *Adv. Drug Deliv. Rev.*, 59 (2007) 1504-1520.
- [176] R. Hoogenboom, H. Schlaad, Bioinspired Poly(2-oxazoline)s, *Polymers*, 3 (2011) 467-488.
- [177] H. Schlaad, C. Diehl, A. Gress, M. Meyer, A.L. Demirel, Y. Nur, A. Bertin, Poly(2-oxazoline)s as Smart Bioinspired Polymers, *Macromol. Rapid Commun.*, 31 (2010) 511-525.
- [178] H. Schlaad, R. Hoogenboom, Poly(2-oxazoline)s and related pseudo-polypeptides, *Macromol. Rapid Commun.*, 33 (2012) 1599.
- [179] O. Sedlacek, B.D. Monnery, S.K. Filippov, R. Hoogenboom, M. Hruby, Poly(2-oxazoline)s-are they more advantageous for biomedical applications than other polymers?, *Macromol. Rapid Commun.*, 33 (2012) 1648-1662.
- [180] K. Aoi., M. Okada., Polymerization of oxazolines., *Prog. Polym. Sci.*, 21 (1996) 151-208.

- [181] M. Glassner, K. Kempe, U.S. Schubert, R. Hoogenboom, C. Barner-Kowollik, One-pot synthesis of cyclopentadienyl endcapped poly(2-ethyl-2-oxazoline) and subsequent ambient temperature Diels-Alder conjugations, *Chem. Commun*, 47 (2011) 10620-10622.
- [182] M.A. Tasdelen, M.U. Kahveci, Y. Yagci, Telechelic polymers by living and controlled/living polymerization methods, *Prog. Polym. Sci.*, 36 (2011) 455-567.
- [183] G. Volet, T.-X. Lav, J. Babinot, C. Amiel, Click-Chemistry: An Alternative Way to Functionalize Poly(2-methyl-2-oxazoline), *Macromol. Chem. Phys.*, 212 (2011) 118-124.
- [184] T.X. Viegas, M.D. Bentley, J.M. Harris, Z. Fang, K. Yoon, B. Dizman, R. Weimer, A. Mero, G. Pasut, F.M. Veronese, Polyoxazoline: chemistry, properties, and applications in drug delivery, *Bioconjug. Chem.*, 22 (2011) 976-986.
- [185] Q. Zhang, C. Weber, U.S. Schubert, R. Hoogenboom, Thermoresponsive polymers with lower critical solution temperature: from fundamental aspects and measuring techniques to recommended turbidimetry conditions, *Mater. Horiz.*, 4 (2017) 109-116.
- [186] V.R. de la Rosa, Poly(2-oxazoline)s as materials for biomedical applications, *J. Mater. Sci.: Mater. Med*, 25 (2014) 1211-1225.
- [187] H. Fael, C. Rafols, A.L. Demirel, Poly(2-Ethyl-2-Oxazoline) as an Alternative to Poly(Vinylpyrrolidone) in Solid Dispersions for Solubility and Dissolution Rate Enhancement of Drugs, *J Pharm Sci*, 107 (2018) 2428-2438.
- [188] E. Boel, A. Smeets, M. Vergaelen, V.R. De la Rosa, R. Hoogenboom, G. Van den Mooter, Comparative study of the potential of poly(2-ethyl-2-oxazoline) as carrier in the formulation of amorphous solid dispersions of poorly soluble drugs, *Eur. J. Pharm. Biopharm*, 144 (2019) 79-90.
- [189] M. Everaerts, A. Tigrine, V.R. de la Rosa, R. Hoogenboom, P. Adriaensens,

C. Clasen, G. Van den Mooter, Unravelling the Miscibility of Poly(2-oxazoline)s: A Novel Polymer Class for the Formulation of Amorphous Solid Dispersions, *Molecules*, 25 (2020).

[190] X. Shan, M.A. Moghul, A.C. Williams, V.V. Khutoryanskiy, Mutual Effects of Hydrogen Bonding and Polymer Hydrophobicity on Ibuprofen Crystal Inhibition in Solid Dispersions with Poly(N-vinyl pyrrolidone) and Poly(2-oxazolines), *Pharmaceutics*, 13 (2021).

[191] B. Claeys, A. Vervaeck, C. Vervaet, J.P. Remon, R. Hoogenboom, B.G. De Geest, Poly(2-ethyl-2-oxazoline) as matrix excipient for drug formulation by hot melt extrusion and injection molding, *Macromol. Rapid Commun.*, 33 (2012) 1701-1707.

[192] M. Glassner, M. Vergaelen, R. Hoogenboom, Poly(2-oxazoline)s: A comprehensive overview of polymer structures and their physical properties, *Polym. Int.*, 67 (2018) 32-45.

[193] W. Fan, S. Yamago, Synthesis of Poly(N-vinylamide)s and Poly(vinylamine)s and Their Block Copolymers by Organotellurium-Mediated Radical Polymerization, *Angewandte Chemie*, 58 (2019) 7113-7116.

[194] N. Jain., S. Tonge., H.U. Mujawar., S. N.Deshmukh., Polyacrylamide pharmaceutical and biomedical applications-A review., *J. Inf. Comput. Sci.*, 10 (2020) 48-53.

[195] T.-H. Yang, Recent Applications of Polyacrylamide as Biomaterials, *Recent Pat. Mater. Sci.*, 1 (2008) 29-40.

[196] N.A. Cortez-Lemus, A. Licea-Claverie, Poly(N-vinylcaprolactam), a comprehensive review on a thermoresponsive polymer becoming popular, *Prog. Polym. Sci.*, 53 (2016) 1-51.

[197] M.N. Mohammed, K.B. Yusoh, J.H.B.H. Shariffuddin, Poly(N-vinyl

caprolactam) thermoresponsive polymer in novel drug delivery systems: A review, Mater. Express., 8 (2018) 21-34.

Chapter 2

Polymer structure and property effects on solid dispersions with haloperidol: Poly(N-vinyl pyrrolidone) and poly(2-oxazolines) studies

This chapter was published as Shan, X.; Williams, A. C.; Khutoryanskiy, V. V., Polymer structure and property effects on solid dispersions with haloperidol: Poly(N-vinyl pyrrolidone) and poly(2-oxazolines) studies. *International journal of pharmaceutics* 2020, 590, 119884.



Polymer structure and property effects on solid dispersions with haloperidol: Poly(N-vinyl pyrrolidone) and poly(2-oxazolines) studies

Xiaoning Shan, Adrian C. Williams, Vitaliy V. Khutoryanskiy*

Reading School of Pharmacy, University of Reading, Whiteknights, PO Box 224, Reading RG66AD, United Kingdom

ARTICLE INFO

Keywords:

Solid dispersions
Poly(N-vinyl pyrrolidone)
Poly(2-oxazolines)
Crystallinity
Hydrophobic drug
Amorphous
Haloperidol

ABSTRACT

Poly(2-methyl-2-oxazoline) (PMOZ), poly(2-propyl-2-oxazoline) (PnPOZ) and poly(2-isopropyl-2-oxazoline) (PiPOZ) were synthesized by hydrolysis of 50 kDa poly(2-ethyl-2-oxazoline) (PEOZ) and subsequent reaction of the resulting poly(ethylene imine) with acetic, butyric and isobutyric anhydrides, respectively. These polymers were characterized by proton nuclear magnetic resonance, FTIR spectroscopy, powder X-ray diffraction, and differential scanning calorimetry. The poly(2-oxazolines) as well as poly(N-vinyl pyrrolidone) (PVP) were used to prepare solid dispersions with haloperidol, a model poorly soluble drug. Dispersions were investigated by powder X-ray diffraction, differential scanning calorimetry and FTIR spectroscopy. Increasing the number of hydrophobic groups (-CH₂- and -CH₃) in the polymer resulted in greater inhibition of crystallinity of haloperidol in the order: PVP > PnPOZ = PEOZ > PMOZ. Interestingly, drug crystallization inhibition by PiPOZ was lower than with its isomeric PnPOZ because of the semi-crystalline nature of the former polymer. Crystallization inhibition was consistent with drug dissolution studies using these solid dispersions, with exception of PnPOZ, which exhibited lower critical solution temperature that affected the release of haloperidol.

1. Introduction

Approximately 40% of approved drugs and almost 90% of newly developed active ingredients are poorly soluble in water (Kalepu and Nekkanti, 2015). Therefore, the development of new medicines using these hydrophobic drug molecules present a challenge for formulation scientists.

Several approaches are currently being exploited to improve the solubility and dissolution profiles of hydrophobic drugs. These include the use of inclusion complexes with cyclodextrins (Carrier et al., 2007; Conceicao et al., 2018; Morrison et al., 2013), formation of salts (He et al., 2017), co-crystals (Blagden et al., 2007), hydrotropic agents (Kim et al., 2010), micellar structures (Qu et al., 2006; Volkova et al., 2019) as well as solid dispersions (Brough and Williams, 2013; Singh and Van den Mooter, 2016).

Solid dispersions are defined as physical mixtures of poorly-soluble drugs with some hydrophilic materials (Vasconcelos et al., 2016) and include eutectic systems, solid solutions (which themselves can be continuous or discontinuous depending on component miscibility) and

systems where a drug can be in an amorphous or partially crystalline state in an amorphous or crystalline carrier. Several classes of hydrophilic polymers have been exploited to prepare amorphous solid dispersions, including poly(N-vinyl pyrrolidone) (Knopp et al., 2016; Li and Buckton, 2015; Niemczyk et al., 2012), cellulose ethers (Chavan et al., 2019), polyethylene oxide (Abu-Diak et al., 2012; Ozeki et al., 1997) and poloxamers (Ali et al., 2010). In some studies, the reduction of drug crystallinity in solid dispersions with various polymers has been explored and related to the chemical structure and properties of water-soluble polymers. For example, in a series of studies of solid dispersions prepared from ibuprofen and PVP, it was demonstrated that reduced drug crystallinity was due to hydrogen bond formation between drug molecules and the polymer (Niemczyk et al., 2012; Rawlinson et al., 2007; Williams et al., 2005). However, systematic studies into the effects of polymer structures on their ability to reduce drug crystallinity are currently lacking because there are limited opportunities to vary polymer structures in a controlled manner; most studies use commercially available polymers.

Haloperidol is an antipsychotic drug used to treat schizophrenia,

Abbreviations: PEI, poly (ethylene imine); POZ, poly(2-alkyl-oxazoline); PEOZ, poly(2-ethyl-2-oxazoline); PMOZ, poly(2-methyl-2-oxazoline); PnPOZ, poly(2-propyl-2-oxazoline); PiPOZ, poly(2-isopropyl-2-oxazoline); PVP, poly(N-vinyl pyrrolidone); HP, haloperidol; SD, solid dispersion; DMA, N, N-dimethylacetamide; TEA, triethylamine; SGF, simulated gastric fluid.

* Corresponding author.

E-mail address: v.khutoryanskiy@reading.ac.uk (V.V. Khutoryanskiy).

<https://doi.org/10.1016/j.ijpharm.2020.119884>

Received 18 March 2020; Received in revised form 10 September 2020; Accepted 11 September 2020

Available online 18 September 2020

0378-5173/© 2020 Elsevier B.V. All rights reserved.

delirium, nausea and vomiting, and other neuropsychiatric disorders (Chaparro et al., 2013; Krause et al., 2018; Zayed et al., 2019). It is a poorly-soluble drug that is commonly formulated as solutions for oral administration or injections, and also as tablets (Demoen., 1961). Previously, solid dispersions with haloperidol were prepared using different weak organic acids (Lee et al., 2017; Singh et al., 2013), PVP (Saluja et al., 2016) and polyethylene glycol (Baird and Taylor, 2011) and dispersions have been made into free flowing tabletable powders by combining with mesoporous metalosilicate (Shah and Serajuddin, 2015).

Poly(2-oxazolines) are an emerging class of polymers, currently attracting substantial interest due to a number of unique physico-chemical properties and lack of toxicity (de la Rosa, 2014; Hoogenboom, 2009; Lorson et al., 2018). Lower members of the poly(2-oxazoline) family exhibit solubility in water: poly(2-methyl-2-oxazoline) (PMOZ), poly(2-ethyl-2-oxazoline) (PEOZ), poly(n-propyl-2-oxazoline) (PnPOZ) and poly(isopropyl-2-oxazoline) (PiPOZ). Recently, poly(2-oxazolines) were used to prepare solid dosage forms as individual polymers and also in combination with some other pharmaceutical excipients (Boel et al., 2019; Fael et al., 2018; Moustafine et al., 2019; Ruiz-Rubio et al., 2018).

Using different water-soluble poly(2-oxazolines) to design solid dispersions offers interesting and previously unexplored opportunities to understand the effect of polymer molecular structure and hydrophilic-hydrophobic balance on the crystallinity of a dispersed drug. In this study, a series of water-soluble poly(2-oxazolines) were synthesized with equivalent degrees of polymerization by hydrolysis of commercially-available PEOZ into linear poly(ethylene imine) (PEI) and subsequent conversion into PMOZ, PnPOZ and PiPOZ. The structure and properties of the resulting polymers were studied by spectroscopic (¹H NMR and FTIR spectroscopies), thermal (differential scanning calorimetry) and powder X-ray diffraction methods. These materials were then used to prepare solid dispersions of haloperidol, a model poorly-soluble active pharmaceutical ingredient, and the effects of polymer structure on drug crystallinity and drug dissolution profiles were explored and compared to PVP-based solid dispersions as a control.

2. Materials and methods

2.1. Materials

Poly(2-ethyl-2-oxazoline) (PEOZ) 50 kDa (polydispersity index, PDI 3–4), poly(N-vinyl pyrrolidone) (PVP) 55 kDa (K-value 30), butyric anhydride (≥97.0%), isobutyric anhydride (≥97.0%), haloperidol (HP) were from Sigma-Aldrich (UK). Hydrochloric acid (37 wt%), N,N-dimethylacetamide (DMA), acetic anhydride (≥99.0%), triethylamine (TEA, 99.7%, extra pure), sodium hydroxide were from Fisher Scientific (UK). Dialysis membrane with a molecular cut-off 3.5 kDa was from Medicell International Ltd., UK.

2.2. Synthesis of PEI

PEOZ was hydrolyzed to linear PEI according to a procedure reported by Sedlacek et al. (2019a). Specifically, PEOZ (20.0 g) was dissolved in 200 mL 18 wt% aqueous hydrochloric acid and heated overnight for 14 h at 100 °C. The PEI solution obtained in hydrochloric acid was then diluted with ice-cold distilled water (1 L). Ice-cold aqueous sodium hydroxide (4 M) was added dropwise to the solution of PEI. Initially PEI solution remained soluble, but with further addition of NaOH the PEI precipitated at pH 10–11. The precipitate was filtered off and washed twice with distilled water and re-precipitated twice then dried under vacuum to obtain PEI as a white powder (yielding 7.6 g (87%)). This material was analyzed by ¹H NMR, PXRD, DSC and FTIR.

2.3. Synthesis of PMOZ, PnPOZ and PiPOZ

PMOZ, PnPOZ and PiPOZ were synthesized according to a procedure developed by (Sedlacek et al., 2019b) for the synthesis of high molecular weight PMOZ. PEI (1 eq. of amines, 1.0 g) was dissolved in DMA (20 mL) upon heating. The mixture was cooled in an ice-water bath (a fine suspension of PEI appeared) and acetic anhydride (2.5 eq, 5.4 mL), butyric anhydride (2.5 eq, 9.4 mL) or isobutyric anhydride (2.5 eq, 9.6 mL) was then added, resulting in immediate dissolution of PEI. TEA (2.5 eq, 4.8 mL) was added. The reaction mixture was purged with nitrogen and allowed to stir at 0 °C for 1 h and then at room temperature overnight. The obtained mixture was then diluted in deionized water and purified by dialysis (MWCO 3.5 kDa) at room temperature for PMOZ and PiPOZ and in a fridge (~5 °C) for PnPOZ. All polymers were recovered by freeze-drying as white solids (yields 89.4%, 88.5% and 88.9% for PMOZ, PnPOZ and PiPOZ, respectively).

2.4. Calculation of hydrophilic-hydrophobic balance (HHB) values for polymers

HHB values for all polymers were calculated according to the following equation taken from (Khtutoryanskiy et al., 2004):

$$HHB = \frac{\sum N_i * EN(\text{carbon, hydrogen})_i}{\sum N_i * EN(\text{oxygen, nitrogen})_i} \quad (1)$$

where N_i is the number of atoms of each chemical element, and EN_i is the electronegativity of each chemical element in the repeating unit of each polymer.

2.5. Preparation of polymer-haloperidol (HP) solid dispersions

Solid dispersions of polymer-HP were prepared in different repeating unit/drug molar ratios by a solvent evaporation. DMA (1 mL) was used to dissolve 25 mg of HP with varying amounts of each polymer depending on the repeating unit/drug molar ratios. After complete dissolution, the solution was transferred to a petri dish and the solvent was removed by evaporation at 50 °C on a heating base. The resultant solid was kept under vacuum for 72–96 h to remove residual DMA. The absence of residual DMA in solid dispersions was confirmed using ¹H NMR spectroscopy.

2.6. Characterization of polymers and solid dispersions

2.6.1. Proton nuclear magnetic resonance (H-NMR)

¹H NMR spectra of polymers were recorded with a Bruker spectrometer operating at 250 MHz using methanol-*d*₄ as the solvent. All chemical shifts are given in ppm.

2.6.2. Powder X-Ray Diffractometry (PXRD)

A small amount of each dry sample (~20 mg) was placed on a silica slide and analyzed in a Bruker D8 ADVANCE PXRD equipped with a LynxEye detector and monochromatic Cu K α ₁ radiation ($\lambda = 1.5406 \text{ \AA}$). Samples were rotated at 30 rpm and data collected over an angular range of 5–64° 2 θ for 1 h, with a step of 0.05° (2 θ) and count time of 1.2 s. The results were analyzed using EVA software.

2.6.3. Differential scanning calorimetry (DSC)

Thermal analysis of pure drug, polymers and solid dispersions was performed using DSC (TA Instruments). Samples (3–5 mg) were loaded into pierced T_{zero} aluminum pans. The thermal behavior of each sample was investigated in a nitrogen atmosphere with a heating/cooling rate of 10 °C/min. The values of the glass transition temperature (T_g) of polymers were determined from the second heating cycle. The degree of sample crystallinity was determined by the specific enthalpy (ΔH) of the drug melting peak by TA universal analysis software and calculated as

the ratio of the ΔH of drug in the solid dispersions to the ΔH of pure HP. Since the drug content in the dispersion is only a fraction of the sample weight, then the degree of crystallinity was normalized according to the following equation:

$$\text{Crystallinity}(\%) = \left(\frac{\Delta H_s \cdot W_s}{W_h} \right) / \Delta H_h \cdot 100 \quad (2)$$

where, ΔH_s is the ΔH of the drug in the solid dispersion, having the melting peak around 150 °C (melting point of HP), ΔH_h is the ΔH of pure HP, W_s is the weight of solid dispersions, W_h is the weight of HP in solid dispersions.

2.6.4. Fourier transform infrared (FTIR) spectroscopy

FTIR spectra were recorded on a Nicolet iS5 spectrometer between 4000 and 400 cm^{-1} at a resolution of 4 cm^{-1} and as an average of 64 scans. The OMNIC software was used for spectral analysis.

2.7. Calculation of solubility parameters

Solubility parameters were calculated using two different methods. The Fedor method (Chokshi et al., 2005; Fedors, 1974; Krevelen, 1990) calculates the solubility parameter δ using the following equation:

$$\delta = \sqrt{\frac{\sum \Delta e_i}{V}} \quad (3)$$

where Δe_i is the energy of vaporization and V is the molar volume.

The Van Krevelen method (Krevelen, 1990) provides:

$$\delta = \sqrt{\delta_d^2 + \delta_p^2 + \delta_h^2} \quad (4)$$

where

$$\delta_d = \frac{\sum F_{di}}{V} \quad \delta_p = \frac{\sqrt{\sum F_{pi}^2}}{V} \quad \delta_h = \frac{\sqrt{\sum E_{hi}}}{V}$$

where δ_d is the contribution from dispersion forces, δ_p is the contribution from polar forces, δ_h is the contribution of hydrogen bonding, F_{di} is the molar attraction constant due to dispersion component, F_{pi} is the molar attraction constant due to polar component, E_{hi} is the hydrogen bonding energy, and V is the molar volume.

For various groups, the values of Δe_i , F_{di} , F_{pi} , E_{hi} , and V (molar volume) were taken from the literature (Fedors, 1974; Krevelen, 1990).

2.8. In vitro dissolution studies

Dissolution of haloperidol from solid dispersions ([Polymer]/[Drug] = 5:1 mol/mol) used USP Apparatus II (paddle method) at 37 ± 0.5 °C with paddles at 50 rpm and simulated gastric fluid (SGF) (0.1 N HCl, pH = 1.2). A pharmaceutical grade empty vegan clear capsule size "0" filled with solid dispersion (equivalent to 25 mg drug) was put into the 900 mL SGF with a sinker. Samples (5 mL) were withdrawn at 2, 5, 10, 20, 40, 60, 80, 100 and 120 min, and filtered using a 0.45- μm syringe filter, an equal volume of the SGF was added to the dissolution medium to maintain the volume. The drug was assayed using a UV-visible spectrophotometric method. All dissolution studies were performed in triplicate.

2.9. Statistical analysis

All solid dispersions for each polymer at all drug loadings were prepared three times independently. All analysis, PXRD, DSC, FTIR as well as dissolution studies, were in triplicate. Data are expressed as mean \pm standard deviation.

3. Results and discussion

3.1. Polymer synthesis and characterization

The synthesis of some members of the poly(2-oxazoline) family such as PMOZ with high molecular weights (above 10 kDa) by living cationic ring-opening polymerization is challenging due to the high probability of chain transfer reactions (Litt et al., 1975; Sedlacek et al., 2019b; Wiesbrock et al., 2005). Recently, Sedlacek et al (Sedlacek et al., 2019b) demonstrated an alternative approach to synthesize well-defined high molecular weight PMOZ through hydrolysis of PEOZ into PEI and subsequent acylation with acetic anhydride.

In this work, a similar strategy was used to synthesize PMOZ, PnPOZ and PiPOZ from commercially-available 50 kDa PEOZ as shown in Fig. 1.

The commercial PEOZ was subjected to an acidic hydrolysis of its side chains to yield linear PEI. The full conversion was confirmed by ^1H NMR spectroscopy, where both signals of PEOZ side chains (δ 2.44 ppm and δ 1.13 ppm) were lost and the main backbone signal shifted to δ 2.75 ppm (Figure S1). Further confirmation was by FTIR: the loss of the characteristic PEOZ amide carbonyl vibration at 1626 cm^{-1} and the presence of new strong peaks at 1474 cm^{-1} and 3263 cm^{-1} (Fig. S3) assigned to the N-H vibration of PEI again confirmed complete hydrolysis of the amide groups of PEOZ.

The prepared linear PEI was then re-acylated with excess acetic anhydride, butyric anhydride or isobutyric anhydride in DMA using TEA as a base. The resultant PMOZ, PnPOZ and PiPOZ were characterized by ^1H NMR and FTIR spectroscopies. The ^1H NMR spectra of these polymers show signals corresponding to the poly(2-oxazolines) backbone at 3.5 ppm (peak a, Figure S1). The signals labelled as b, c and d are attributed to poly(2-oxazoline) side chains (Boerman et al., 2016; Funtan et al., 2016; Li et al., 2015; Mees et al., 2016; Sedlacek et al., 2019b). Complete conversion from PEI to PMOZ, PnPOZ and PiPOZ was shown not only through the loss of PEI's ^1H NMR signals (Figure S1) but also by loss of the PEI's N-H vibration at 3263 cm^{-1} in FTIR spectra, with a strong feature appearing at 1626 cm^{-1} corresponding to the amide carbonyl vibration (Figure S3). In detail, the FTIR spectrum for PEOZ shows the following bands: 2977 cm^{-1} (CH_2 stretch), 1626 cm^{-1} (C=O stretch), 1470 cm^{-1} (C-H bending), 1420 cm^{-1} (CH bending), and 1240 cm^{-1} (C-N stretch). The spectrum for PEI shows the bands at 3263 cm^{-1} (N-H stretch), 1474 cm^{-1} (N-H bending), 1132 cm^{-1} (C-N stretch) and 750 cm^{-1} (N-H bending) typical for this polymer. The spectra from the different poly(2-oxazoline) derivatives (PMOZ, PEOZ, PnPOZ and PiPOZ) essentially show the same molecular modes, most noticeably the strong C=O stretching mode around 1630 cm^{-1} .

The parent polymer, the intermediate PEI and resulting poly(2-oxazoline) derivatives were also analyzed by differential scanning calorimetry (DSC) and powder X-ray diffraction (PXRD). Fig. 2 shows DSC thermograms for all poly(2-oxazolines), alongside poly(N-vinyl pyrrolidone) (PVP) which was used as a positive control in subsequent solid dispersion studies. PVP, PMOZ, PiPOZ, PEOZ and PnPOZ show glass transition temperatures (T_g) at 163.1, 82.7, 69.3, 58.9 and 39.4 °C, respectively, in good agreement with the literature (Gatica et al., 2013; Glassner et al., 2018; Oleszko et al., 2015; Sessa et al., 2011). The decrease in T_g with increasing number of carbon atoms in the side chain in poly(2-oxazoline) series can be explained by the increased flexibility of the longer side-chains. It is clearly seen that T_g values recorded for poly(2-oxazolines) are substantially lower (82.7, 69.3, 58.9 and 39.4 °C) than the T_g of PVP (163.1 °C). Typically, carriers with higher T_g 's are regarded as more desirable for preparing solid dispersions because of their greater rigidity and enhanced ability to inhibit drug crystallization (Huang and Dai, 2014).

The DSC analysis of linear PEI showed it melting at 66.2 °C, also in good agreement with the literature (Saegusa et al., 1972); no glass transition could be detected for linear PEI, which is consistent with the observations reported by Lambermont-Thijs et al (2010).

Due to the absence of side groups and the presence of both hydrogen

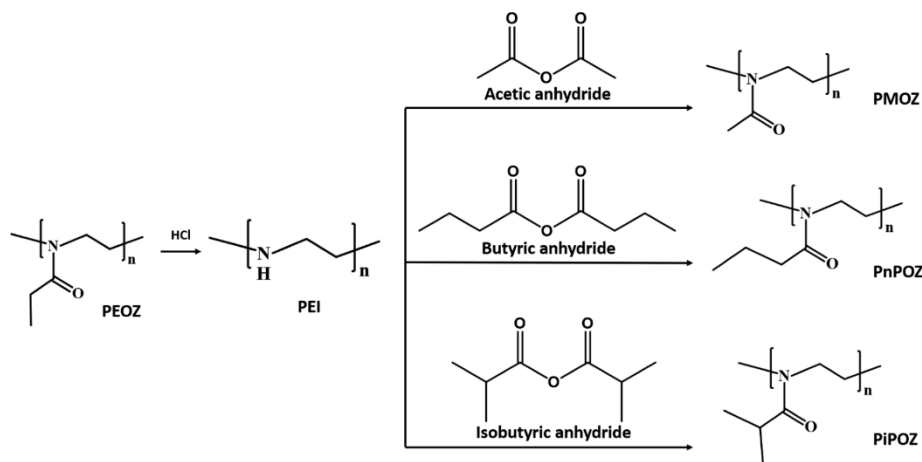


Fig. 1. Synthesis of high molar weight PMOZ, PnPOZ and PiPOZ by hydrolysis of PEOZ and subsequent acylation of linear PEI.

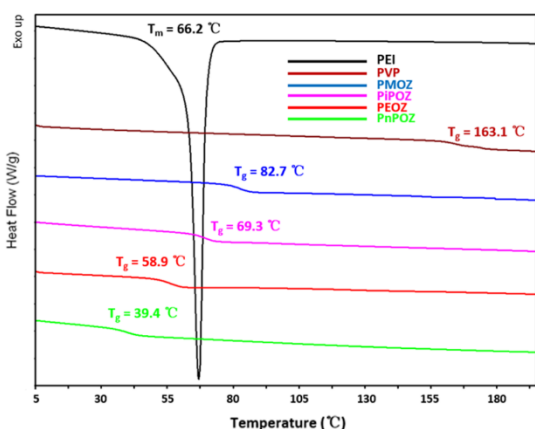


Fig. 2. DSC thermograms (second scan) of PVP, PEOZ and synthesized PEI, PMOZ, PnPOZ and PiPOZ showing decreasing glass transition temperatures with increasing numbers of carbon atoms in the side chain.

bond donating and accepting $-\text{NH}-$ groups, linear PEI has a strong tendency to crystallize (Lambert-Thijs et al., 2010), which was confirmed here by PXRD (Fig. 3): three main crystalline peaks were observed at $2\theta = 18.7^\circ$, 20.7° and 27.9° .

It is interesting that, by x-diffractometry, PiPOZ appears to be semi-crystalline. By DSC, a melting peak occurred at $203.5\text{ }^\circ\text{C}$ during the first heating cycle, which was lost during a subsequent second scan, possibly as a result of thermal disruption of crystallinity at higher temperature, as seen in Fig. S2 (Demirel et al., 2007). According to the PiPOZ unit cell model proposed (Demirel et al., 2007; Oleszko et al., 2015), the isopropyl groups alternately align along the [100] direction (the sharp peak at $2\theta = 8.14^\circ$) to either side of the backbone, with the amide dipoles alternately oriented along the [010] direction (the other broad peak at $2\theta = 18.5^\circ$) (Fig. 3). The significantly different T_g values for the isomers PiPOZ ($69.3\text{ }^\circ\text{C}$) and PnPOZ ($39.4\text{ }^\circ\text{C}$) as well as PiPOZ's semi-crystalline nature can be attributed to the different d-spacing (distance between the main chains) together with the more compact isopropyl groups that are less flexible than the n-propyl groups, thereby facilitating their packing into crystallites (Demirel et al., 2016).

PXRD results also confirmed that PVP, PMOZ, PEOZ and PnPOZ are

predominantly amorphous.

3.2. Preparation and characterization of solid dispersions

In order to evaluate the effects of different polymers on the crystallinity of haloperidol (HP), solid dispersions (SDs) were prepared by solvent evaporation and were characterized by DSC, PXRD and FTIR, with DSC and PXRD used to calculate the crystallinity of HP in the dispersions. Differences in solvent polarities, boiling points and the evaporation rate all affect the interaction of the drug with polymer. Thus, several solvents and solvent mixtures were initially screened including DMA, ethanol, acetone, chloroform, chloroform-ethanol mixtures and acetone-ethanol mixtures. Only DMA acted as a common solvent to dissolve all polymers and HP.

The X-ray diffractogram of HP (Fig. 4) shows multiple distinctive peaks, notably at 6.6° , 11.9° , 13.1° , 15.1° , 16.4° , 20.0° , 22.8° , 24.9° , 26.3° and 31.9° , demonstrating the crystalline structure of pure HP.

A gradual decrease in the drug crystallinity was observed in solid dispersions as the quantity of each polymer increased. For example, solid dispersions with PVP showed the presence of crystalline HP at the following molar ratios [PVP]/[HP] = 0.3:1, 1:1 and 2:1. A fully amorphous solid dispersion was observed only at [PVP]/[HP] = 5:1 (Fig. 4a). Solid dispersions with PEOZ and PnPOZ showed the presence of crystalline HP at [PEOZ]/[HP] and [PnPOZ]/[HP] molar ratios of 0.3:1, 1:1, 2:1, 5:1 and 10:1 but were amorphous at 15:1 (Fig. 4b and Figure S4b).

It is interesting to note that when PiPOZ was used to prepare solid dispersions, haloperidol was amorphous only when the [PiPOZ]/[HP] molar ratio reached 20:1 (Figure S4c). PXRD analysis of these dispersions revealed that the peak at $2\theta = 8.14^\circ$ representing the crystalline domains of PiPOZ strengthened with increasing concentrations of polymer [PiPOZ]/[HP] from 0.3:1 to 15:1. However, when the drug was amorphous at [PiPOZ]/[HP] = 20:1, the intensity of the polymer-derived crystalline peak decreased (Figure S4c). This indicates that the crystalline domains of PiPOZ are also affected by the interaction with HP. Interestingly, a new peak that appeared at $2\theta = 7.8^\circ$ in PnPOZ-HP dispersions (Figure S4b) suggesting that the interactions with the drug had also increased the crystallinity of the polymer. X-ray analysis of the dispersions formed using PMOZ shown that HP remains crystalline even at the lowest drug loading of [PMOZ]/[HP] = 25:1 (Fig. S4a).

FTIR spectroscopy was used to investigate molecular interactions between the drug and the polymers in these solid dispersions. Hydrogen bonding was expected between the hydroxyl group of HP with carbonyl groups of PVP (Chadha et al., 2006) or with nitrogen atoms of POZ

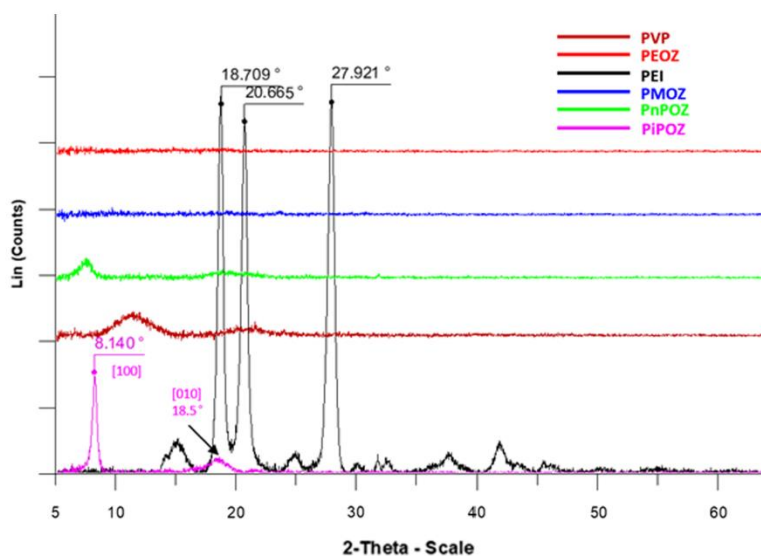


Fig. 3. X-ray diffraction diffractograms of PVP, PEOZ and synthesized PEI, PMOZ, PnPOZ and PiPOZ.

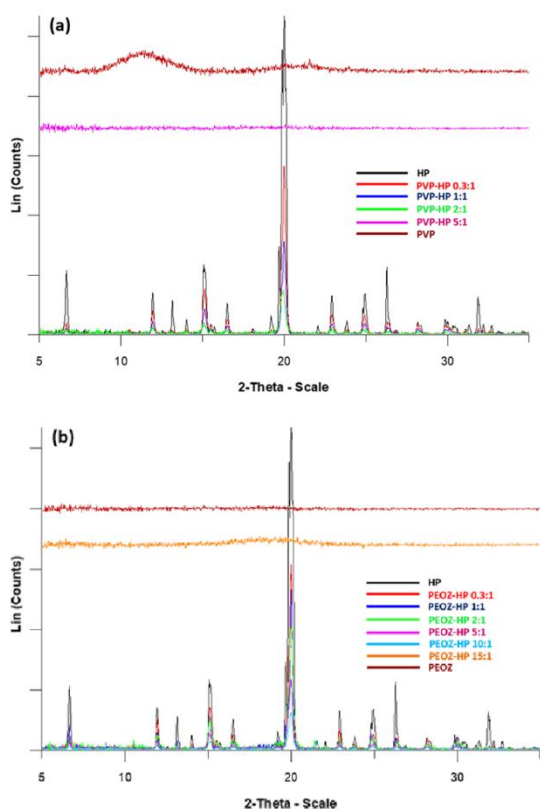


Fig. 4. X-ray diffraction diagrams of PVP-HP SDs (a) and PEOZ-HP SDs (b).

(Moustafine et al., 2019). Such interactions can be confirmed by broadening and shifting in the absorption bands of the interacting groups (He et al., 2004). Fig. 5 presents example spectra of haloperidol, PVP and PVP-HP solid dispersions (2:1 and 5:1) between 1550 and 1750 cm^{-1} which demonstrates these interactions and Figure S5 shows all other spectra in a broader spectral region.

The spectrum of HP showed characteristic peaks at 3100 cm^{-1} assigned to the hydroxyl group, 1680 cm^{-1} assigned to carbonyl group and 1595 cm^{-1} due to the benzene ring. Characteristic carbonyl peaks are observed in POZ and PVP spectra at 1626 cm^{-1} and 1655 cm^{-1} , respectively. The HP hydroxyl group peak at 3100 cm^{-1} was lost concomitantly with a broad peak at 3408 cm^{-1} forming as the molar ratio [PVP]/[HP] increased to 2:1. This new broad peak shifted to 3440 cm^{-1} as the molar ratio increased to 5:1, suggesting a change in the environment of the hydroxyl groups, potentially due to hydrogen bonding between the drug and PVP. This is in good agreement with the study reported by Saluja et al. (2016). Similar loss of the 3100 cm^{-1} peak

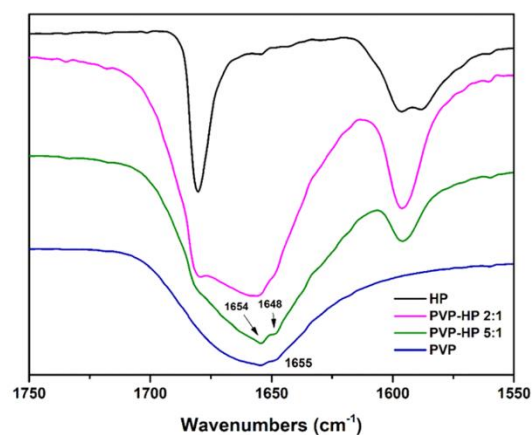


Fig. 5. FTIR spectra of HP, PVP and PVP-HP solid dispersions in the range of 1750–1550 cm^{-1} .

and a shift to higher wavenumber were also observed in POZ-HP spectra, but proof of hydrogen bonding between the drug and poly(2-oxazolines) is confounded since the peak around 3400 cm^{-1} can also be attributed to water, considering the hydrophilic nature of these polymers. Moreover, there was neither peak shifting nor broadening observed for the amide groups in the spectra of solid dispersions, suggesting that very weak or no hydrogen bonding exist between the drug and the poly(2-oxazolines). This is exemplified by comparing FTIR spectra from PEOZ-HP physical mixtures and solid dispersions (15:1) (Figure S6). The spectrum of the physical mixture clearly shows characteristic peaks of both PEOZ and the drug, notably the 1680 cm^{-1} feature assigned to the drug carbonyl group and the broad 1626 cm^{-1} peak assigned to the same mode in PEOZ. Though the peaks overlap, these features are also apparent at the same wavenumber values in the solid dispersion, and the amide feature at 1595 cm^{-1} was also invariant again providing no evidence for significant hydrogen bonding between the drug and carrier.

DSC experiments were also conducted to further investigate the thermal behavior of the solid dispersions. The DSC thermogram of pure HP showed a single characteristic melting peak at $150\text{ }^\circ\text{C}$, confirming its crystalline nature (Fig. 6), and in agreement with previous reports (Solanki et al., 2018; Yasir et al., 2016). The DSC curves of solid dispersions showed broader and reduced melting peaks corresponding to the crystalline drug as the amounts of polymer in the dispersions increased (Fig. 6 and Figure S7). The HP melting peak was absent in solid dispersions with [PVP]/[HP] = 5:1 (Fig. 6a), [PEOZ]/[HP] = 15:1

(Fig. 6b), [PnPOZ]/[HP] = 15:1 (Figures S7c and 7d) and [PiPOZ]/[HP] = 20:1 (Figure S7b), indicating that the drug was amorphous. However, HP was still crystalline in the dispersions with PEOZ even at [PMOZ]/[HP] = 25:1, in agreement with the earlier X-ray data (Figure S7a).

As can be seen from Figure S7b, Figure S8 and Table S2, as the amount of PiPOZ increased, a second endothermic peak appeared at [PiPOZ]/[HP] = 5:1, 10:1, 15:1 and 20:1, which could be attributed to the crystalline nature of PiPOZ. PiPOZ apparently became increasingly crystalline up to [PiPOZ]/[HP] = 15:1, but the polymer crystallinity fell at a ratio of 20:1 where HP crystallinity was lost (Figure S8). Confirming the earlier X-ray studies, the thermal data also suggests that the crystallinity of PiPOZ was affected by interaction with HP. The parameters of peak 2 including the T_m , ΔH_f and degree of crystallinity calculated using equation (S1) and equation (S2) are summarized in Table S2.

It is worth noting that there were also two melting peaks apparent in the DSC curves of PnPOZ-HP (1:1, 2:1, 5:1 and 10:1). The T_m of the two peaks obtained from the second cycle after quenching using different method are summarized in Table S1. The T_m of peak 2 was around $112\text{ }^\circ\text{C}$ at 1:1, 2:1 and 5:1, whereas the T_m of peak 1 corresponding to HP decreased from $150.9\text{ }^\circ\text{C}$ at 1:1 to $134.6\text{ }^\circ\text{C}$ at 5:1 as the crystalline HP was disordered as it distributed and interacted with the polymer. At a polymer:drug ratio of 10:1, only a single melting event was seen as the two peaks combined. When the first heating cycle temperature was raised from 100 to $120\text{ }^\circ\text{C}$, and then cooled, this melting event was lost from the thermogram. It is extremely unlikely that the peak results from a polymorph of HP since none have been reported to date. For example, a search of the Cambridge Structural Database V5.40 (Groom et al., 2016) revealed only a single, monoclinic crystalline form of HP and an extensive search of the literature found no evidence to support the existence of another known polymorphic form. Indeed, a recent review by Santos (Santos et al., 2014) identified HP as having only a single known crystalline form. As such, it is unlikely that the broad peak at $2\theta = 7.8^\circ$ is attributable to a previously unreported crystalline form of HP. Rather, given its broad nature, it seems more likely that this diffraction feature is attributable to crystallization of the polymer. The crystalline character of PnPOZ formed in PnPOZ-HP SDs might result from the interaction with the drug such that the arrangement or density of the polymer has been changed, for example, increasing the average distance between the amide dipoles of different polymer chains could decrease the average strength of dipolar interactions. Weaker dipolar interactions would allow faster relaxation of the PnPOZ chain backbones towards equilibrium crystalline structures. Additionally, the three carbon atoms in the propyl side chain has been reported as the critical number between amorphous and crystalline poly(2-oxazolines) (Demirel et al., 2016). The balance between amorphous PnPOZ and crystalline PnPOZ might be broken because of the involvement of HP. The loss of the second melting peak might be explained by thermal damage to the polyamide at higher temperatures which would also explain the loss of melting peak of PiPOZ in the second cycle after quenching. Although the specific crystallinity of PnPOZ in solid dispersions cannot be calculated because pure PnPOZ is amorphous, it can be seen from the enlargement of Figure S7c that PnPOZ crystallinity increases with increasing PnPOZ-HP molar ratio from 1:1 to 5:1. Nevertheless, it became amorphous again at 15:1 where the drug also became amorphous, probably because the drug content was below a level where it impacted on the gross structure of PnPOZ.

All T_g of PMOZ-HP SD, PiPOZ-HP SD and PEOZ-HP SD and PnPOZ-HP SD at 15:1 were below the T_g of the pure polymer (Fig. 7). The decreased T_g was likely resulting from plasticization caused by the interaction of the polymer with drug molecules.

PVP is often used as a standard for preparing solid dispersions due to its high hydrophilicity and ability to form stable dispersions (Chadha et al., 2006; Sharma and Jain, 2010). However, there are some reports introducing poly(2-oxazolines) such as PEOZ as dispersion carriers (Boel et al., 2019; Fael et al., 2018). Therefore, PEOZ, PMOZ, PnPOZ and PiPOZ were studied and compared with each other and with PVP. The drug crystallinity in polymer-haloperidol solid dispersions was

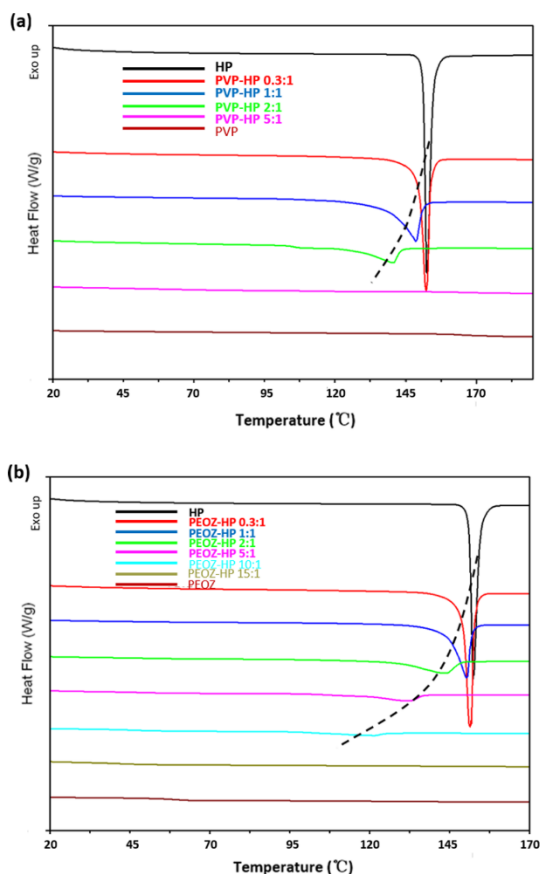


Fig. 6. DSC thermograms of PVP-HP (a) and PEOZ-HP (b) solid dispersions. Dashed curve shows the trend in the endothermic events.

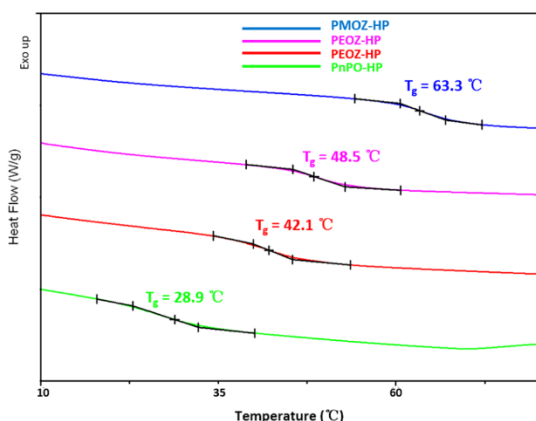


Fig. 7. DSC thermograms of solid dispersions formed by PMOZ, PiPOZ, PEOZ and PnPOZ at [polymer]/[drug] = 15:1 M ratio.

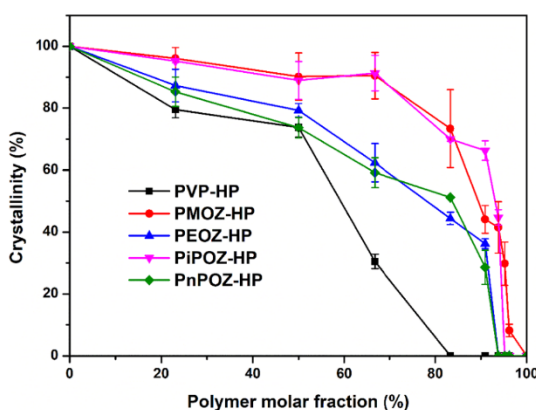


Fig. 8. Crystallinity of polymer-HP solid dispersions as a function of polymer molar fraction.

calculated by the specific enthalpy of the melting peak. As can be seen from Fig. 8, HP crystallinity was reduced in all dispersions with PVP and was essentially amorphous at a molar ratio of 5:1. By contrast, the HP in solid dispersions with poly(2-oxazolines) had a lower propensity to be disordered and was amorphous at the higher polymer-drug ratio of 15:1.

The differing effects are believed to result from the stronger hydrogen-accepting ability of PVP compared to POZ. Oxygen atoms in the tertiary amide group of PVP and nitrogen atoms in the tertiary amide group of POZ can act as hydrogen acceptors to interact with the hydroxyl group of haloperidol via hydrogen bonding. However, the convex and conspicuous cyclic amide group of PVP provides a steric environment that allows its carbonyl group to be more available for hydrogen bonding than the nitrogen atom on the backbone of POZ.

The ability of poly(2-oxazolines) and PVP to reduce the crystallinity of haloperidol has shown an interesting trend that is partially influenced by the hydrophobic-hydrophilic balance (HHB) of each polymer. The most hydrophilic PMOZ (HHB = 3.95) has poor ability to reduce crystallinity of haloperidol. The two more hydrophobic members of poly(2-oxazoline) family, PEOZ (HHB = 5.02) and PnPOZ (HHB = 6.10), have similar and better ability to reduce drug crystallinity. This is logical as non-polar haloperidol molecules will be more likely molecularly dispersed in the hydrophobic domains of PEOZ and PnPOZ. It is

interesting to note that PVP has a hydrophobic-hydrophilic balance intermediate between PEOZ and PnPOZ (HHB 5.42), but its ability to reduce drug crystallinity is superior compared to these two polymers. This is possibly related to its better capability to form hydrogen bonds with haloperidol as discussed above.

The ability of PiPOZ, whose HHB is similar to PnPOZ due to their structural isomerism (HHB = 6.10), to reduce drug crystallinity is as poor as the most hydrophilic polymer used (PMOZ). The possible reason for this is its semi-crystalline nature, where haloperidol molecules will be less capable of penetrating into densely packed crystalline domains of PiPOZ to form molecular dispersion. Fig. 9 schematically shows the difference in the structure of solid dispersions formed by fully amorphous and semi-crystalline polymers.

3.3. Theoretical evaluation of drug-polymer miscibility

The miscibility between haloperidol and the polymers was estimated using the Fedor and Van Krevelen methods. The calculated solubility parameters for haloperidol, PVP, PMOZ, PEOZ, PnPOZ and PiPOZ are in Table 1.

Compounds with similar values of δ are more likely to be miscible, because the cohesive energy within each component is balanced by the energy released by interactions between the components. It has been demonstrated that two compounds with a $\Delta\delta$ less than $7.0 \text{ MPa}^{1/2}$ are likely to be miscible in the molten state whereas compounds with $\Delta\delta > 10.0 \text{ MPa}^{1/2}$ are likely to be immiscible (Greenhalgh et al., 1999). It can be seen from Table 1 that all the polymers are expected to be miscible with haloperidol with $\Delta\delta$ values ranging from 0.4 to 2.5. Interestingly, solubility parameters for PEOZ and PnPOZ most closely match that of haloperidol, and these polymers showed greatest crystallinity inhibition compared to the other poly(2-oxazolines). However, the discrepancy in $\Delta\delta$ with PVP is 2, yet this polymer showed the greatest crystallinity inhibition efficiency; again, this probably results from hydrogen bond formation between PVP macromolecules and the drug which was absent when using the poly(2-oxazolines) carriers. Further, it should be noted that the solubility parameter approach only considers contact energies between the components and does not allow for the effects of entropy or the free volume of the amorphous state (Jankovic et al., 2019).

3.4. Phase diagrams

According to the Flory-Huggins polymer solution theory (Flory, 1953), a drug-polymer temperature-composition phase diagram can be constructed if the change in drug-polymer interaction parameter χ with temperature is known. The relationship between the melting temperature of the pure drug (T_m^0) and the depressed melting point of the drug in the drug-polymer system (T_m) can be described by the following equation (Huang and Dai, 2014; Lin and Huang, 2010; Moseson and Taylor, 2018):

$$\frac{1}{T_m} - \frac{1}{T_m^0} = -\frac{R}{\Delta H} \left(\ln \phi + \left(1 - \frac{1}{m}\right)(1 - \phi) + \chi(1 - \phi)^2 \right) \quad (5)$$

where R is the gas constant ($8.31 \text{ J/mol}\cdot\text{K}$), ΔH is the heat of fusion of the pure drug, ϕ is the volume fraction of the drug in the solid dispersion (i. e., drug loading), m is the volume ratio between polymer and drug, and χ is the drug-polymer interaction parameter representing the difference between the drug-polymer contact interaction and the average self-contact interactions of drug-drug and polymer-polymer (Huang and Dai, 2014). A negative χ indicates that the interaction between a polymer and a drug is stronger than the attraction within polymer-polymer and drug-drug pairs. More negative values of χ indicate better affinity between the polymer and the drug and, for example, could be caused by hydrogen bonding between the drug and the polymer. Positive χ values indicate that drug molecules and polymer segments have stronger affinity to interact with those of their own kind rather than interacting

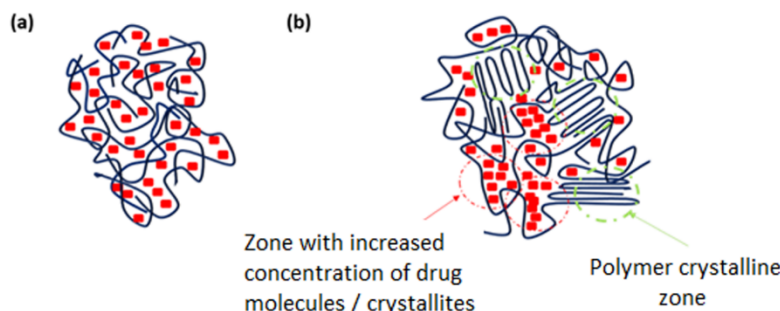


Fig. 9. Structures of solid dispersions formed by fully amorphous (a) and semi-crystalline (b) polymers. Red tetragonal symbols represent drug molecules and curved lines represent polymer chains.

Table 1
Solubility parameters of drug and polymers.

Drug and polymers	Solubility parameters (δ) (MPa ^{1/2})				$\Delta\delta$	Group classification
	Fedor method	Van Krevelen Method	Average			
Haloperidol	24.3	24.0	24.2			
PVP	26.0	26.3	26.2	2.0		Miscible
PMOZ	26.3	27.0	26.7	2.5		Miscible
PEOZ	24.7	24.5	24.6	0.4		Miscible
PnPOZ	23.7	22.9	23.3	0.9		Miscible
PiPOZ	23.3	22.5	22.9	1.		Miscible
				3		

with each other (Lin and Huang, 2010).

Eq. (5) can be rearranged (Moseson and Taylor, 2018):

$$\left(-\frac{\Delta H}{R}\right)\left(\frac{1}{T_m} - \frac{1}{T_m^0}\right) - \left[\ln \phi + \left(1 - \frac{1}{m}\right)(1 - \phi)\right] = \chi(1 - \phi)^2 \quad (6)$$

$$A = \chi \times B$$

where A and B values can be derived from melting point depression data. Thus, by measuring melting points of drugs in solid dispersion at different drug/polymer ratios, a series of A and B values can be generated at different T_m . By plotting A versus B, a χ value can be obtained (Figure S9, Supplementary information) and used to predict T_m at any drug/polymer ratio according to Eq. (5).

The Gordon-Taylor relationship has been used to predict the glass transition in a polymer-drug mixture $T_{g\text{mix}}$ (Hancock and Zografi, 1994; Verma and Rudraraju, 2014):

$$T_{g\text{mix}} = \frac{W_1 T_{g1} + K W_2 T_{g2}}{W_1 + K W_2} \quad K = \frac{T_{g1} \rho_1}{T_{g2} \rho_2} \quad (7)$$

where T_g is glass transition temperature, W_1 and W_2 are the weight fractions of components 1 and 2, and K is calculated from the densities (ρ) and T_g of the respective components.

The data generated through the use of the Flory-Huggins theory and Gordon-Taylor relationship can be used to build the complete phase diagrams (Fig. 10).

Good agreement of the experimental data and modeled liquid-solid phase transition curve is observed. The negative values of $\chi = -2.40$ for PVP-HP, $\chi = -1.21$ for PEOZ-HP and $\chi = -0.76$ for PnPOZ-HP indicate that these polymer-HP systems are miscible. It is worth noting that the interaction parameter of PVP-HP system showed the most negative value, again related to hydrogen bonding between the drug and polymer chains. However, the A versus B plots for PMOZ-HP and PiPOZ-HP solid dispersions did not give a linear trend (Figure S9, Supplementary information) so a single interaction parameter could not be determined and the phase diagram for these systems could not be built.

The interaction parameters at polymer-HP = 10:1 and 15:1 mol/mol were positive values, meaning that PMOZ-HP and PiPOZ-HP were not fully miscible. Therefore, based on the values of χ , the solid dispersions can be arranged in the following order from greater drug-polymer interaction to minimal interaction: PVP-HP > PEOZ-HP \approx PnPOZ-HP > PiPOZ-HP \approx PMOZ-HP. It can be clearly seen that this order is consistent with the crystallinity inhibition efficiency of these polymers discussed in Section 3.2.

The predicted melting temperature T_m forms the liquid-solid phase transition curve in the phase diagram. The experimental results are in good agreement with the predicted T_m values, but the experimental T_g deviates significantly from the predicted values. This deviation could be related to the presence of specific interactions between the drug molecules and macromolecules. Positive deviations from predicted relationships is typical for strongly interactive systems (Kawakami et al., 2012), whereas negative deviation is observed when the drug-polymer interaction is weaker than drug-drug interaction. Additionally, the presence of water traces in the solid dispersion could contribute to a negative deviation due to plasticization effects (Müllertz et al., 2016).

The liquid-solid phase transition curves were extrapolated to Drug Weight Fraction = 0 (dashed red curves in Fig. 10). When this curve intersects the T_g curve this allows estimation of the solubility of HP in PVP, PEOZ and PnPOZ at temperatures where the saturated solutions exist at T_g . It can be seen from Fig. 10a that the solubility of HP in PVP is approximately 40% w/w at 122 °C and this saturated solution exists at T_g . However, the saturated PEOZ-HP and PnPOZ-HP solutions do not exist at T_g . At room temperature of 25 °C, which is characterized by $T < T_m$ and $T < T_g$, these drug/polymer solutions are able to crystallize.

3.5. In vitro dissolution studies

The dissolution profiles of HP and polymer-HP (all 5:1 mol/mol) solid dispersions are presented in Fig. 11. The dissolution of pure HP within 120 min was below 70%, with 57% released in the first 20 min. As expected from the crystallinity data (Fig. 8), the fastest dissolution was observed from solid dispersions with PVP where haloperidol is essentially amorphous: over 90% of the drug was released in the first 20 mins. Drug release from solid dispersions with poly(2-oxazolines) was slower compared to PVP, but (other than PnPOZ) faster than HP alone. The release data reflected the fraction of the drug that was amorphous in the dispersions. Thus, solid dispersions with PEOZ which contains ~56%:44% amorphous:crystalline haloperidol gave around 80% of the drug released in 20 mins. Dispersions formed with PMOZ and PiPOZ contain approximately 30% of the drug in an amorphous form and gave statistically similar release profiles with around 70% drug released in 20 mins. Again, surprising results were observed for solid dispersions with PnPOZ. Fig. 8 shows this system contains approximately 50% of the drug in an amorphous form and so it was expected to exhibit release performance similar to PEOZ; however, its solid dispersions showed even

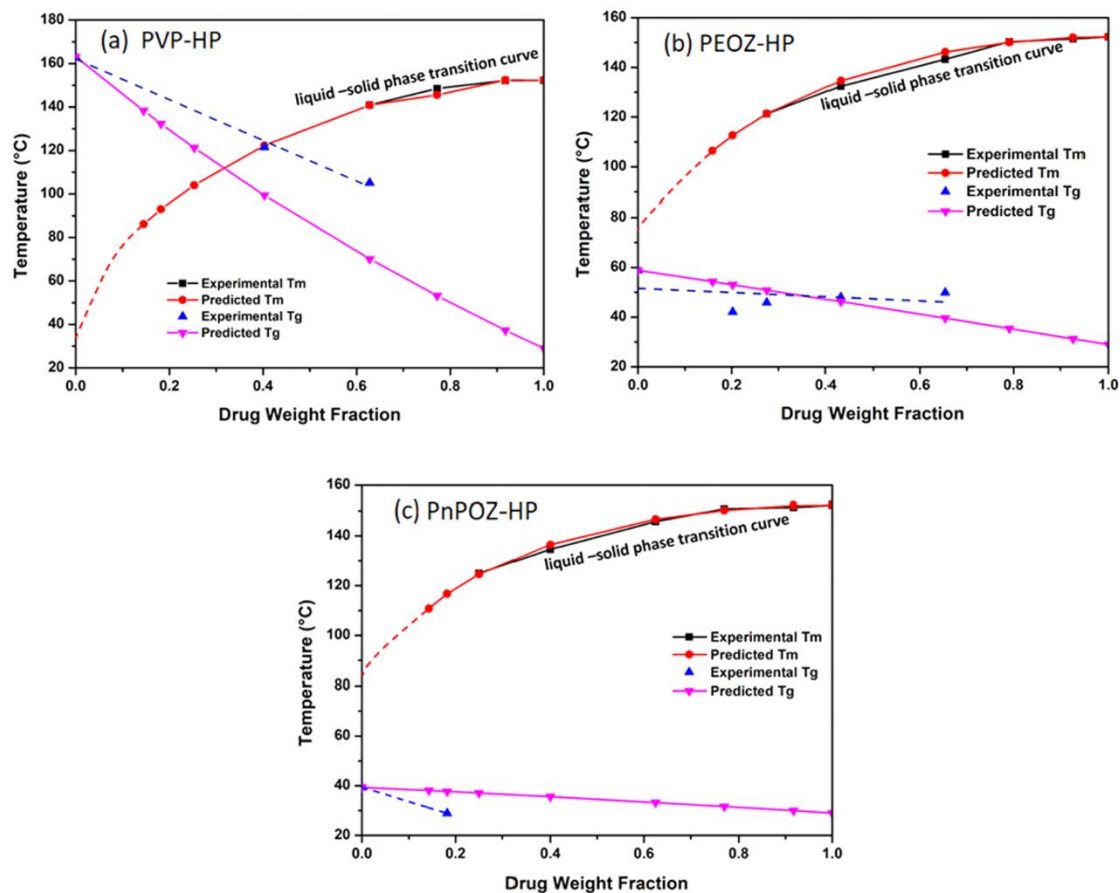


Fig. 10. Temperature-composition phase diagrams of polymer-haloperidol solid dispersions showing the experimental and predicted melting temperatures T_m (liquid-solid phase transition curve) as well as experimental and predicted glass transition temperatures. Error bars reflect one standard deviation ($n = 3$) but are within the symbols for the experimental results.

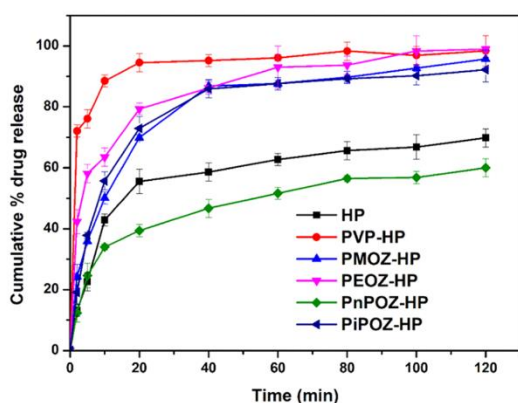


Fig. 11. Dissolution profiles of pure haloperidol and from different polymer-haloperidol solid dispersions. Cumulative % drug release with standard error of mean has been plotted against time.

slower dissolution compared to pure crystalline haloperidol, with less than 40% released in 20 mins. This unexpected result could be explained by the Lower Critical Solution Temperature (LCST) in this polymer at $\sim 25^\circ\text{C}$ (Bouten et al., 2015; Park and Kataoka, 2007) which is much lower than the temperature used in the dissolution studies (37°C). Under these conditions PnPOZ remains insoluble in the dissolution medium, which limits drug release from these solid dispersions. Clearly by using polymers that inhibit haloperidol crystallisation, then the generation of supersaturated systems at the dissolution surface or within the bulk fluid is a possibility (Han and Lee, 2017).

Potentially, more detailed dissolution study of these formulations will be of interest in the future, for example, to evaluate the extent of haloperidol supersaturation on the evolution of kinetic solubility profiles (Han and Lee, 2017).

4. Conclusion

A series of poly(2-oxazolines) were synthesized in this work by hydrolysis of poly(2-ethyl-2-oxazoline) into poly(ethylene imine) and its subsequent reaction with acetic, butyric and isobutyric anhydrides. These polymers were fully characterized using ^1H NMR and FTIR spectroscopies, differential scanning calorimetry and powder X-ray diffraction.

Solid dispersions of haloperidol were prepared using these poly(2-oxazolines) and poly(N-vinyl pyrrolidone). Polymer structure and properties were found to influence the crystallinity of the drug and its release from solid dispersions. Poly(N-vinyl pyrrolidone) was superior in its ability to reduce crystallinity of haloperidol and gave rapid drug release from solid dispersions. This is related to its ability to form hydrogen bonds with the drug molecules and also with its relatively high hydrophobicity. An increase in the hydrophobicity in a series of poly(2-oxazolines) also favored drug crystallinity reduction. However, poly(2-isopropyl-2-oxazoline) has shown very poor ability to reduce crystallinity of haloperidol, which is related to a semi-crystalline nature of this polymer. The theoretical analysis of these solid dispersions using solubility parameters, Flory-Huggins polymer solution theory and the Gordon-Taylor relationship provided results which are in good agreement with the experimental data.

The dissolution studies indicated good agreement with the levels of drug crystallinity in solid dispersions. However, solid dispersions with poly(n-propyl-2-oxazoline) were found to release drug very slowly due to its lower critical solution temperature and hence insolubility of this polymer in the dissolution medium. By synthesizing polymers with equivalent degrees of polymerization, the effects of polymer hydrophobic-hydrophilic properties, their semi-crystalline nature, hydrogen bonding strengths, and lower critical solution temperature (influencing polymer solubility) on the structure of solid dispersions and drug release have been demonstrated. Our studies show that, when selecting a carrier for solid dispersions, it is important to consider not only the hydrogen bonding capabilities of the polymer but also its broader properties including their semi-crystallinity, steric properties and lower critical solution temperatures.

CRedit authorship contribution statement

Xiaoning Shan: Methodology, Investigation, Validation, Writing - original draft. **Adrian C. Williams:** Writing - review & editing, Supervision. **Vitaliy V. Khutoryanskiy:** Conceptualization, Writing - review & editing, Supervision.

Declaration of Competing Interest

The authors declare that they have no known competing financial interests or personal relationships that could have appeared to influence the work reported in this paper.

Acknowledgments

The authors are grateful to the University of Reading and China Scholarship Council (201707040071) for funding the PhD studentship of X.S. The assistance of staff at the Chemical Analysis Facility (CAF, University of Reading) with ¹H-NMR, DSC and PXRD experiments is also acknowledged. The authors are also grateful to Prof Kenneth Shankland for his help in PXRD experiments and valuable advice in interpreting crystallinity data.

Appendix A. Supplementary data

Supplementary data to this article can be found online at <https://doi.org/10.1016/j.ijpharm.2020.119884>.

References

- Abu-Diak, O.A., Jones, D.S., Andrews, G.P., 2012. Understanding the performance of melt-extruded poly(ethylene oxide)-bicalutamide solid dispersions: characterisation of microstructural properties using thermal, spectroscopic and drug release methods. *J. Pharm. Sci.* 101, 200–213.
- Ali, W., Williams, A.C., Rawlinson, C.F., 2010. Stoichiometrically governed molecular interactions in drug: Poloxamer solid dispersions. *Int. J. Pharm.* 391, 162–168.

- Baird, J.A., Taylor, L.S., 2011. Evaluation and modeling of the eutectic composition of various drug-polyethylene glycol solid dispersions. *Pharm. Dev. Technol.* 16, 201–211.
- Blagden, N., de Matas, M., Gavan, P.T., York, P., 2007. Crystal engineering of active pharmaceutical ingredients to improve solubility and dissolution rates. *Adv. Drug Deliv. Rev.* 59, 617–630.
- Boel, E., Smeets, A., Vergaelen, M., De la Rosa, V.R., Hoogenboom, R., Mooter, G.V.D., 2019. Comparative study of the potential of poly(2-ethyl-2-oxazoline) as carrier in the formulation of amorphous solid dispersions of poorly soluble drugs. *Eur. J. Pharm. Biopharm.* 144, 79–90.
- Boerman, M.A., Van der Laan, H.L., Bender, J.C.M.E., Hoogenboom, R., Jansen, J.A., Leeuwenburgh, S.C., Van Hest, J.C.M., 2016. Synthesis of pH- and thermoresponsive poly(2-n-propyl-2-oxazoline) based copolymers. *J. Polym. Sci., Part A: Polym. Chem.* 54, 1573–1582.
- Bouten, P.J.M., Lava, K., Van Hest, J.C.M., Hoogenboom, R., 2015. Thermal properties of methyl ester-containing poly(2-oxazolines). *Polymers* 7 (10), 1998–2008. <https://doi.org/10.3390/polym7101494>.
- Brough, C., Williams 3rd, R.O., 2013. Amorphous solid dispersions and nano-crystal technologies for poorly water-soluble drug delivery. *Int. J. Pharm.* 453, 157–166.
- Bruno C. Hancock, Zografis, G., 1994. The relationship between the glass transition temperature and the water content of amorphous pharmaceutical solids. *Pharmaceutical research* 11, 471–477.
- Carrier, R.L., Miller, L.A., Ahmed, I., 2007. The utility of cyclodextrins for enhancing oral bioavailability. *J. Controlled Release* 123, 78–99.
- Chadha, R., Kapoor, V.K., Kumar, A., 2006. Analytical techniques used to characterize drug-polyvinylpyrrolidone systems in solid and liquid states-An overview. *J. Sci. Ind. Res.* 65, 459–469.
- Chaparro, C., Moreno, D., Ramirez, V., Fajardo, A., González, D., Sanín, A., Grueso, R., 2013. Haloperidol as prophylactic treatment for postoperative nausea and vomiting: systematic literature review. *Rev. Colomb. Anestesiol.* 41, 34–43.
- Chavan, R.B., Rathi, S., Jyothi, V.G.S.S., Shastri, N.R., 2019. Cellulose based polymers in development of amorphous solid dispersions. *Asian J. Pharm. Sci.* 14, 248–264.
- Chokshi, R.J., Sandhu, H.K., Iyer, R.M., Shah, N.H., Malick, A.W., Zia, H., 2005. Characterization of physico-mechanical properties of indomethacin and polymers to assess their suitability for hot-melt extrusion process as a means to manufacture solid dispersion/solution. *J. Pharm. Sci.* 94, 2463–2474.
- Conceicao, J., Adeoye, O., Cabral-Marques, H.M., Lobo, J.M.S., 2018. Cyclodextrins as excipients in tablet formulations. *Drug Discovery Today* 23, 1274–1284.
- de la Rosa, V.R., 2014. Poly(2-oxazolines) as materials for biomedical applications. *Journal of materials science. Mater. Med.* 25, 1211–1225.
- Demirel, A.L., Meyer, M., Schlaad, H., 2007. Formation of polyamide nanofibers by directional crystallization in aqueous solution. *Angew. Chem. Int. Ed.* 46, 8622–8624.
- Demirel, A.L., Tatar Güner, P., Verbraeken, B., Schlaad, H., Schubert, U.S., Hoogenboom, R., 2016. Revisiting the crystallization of poly(2-alkyl-2-oxazolines). *J. Polym. Sci., Part B: Polym. Phys.* 54, 721–729.
- Demoen, 1961. Properties and analysis of haloperidol and its dosage forms. *J. Pharm. Sci.* 50, 350–353.
- Fael, H., Rafols, C., Demirel, A.L., 2018. Poly(2-ethyl-2-oxazoline) as an alternative to poly(vinylpyrrolidone) in solid dispersions for solubility and dissolution rate enhancement of drugs. *J. Pharm. Sci.* 107, 2428–2438.
- Fedors, R.F., 1974. A method for estimating both the solubility parameters and molar volumes of liquids. *Polymer Eng. Sci.* 14, 147–154.
- Flory, P.J., 1953. Principles of polymer chemistry. Cornell University Press.
- Funtan, S., Evgrafova, Z., Adler, J., Huster, D., Binder, W.H., 2016. Amyloid beta aggregation in the presence of temperature-sensitive polymers. *Polymers* 8 (5), 178. <https://doi.org/10.3390/polym8050178>.
- Gatica, N., Soto, L., Moraga, C., Vergara, L., 2013. Blends of poly(N-vinyl-2-pyrrolidone) and dihydric phenols: thermal and infrared spectroscopic studies. Part IV. *J. Chilean Chem. Soc.* 58, 2048–2052.
- Glassner, M., Vergaelen, M., Hoogenboom, R., 2018. Poly(2-oxazolines): a comprehensive overview of polymer structures and their physical properties. *Polym. Int.* 67, 32–45.
- Greenhalgh, D.J., Williams, A.C., Timmins, P., 1999. Solubility parameters as predictors of miscibility in solid dispersions. *J. Pharm. Sci.* 88, 1182–1190.
- Groom, C.R., Bruno, I.J., Lightfoot, M.P., Ward, S.C., 2016. The Cambridge structural database. *Acta Crystallographica Sect. B, Struct. Sci., Crystal Eng. Mater.* 72, 171–179.
- Han, Y.R., Lee, P.I., 2017. Effect of extent of supersaturation on the evolution of kinetic solubility profiles. *Mol. Pharm.* 14, 206–220.
- He, Y., Ho, C., Yang, D., Chen, J., Orton, E., 2017. Measurement and accurate interpretation of the solubility of pharmaceutical salts. *J. Pharm. Sci.* 106, 1190–1196.
- He, Y., Zhu, B., Inoue, Y., 2004. Hydrogen bonds in polymer blends. *Prog. Polym. Sci.* 29, 1021–1051.
- Hoogenboom, R., 2009. Poly(2-oxazolines): a polymer class with numerous potential applications. *Angew. Chem.* 48, 7978–7994.
- Huang, Y., Dai, W.G., 2014. Fundamental aspects of solid dispersion technology for poorly soluble drugs. *Acta Pharmaceutica Sinica B* 4, 18–25.
- Jankovic, S., Tsakiridou, G., Ditzinger, F., Koehl, N.J., Price, D.J., Ilie, A.R., Kalantzis, L., Kimpe, K., Holm, R., Nair, A., Griffin, B., Saal, C., Kuentz, M., 2019. Application of the solubility parameter concept to assist with oral delivery of poorly water-soluble drugs - a PEARRL review. *J. Pharm. Pharmacol.* 71, 441–463.
- Kalepu, S., Nekkanti, V., 2015. Insoluble drug delivery strategies: review of recent advances and business prospects. *Acta Pharmaceutica Sinica B* 5, 442–453.

- Kawakami, K., Usui, T., Hattori, M., 2012. Understanding the glass-forming ability of active pharmaceutical ingredients for designing supersaturating dosage forms. *J. Pharm. Sci.* 101, 3239–3248.
- Khutoryanskiy, V.V., Mun, G.A., Nurkeeva, Z.S., Dubolazov, A.V., 2004. pH and salt effects on interpolymer complexation via hydrogen bonding in aqueous solutions. *Polym. Int.* 53, 1382–1387.
- Kim, J.Y., Kim, S., Papp, M., Park, K., Pinal, R., 2010. Hydrotropic solubilization of poorly water-soluble drugs. *J. Pharm. Sci.* 99, 3953–3965.
- Knopp, M.M., Nguyen, J.H., Becker, C., Francke, N.M., Jorgensen, E.B., Holm, P., Holm, R., Mu, H., Rades, T., Langguth, P., 2016. Influence of polymer molecular weight on in vitro dissolution behavior and in vivo performance of celecoxib:PVP amorphous solid dispersions. *Eur. J. Pharmaceut. Biopharmaceut.* 101, 145–151.
- Krause, M., Huhn, M., Schneider-Thoma, J., Rothe, P., Smith, R.C., Leucht, S., 2018. Antipsychotic drugs for elderly patients with schizophrenia: A systematic review and meta-analysis. *Eur. Neuropsychopharmacol.: J. Eur. College Neuropsychopharmacol.* 28, 1360–1370.
- Krevelen, D.W.V., 1990. Properties of polymers. Elsevier 189–221.
- Lambermont-Thijs, H.M.L., Bonami, L., Prez, F.E.D., Hoogenboom, R., 2010. Linear poly(alkyl ethylene imine) with varying side chain length. Synthesis and physical properties. *Polym. Chem.* 1, 747–754.
- Lee, H.L., Vasoya, J.M., Criqueira, M.L., Yeh, K.L., Lee, T., Serajuddin, A.T., 2017. Continuous preparation of 1:1 haloperidol-maleic acid salt by a novel solvent-free method using a twin screw melt extruder. *Mol. Pharm.* 14, 1278–1291.
- Li, T., Tang, H., Wu, P., 2015. Molecular evolution of poly(2-isopropyl-2-oxazoline) aqueous solution during the liquid-liquid phase separation and phase transition process. *Langmuir: ACS J. Surf. Colloids* 31, 6870–6878.
- Li, W., Buckton, G., 2015. Using DVS-NIR to assess the water sorption behaviour and stability of a griseofulvin/PVP K30 solid dispersion. *Int. J. Pharm.* 495, 999–1004.
- Lin, D., Huang, Y., 2010. A thermal analysis method to predict the complete phase diagram of drug-polymer solid dispersions. *Int. J. Pharm.* 399, 109–115.
- Litt, M., Levy, A., Herz, J., 1975. Polymerization of cyclic imino ethers. X. Kinetics, chain transfer, and repolymerization. *J. Macromol. Sci.: Part A – Chem.* 9, 703–727.
- Lorson, T., Lübtow, M.M., Wegener, E., Haider, M.S., Borova, S., Nahm, D., Jordan, R., Sokolski-Papkov, M., Kabanov, A.V., Luxenhofer, R., 2018. Poly(2-oxazoline)s based biomaterials: a comprehensive and critical update. *Biomaterials* 178, 204–280.
- Mees, M., Haladjova, E., Momekova, D., Momekov, G., Shestakova, P.S., Tsvetanov, C.B., Hoogenboom, R., Rangelov, S., 2016. Partially hydrolyzed poly(n-propyl-2-oxazoline): synthesis, aqueous solution properties, and preparation of gene delivery systems. *Biomacromolecules* 17, 3580–3590.
- Morrison, P.W., Connon, C.J., Khutoryanskiy, V.V., 2013. Cyclodextrin-mediated enhancement of riboflavin solubility and corneal permeability. *Mol. Pharm.* 10, 756–762.
- Moseson, D.E., Taylor, L.S., 2018. The application of temperature-composition phase diagrams for hot melt extrusion processing of amorphous solid dispersions to prevent residual crystallinity. *Int. J. Pharm.* 553, 454–466.
- Moustafine, R.I., Viktorova, A.S., Khutoryanskiy, V.V., 2019. Interpolymer complexes of carbopol(R) 971 and poly(2-ethyl-2-oxazoline): physicochemical studies of complexation and formulations for oral drug delivery. *Int. J. Pharm.* 558, 53–62.
- Müllertz, A., Perrie, Y., Rades, T., 2016. Analytical techniques in the pharmaceutical sciences. Springer, ISSN 2192-6204.
- Niemczyk, A.I., Williams, A.C., Rawlinson-Malone, C.F., Hayes, W., Greenland, B.W., Chappell, D., Khutoryanskiy, A., Timmins, P., 2012. Novel polyvinylpyrrolidones to improve delivery of poorly water-soluble drugs: from design to synthesis and evaluation. *Mol. Pharm.* 9, 2237–2247.
- Oleszko, N., Utrata-Wesotek, A., Watach, W., Libera, M., Hercog, A., Szeluga, U., Domański, M., Trzebicka, B., Dworak, A., 2015. Crystallization of poly(2-isopropyl-2-oxazoline) in organic solutions. *Macromolecules* 48, 1852–1859.
- Ozeki, T., Yuasa, H., Kanaya, Y., 1997. Application of the solid dispersion method to the controlled release of medicine. IX. Difference in the release of flurbiprofen from solid dispersions with poly(ethylene oxide) and hydroxypropylcellulose and the interaction between medicine and polymers. *Int. J. Pharm.* 155, 209–217.
- Park, J.-S., Kataoka, K., 2007. Comprehensive and accurate control of thermosensitivity of poly(2-alkyl-2-oxazoline)s via well-defined gradient or random copolymerization. *Macromolecules* 40 (10), 3599–3609.
- Qu, X., Khutoryanskiy, V.V., Stewart, A., Rahman, S., Papahadjopoulos-Sternberg, B., Christine Dufes, D.M., Clive G. Wilson, R.L., Carter, K.C., Schätzlein, A., Uchegbu, I. F., 2006. Carbohydrate-based micelle clusters which enhance hydrophobic drug bioavailability by up to 1 order of magnitude. *Biomacromolecules* 7, 3452–3459.
- Rawlinson, C.F., Williams, A.C., Timmins, P., Grimsey, I., 2007. Polymer-mediated disruption of drug crystallinity. *Int. J. Pharm.* 336, 42–48.
- Ruiz-Rubio, L., Alonso, M.L., Perez-Alvarez, L., Alonso, R.M., Vilas, J.L., Khutoryanskiy, V.V., 2018. Formulation of carbopol(R)/poly(2-ethyl-2-oxazoline) mucoadhesive tablets for buccal delivery of hydrocortisone. *Polymers* 10.
- Saegusa, T., Ikeda, H., Fujii, H., 1972. Crystalline Polyethylenimine. *Macromolecules* 5, 108–108.
- Saluja, H., Mehanna, A., Panicucci, R., Atef, E., 2016. Hydrogen bonding: between strengthening the crystal packing and improving solubility of three haloperidol derivatives. *Molecules* 21.
- Santos, O.M.M., Reis, M.E.D., Jacon, J.T., Lino, M.E.d.S., Simões, J.S., Doriguetto, A.C., 2014. Polymorphism: an evaluation of the potential risk to the quality of drug products from the Farmácia Popular Rede Própria. *Brazilian J. Pharm. Sci.* 50, 1–24.
- Sedlacek, O., Janouskova, O., Verbraeken, B., Hoogenboom, R., 2019a. Straightforward route to superhydrophilic poly(2-oxazoline)s via acylation of well-defined polyethylenimine. *Biomacromolecules* 20, 222–230.
- Sedlacek, O., Monnery, B.D., Hoogenboom, R., 2019b. Synthesis of defined high molar mass poly(2-methyl-2-oxazoline). *Polym. Chem.* 10, 1286–1290.
- Sessa, D.J., Woods, K.K., Mohamed, A.A., Palmquist, D.E., 2011. Melt-processed blends of zein with polyvinylpyrrolidone. *Ind. Crops Prod.* 33, 57–62.
- Shah, A., Serajuddin, A.T., 2015. Conversion of solid dispersion prepared by acid-base interaction into free-flowing and tabletable powder by using Neusilin(R) US2. *Int. J. Pharm.* 484, 172–180.
- Sharma, A., Jain, C.P., 2010. Preparation and characterization of solid dispersions of carvedilol with PVP K30. *Res. Pharm. Sci.* 5, 49–56.
- Singh, A., Van den Mooter, G., 2016. Spray drying formulation of amorphous solid dispersions. *Adv. Drug Deliv. Rev.* 100, 27–50.
- Singh, S., Parikh, T., Sandhu, H.K., Shah, N.H., Malick, A.W., Singhal, D., Serajuddin, A. T., 2013. Supersolubilization and amorphization of a model basic drug, haloperidol, by interaction with weak acids. *Pharm. Res.* 30, 1561–1573.
- Solanki, N.G., Tahsin, M., Shah, A.V., Serajuddin, A.T.M., 2018. Formulation of 3D printed tablet for rapid drug release by fused deposition modeling: screening polymers for drug release, drug-polymer miscibility and printability. *J. Pharm. Sci.* 107, 390–401.
- Vasconcelos, T., Marques, S., das Neves, J., Sarmiento, B., 2016. Amorphous solid dispersions: Rational selection of a manufacturing process. *Adv. Drug Deliv. Rev.* 100, 85–101.
- Verma, S., Rudraraju, V.S., 2014. A systematic approach to design and prepare solid dispersions of poorly water-soluble drug. *AAPS PharmSciTech* 15, 641–657.
- Volkova, T., Kumeev, R., Kochkina, N., Terekhova, I., 2019. Impact of Pluronic of different structure on pharmacologically relevant properties of sulfasalazine and methotrexate. *J. Mol. Liq.* 289, 111076.
- Wiesbrock, F., Hoogenboom, R., Leenen, M.A.M., Meier, M.A.R., Schubert, U.S., 2005. Investigation of the living cationic ring-opening polymerization of 2-methyl-, 2-ethyl-, 2-nonyl-, and 2-phenyl-2-oxazoline in a single-mode microwave reactor. *Macromolecules* 38, 5025–5034.
- Williams, A.C., Timmins, P., Lu, M., Forbes, R.T., 2005. Disorder and dissolution enhancement: deposition of ibuprofen on to insoluble polymers. *Eur. J. Pharm. Sci.: Off. J. Eur. Federation Pharm. Sci.* 26, 288–294.
- Yasir, M., Singh Sara, U.V., Som, I., Singh, L., 2016. Development and validation of a new HPLC method for in-vitro studies of haloperidol in solid lipid nanoparticles. *J. Anal. Bioanal. Techniques* 7, 339.
- Zayed, Y., Barbarawi, M., Kheiri, B., Banifadel, M., Haykal, T., Chahine, A., Rashdan, L., Aburahma, A., Bachuwa, G., Seedahmed, E., 2019. Haloperidol for the management of delirium in adult intensive care unit patients: A systematic review and meta-analysis of randomized controlled trials. *J. Crit. Care* 50, 280–286.

Supporting information to the paper

Polymer structure and property effects on amorphous solid dispersions with haloperidol:

poly(N-vinyl pyrrolidone) and poly(2-oxazolines) studies

Xiaoning Shan, Adrian C. Williams, Vitaliy V. Khutoryanskiy*

Reading School of Pharmacy, University of Reading, Whiteknights, PO
Box 224, Reading RG66AD, United Kingdom, email:
v.khutoryanskiy@reading.ac.uk

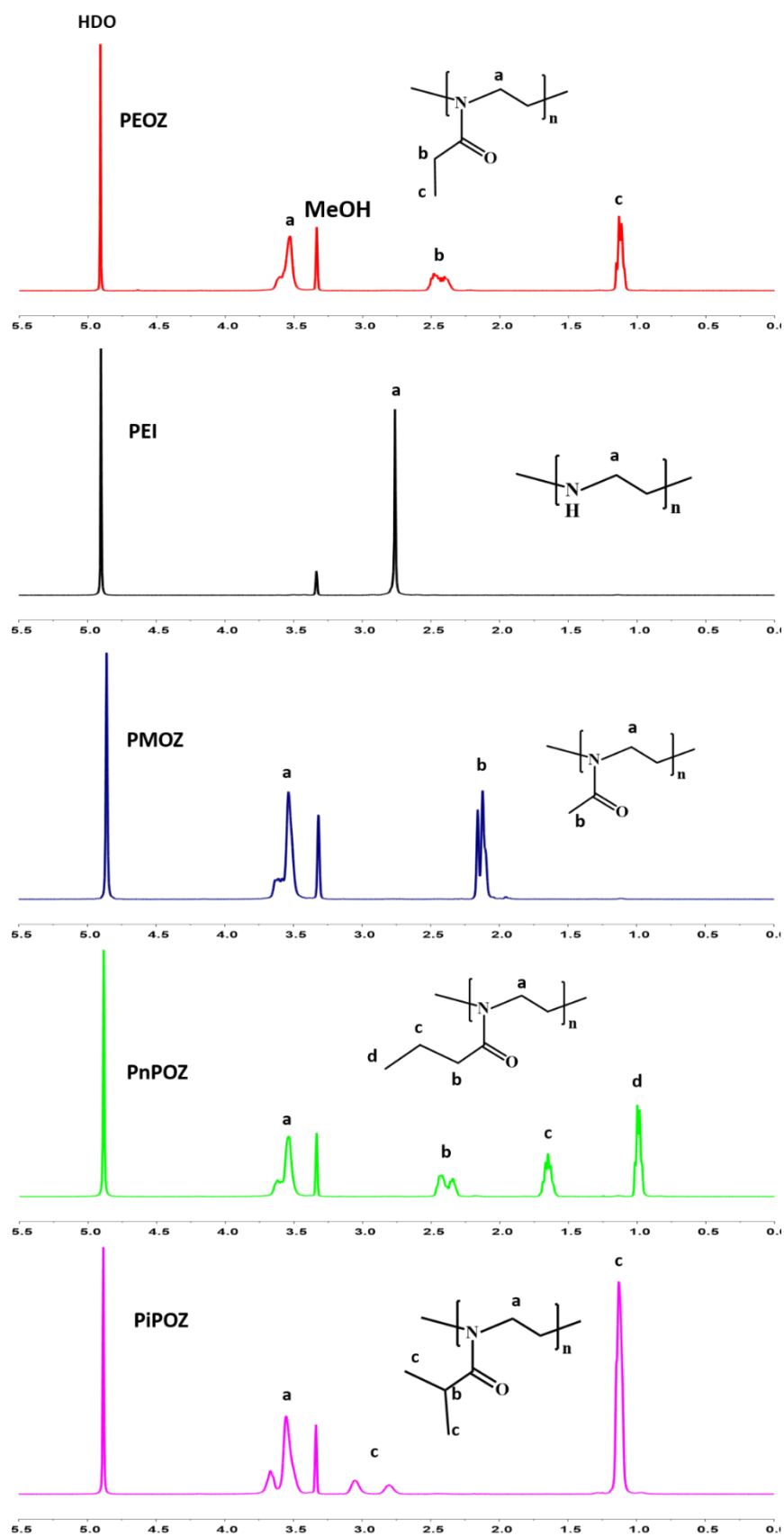


Fig. S1. ^1H -NMR spectra of synthesized PMOZ, PnPOZ and PiPOZ in

CD₃OD.

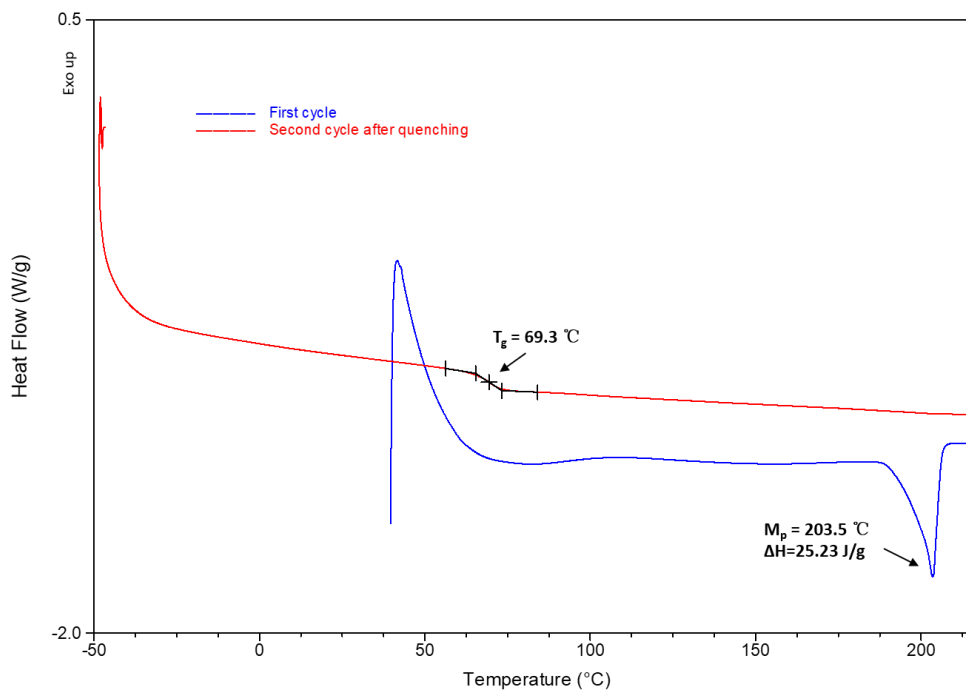


Fig. S2. DSC trace of PiPOZ, at a heating rate of 10 °C/min. The first run started from 25 °C to 220 °C, the second run after quenching started from -50 °C to 220 °C.

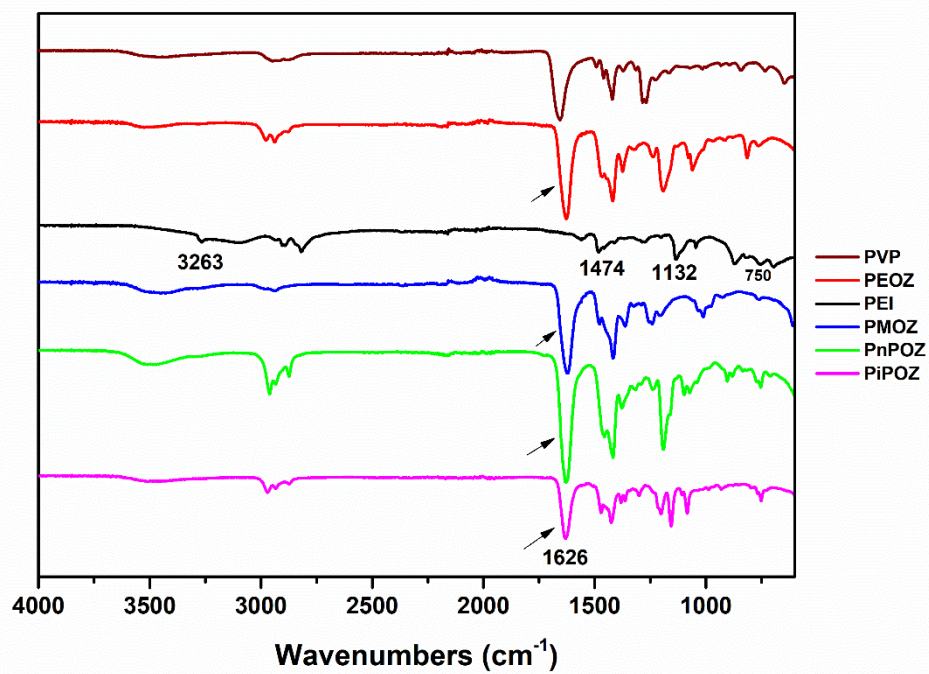
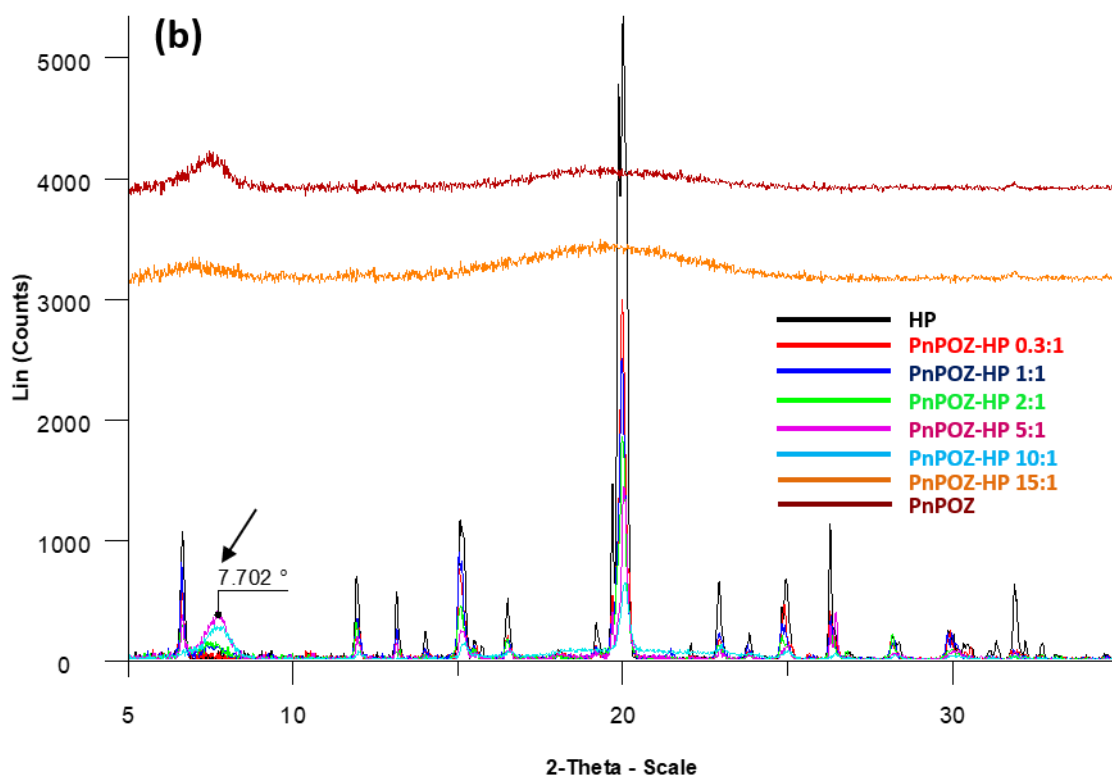
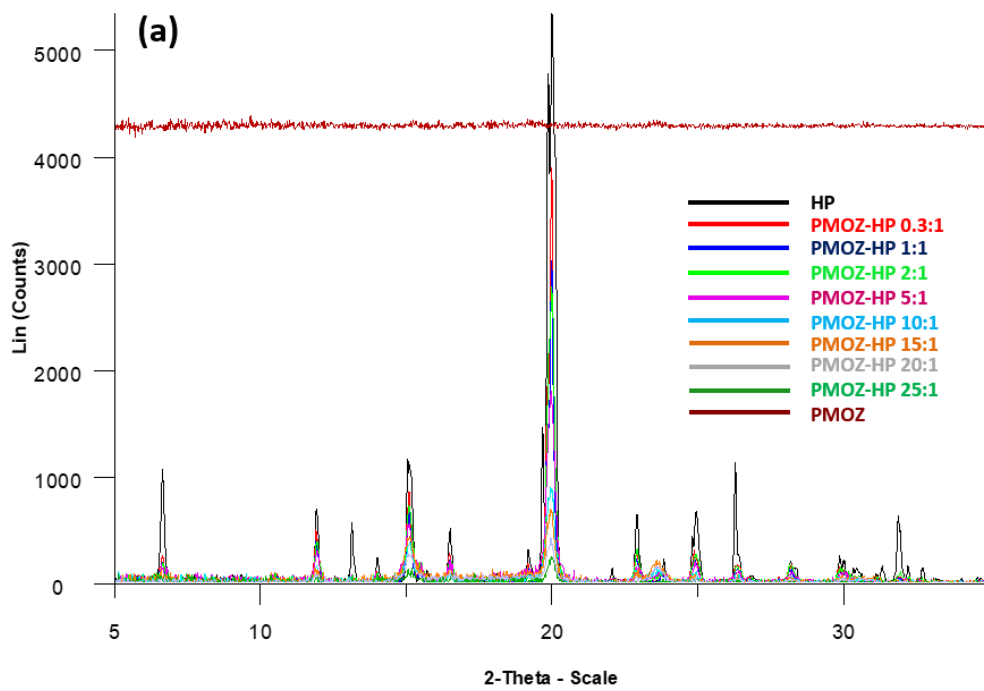


Fig. S3. FTIR spectra of PVP, PEOZ and synthesized PEI, PMOZ, PnPOZ and PiPOZ. Spectra are offset for clarity.



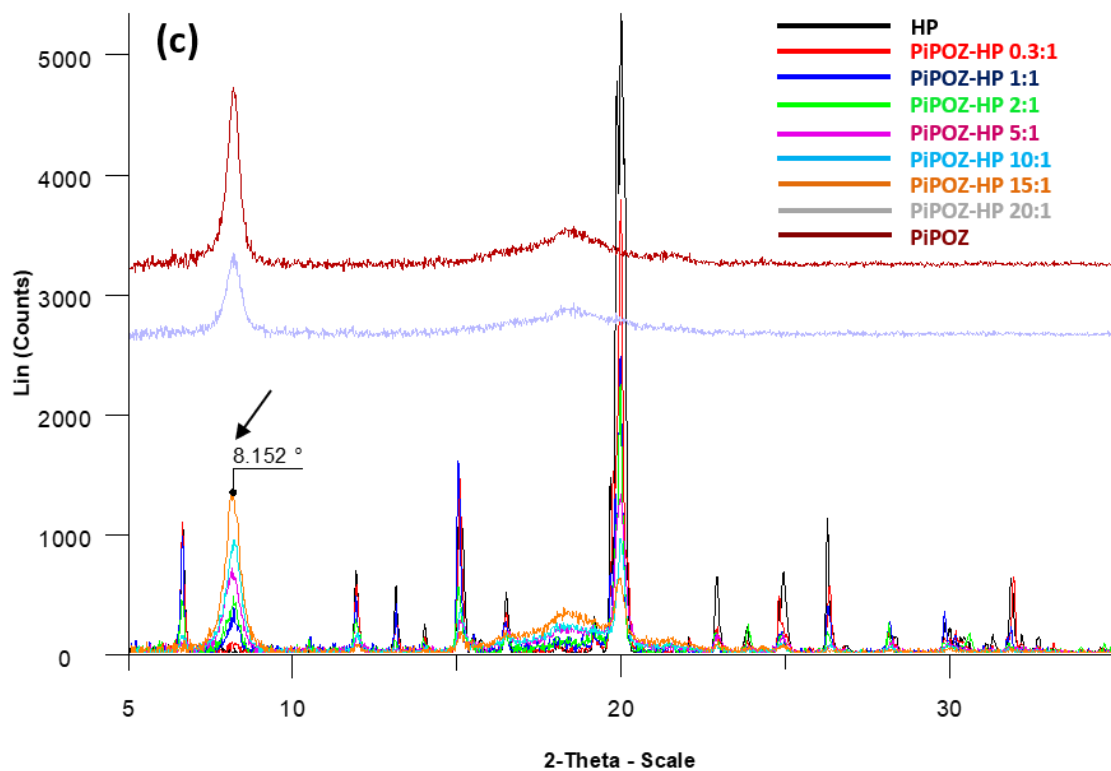
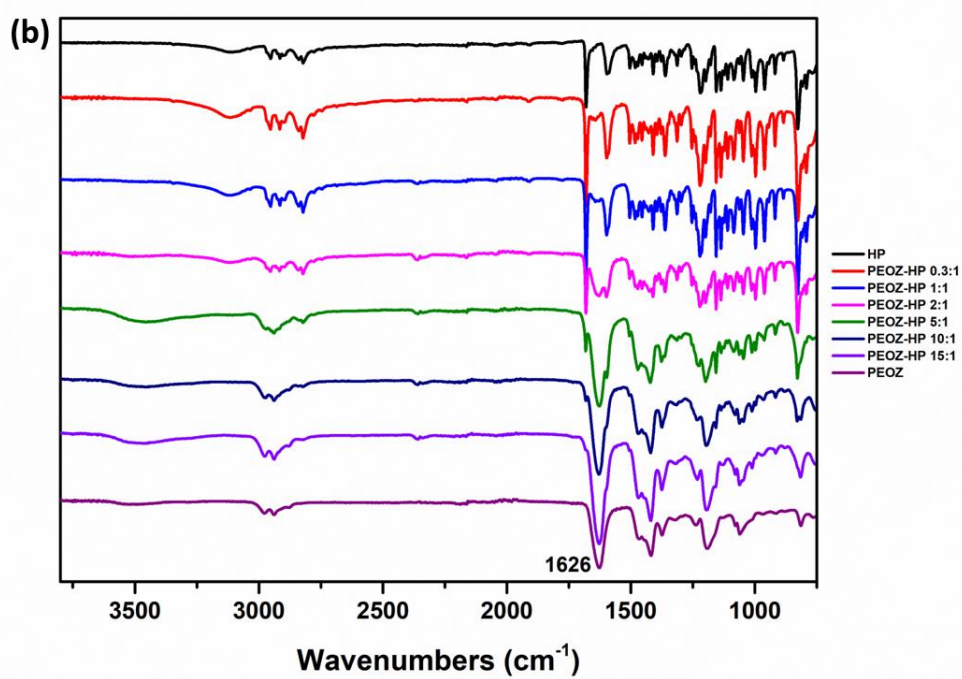
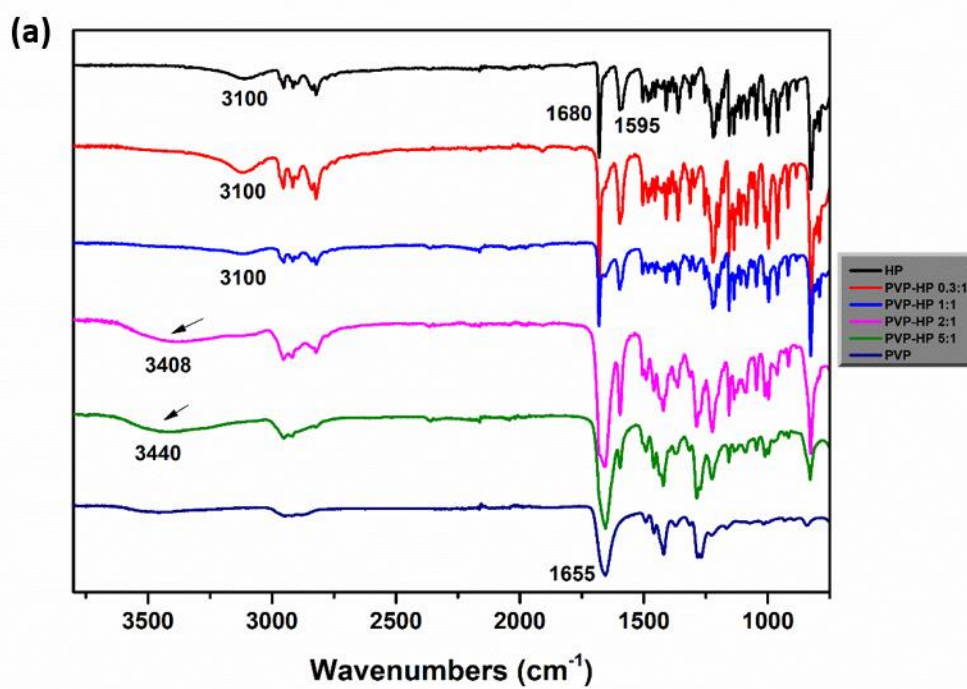
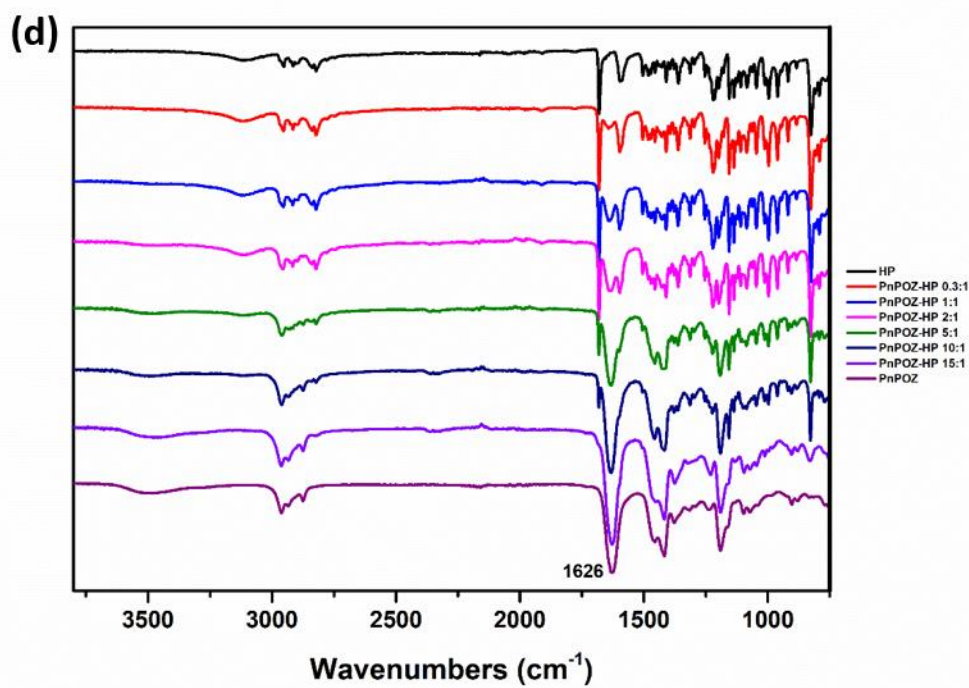
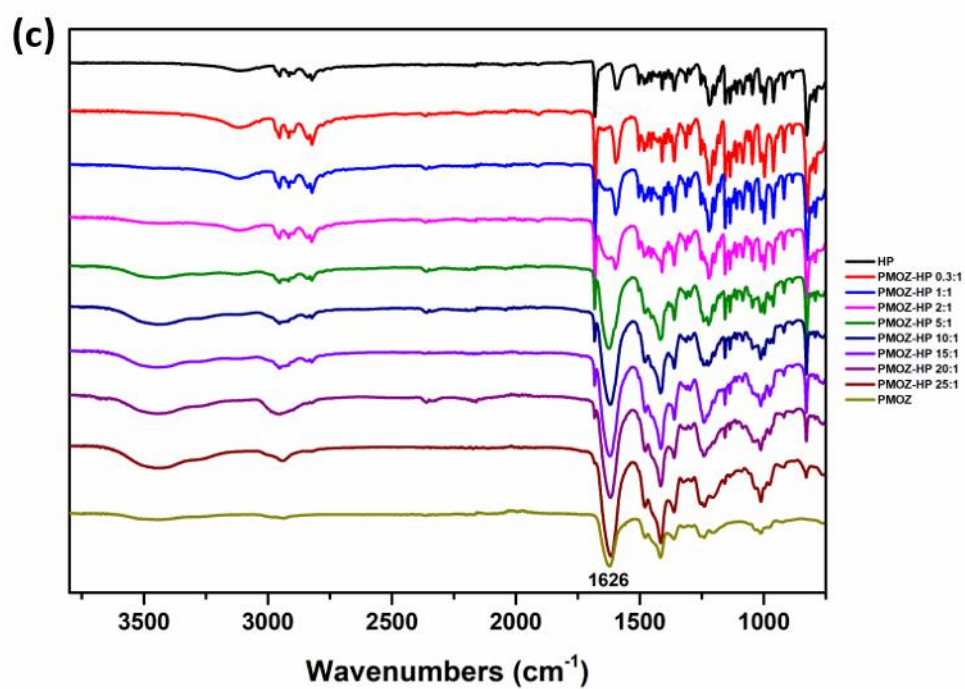


Fig. S4. X-ray diffraction patterns of PMOZ-HP SDs (a), PnPOZ-HP SDs (b) and PiPOZ-HP SDs (c). Patterns are offset for clarity.





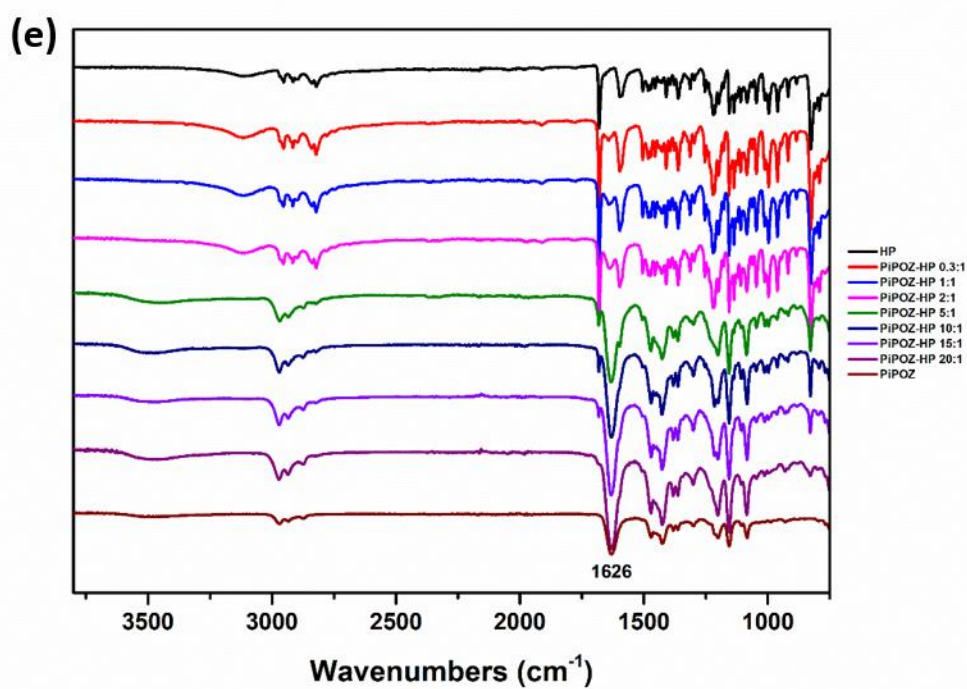


Fig. S5. FTIR spectra of PVP-HP SDs (a), PEOZ-HP SDs (b), PMOZ-HP SDs (c), PnPOZ-HP SDs (d) and PiPOZ-HP SDs (e). Spectra are offset for clarity.

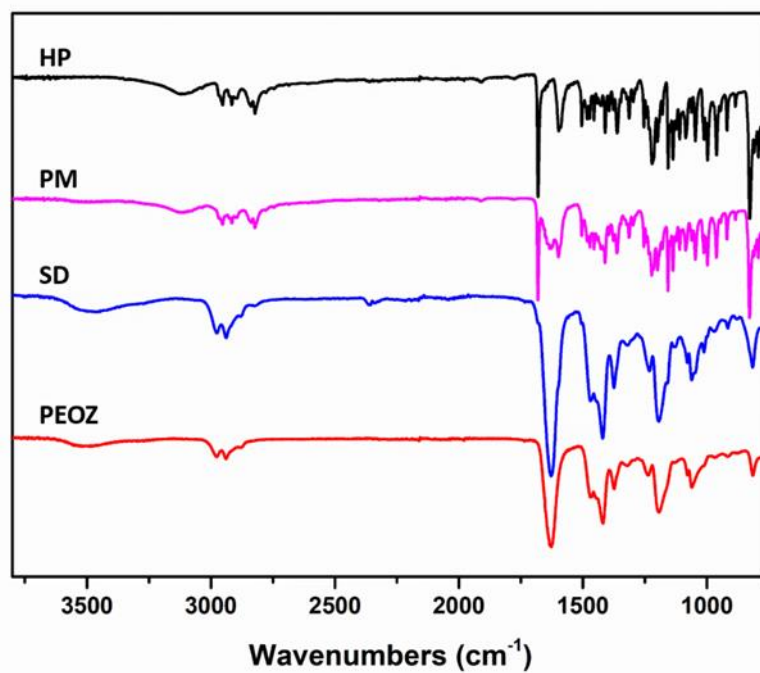
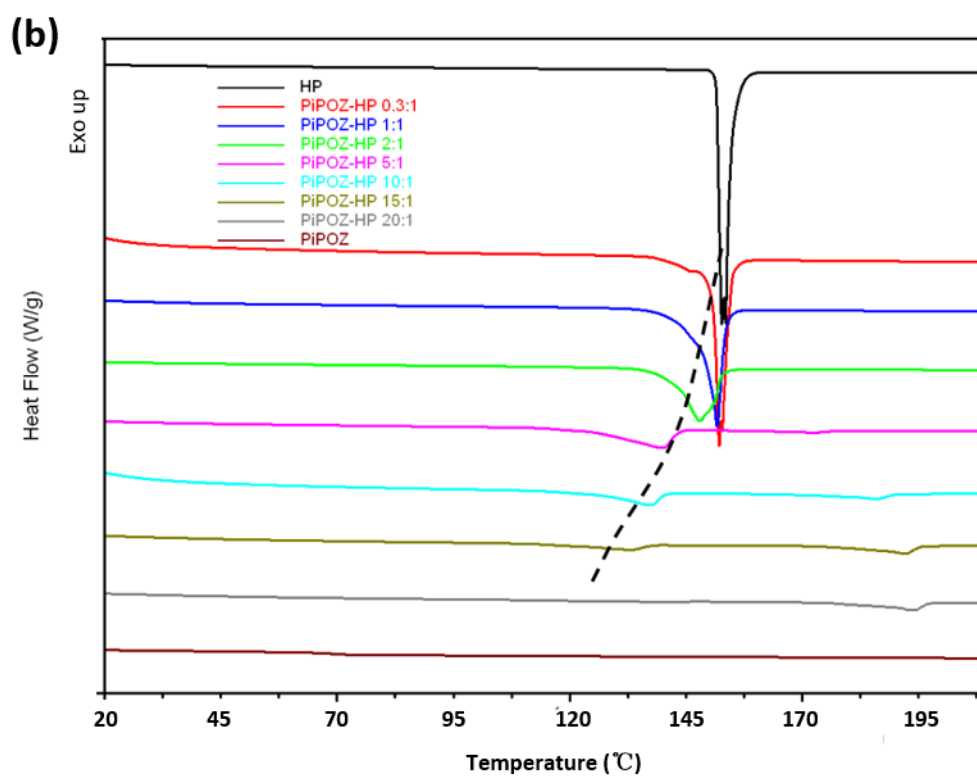
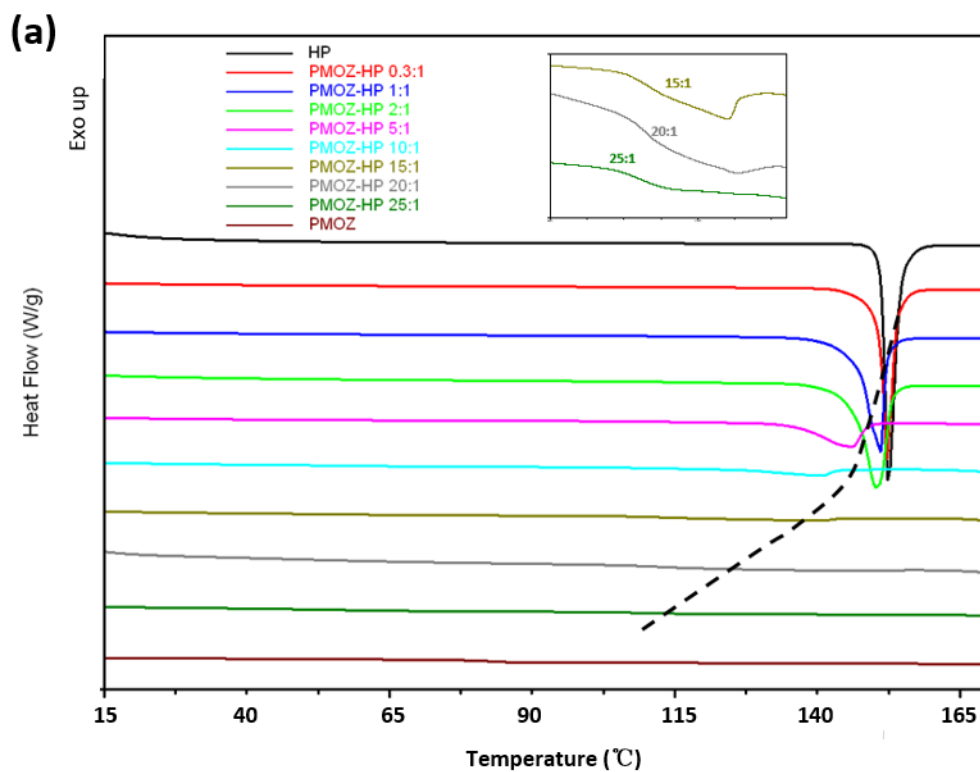


Fig. S6. FTIR spectra of individual PEOZ and HP as well as PEOZ-HP 15:1 mol as physical mixtures (PM) and solid dispersions (SD).



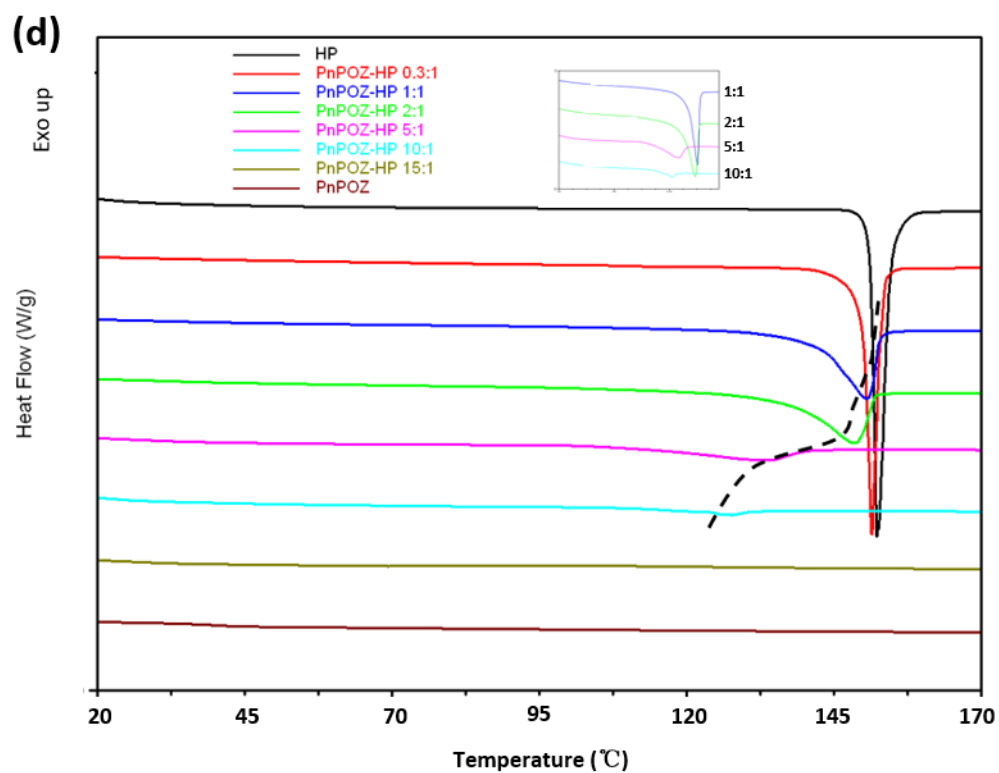
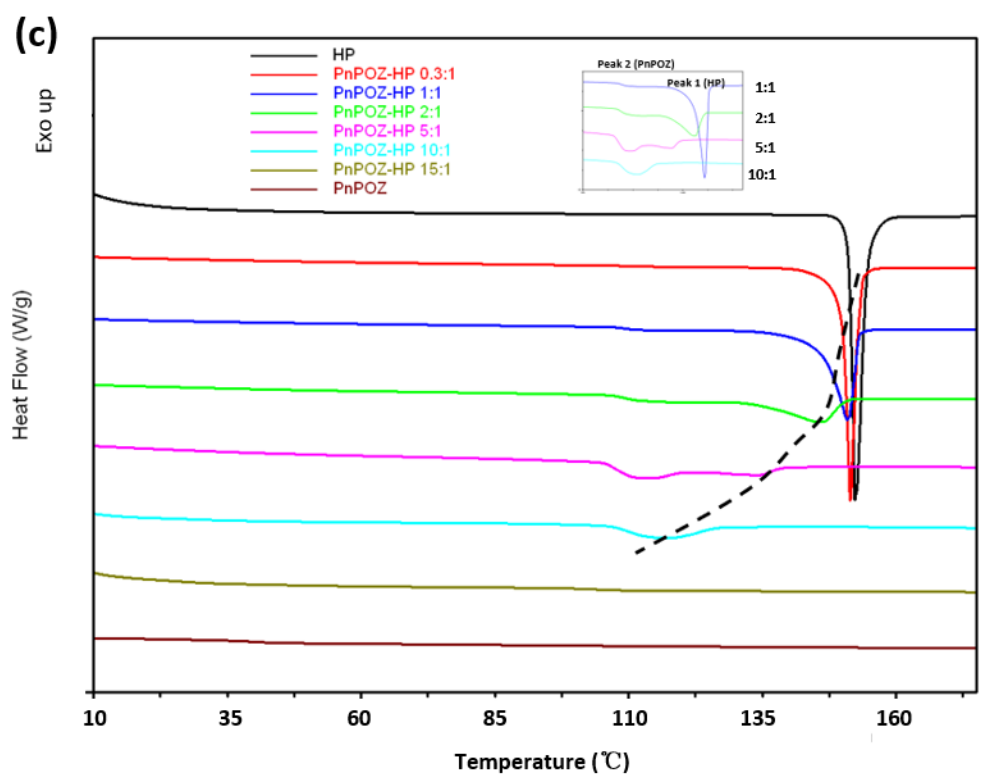


Fig. S7. DSC thermograms of PMOZ-HP SDs (a), PiPOZ-HP SDs (b),

PnPOZ-HP SDs (c) analyzed using Method 1 and PnPOZ-HP SDs (d) analyzed using Method 2. Traces are offset for clarity.

Note 1: Inserts are enlargements at some molar ratios for clarity.

Note 2: All polymer-HP SDs were analysed by heating the sample to 100 °C in the first cycle (Method 1). Samples were also analysed by heating to 120 °C in the first cycle (Method 2). Thermograms for PnPOZ dispersions are obtained by heating to 120 °C in the first cycle (Method 2) whilst all other data is obtained by heating to 100 °C in the first cycle (Method 1).

Table.S1: Melting temperatures of haloperidol in solid dispersions with PnPOZ analysed by two methods.

	Method 1		Method 2
	T _m of Peak 2 (°C)	T _m of Peak 1 (°C)	T _m of Peak (°C)
PnPOZ-HP 1:1	112.5	150.9	150.6
PnPOZ-HP 2:1	112.7	146.2	148.4
PnPOZ-HP 5:1	112.1	134.6	133.5
PnPOZ-HP 10:1		116.2	125.7

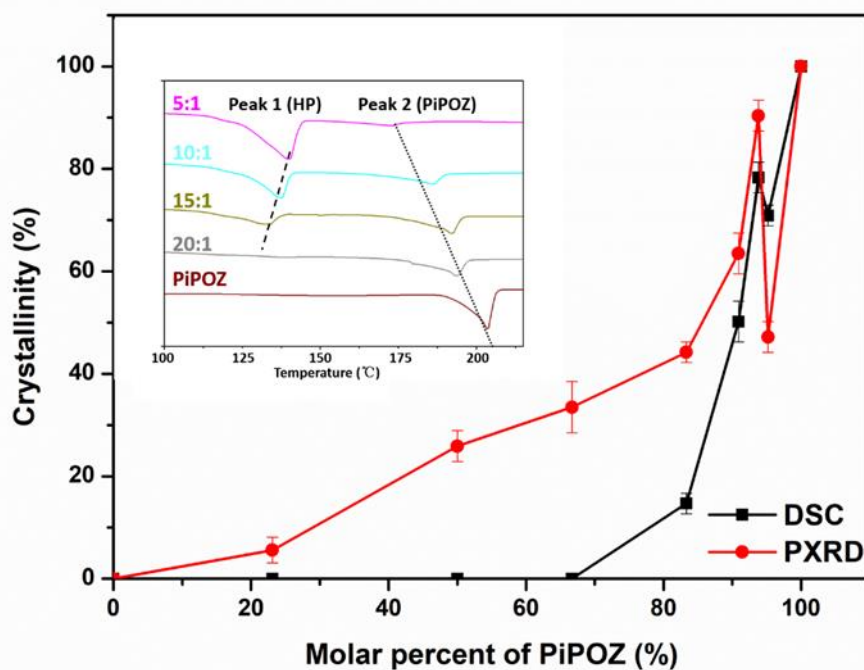


Fig. S8. Crystallinity of PiPOZ in SDs calculated by DSC and PXRD and (insert) enlarged DSC traces of PiPOZ-HP SDs

Table. S2: Crystallinity (%) of PiPOZ calculated from DSC and PXRD data.

Formula	T_m of Peak 2 ($^{\circ}\text{C}$)	ΔH_s (J/g)	Crystallinity (%)	
			DSC	PXRD
PiPOZ-HP 0.3:1	*NA	*NA	*NA	5.6
PiPOZ-HP 1:1	*NA	*NA	*NA	25.9
PiPOZ-HP 2:1	*NA	*NA	*NA	33.5
PiPOZ-HP 5:1	172.5	2.21	14.7	44.2
PiPOZ-HP 10:1	186.4	9.47	50.2	63.5
PiPOZ-HP 15:1	192.2	16.11	78.3	90.4
PiPOZ-HP 20:1	193.9	15.27	70.9	47.2
PiPOZ	203.5	$\Delta H_p = 25.13$ (J/g)	100	100

*NA: not available.

the degree of crystallinity of PiPOZ calculated by PXRD was normalised according to the following equation:

$$\text{Crystallinity (\%)} = \left(\frac{I_s}{I_p} \right) * 100 \quad (\text{S1})$$

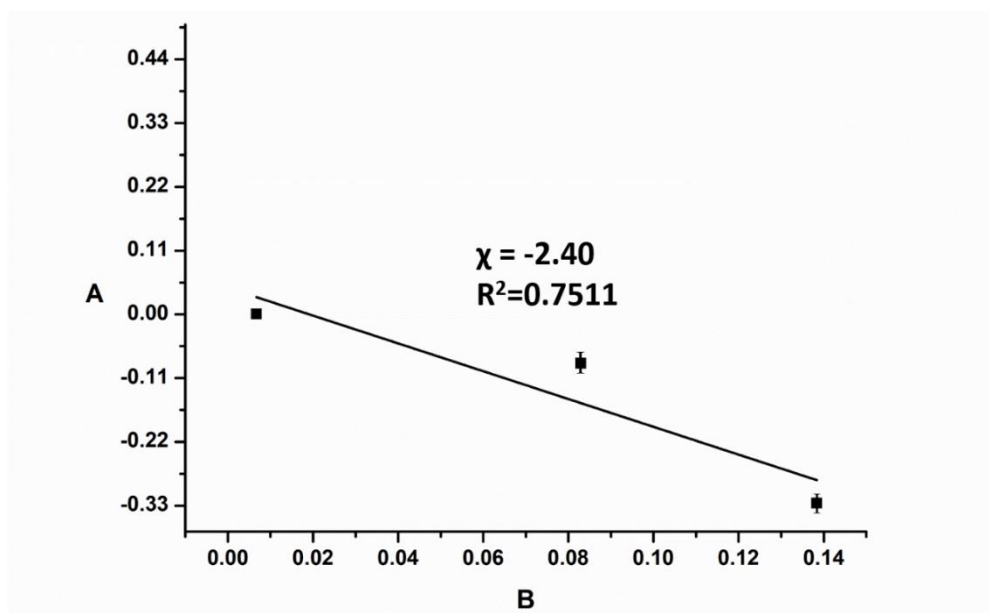
where, I_s is the intensity of the sample at peak $8.152^\circ 2\theta$, I_p is the intensity of the pure PiPOZ at characteristic peak $8.152^\circ 2\theta$.

the degree of crystallinity of PiPOZ calculated by DSC was normalised according to the following equation:

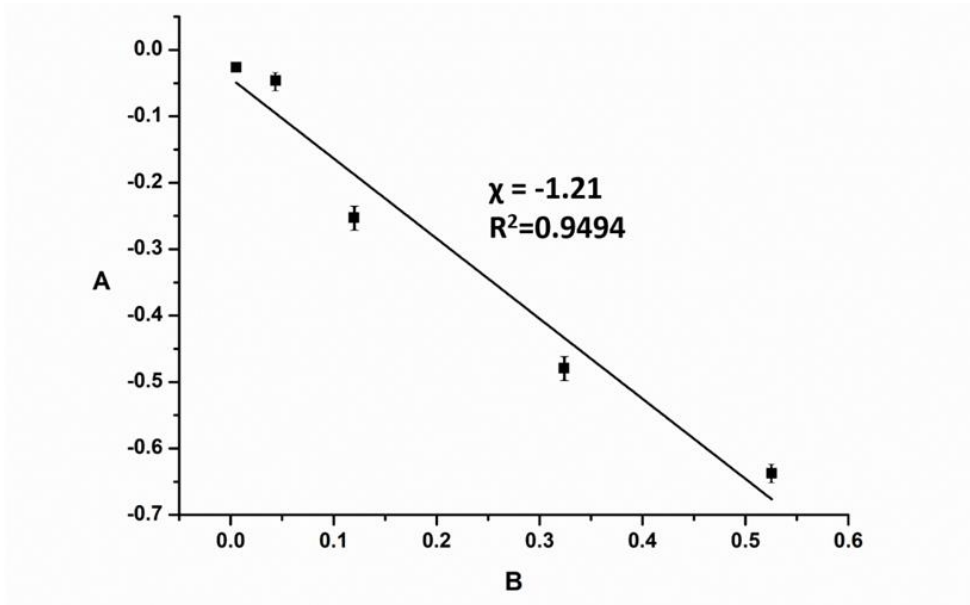
$$\text{Crystallinity (\%)} = \left(\Delta H_s * \frac{W_s}{W_p} \right) / \Delta H_p * 100 \quad (\text{S2})$$

where, ΔH_s is the enthalpy for the melting PiPOZ at around 200°C , ΔH_p is the melting enthalpy of pure PiPOZ, W_s is the weight of SDs, W_p is the weight of PiPOZ in SDs.

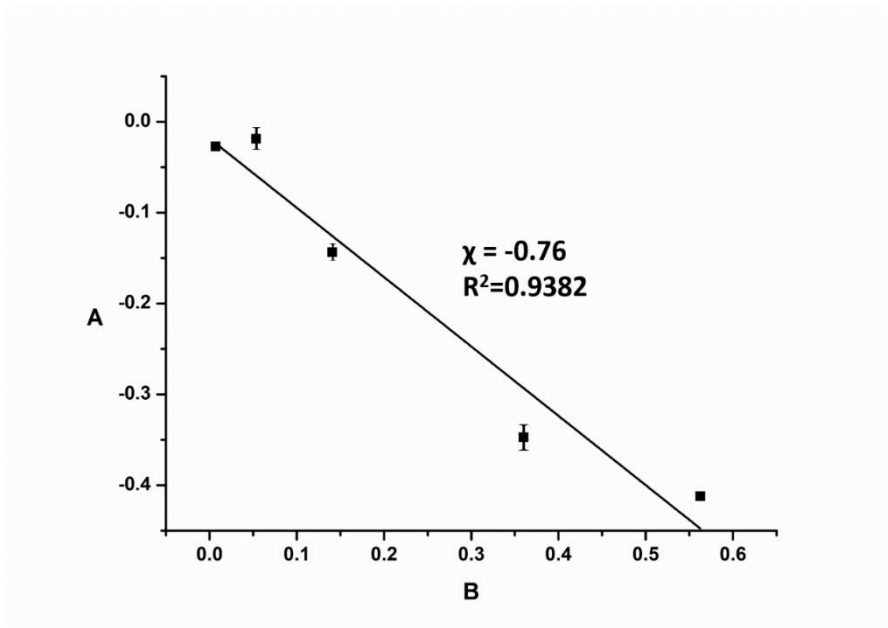
(a)



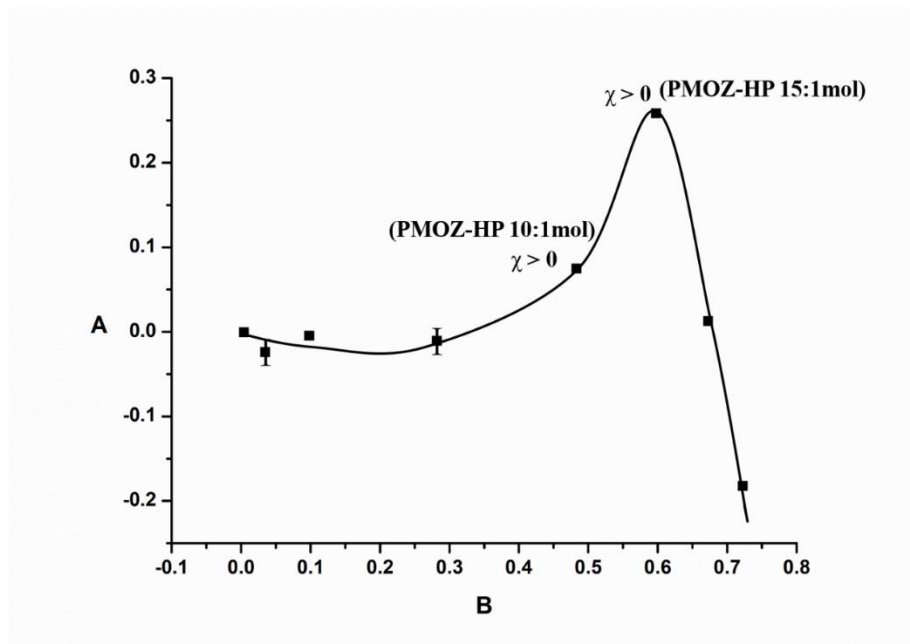
(b)



(c)



(d)



(e)

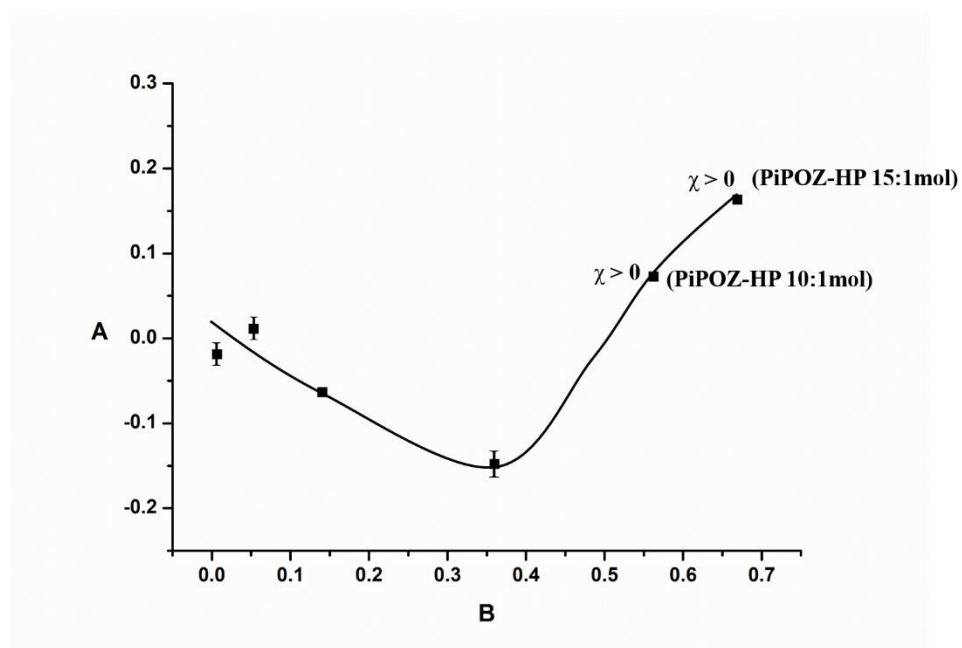


Fig.S9. The A~B plots for PVP-HP (a), PEOZ-HP (b), PnPOZ-HP (c), PMOZ-HP (d) and PiPOZ-HP (e) solid dispersions. Error bars show standard deviation (n=3).

Chapter 3

Mutual Effects of Hydrogen Bonding and Polymer Hydrophobicity on Ibuprofen Crystal Inhibition in Solid Dispersions with Poly(N-vinyl pyrrolidone) and Poly(2-oxazolines)

This chapter was published as Shan, X.; Moghul, M. A.; Williams, A. C.; Khutoryanskiy, V. V., Mutual Effects of Hydrogen Bonding and Polymer Hydrophobicity on Ibuprofen Crystal Inhibition in Solid Dispersions with Poly(N-vinyl pyrrolidone) and Poly(2-oxazolines). *Pharmaceutics* 2021, 13, (5).

Article

Mutual Effects of Hydrogen Bonding and Polymer Hydrophobicity on Ibuprofen Crystal Inhibition in Solid Dispersions with Poly(*N*-vinyl pyrrolidone) and Poly(2-oxazolines)

Xiaoning Shan, Maryam A. Moghul, Adrian C. Williams and Vitaliy V. Khutoryanskiy *

Reading School of Pharmacy, University of Reading, Whiteknights, PO Box 224, Reading RG6 6AD, UK; Xiaoning.Shan@pgr.reading.ac.uk (X.S.); mmoghul.01@gmail.com (M.A.M.); a.c.williams@reading.ac.uk (A.C.W.)

* Correspondence: v.khutoryanskiy@reading.ac.uk; Tel: +44-118-3786119

Abstract: Poly(*N*-vinyl pyrrolidone) (PVP), poly(2-methyl-2-oxazoline) (PMOZ), poly(2-ethyl-2-oxazoline) (PEOZ), poly(2-*n*-propyl-2-oxazoline) (PnPOZ), and poly(2-isopropyl-2-oxazoline) (PiPOZ) were used to prepare solid dispersions with ibuprofen (IB), a model poorly-water soluble drug. Dispersions, prepared by solvent evaporation, were investigated using powder X-ray diffractometry, differential scanning calorimetry, and FTIR spectroscopy; hydrogen bonds formed between IB and all polymers in solid dispersions. PMOZ, the most hydrophilic polymer, showed the poorest ability to reduce or inhibit the crystallinity of IB. In contrast, the more hydrophobic polymers PVP, PEOZ, PnPOZ, and PiPOZ provided greater but similar abilities to reduce IB crystallinity, despite the differing polymer hydrophobicity and that PiPOZ is semi-crystalline. These results indicate that crystallinity disruption is predominantly due to hydrogen bonding between the drug molecules and the polymer. However, carrier properties affected drug dissolution, where PnPOZ exhibited lower critical solution temperature that inhibited the release of IB, whereas drug release from other systems was consistent with the degree of ibuprofen crystallinity within the dispersions.

Keywords: solid dispersions; hydrogen bonding; hydrophobicity; poly(*N*-vinyl pyrrolidone); poly(2-oxazolines); crystallinity; hydrophobic drug; amorphous; ibuprofen

Citation: Shan, X.; Moghul, M.A.; Williams, A.C.; Khutoryanskiy, V.V. Mutual Effects of Hydrogen Bonding and Polymer Hydrophobicity on Ibuprofen Crystal Inhibition in Solid Dispersions with Poly(*N*-vinyl pyrrolidone) and Poly(2-oxazolines). *Pharmaceutics* **2021**, *13*, 659. <https://doi.org/10.3390/pharmaceutics13050659>

Academic Editor: Wouter L. J. Hinrichs

Received: 14 March 2021

Accepted: 28 April 2021

Published: 4 May 2021

Publisher's Note: MDPI stays neutral with regard to jurisdictional claims in published maps and institutional affiliations.



Copyright: © 2021 by the authors. Licensee MDPI, Basel, Switzerland. This article is an open access article distributed under the terms and conditions of the Creative Commons Attribution (CC BY) license (<http://creativecommons.org/licenses/by/4.0/>).

1. Introduction

Whilst oral delivery remains the most common route for drug administration, most new active pharmaceutical ingredients are poorly water soluble and thus not well-absorbed after oral administration. Solid dispersion, defined as the dispersion of one or more active ingredient in a carrier or matrix at solid state, is an established platform technology to enhance the dissolution rate and improve the apparent solubility of a drug and, hence, increase the bioavailability of a range of poorly water soluble drugs [1–3]. Several classes of hydrophilic polymers have been used as carriers to prepare solid dispersions, including PVP [4–6] and its derivatives [7–9], polyethylene glycols [10,11], cellulose ethers [12,13] and poloxamers [14,15].

In solid dispersions, polymer–drug interactions can provide stability to the system by restricting the mobility of the drug molecules in the polymer matrix. Common interactions between drugs and polymers include ionic, hydrophobic, dipole–dipole, Van der Waals, and hydrogen bonding [16–18]. Hydrogen bonding is typically detected between drugs and polymers in solid dispersions, as reported extensively, for example, between IB and PVP [19,20], esomeprazole and hydroxypropyl methylcellulose (HPMC) [21],

flurbiprofen and poly(ethylene oxide) [22], and for nifedipine and Eudragit® [23], indicating that this is a key mechanism in the successful formation of amorphous or semi-crystalline solid dispersions. In contrast, there are relatively few studies exploring the effects of carrier hydrophobicity on crystallization inhibition [16,24,25]. However, research typically focuses on hydrogen bonding or hydrophobicity, with little consideration given to the mutual effects of hydrogen bonding and polymer hydrophobicity on drug crystal inhibition.

Poly(2-oxazolines) have been reported as an alternative to PVP in solid dispersions for solubility and dissolution rate enhancement of poorly-water soluble drugs. For example, Fael et al. [26] found that a lower molecular weight of PEOZ (5000 g/mol) was superior to a higher molecular weight of the polymer (50,000 g/mol) in improving the dissolution behavior of glipizide. Boel et al. [27] showed that PEOZ maintained supersaturation of itraconazole and fenofibrate to a similar extent as PVP, poly(vinylpyrrolidone-co-vinyl acetate) (PVP-VA), and HPMC. Everaerts et al. [28] selected PEOZ, PnPOZ, poly(2-sec-butyl-2-oxazoline) (PsecBuOZ), and a combination of PEOZ with either PnPOZ or PsecBuOZ as carriers for amorphous solid dispersions with six drugs, and highlighted the potential of poly(2-oxazolines) as a novel polymer carrier to form amorphous solid dispersions.

In our previous work [29], PVP and a series of water-soluble poly(2-oxazolines) including PMOZ, PEOZ, PnPOZ, and PiPOZ were used to prepare solid dispersions with haloperidol. The effects of polymer hydrophobicity and their semi-crystalline nature on drug crystallinity were demonstrated. However, hydrogen bonding between haloperidol and poly(2-oxazolines) was almost absent due to the poor hydrogen bond donating ability of the haloperidol hydroxyl group.

In order to explore the impacts of both polymer hydrophobicity and drug-polymer hydrogen bonding, we selected IB, a hydrophobic crystalline drug and strong hydrogen bond donor (because of its carboxylic group), to prepare solid dispersions with poly(2-oxazolines) and PVP. Dispersions were prepared by solvent evaporation and characterized using FTIR spectroscopy, differential scanning calorimetry, and powder X-ray diffractometry. Solubility parameters and Flory-Huggins interaction parameters were calculated to predict drug-polymer miscibility, and drug dissolution studies were conducted to further explore the relationship between IB crystallization inhibition and release from the dispersions.

2. Materials and Methods

2.1. Materials

Poly(2-ethyl-2-oxazoline) (PEOZ), 50 kDa (polydispersity index, PDI 3-4); poly(*N*-vinyl pyrrolidone) (PVP), 55 kDa (K-value 30); and buffer tablets, pH 6.8 were from Sigma-Aldrich (Gillingham, UK). Poly(2-methyl-2-oxazoline) (PMOZ), poly(2-*n*-propyl-2-oxazoline) (PnPOZ), and poly(2-isopropyl-2-oxazoline) (PiPOZ) were synthesized according to our previously reported procedure [29]. Ibuprofen (IB) was from Tokyo Chemistry Industry (Japan). *N,N*-dimethylacetamide (DMA) was from Fisher Scientific (Loughborough, UK).

2.2. Preparation of Polymer-IB Solid Dispersions

Solid dispersions of polymer-IB were prepared in different repeating unit/drug molar ratios by solvent evaporation. DMA (1 mL) was used to dissolve 25 mg of IB with varying amounts of each polymer depending on the repeating unit/drug molar ratios. After dissolution, the solution was transferred to a Petri dish and the solvent was removed by evaporation at 50 °C on a heating base. The resultant solid was kept under vacuum for 72-96 h to remove residual DMA.

2.3. Characterization of Solid Dispersions

2.3.1. Powder X-Ray Diffractometry (PXRD)

A small amount of each dry sample (~20 mg) was placed on a silica plate and analyzed in a Bruker D8 ADVANCE PXRD using Cu K α radiation ($\lambda = 1.5406 \text{ \AA}$) over 5–64° for 1 h, with a step of 0.05°(2 θ) and count time of 1.2 s at 40 mV, 40 mA, with the sample rotated at 30 rpm. The results were analyzed using EVA software and the background for each sample was removed.

2.3.2. Differential Scanning Calorimetry (DSC)

Thermal analysis of pure drug, polymers, and solid dispersions was performed using DSC (TA Instruments). Samples (3–5 mg) were loaded into pierced T_{zero} aluminum pans. The thermal behavior of each sample was investigated in a nitrogen atmosphere from 10 to a maximum of 220 °C at 10 °C/min. The degree of sample crystallinity was determined by the specific enthalpy (ΔH) of the drug melting peak using TA universal analysis software and was calculated as the ratio of ΔH of the drug in the solid dispersions to ΔH of pure IB (taken as 100% crystalline). Since the drug content in the dispersion was only a fraction of the sample weight, the degree of crystallinity was normalized according to the following equation:

$$\text{Crystallinity (\%)} = \left(\Delta H_s \times \frac{W_s}{W_i} \right) / \Delta H_i \times 100 \quad (1)$$

where ΔH_s is the ΔH of the drug in the solid dispersion, melting around 76 °C (melting point of IB), ΔH_i is the ΔH of pure IB, W_s is the weight of solid dispersions, and W_i is the weight of IB in solid dispersions.

2.3.3. Fourier Transform Infrared (FTIR) Spectroscopy

FTIR spectra were recorded on a Nicolet iS5 spectrometer using a diamond ATR (attenuated total reflection) accessory. After a background scan was collected, samples were placed on the crystal and scanned from 4000–400 cm⁻¹ at a resolution of 4 cm⁻¹ and with an average of 64 scans. OMNIC software was used for spectral analysis.

2.4. In Vitro Dissolution Studies

Dissolution of IB from solid dispersions ([polymer repeat unit]/[drug] = 1:1 mol/mol) used USP Apparatus II (paddle method) at 37 ± 0.5 °C with paddles at 50 rpm and simulated intestinal fluid (SIF) (PBS, pH = 6.8). A pharmaceutical grade empty vegan clear capsule size “0” filled with solid dispersion (equivalent to 100 mg drug) was placed in 900 mL SIF with a sinker. Samples (5 mL) were withdrawn at 2, 5, 10, 20, 40, 60, 80, 100, and 120 min, and filtered using a 0.45- μm syringe filter; an equal volume of SIF was added to the dissolution medium to maintain the volume. The drug was assayed by UV-visible spectroscopy at 265 nm. All dissolution studies were performed in triplicate.

2.5. Statistical Analysis

All solid dispersions for each polymer at all drug loadings were prepared three times independently. All analyses, PXRD, DSC, FTIR, and dissolution studies were in triplicate. Data are expressed as mean ± standard deviation.

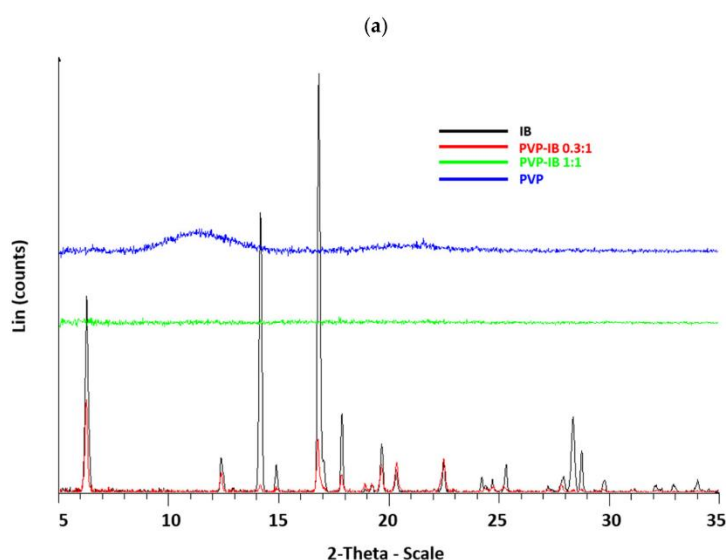
3. Results and Discussion

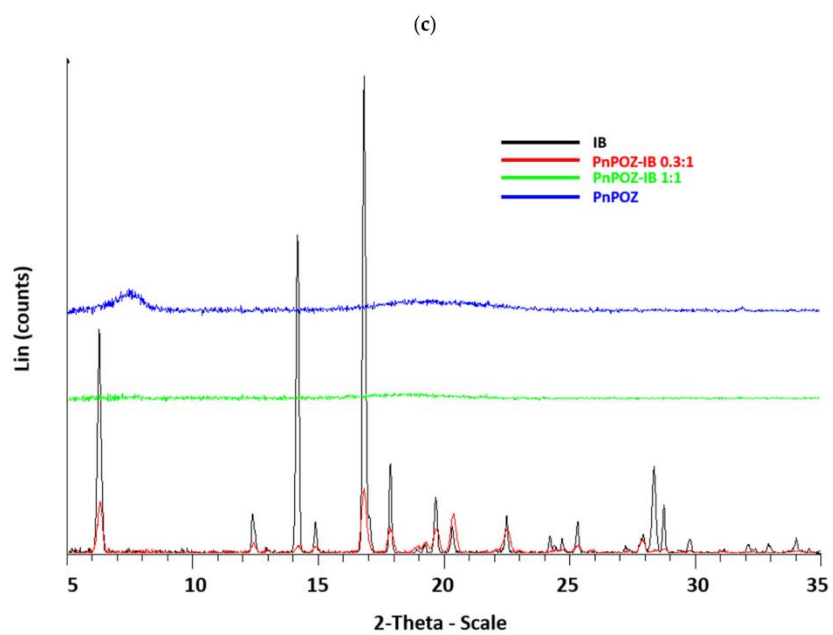
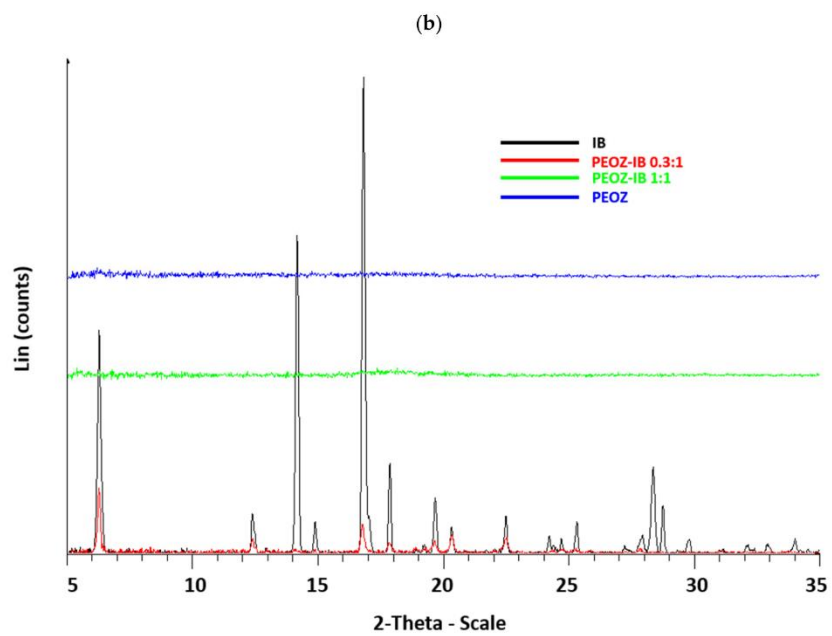
3.1. Preparation and Characterization of Solid Dispersions

To evaluate the effects of different polymers on the crystallinity of IB, solid dispersions were prepared by solvent evaporation and were characterized by DSC, PXRD, and FTIR, with DSC used to calculate the crystallinity of IB in the dispersions. The X-ray diffractogram of IB (Figure 1) shows multiple distinctive peaks, notably at 6.2°, 12.3°, 14.1°, 14.9°, 16.8°, 17.9°, 19.6°, 20.3°, 22.5°, 25.3°, 28.4°, and 28.8°, in agreement with the literature [30] and demonstrating the crystalline nature of pure IB.

Clearly, the drug is diluted when included in the polymer dispersion, and so peak intensities fall in all solid dispersions with PVP, PEOZ, PnPOZ, and PiPOZ at molar ratio [polymer]/[IB] = 0.3:1. In these systems, the drug is in excess of the polymer hydrogen bond acceptor repeat units and so is expected to remain largely crystalline. However, when the molar ratio of polymer repeat unit to IB is 1:1, the X-ray data in Figure 1 indicate that IB crystallinity is completely lost (although PMOZ systems showed some anomalous results, discussed below). It is also interesting to note that PiPOZ alone is semi-crystalline and presents a feature at $8.14^\circ 2\theta$, but this is lost at both 0.3:1 (where IB is in excess) and at a 1:1 mole ratio with the drug (highlighted in Figure 1d). This demonstrates that whilst solid dispersion studies typically focus on disruption of drug crystallinity, clearly the interactions between drug and carrier can also affect the nature and properties of the polymeric dispersant.

When dispersed in PMOZ, the X-ray data indicate different behavior for ibuprofen. As above, at a 0.3:1 molar ratio, where the drug is in excess, there is a reduction in the intensity of the peaks from ibuprofen due to the dilution effect. Some peaks observed in samples at this ratio were slightly shifted from their positions seen with pure ibuprofen at 19.6° , 20.3° , and 22.5° (denoted as 4, 5, and 6, respectively, in Figure 1e) while the characteristic peak of IB at $16.8^\circ 2\theta$ did not significantly move, indicating that IB was predominantly in its original form. However, in contrast with the other polymers, it is clear that ibuprofen has some structure in PMOZ at 1:1, 1:2, and 1:5 drug:polymer compositions, with a series of broader diffraction features seen between 16 and 20° ; again, these features show reduced intensities as the drug is further diluted in the polymer. For these systems, the original strong diffraction peak from the initial crystalline ibuprofen at $16.8^\circ 2\theta$ is lost, and broader features at 16.1° , 17.2° , and $19.5^\circ 2\theta$ are seen (peaks 2, 3, and 4, respectively, in Figure 1e). Further, a new feature at 10.5° is seen in these systems, which is absent from the pure ibuprofen diffractogram (peak 1). The changes to the diffraction peak positions and breadth of the new features are consistent with a semi-crystalline structure, but one that differs from the initial ibuprofen crystal lattice. Racemic ibuprofen is known to be polymorphic, but the diffraction peaks seen for the drug when dispersed in PMOZ are not consistent with the reported form II polymorph [31]. Thus, in our system, it is feasible that a semi-crystalline PMOZ-IB complex is formed. Finally, at a 1:10 drug:polymer composition, all diffraction peaks were lost, suggesting the formation of an amorphous dispersion.





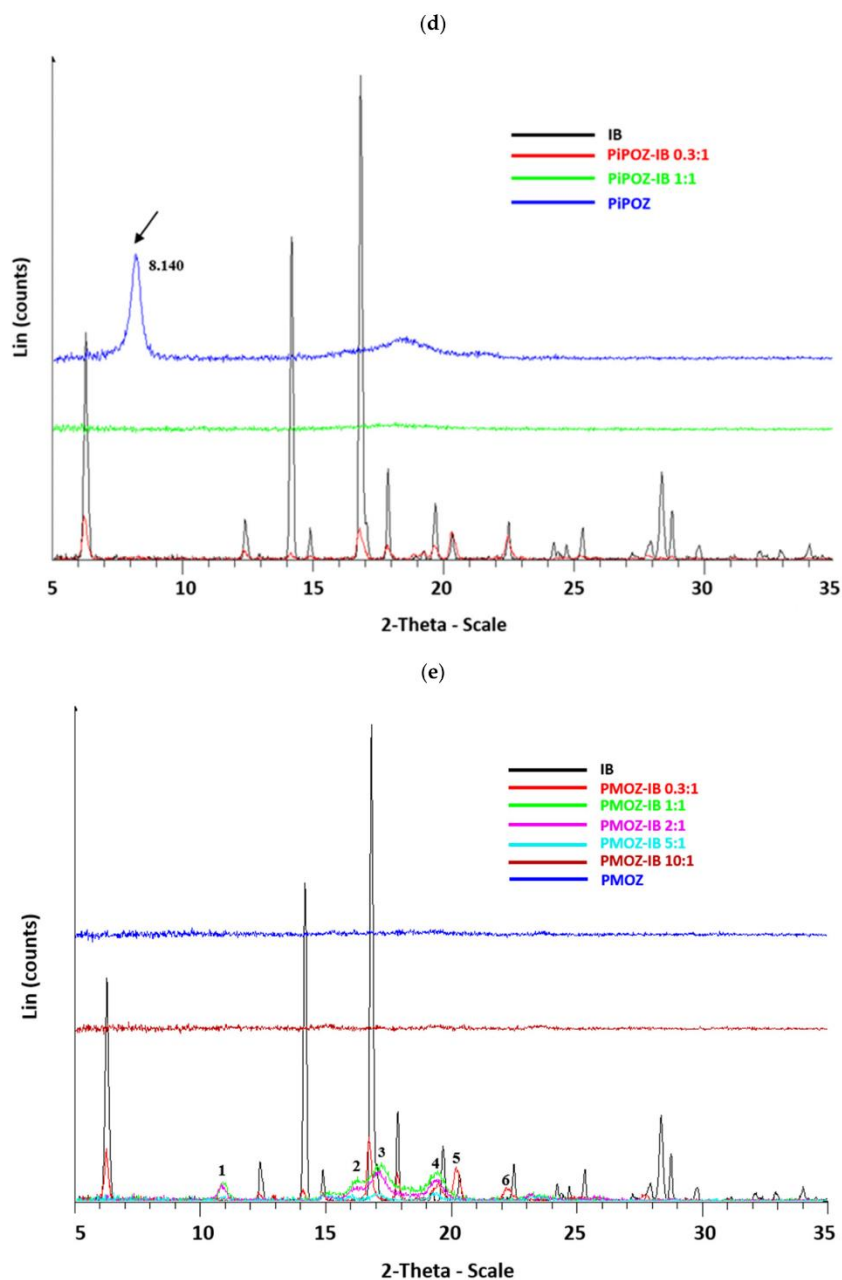


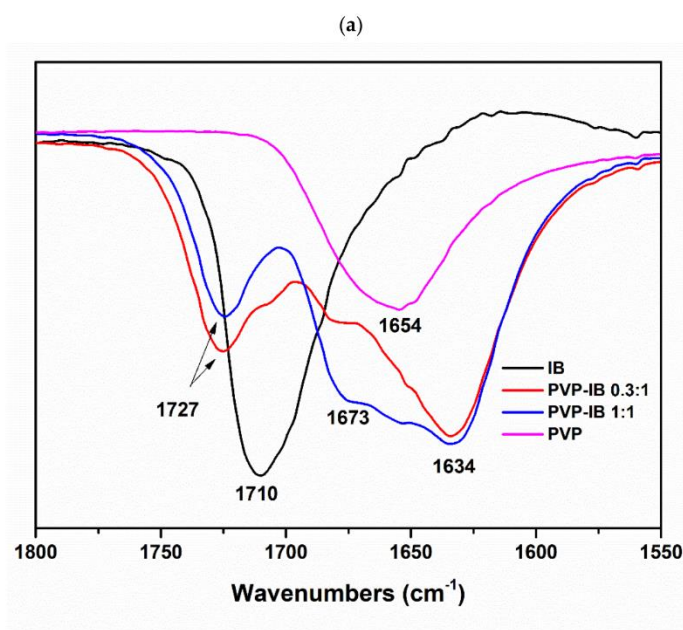
Figure 1. X-ray diffraction diagrams of PVP-IB SDs (a), PEOZ-IB SDs (b), PnPOZ-IB SDs (c), PiPOZ-IB SDs (d), and PMOZ-IB SDs (e).

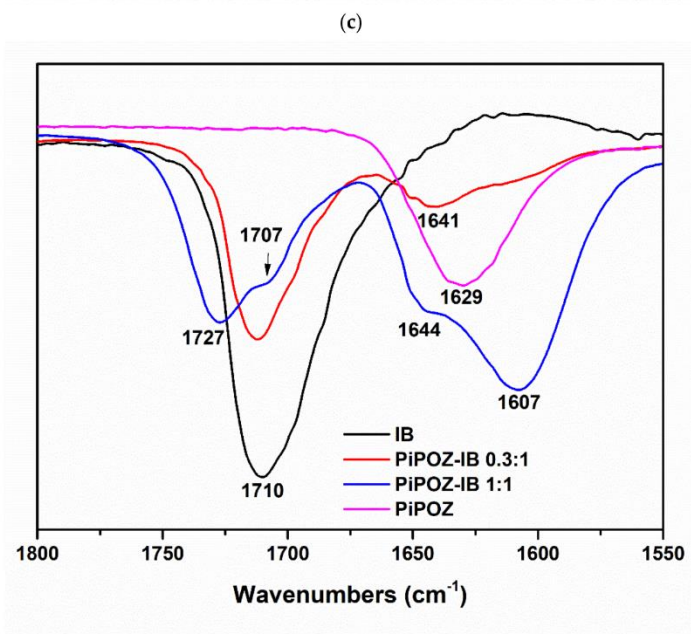
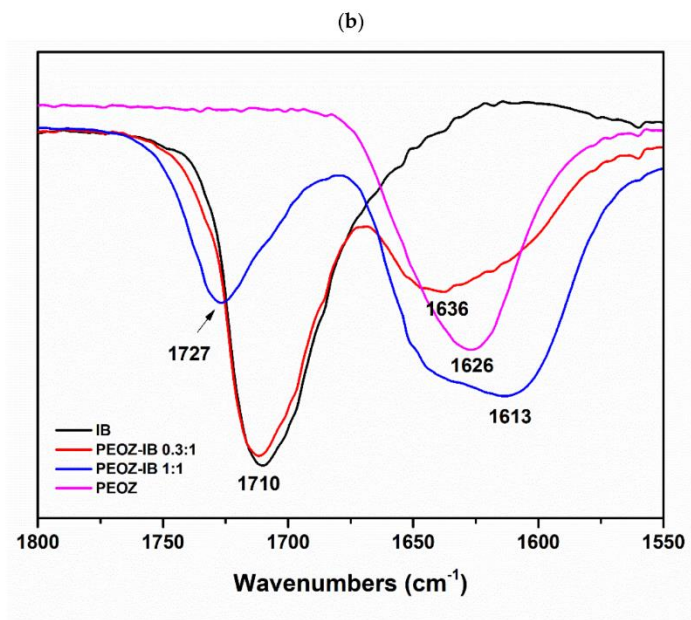
FTIR spectra were recorded from the components and dispersions to probe molecular interactions. Functional groups of particular interest are the carboxyl group of IB

[$-\text{C}=\text{O}(\text{OH})$], where the $-\text{OH}$ acts as a proton donor, and the carbonyl group ($-\text{C}=\text{O}$) and the nitrogen atom of polymers, which act as proton acceptors. In addition, correlation between frequency shifts and intermolecular interaction between drugs and polymers in solid dispersions is well known [32–34], and so was used to investigate hydrogen bonding in our polymer–drug solid dispersion systems.

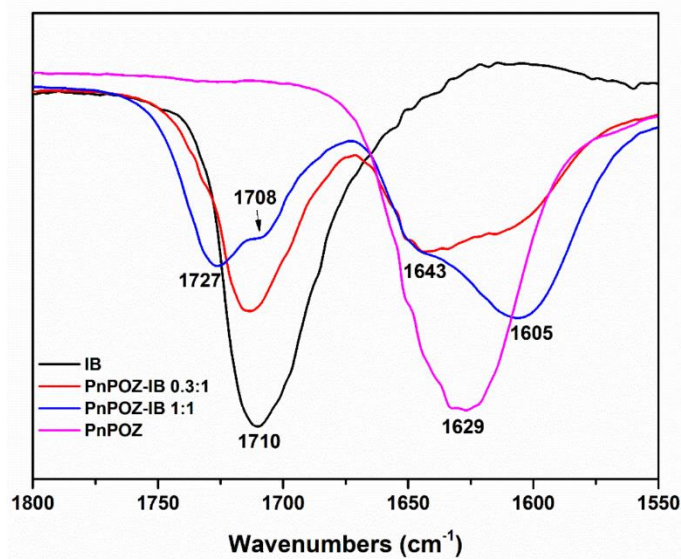
The FTIR spectra of IB, polymers, and polymer–IB solid dispersions are shown in Figures S1 and S2. For clarity, the spectra are expanded between 1800–1550 cm^{-1} in Figure 2. IB vibrational frequencies and their assignments are given in Table S1 and agree with the literature [35]. Briefly, absorption bands between 3100–2800 cm^{-1} are attributed to C–H stretching modes, with peak intensities gradually reducing as the drug quantity falls in the solid dispersions (Figure S2). Two medium intensity features, appearing at 2725 cm^{-1} and 2633 cm^{-1} in the spectrum of IB, can be assigned to the stretching vibration of the cyclic dimerized hydroxyl groups, which is subjected to intermolecular hydrogen bonding [19,36] (Figure S1). However, these bands are lost in the spectra of amorphous solid dispersions, indicating that the drug dimeric structure is lost as a result of interaction with the polymers.

The FTIR spectrum of IB shows a strong carbonyl stretching mode at 1710 cm^{-1} (Figure 2), which shifted to higher wavenumbers when dispersed in the polymers, and especially at ratios where X-ray diffraction showed no drug crystallinity (i.e., 1:1 ratios). These red shifts are summarized in Table 1. In contrast to the polyoxazoline carriers, the spectra of 0.3:1 mol PVP:IB showed that the IB carbonyl stretching mode shifted from 1710 cm^{-1} to 1727 cm^{-1} , despite the excess of IB to polymer monomer units, indicating the strong hydrogen bonding between IB with PVP may have consequential disruption to the IB crystal lattice. Furthermore, the carbonyl stretching mode for PVP at 1654 cm^{-1} was replaced by two peaks at 1634 cm^{-1} and 1673 cm^{-1} , with this latter peak strengthening at [PVP]/[IB] = 1:1 (Figure 2a).





(d)



(e)

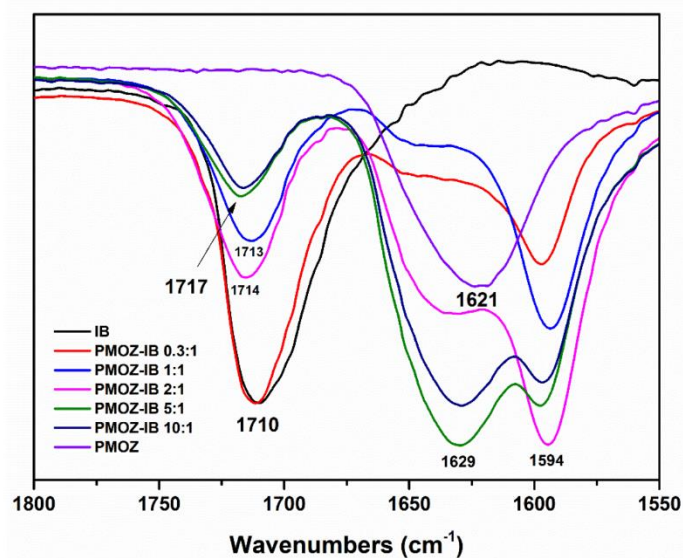


Figure 2. FTIR spectra of PVP-IB SDs (a), PEOZ-IB SDs (b), PnPZOZ-IB SDs (c), PiPOZ-IB SDs (d), and PMOZ-IB SDs (e) in the range of 1800–1550 cm^{-1} .

The 1:1 ratio of IB in dispersions with PEOZ, PnPZOZ, and PiPOZ showed similar infrared spectra, in agreement with that for PVP. The carbonyl stretching mode of IB showed a consistent red shift of 17 cm^{-1} from 1710 cm^{-1} to 1727 cm^{-1} , and the carbonyl stretch in the polymers split from the single peak at 1626 or 1629 cm^{-1} to give features at both higher and lower wavenumbers. At higher drug loadings (polymer: drug 0.3:1), the

data suggest some drug–polymer interactions occurred, but these are somewhat obscured by the “free” excess IB within the systems.

As with the X-ray investigation, dispersions with PMOZ showed different molecular interactions than for the other polyoxazolines. A modest red shift in the IB carbonyl feature of 3 cm^{-1} was seen at a 1:1 stoichiometry, and when excess polymer was employed (10:1 polymer repeat unit: IB), the shift was still modest at 7 cm^{-1} . The PMOZ carbonyl mode was seen at 1621 cm^{-1} in the polymer alone (Figure 2e). There is again evidence for this mode splitting in the dispersion with peaks consistently at $\sim 1594\text{ cm}^{-1}$ and $\sim 1650\text{ cm}^{-1}$ in the samples at 0.3:1 and 1:1 mole ratios. This peak apparently moves towards $\sim 1629\text{ cm}^{-1}$ as the polymer content increases, but in fact is due to the increased contribution of the “excess” (or “free”) PMOZ carbonyl peak intensity, which overlaps and obscures the carbonyl group of PMOZ that interacts with IB. The weaker interaction of PMOZ with IB compared with that in other polyoxazoline dispersions can be attributed to PMOZ’s relatively high hydrophilicity, which inhibits its ability to disorder the hydrophobic drug molecules [29].

From the IR data, there is no evidence for hydrogen bonding between the carboxylic groups of IB and nitrogen atoms in the polymers, given the invariant C–N stretching mode (Figure S3). Although PVP can form hydrogen bonds either through the nitrogen or carbonyl group [37], steric hindrance constrains the involvement of nitrogen atom in intermolecular interactions, so the carbonyl group is more favorable for hydrogen bonding [38,39].

Overall, the changes in the carbonyl band of IB and polymers indicate a modified carbonyl environment caused by the hydrogen bonding between the carboxylic groups of IB and carbonyl groups of the polymers. The relatively high red shift of the carbonyl mode of IB at $[\text{PVP}]/[\text{IB}] = 0.3:1$ mol confirmed strong hydrogen bonding between the drug and PVP, and at 1:1 mole ratio, the dispersions with PVP, PEOZ, PnPOZ, and PiPOZ all showed similar red shifts of this feature, suggesting near equivalent hydrogen bond interaction strengths. In contrast, the interaction between PMOZ and IB was relatively weak as a result of PMOZ’s high hydrophilicity, but no new spectral features were found to demonstrate the presence of a novel drug: PMOZ complex.

Table 1. The red shift of the carbonyl stretching mode from the carboxylic acid of IB at 1710 cm^{-1} in (polymer)/(IB) = 0.3 mol and 1:1 mol solid dispersions.

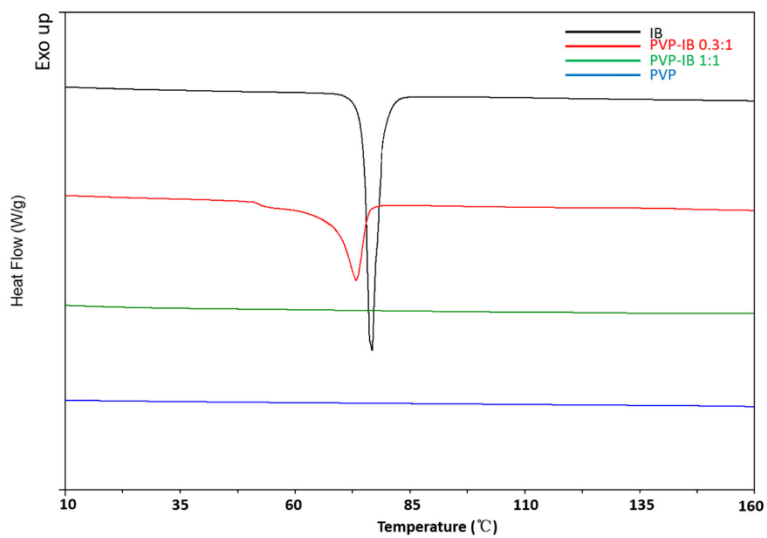
Polymer–Drug	Wavenumbers (cm^{-1})			
	0.3:1 mol	Red Shift	1:1 mol	Red Shift
PVP-IB	1727	17	1727	17
PMOZ-IB	1710	0	1713	3
PEOZ-IB	1711	1	1727	17
PnPOZ-IB	1713	3	1727	17
PiPOZ-IB	1712	2	1727	17

DSC experiments were used to investigate the thermal behavior of the solid dispersions and to estimate drug crystallinity within the dispersions. The DSC thermogram of pure IB showed a single characteristic melting peak at $76\text{ }^{\circ}\text{C}$, confirming its crystalline nature (Figure 3) and in agreement with previous reports [40,41]. In all dispersions at 0.3:1 mole ratio, the excess IB was seen to melt at a lower temperature, and the broadening of the melting event is consistent with disorder being introduced into the crystal lattice and interactions with the polymer occurring. At 1:1 mole ratio, the drug melting peak was lost in all dispersions except in dispersion with PMOZ, in agreement with the X-ray data.

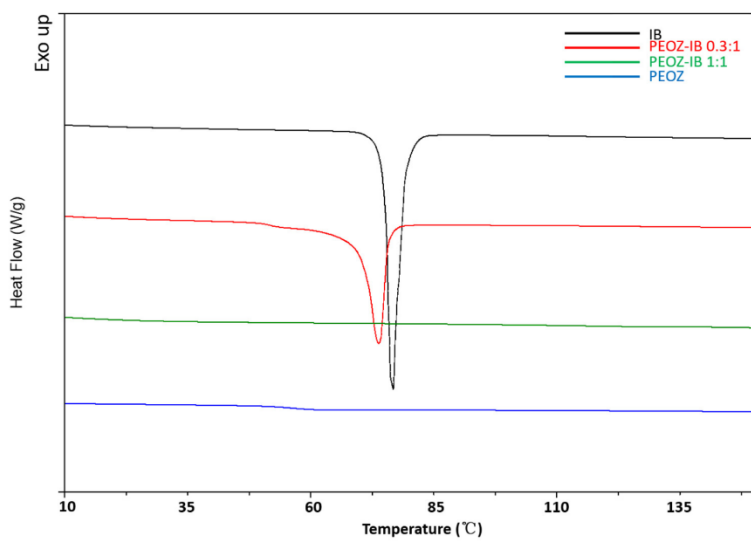
With PMOZ, a second endothermic peak appeared at $121.2\text{ }^{\circ}\text{C}$ in $(\text{PMOZ})/(\text{IB}) = 0.3:1$, at $137.7\text{ }^{\circ}\text{C}$ in $(\text{PMOZ})/(\text{IB}) = 1:1$, at $137.9\text{ }^{\circ}\text{C}$ in $(\text{PMOZ})/(\text{IB}) = 2:1$, and at $128.3\text{ }^{\circ}\text{C}$ in $(\text{PMOZ})/(\text{IB}) = 5:1$, potentially due to semi-crystalline IB or a PMOZ-IB complex. In addition, the melting peak seen at $203.5\text{ }^{\circ}\text{C}$ for semi-crystalline PiPOZ was lost in $(\text{PiPOZ})/(\text{IB})$ solid dispersions; whilst reports tend to focus on the disruption to drug crystallinity in

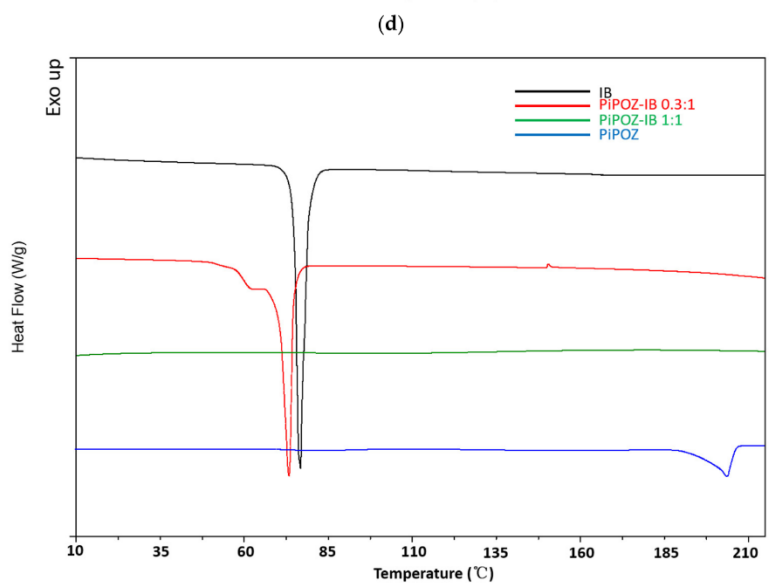
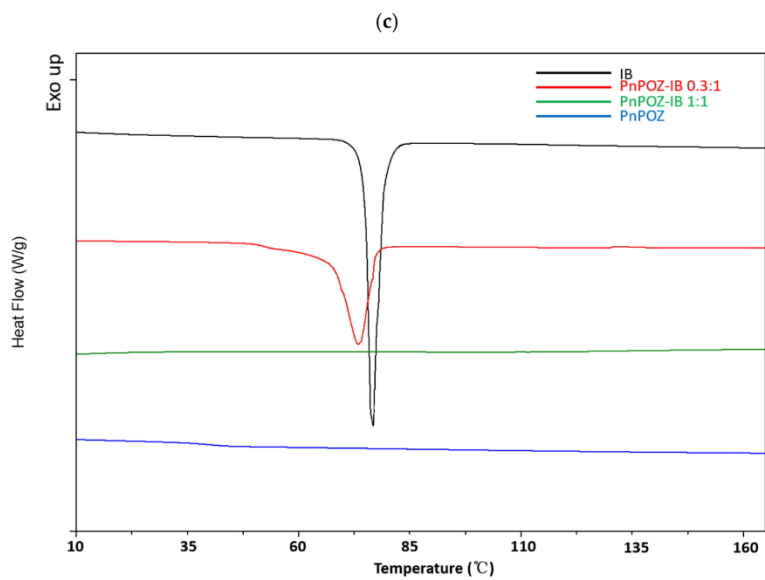
solid dispersions, clearly the drug also has the potential to disrupt the structure of the polymeric carrier, as indicated here.

(a)



(b)





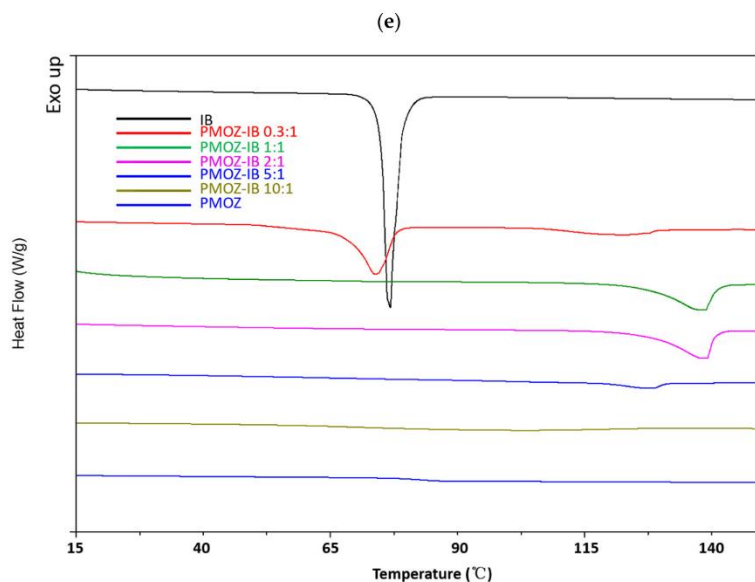


Figure 3. DSC thermograms of PVP-IB SDs (a), PEOZ-IB SDs (b), PnPOZ-IB SDs (c), PiPOZ-IB SDs (d), and PMOZ-IB SDs (e).

Drug crystallinity in polymer-IB solid dispersions was calculated from the specific enthalpy of the melting peak. As can be seen from Figure 4, IB crystallinity was reduced in all dispersions with PVP, PEOZ, PnPOZ, and PiPOZ, and the drug was essentially amorphous at a molar ratio of 1:1. The crystallinity of IB in dispersions with PMOZ could not be quantified by this approach due to the formation of new thermal features and the potential formation of a complex with this polymer.

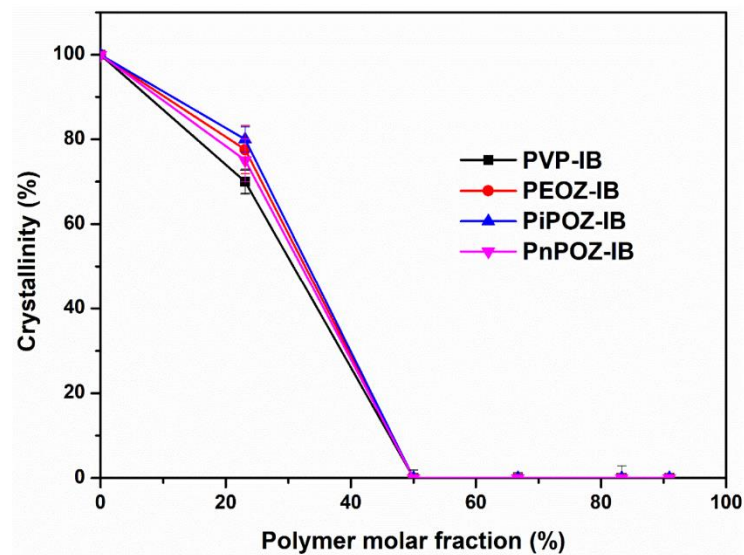


Figure 4. Crystallinity of polymer-IB solid dispersions as a function of polymer molar fraction.

3.2. Theoretical Evaluation of Drug-Polymer Miscibility

3.2.1. Solubility Parameters

The solubility parameter is a measure of cohesive energy density (CED: the cohesive energy per unit volume) of a material. The cohesive energy represents the total attractive forces within a condensed state material and can be defined as the quantity of energy needed to separate the atoms/molecules of a solid or liquid to a distance where the atoms or molecules possess no potential energy, that is, no interactions occur between atoms and molecules [30]. Consequently, solubility parameters have been used to predict the solubility/miscibility of one component into/with another component [42]. For this study, the solubility parameters were calculated using the Van Krevelen method [43], rather than the Fedors method [44,45], since the former considers hydrogen bonding. The Van Krevelen method provides:

$$\delta = \sqrt{\delta_d^2 + \delta_p^2 + \delta_h^2} \quad (2)$$

$$\text{where } \delta_d = \frac{\sum F_{di}}{V} \quad \delta_p = \frac{\sqrt{\sum F_{pi}^2}}{V} \quad \delta_h = \frac{\sqrt{\sum E_{hi}}}{V}$$

where δ is the total solubility parameter; δ_d , the contribution from dispersion forces; δ_p , the contribution from polar forces; δ_h , the contribution of hydrogen bonding; F_{di} , the molar attraction constant due to dispersion component; F_{pi} , the molar attraction constant due to polar component; E_{hi} , the hydrogen bonding energy; and V , the molar volume. For various groups, the values of F_{di} , F_{pi} , E_{hi} , and V (molar volume) are given in the literature [43,45]. The solubility parameters of these five polymers were taken from our previous study [29] and the solubility parameters calculated for IB and PVP are in good agreement with the literature [46].

Compounds with similar values of δ are likely to be miscible because the energy required to break interactions within each component is balanced by the energy released by interaction between the components. Greenhalgh et al. [30] classified dispersions based on the difference between the solubility parameters of excipients and drugs ($\Delta\delta$). The authors demonstrated that compounds with $\Delta\delta < 7.0 \text{ MPa}^{1/2}$ are likely to be miscible. However, compounds with $\Delta\delta > 10.0 \text{ MPa}^{1/2}$ are likely to be immiscible. The calculated solubility parameters for IB, PVP, PMOZ, PEOZ, PnPOZ, and PiPOZ are summarized in Table 2.

Table 2. Solubility parameters of drug and polymers.

Drug and Polymers	Solubility Parameters (δ) ($\text{MPa}^{1/2}$)		Group Classification
	Van Krevelen Method	$\Delta\delta$	
IB	19.4		
PVP	26.3	6.9	Miscible
PMOZ	27.0	7.6	Not miscible
PEOZ	24.5	5.1	Miscible
PnPOZ	22.9	3.5	Miscible
PiPOZ	22.5	3.1	Miscible

It can be seen from Table 2 that all the polymers are expected to be miscible with IB with $\Delta\delta$ values ranging from 3.1 to 6.9, except for PMOZ ($\Delta\delta = 7.6$). The rank order values for $\Delta\delta$ miscibility (PiPOZ; PnPOZ; PEOZ; PVP) are inconsistent with their ability to disrupt ibuprofen crystallinity, which may be explained by confounding factors such as the stronger hydrogen bonding seen between PVP and IB, as suggested from the FTIR data (Table 1). Although widely used, this approach has limitations and tends to be most widely applicable for drug-polymer systems where Van der Waals interactions play a major role, whereas for drug-polymer mixtures forming highly directional interactions such as hydrogen bonds or long range forces such as ionic interactions, this method can yield erroneous results [1,47].

3.2.2. Flory–Huggins Interaction Parameter

Flory–Huggins theory considers melting point depression as an indicator of miscibility. According to this [48], the relationship between the melting temperature of the pure drug (T_m^0) and the depressed melting point of the drug in the drug–polymer system (T_m) can be described by the following equation [49–51]:

$$\frac{1}{T_m} - \frac{1}{T_m^0} = -\frac{R}{\Delta H} \left(\ln \phi + \left(1 - \frac{1}{m}\right) (1 - \phi) + \chi (1 - \phi)^2 \right) \quad (3)$$

where R is the gas constant (8.31 J/mol·K), ΔH is the heat of fusion of the pure drug, ϕ is the volume fraction of the drug in the solid dispersion (i.e., drug loading), m is the volume ratio between polymer and drug, and χ is the drug–polymer interaction parameter representing the difference between the drug–polymer contact interaction and the average self-contact interactions of drug–drug and polymer–polymer [49]. A negative χ value indicates that the interaction between a polymer and a drug is stronger than the attraction within polymer–polymer and drug–drug pairs. More negative values of χ indicate better affinity between the polymer and the drug and, for example, could be caused by hydrogen bonding between the drug and the polymer. Positive χ values indicate that drug molecules and polymer segments have stronger affinity to interact with those of their own kind rather than interacting with each other [50].

Given that all the polymer–IB solid dispersion systems showed depressed drug melting points at (polymer)/(drug) = 0.3:1 mol, the χ values of these dispersions were calculated and are listed in Table 3. Again, the PMOZ-IB system could not be investigated by this method.

Table 3. Flory–Huggins interaction parameters of polymer–IB solid dispersion systems at the molar ratio of 0.3:1.

Polymer–Drug	$V_{\text{polymer repeat unit}}^a$ (cm ³ /mol)	V_{polymer}^b (cm ³ /mol)	V_{drug}^c (cm ³ /mol)	M^d	T_m (°C)	χ
PVP-IB	80.0	40,000		204.60	73.27	−3.71
PEOZ-IB	74.1	37,050	195.5	189.51	73.80	−3.85
PnPOZ-IB	90.2	45,100		230.69	73.50	−3.32
PiPOZ-IB	90.5	45,250		231.46	73.34	−3.52

a is the molecular volume of polymer repeating unit, calculated from the literature [43,45]. b is the molecular volume of polymer, calculated by multiplying $V_{\text{polymer repeat unit}}$ by the repeat unit number. c is the molecular volume of IB, calculated from the literature [43,45], and is in agreement with the value taken from [52]. d is the volume ratio between the polymer and the drug.

As can be seen, the drug–polymer interaction parameters are all negative and broadly similar, ranging from −3.85 for PEOZ-IB to −3.32 for PnPOZ-IB. Interestingly, the Flory–Huggins approach suggests a rank order of (greatest interactions to least) of PEOZ > PVP > PiPOZ > PnPOZ, whereas the rank order of solubility parameter miscibility was PiPOZ > PnPOZ > PEOZ > PVP. Clearly, both approaches provide approximations (almost a “yes/no” guide), rather than a predictive ability to develop the optimal solid dispersion, since other factors influence the polymer’s ability to disrupt the drug’s crystallinity.

The X-ray, thermal, and infrared studies showed that PMOZ has a lower propensity to disorder ibuprofen than the other polymers. Its solubility parameter difference to ibuprofen ($\Delta\delta$) was 7.6 MPa^{1/2}, and thus beyond the notional value of 7 for miscibility but close to the borderline value 6.9 MPa^{1/2} calculated for PVP, which has the greatest tendency to disorder the drug. An alternative explanation is that the hydrophobic–hydrophilic balance (HHB) value for PMOZ (3.95) demonstrates that it is highly hydrophilic, and so the hydrophobic IB molecules will be less likely to molecularly disperse into the hydrophilic domains of PMOZ, consistent with our earlier findings on the non-hydrogen bonding dispersions with haloperidol where, again, PMOZ showed reduced interactions compared with the more hydrophobic carriers [29]. The importance of polymer hydrophobicity for crystal growth inhibitors has previously been reported [16].

3.3. In Vitro Dissolution Studies

The dissolution profiles of IB and polymer-IB (all 1:1 mol/mol) solid dispersions are shown in Figure 5. The dissolution of pure IB within 60 min was below 70%, with ~50% released in the first 20 min. As expected from the crystallinity data (Figure 4), dissolution was rapid from solid dispersions with PVP, PEOZ, and PiPOZ, where over 80% of the drug was released in the first 20 min. Drug release from solid dispersion with PMOZ was slower compared to PVP, PEOZ, and PiPOZ, but faster than IB alone, with ~70% of the drug released in 20 min, consistent with the analytical and theoretical discussions above. Despite the reduction of drug crystallinity and the system being essentially amorphous as determined by XRD and DSC, dispersions formed with PnPOZ showed slower dissolution than pure crystalline IB, with less than 30% released in 20 min. This result is consistent with our previous study [29] and can be explained by this polymer's lower critical solution temperature (LCST) of ~25 °C [53,54], which is much lower than the temperature used in the dissolution studies (37 °C). Under these conditions, PnPOZ remains insoluble in the dissolution medium, which limits drug release from these solid dispersions. Further detailed dissolution studies of these formulations will be of interest in the future, for example, in assessing release below 25 °C and evaluating the extent of IB supersaturation on the evolution of kinetic solubility profiles [55].

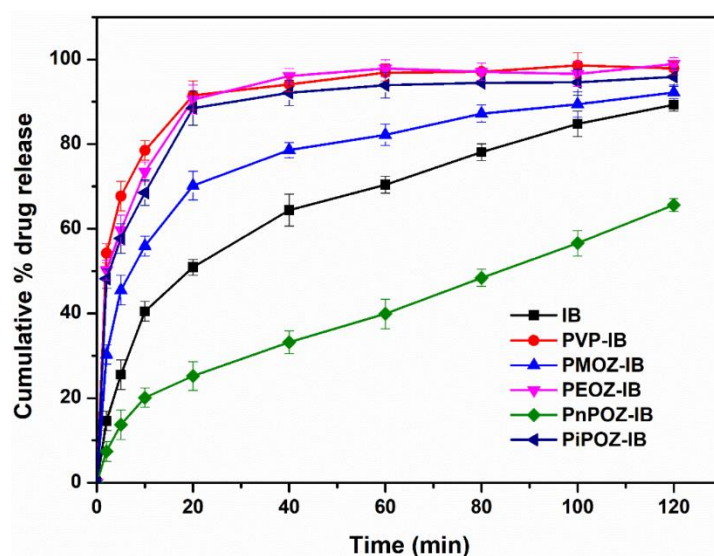


Figure 5. Dissolution profiles of pure IB and from different polymer-IB solid dispersions ((polymer repeat unit)/(drug) = 1:1 mol/mol). Cumulative % drug release with standard error of mean has been plotted against time.

4. Conclusions

Solid dispersions of IB were prepared using the poly(2-oxazolines) and PVP. Physical characterization of the dispersions showed that the polymers were able to disrupt the ibuprofen crystallinity, forming apparently amorphous dispersion at 1:1 mole ratios, and that hydrogen bonding was the prime mechanism for the interaction; however, the interactions between PMOZ and ibuprofen were more complex and hydrogen bonding was less prominent. The theoretical approach using the differences in solubility parameters between the drug and carrier or calculating the Flory-Huggins interaction parameters suggested compatibility between the drug and carriers, but the rank order of the predicted

interactions varied between the two approaches. The purpose of generating solid dispersions is to enhance the dissolution rate of a poorly water soluble drug, and our studies demonstrated that the dispersions were able to significantly increase ibuprofen dissolution. However, our studies also show that other factors can significantly impact the performance of a solid dispersion. Physical characterization, for example, XRD showing that the drug is amorphous, can be assumed to result in enhanced dissolution. However, we show that not only is the crystallinity of a drug affected by dispersion, but so too is the structure of a semi-crystalline polymer (PiPOZ). The hydrophilicity of a carrier may reduce interactions with a hydrophobic drug, and so HHB may be an additional factor. Furthermore, the solution behavior of the carrier can also influence performance; physical characterization and theoretical models implied that dispersions with PnPOZ would be as effective as the other carriers, but the lower critical solution temperature (~25 °C) meant that this amorphous dispersion performed worse than the ibuprofen alone in the dissolution studies. Thus, both physical interactions, such as hydrogen bonding, and polymer properties, such as hydrophobicity, need to be considered when selecting carriers for solid dispersions.

Supplementary Materials: The following are available online at www.mdpi.com/1999-4923/13/5/659/s1, Figure S1: FTIR of ibuprofen. Figure S2: FTIR full spectra of PVP-IB SDs (a), PEOZ-IB SDs (b), PnPOZ-IB SDs (c), PiPOZ-IB SDs (d) and PMOZ-IB SDs (e) Figure S3: FTIR spectra of PVP-IB SDs and POZ-IB SDs in the range of 1400~900 cm⁻¹. The peaks (marked with an arrow) are attributed to C-N mode. Table S1: FTIR spectral data of ibuprofen (s- strong; w- weak; sym-symmetrical; asym-asymmetrical; str-stretching; m- medium; vs- very strong; vw - very weak.).

Author Contributions: Conceptualization, V.V.K. and A.C.W.; methodology, X.S. and M.A.M.; software, X.S. and M.A.M.; validation, X.S. and M.A.M.; formal analysis, X.S.; investigation, X.S.; resources, X.S.; data curation, X.S.; writing—original draft preparation, X.S.; writing—review and editing, V.V.K. and A.C.W.; visualization, X.S.; supervision, V.V.K. and A.C.W.; project administration, funding acquisition, V.V.K. All authors have read and agreed to the published version of the manuscript.

Funding: This research received no external funding.

Institutional Review Board Statement: Not applicable

Informed Consent Statement: Not applicable

Data Availability Statement: Data is contained within the article and in supplementary material.

Acknowledgments: The authors are grateful to the University of Reading and the China Scholarship Council (201707040071) for funding the PhD studentship of X.S. The assistance of staff at the Chemical Analysis Facility (CAF, University of Reading) with DSC and PXRD experiments is also acknowledged. The authors are also grateful to Kenneth Shankland for his valuable advice in interpreting PXRD and DSC data.

Conflicts of Interest: The authors declare no conflict of interest.

References

1. Baghel, S.; Cathcart, H.; O'Reilly, N.J. Polymeric amorphous solid dispersions: A review of amorphization, crystallization, stabilization, solid-state characterization, and aqueous solubilization of biopharmaceutical classification system class ii drugs. *J. Pharm. Sci.* **2016**, *105*, 2527–2544.
2. Kim, K.T.; Lee, J.Y.; Lee, M.Y.; Song, C.K.; Choi, J.H.; Kim, D.D. Solid dispersions as a drug delivery system. *J. Pharm. Investig.* **2011**, *41*, 125–142.
3. Tekade, A.R.; Yadav, J.N. A review on solid dispersion and carriers used therein for solubility enhancement of poorly water soluble drugs. *Adv. Pharm. Bull.* **2020**, *10*, 359–369.
4. Biswal, S.; Sahoo, J.; Murthy, P.N. Physicochemical properties of solid dispersions of gliclazide in polyvinylpyrrolidone k90. *AAPS Pharm. Sci. Tech* **2009**, *10*, 329–334.
5. Franco, P.; De Marco, I. The use of poly(N-vinyl pyrrolidone) in the delivery of drugs: A review. *Polymers* **2020**, *12*, 1114. doi:10.3390/polym12051114.

6. Rumondor, A.C.; Ivanisevic, I.; Bates, S.; Alonzo, D.E.; Taylor, L.S. Evaluation of drug-polymer miscibility in amorphous solid dispersion systems. *Pharm. Res.* **2009**, *26*, 2523–2534.
7. Indulkar, A.S.; Lou, X.; Zhang, G.G.Z.; Taylor, L.S. Insights into the dissolution mechanism of ritonavir-copovidone amorphous solid dispersions: Importance of congruent release for enhanced performance. *Mol. Pharm.* **2019**, *16*, 1327–1339.
8. Panini, P.; Rampazzo, M.; Singh, A.; Vanhoutte, F.; Van den Mooter, G. Myth or truth: The glass forming ability class iii drugs will always form single-phase homogenous amorphous solid dispersion formulations. *Pharmaceutics* **2019**, *11*, 529, doi:10.3390/pharmaceutics11100529.
9. Que, C.; Lou, X.; Zemlyanov, D.Y.; Mo, H.; Indulkar, A.S.; Gao, Y.; Zhang, G.G.Z.; Taylor, L.S. Insights into the dissolution behavior of ledipasvir-copovidone amorphous solid dispersions: Role of drug loading and intermolecular interactions. *Mol. Pharm.* **2019**, *16*, 5054–5067.
10. Biswal, S.; Sahoo, J.; Murthy, P.N.; Giradkar, R.P.; Avari, J.G. Enhancement of dissolution rate of gliclazide using solid dispersions with polyethylene glycol 6000. *AAPS Pharm. Sci. Tech* **2008**, *9*, 563–570.
11. Urbanetz, N.A. Stabilization of solid dispersions of nimodipine and polyethylene glycol 2000. *Eur. J. Pharm. Sci.* **2006**, *28*, 67–76.
12. Ghosh, I.; Snyder, J.; Vippagunta, R.; Alvine, M.; Vakil, R.; Tong, W.Q.; Vippagunta, S. Comparison of hpmc based polymers performance as carriers for manufacture of solid dispersions using the melt extruder. *Int. J. Pharm.* **2011**, *419*, 12–19.
13. Li, B.; Harich, K.; Wegiel, L.; Taylor, L.S.; Edgar, K.J. Stability and solubility enhancement of ellagic acid in cellulose ester solid dispersions. *Carbohydr. Polym.* **2013**, *92*, 1443–1450.
14. Ali, W.; Williams, A.C.; Rawlinson, C.F. Stoichiometrically governed molecular interactions in drug: Poloxamer solid dispersions. *Int. J. Pharm.* **2010**, *391*, 162–168.
15. Newa, M.; Bhandari, K.H.; Oh, D.H.; Kim, Y.R.; Sung, J.H.; Kim, J.O.; Woo, J.S.; Choi, H.G.; Yong, C.S. Enhanced dissolution of ibuprofen using solid dispersion with poloxamer 407. *Arch. Pharm. Res.* **2008**, *31*, 1497–1507.
16. Ilevbare, G.A.; Liu, H.; Edgar, K.J.; Taylor, L.S. Understanding polymer properties important for crystal growth inhibition—impact of chemically diverse polymers on solution crystal growth of ritonavir. *Cryst. Growth Des.* **2012**, *12*, 3133–3143.
17. Li, Y.; Pang, H.; Guo, Z.; Lin, L.; Dong, Y.; Li, G.; Lu, M.; Wu, C. Interactions between drugs and polymers influencing hot melt extrusion. *J. Pharm. Pharmacol.* **2014**, *66*, 148–166.
18. Tran, T.T.D.; Tran, P.H.L. Molecular interactions in solid dispersions of poorly water-soluble drugs. *Pharmaceutics* **2020**, *12*, 745, doi:10.3390/pharmaceutics12080745.
19. Niemczyk, A.I.; Williams, A.C.; Rawlinson-Malone, C.F.; Hayes, W.; Greenland, B.W.; Chappell, D.; Khutoryanskaya, O.; Timmins, P. Novel polyvinylpyrrolidones to improve delivery of poorly water-soluble drugs: From design to synthesis and evaluation. *Mol. Pharm.* **2012**, *9*, 2237–2247.
20. Rawlinson, C.F.; Williams, A.C.; Timmins, P.; Grimsey, I. Polymer-mediated disruption of drug crystallinity. *Int. J. Pharm.* **2007**, *336*, 42–48.
21. Van Nguyen, H.; Baek, N.; Lee, B.J. Enhanced gastric stability of esomeprazole by molecular interaction and modulation of microenvironmental pH with alkalizers in solid dispersion. *Int. J. Pharm.* **2017**, *523*, 189–202.
22. Ozeki, T.; Yuasa, H.; Kanaya, Y. Application of the solid dispersion method to the controlled release of medicine. IX. Difference in the release of flurbiprofen from solid dispersions with poly(ethylene oxide) and hydroxypropylcellulose and the interact. *Int. J. Pharm.* **1997**, *155*, 209–217.
23. Huang, J.; Wigent, R.J.; Schwartz, J.B. Drug-polymer interaction and its significance on the physical stability of nifedipine amorphous dispersion in microparticles of an ammonio methacrylate copolymer and ethylcellulose binary blend. *J. Pharm. Sci.* **2008**, *97*, 251–262.
24. Rasenack, N.; Hartenhauer, H.; Müller, B.W. Microcrystals for dissolution rate enhancement of poorly water-soluble drugs. *Int. J. Pharm.* **2003**, *254*, 137–145.
25. Zimmermann, A.; Millqvist-Fureby, A.; Elema, M.R.; Hansen, T.; Mullertz, A.; Hovgaard, L. Adsorption of pharmaceutical excipients onto microcrystals of siramesine hydrochloride: Effects on physicochemical properties. *Eur. J. Pharm. Biopharm.* **2009**, *71*, 109–116.
26. Fael, H.; Rafols, C.; Demirel, A.L. Poly(2-ethyl-2-oxazoline) as an alternative to poly(vinylpyrrolidone) in solid dispersions for solubility and dissolution rate enhancement of drugs. *J. Pharm. Sci.* **2018**, *107*, 2428–2438.
27. Boel, E.; Smeets, A.; Vergaelen, M.; De la Rosa, V.R.; Hoogenboom, R.; Van den Mooter, G. Comparative study of the potential of poly(2-ethyl-2-oxazoline) as carrier in the formulation of amorphous solid dispersions of poorly soluble drugs. *Eur. J. Pharm. Biopharm.* **2019**, *144*, 79–90.
28. Everaerts, M.; Tigrine, A.; de la Rosa, V.R.; Hoogenboom, R.; Adriaensens, P.; Clasen, C.; Van den Mooter, G. Unravelling the miscibility of poly(2-oxazoline)s: A novel polymer class for the formulation of amorphous solid dispersions. *Molecules* **2020**, *25*, 3587, doi:10.3390/molecules25163587.
29. Shan, X.; Williams, A.C.; Khutoryanskiy, V.V. Polymer structure and property effects on solid dispersions with haloperidol: Poly(n-vinyl pyrrolidone) and poly(2-oxazolines) studies. *Int. J. Pharm.* **2020**, *590*, 119884.
30. Greenhalgh, D.J.; Williams, A.C.; Timmins, P.; York, P. Solubility parameters as predictors of miscibility in solid dispersions. *J. Pharm. Sci.* **1999**, *88*, 1182–1190.
31. Dudognon, E.; Danede, F.; Descamps, M.; Correia, N.T. Evidence for a new crystalline phase of racemic ibuprofen. *Pharm. Res.* **2008**, *25*, 2853–2858.

32. Rostkowska, H.; Nowak, M.J.; Lapinski, L.; Adamowicz, L. Ir spectral and theoretical characterization of intramolecular hydrogen bonds closing five-membered rings. *Phys. Chem. Chem. Phys.* **2001**, *3*, 3012–3017.
33. Rumondor, A.C.; Wikstrom, H.; Van Eerdenbrugh, B.; Taylor, L.S. Understanding the tendency of amorphous solid dispersions to undergo amorphous-amorphous phase separation in the presence of absorbed moisture. *AAPS Pharm. Sci. Tech* **2011**, *12*, 1209–1219.
34. Teberekidis, V.I.; Sigalas, M.P. Theoretical study of hydrogen bond interactions of felodipine with polyvinylpyrrolidone and polyethyleneglycol. *J. Mol. Struct.* **2007**, *803*, 29–38.
35. Ramukutty, S.; Ramachandran, E. Growth, spectral and thermal studies of ibuprofen crystals. *Cryst. Res. Technol.* **2012**, *47*, 31–38.
36. Bogdanova, S.; Pajeva, I.; Nikolova, P.; Tsakovska, I.; Müller, B. Interactions of poly(vinylpyrrolidone) with ibuprofen and naproxen: Experimental and modeling studies. *Pharm. Res.* **2005**, *22*, 806–815.
37. Iannuccelli, V.; Coppi, G.; Leo, E.; Fontana, F.; Bernabei, M.T. Pvp solid dispersions for the controlled release of furosemide from a floating multiple-unit system. *Drug Dev. Ind. Pharm.* **2000**, *26*, 595–603.
38. Chadha, R.; Kapoor, V.K.; Kumar, A. Analytical techniques used to characterize drug-polyvinylpyrrolidone systems in solid and liquid states—An overview. *J. Sci. Ind. Res.* **2006**, *65*, 459–469.
39. Hosono, T.; Tsuchiya, S.; Matsumaru, H. Model of interaction of ajmaline with polyvinylpyrrolidone. *J. Pharm. Sci.* **1980**, *69*, 824–826.
40. Sekizaki, H.; Danjo, K.; Eguchi, H.; Yonezawa, Y.; Sunada, H.; Otsuka, A. Solid-state interaction of ibuprofen with polyvinylpyrrolidone. *Chem. Pharm. Bull.* **1995**, *43*, 988–993.
41. Williams, A.C.; Timmins, P.; Lu, M.; Forbes, R.T. Disorder and dissolution enhancement: Deposition of ibuprofen on to insoluble polymers. *Eur. J. Pharm. Sci.* **2005**, *26*, 288–294.
42. Jankovic, S.; Tsakiridou, G.; Ditzinger, F.; Koehl, N.J.; Price, D.J.; Ilie, A.R.; Kalantzi, L.; Kimpe, K.; Holm, R.; Nair, A.; et al. Application of the solubility parameter concept to assist with oral delivery of poorly water-soluble drugs—A PEARRL review. *J. Pharm. Pharmacol.* **2019**, *71*, 441–463.
43. Krevelen, D.W.V. *Properties of Polymers*; Elsevier: Amsterdam, The Netherlands, 1990; pp. 189–221.
44. Chokshi, R.J.; Sandhu, H.K.; Iyer, R.M.; Shah, N.H.; Malick, A.W.; Zia, H. Characterization of physico-mechanical properties of indomethacin and polymers to assess their suitability for hot-melt extrusion processes as a means to manufacture solid dispersion/solution. *J. Pharm. Sci.* **2005**, *94*, 2463–2474.
45. Fedors, R.F. A method for estimating both the solubility parameters and molar volumes of liquids. *Polym. Eng. Sci.* **1974**, *14*, 147–154.
46. Kitak, T.; Dumicic, A.; Planinsek, O.; Sibanc, R.; Srcic, S. Determination of solubility parameters of ibuprofen and ibuprofen lysinate. *Molecules* **2015**, *20*, 21549–21568.
47. Barton, A.F.M. Solubility parameters. *Chem. Rev.* **1975**, *75*, 731–753.
48. Flory, P.J. *Principles of Polymer Chemistry*; Cornell University Press: Ithaca, NY, USA, 1953.
49. Huang, Y.; Dai, W.G. Fundamental aspects of solid dispersion technology for poorly soluble drugs. *Acta Pharm. Sin. B* **2014**, *4*, 18–25.
50. Lin, D.; Huang, Y. A thermal analysis method to predict the complete phase diagram of drug-polymer solid dispersions. *Int. J. Pharm.* **2010**, *399*, 109–115.
51. Moseson, D.E.; Taylor, L.S. The application of temperature-composition phase diagrams for hot melt extrusion processing of amorphous solid dispersions to prevent residual crystallinity. *Int. J. Pharm.* **2018**, *553*, 454–466.
52. Kong, C.Y.; Sugiura, K.; Funazukuri, T.; Miyake, K.; Okajima, I.; Badhulika, S.; Sako, T. The retention factors and partial molar volumes of ibuprofen at infinite dilution in supercritical carbon dioxide at $t = (308.15, 313.15, 323.15, 333.15, 343.15 \text{ and } 353.15) \text{ K}$. *J. Mol. Liq.* **2019**, *296*, 111849.
53. Bouten, P.; Lava, K.; van Hest, J.; Hoogenboom, R. Thermal properties of methyl ester-containing poly(2-oxazoline)s. *Polymers* **2015**, *7*, 1998–2008.
54. Park, J.S.; Kataoka, K. Comprehensive and accurate control of thermosensitivity of poly(2-alkyl-2-oxazoline)s via well-defined gradient or random copolymerization. *Macromolecules* **2007**, *40*, 3599–3609.
55. Han, Y.R.; Lee, P.I. Effect of extent of supersaturation on the evolution of kinetic solubility profiles. *Mol. Pharm.* **2017**, *14*, 206–220.

Supplementary Materials: Mutual Effects of Hydrogen Bonding and Polymer Hydrophobicity on Ibuprofen Crystal Inhibition in Solid Dispersions with Poly(*N*-vinyl pyrrolidone) and Poly(2-oxazolines)

Xiaoning Shan, Maryam A. Moghul, Adrian C. Williams and Vitaliy V. Khutoryanskiy

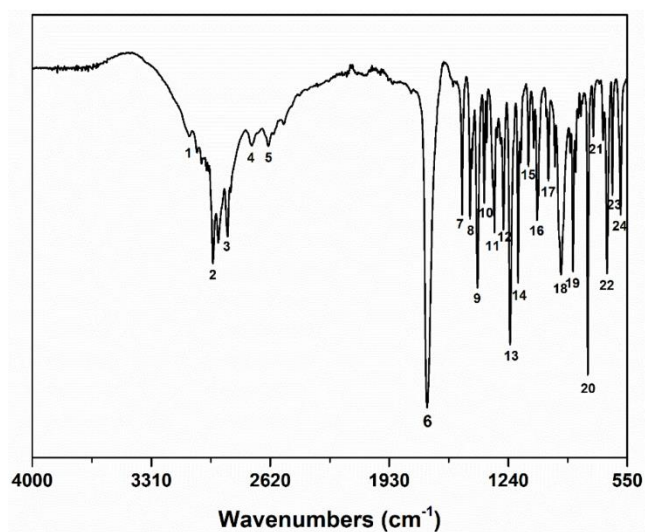
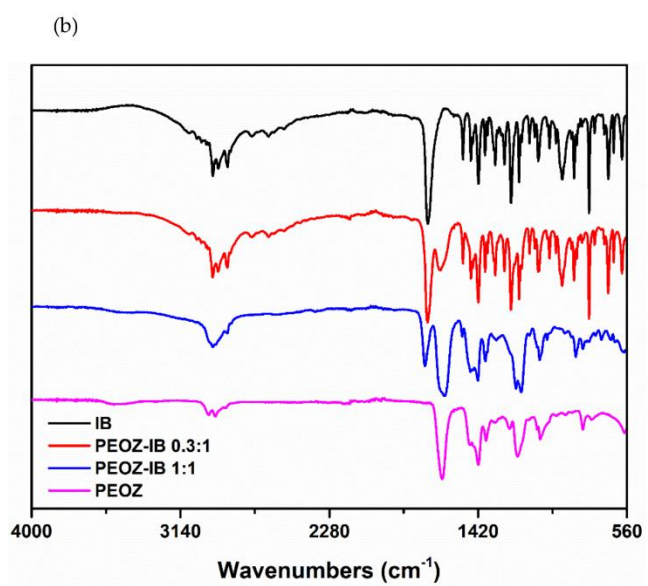
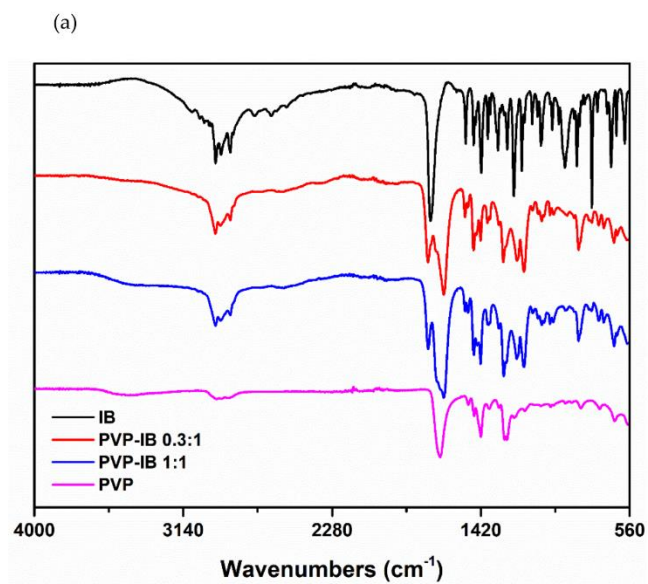
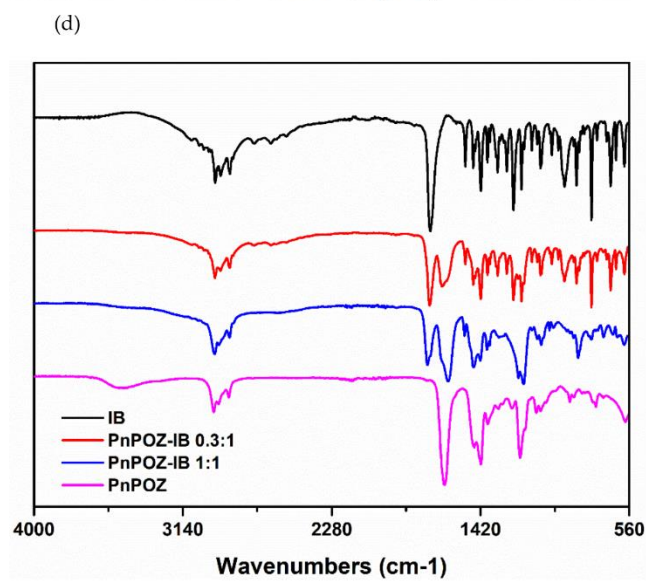
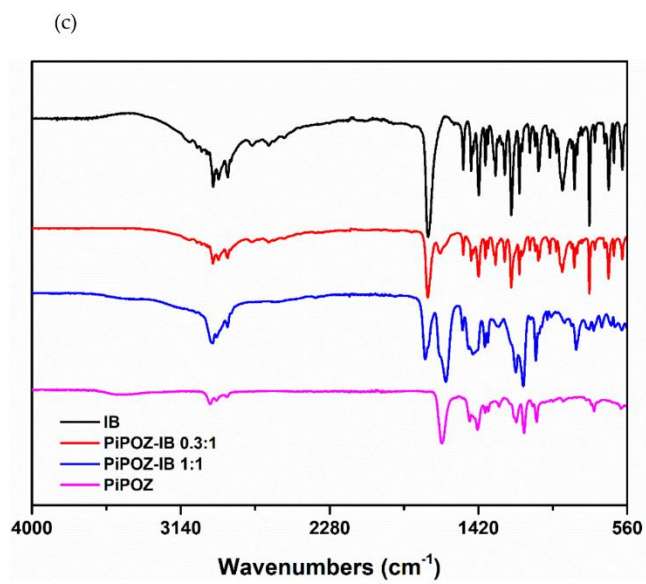


Figure S1. FTIR of ibuprofen.





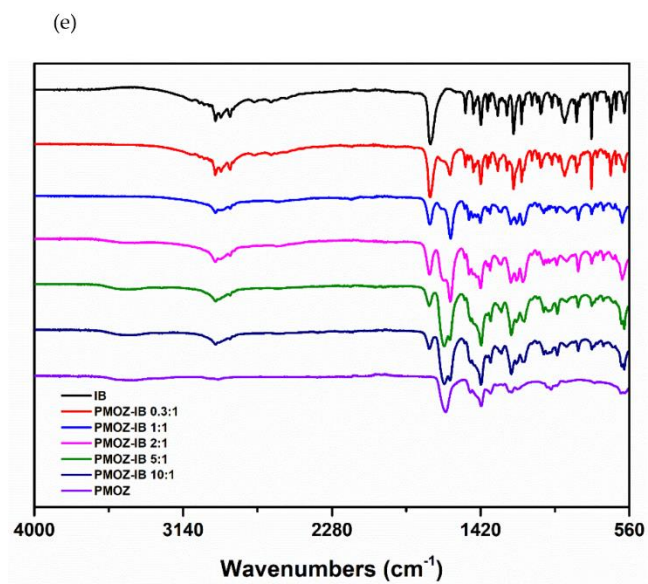


Figure S2. FTIR full spectra of PVP-IB SDs (a), PEOZ-IB SDs (b), PnPOZ-IB SDs (c), PiPOZ-IB SDs (d) and PMOZ-IB SDs (e).

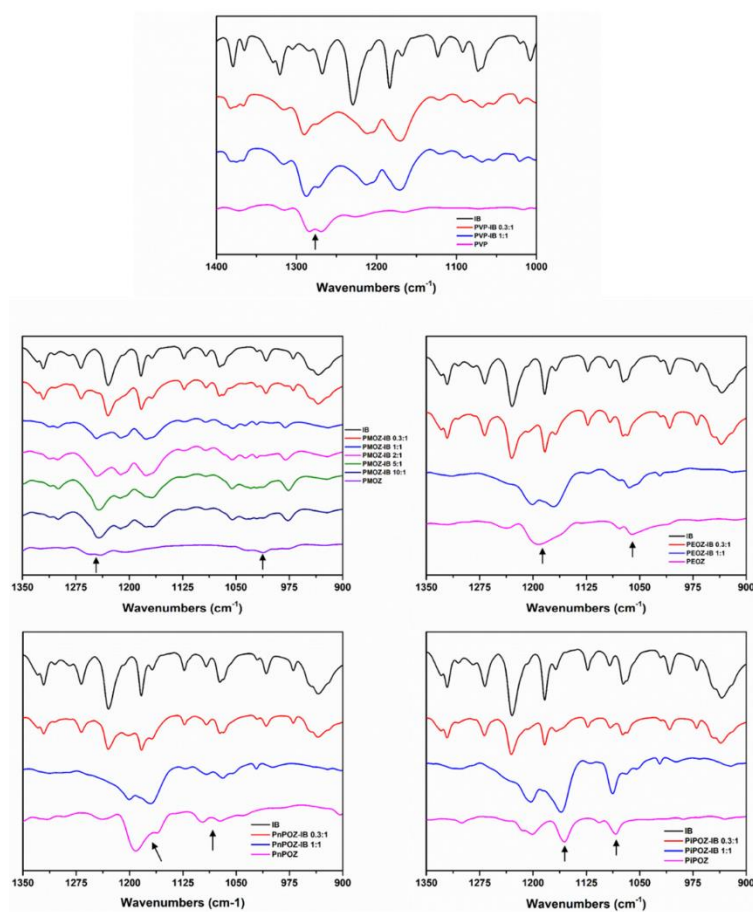


Figure S3. FTIR spectra of PVP-IB SDs and POZ-IB SDs in the range of 1400~900 cm^{-1} . The peaks (marked with an arrow) are attributed to C-N mode.

Table S1. FTIR spectral data of ibuprofen (s- strong; w- weak; sym-symmetrical; asym-asymmetrical; str-stretching; m-medium; vs- very strong; vw – very weak.).

Band	Wavenumbers (cm^{-1})	Assignments
1	3088 m	CH_2 asym str
2	2955 vs	CH_3 asym str
3	2869 m	CH_2 sym str
4	2725 m	O-H...O valence str
5	2633 m	O-H...O valence str
6	1710 vs	C=O str
7	1507 s	aromatic C=C str
8	1462 s	CH_3 asym deformation, CH_2 scissoring
9	1416 s	CH-CO deformation
10	1380 s	CH_3 sym str
11	1320 s	OH in plane deformation
12	1268 s	=C-H in plane deformation
13	1230 vs	C...C str
14	1183 s	C-O str

15	1123 w	=C-H in plane deformation
16	1071 m	=C-H in plane deformation
17	1008 m	C-H in plane deformation
18	936 s	CH ₃ rocking vibration
19	866 s	C-H out of plane vibration
20	779 s	CH ₂ rocking
21	746 w	C=C ring str, C...C skeletal vibration
22	668 s	C-H out of plane deformation
23	636 w	C-H in plane ring deformation
24	588 m	C...C deformation

Chapter 4

Synthesis and Evaluation of Methacrylated Poly(2-ethyl-2-oxazoline) as a Mucoadhesive Polymer for Nasal Drug Delivery

This chapter was published as Shan, X.; Aspinall, S.; Kaldybekov, D.B.; Buang, F.; Williams, A.C.; Khutoryanskiy, V.V., Synthesis and Evaluation of Methacrylated Poly(2-ethyl-2-oxazoline) as a Mucoadhesive Polymer for Nasal Drug Delivery. ACS Applied Polymer Materials 2021, 3, 5882-5992.

Synthesis and Evaluation of Methacrylated Poly(2-ethyl-2-oxazoline) as a Mucoadhesive Polymer for Nasal Drug Delivery

Xiaoning Shan, Sam Aspinall, Dautlet B. Kaldybekov, Fhataheya Buang, Adrian C. Williams, and Vitaliy V. Khutoryanskiy*

Cite This: *ACS Appl. Polym. Mater.* 2021, 3, 5882–5892

Read Online

ACCESS |

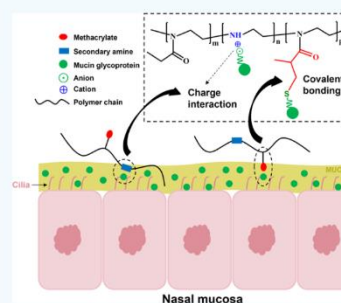
Metrics & More

Article Recommendations

Supporting Information

ABSTRACT: Methacrylated poly(2-ethyl-2-oxazoline) (PEOZ) was synthesized by partial hydrolysis of 500 kDa PEOZ, and the resulting poly[(2-ethyl-2-oxazoline)-*co*-ethylenimine] P(EOZ-*co*-EI) was subsequently reacted with methacrylic anhydride. The successful synthesis of methacrylated PEOZ (MAPEOZ) was confirmed by proton nuclear magnetic resonance (^1H NMR), infrared spectroscopy, and differential scanning calorimetry. The degrees of hydrolysis and methacrylation were determined by ^1H NMR spectra. MAPEOZ exhibited temperature-responsive properties, which were dependent on the degree of methacrylation. On that basis, three soluble MAPEOZ derivatives with different degrees of methacrylation were selected and investigated in cell toxicity studies, showing no significant cytotoxicity against the HEK293 cell line. A slug mucosal irritation assay showed that PEOZ and MAPEOZ do not cause mucosal irritation. The presence of methacryloyl groups and residual amines had a remarkable synergistic effect on the mucoadhesive properties of these polymers. These poly(2-ethyl-2-oxazoline) derivatives have excellent potential as mucoadhesive materials for developing formulations for drug delivery via mucosal routes of administration.

KEYWORDS: poly(2-ethyl-2-oxazoline), mucoadhesion, mucoadhesive materials, methacrylated polymers, nasal drug delivery



1. INTRODUCTION

Nasal administration is a readily accessible route for non-invasive treatment of rhinitis or nasal polyposis. Moreover, the human nasal mucosa surface area is around 150 cm², and, as a tissue with a relatively high vascularization and permeability, the nose is not only a therapeutic target but also a gateway for systemic drug delivery.^{1,2} Consequently, dosage forms have been developed for various therapeutic purposes, including hormone replacement therapy,³ osteoporosis,⁴ migraine,⁵ and prostate cancer,^{6,7} and have the potential to treat different neurodegenerative disorders such as Alzheimer's, Parkinson's, and Huntington's diseases.⁸

However, the nasal cavity mucus layer can function as a barrier to drug diffusion to the nasal epithelium, which can result in poor drug bioavailability. To optimize nasal administration, bioadhesive or, more appropriately, mucoadhesive dosage forms such as microspheres,^{9–11} liposomes,^{12–14} and gels^{15,16} have been studied to prolong their residence in the nasal cavity. Polymeric dosage forms exhibiting mucoadhesive properties are usually formulated using hydrophilic polymers, which often demonstrate strong mucoadhesion. Cationic polymers such as chitosan show strong mucoadhesive properties due to interactions with mucosal surfaces.^{17–21} In addition, some hydrophilic polymers with methacryloyl groups,²² acryloyl groups,^{23–26} and maleimide^{27–29} can covalently bond with the thiols present in mucus glycoproteins

through a Michael-type addition;³⁰ catechol-functionalized polymers formed covalent bonds with thiols in mucus glycoproteins via catechol oxidation.³¹ Further, polymeric thiomers, defined as polymers with $-\text{SH}$ groups, formed covalent disulfide bridges with thiols in mucus glycoproteins.^{32–34} Phenylboronic acid-decorated polymers can interact with mucosal surfaces either through a covalent linkage with the sialic acid present in mucins to form reversible covalent complexes^{35–37} or via hydrogen bonds with the hydroxyl groups present in oligosaccharide side chains.³⁸

Poly(2-oxazolines) are an emerging class of polymers that are attracting significant interest due to their unique physicochemical properties and lack of toxicity.^{39–42} Poly(2-methyl-2-oxazoline), poly(2-ethyl-2-oxazoline) (PEOZ), and poly(*n*-propyl-2-oxazoline) are of particular interest as drug delivery vehicles due to their solubility in water.⁴³ However, poly(2-oxazolines) themselves tend to be poorly mucoadhesive. For example, we showed that thiolated silica nanoparticles are mucoadhesive, but POZylated (functionalized with short-

Received: August 27, 2021

Accepted: October 22, 2021

Published: November 3, 2021



chain 5 kDa poly(2-oxazolines)) nanoparticles became non-mucoadhesive in an *ex vivo* rat intestinal mucosal model⁴⁴ and enhanced mucus penetration through porcine stomach mucosa.⁴⁵ Larger molecular weight PEOZ (50, 200, and 500 kDa) exhibited weak mucoadhesive properties that were improved by complexation or mixing with Carbopol,⁴⁶ and similarly, films formed from chitosan and PEOZ blends demonstrated mucoadhesive properties with respect to bovine cornea⁴⁷ and sheep vaginal tissue.⁴⁸ These studies indicate that nonionic water-soluble poly(2-oxazolines) exhibit poor mucoadhesive properties unless mixed with more mucoadhesive materials such as chitosan or Carbopol.

To enhance the mucoadhesion of poly(2-oxazolines), here we have chemically modified the PEOZ backbone through partial hydrolysis and a subsequent reaction of the resulting poly[(2-ethyl-2-oxazoline)-*co*-ethylenimine] P(EOZ-*co*-EI) with methacrylic anhydride, forming methacrylated (or methacryloylated) polymers. The products were characterized using spectroscopic (¹H nuclear magnetic resonance (NMR), Fourier transform infrared (FTIR), and UV-vis) and thermal (differential scanning calorimetry (DSC)) methods. The biocompatibility of the parent PEOZ and its hydrolyzed and methacrylated derivatives was studied in the HEK293 cell line and by using an *in vivo* slug mucosal irritation (SMI) assay. Aqueous solutions of PEOZ and its methacrylated derivatives containing sodium fluorescein were prepared and their retention on sheep nasal mucosa was evaluated using a fluorescence flow-through assay.

2. EXPERIMENTAL SECTION

2.1. Materials. Poly(2-ethyl-2-oxazoline) (PEOZ, 500 kDa, dispersity $D = 3-4$), methacrylic anhydride, dimethyl sulfoxide (DMSO), deuterated DMSO (DMSO-*d*₆), deuterium oxide (D₂O), sodium fluorescein, glycol chitosan, benzalkonium chloride (BAC), calcium chloride dihydrate (CaCl₂·2H₂O), sodium chloride (NaCl), and potassium chloride (KCl) were obtained from Sigma-Aldrich (Gillingham, U.K.). Hydrochloric acid (HCl; 37 wt %), triethylamine (TEA; 99.7%, extra pure), and phosphate-buffered saline (PBS) tablets were obtained from Fisher Scientific (Loughborough, U.K.). Dialysis membrane with a molecular weight cutoff of 7 kDa was purchased from Mediatech Membranes Ltd. (U.K.). DMEM high glucose was purchased from Capricorn Scientific (Germany). Fetal calf serum (10%) was purchased from GE Healthcare Life Sciences. Penicillin/streptomycin (1%) was purchased from Nacalai Tesque Inc. (Japan). CellTiter 96 Aqueous MTS Reagent Powder was purchased from Promega Corporation. Phenazine methosulfate was purchased from Thermo Fisher Scientific.

2.2. Partial Hydrolysis of Poly(2-ethyl-2-oxazoline). PEOZ was partially hydrolyzed to poly[(2-ethyl-2-oxazoline)-*co*-ethylenimine], P(EOZ-*co*-EI), copolymers according to reported procedures^{49,50} with minor changes. To study the hydrolysis kinetics, PEOZ (20.0 g) was dissolved in 200 mL of 18 wt % aqueous HCl and heated for 0.5, 1, 1.5, 2, 2.5, and 3 h at 100 °C. Subsequently, the mixture was cooled in an ice-water bath to quench the reaction. The obtained mixture was then mixed with a portion of deionized water and purified by dialysis via a cellulose-based membrane with 7 kDa MWCO at room temperature. All copolymers were recovered by freeze-drying.

2.3. Synthesis of Methacrylated Poly(2-ethyl-2-oxazoline). Methacrylated poly(2-ethyl-2-oxazoline) (MAPEOZ) was synthesized by reacting ethylenimine groups of P(EOZ-*co*-EI) with methacrylic anhydride to generate four derivatives (with four degrees of methacrylation) according to the reported method²² with slight modifications. Briefly, P(EOZ-*co*-EI) (1 equiv of amines) was dissolved in a mixture of DMSO and deionized water (1:1 v/v). Methacrylic anhydride (2.5 equiv) and TEA (2.5 equiv) were added

to the reaction mixture, which was stirred at 40 °C overnight. The products were then redispersed in deionized water and purified by dialysis at room temperature. All polymers were then recovered by freeze-drying.

2.4. Characterization of Methacrylated Poly(2-ethyl-2-oxazoline).
2.4.1. Proton Nuclear Magnetic Resonance (¹H NMR). ¹H NMR spectra of polymers were recorded in D₂O and DMSO-*d*₆ (15 mg/mL) using a 400 MHz Bruker spectrometer (Nanobay). All chemical shifts are given in ppm. MestReNova software was used for spectral analysis.

2.4.2. Fourier Transform Infrared (FTIR) Spectroscopy. FTIR spectra were recorded using a diamond attenuated total reflection (ATR) accessory on a Nicolet iS5 spectrometer. After a background scan, data were collected between 4000 and 400 cm⁻¹ at a resolution of 4 cm⁻¹ as an average of 64 scans; OMNIC software was used for spectral analysis.

2.4.3. Differential Scanning Calorimetry (DSC). Samples (3–5 mg) were placed in pierced T_{zero} aluminum pans. The thermal properties of each sample were investigated using a DSC (TA Instruments) in a nitrogen atmosphere with a heating/cooling rate of 10 °C/min from 10 to 150 °C. The values of the glass-transition temperature (T_g) were determined from the second heating cycle of each sample.

2.4.4. ¹H NMR to Calculate PEOZ Hydrolysis. Hydrolysis of poly(2-ethyl-2-oxazoline) to poly[(2-ethyl-2-oxazoline)-*co*-ethylenimine] was determined from ¹H NMR spectra in D₂O using the signals (as shown in Figure S1) and the integrated areas (*I*) of the peaks assigned to either PEOZ or its hydrolysis product; conversion was calculated according to⁴⁵

$$\% \text{ conversion PEOZ} = \frac{I[\text{EI}]}{I[\text{EI}] + I[\text{EOZ}]} \times 100 \quad (1)$$

where $I[\text{EOZ}]$ is the integral value of EOZ moieties and $I[\text{EI}]$ is the integral value of EI moieties.

2.4.5. ¹H NMR to Determine the Composition of MAPEOZ Samples. The degree of methacrylation was calculated from ¹H NMR spectra in D₂O using the integrated areas (*I*) from the methacrylated products (Figure S3).

$$\text{methacrylation \%} = \frac{I[\text{MA}]}{I[\text{EOZ}] + I[\text{EI}] + I[\text{MA}]} \times 100 \quad (2)$$

$$\text{EI \%} = \frac{I[\text{EI}]}{I[\text{EOZ}] + I[\text{EI}] + I[\text{MA}]} \times 100 \quad (3)$$

$$\text{EOZ \%} = \frac{I[\text{EOZ}]}{I[\text{EOZ}] + I[\text{EI}] + I[\text{MA}]} \times 100 \quad (4)$$

where $I[\text{MA}]$ is the integral value of the backbone of methacrylated moieties, $I[\text{EOZ}]$ is the integral value of the backbone of EOZ groups, and $I[\text{EI}]$ is the integral value of EI groups.

Given that the signal of EOZ groups overlapped with the signal of MA (Figure 2), according to

$$\frac{I[\text{MA}]}{4} = \frac{I[\text{MA CH}_3]}{3} \quad \text{and} \quad \frac{I[\text{EOZ}]}{4} = \frac{I[\text{PEOZ CH}_3]}{3}$$

where $I[\text{MA CH}_3]$ is the integral value of $-\text{CH}_3$ of methacrylated moieties and $I[\text{PEOZ CH}_3]$ is the integral value of $-\text{CH}_3$ of EOZ moieties, eqs 2, 3, and 4 were modified to

$$\text{methacrylation \%} = \frac{4I[\text{MA CH}_3]}{4I[\text{EOZ CH}_3] + 3I[\text{EI}] + 4I[\text{MA CH}_3]} \times 100 \quad (5)$$

$$\text{EI \%} = \frac{3I[\text{EI}]}{4I[\text{PEOZ CH}_3] + 3I[\text{EI}] + 4I[\text{MA CH}_3]} \times 100 \quad (6)$$

$$\text{EOZ \%} = \frac{4I[\text{EOZ CH}_3]}{4I[\text{EOZ CH}_3] + 3I[\text{EI}] + 4I[\text{MA CH}_3]} \times 100 \quad (7)$$

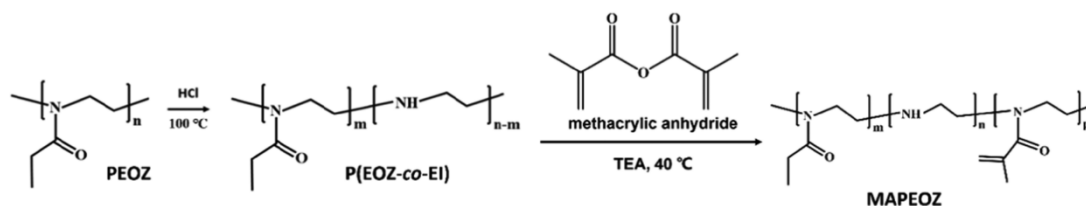


Figure 1. Synthesis of methacrylated poly(2-ethyl-2-oxazoline) (MAPEOZ).

2.4.6. Turbidity Measurements. Turbidity measurements were performed with a Cary 100 UV–vis spectrometer equipped with a Cary temperature controller (Agilent Technologies). All polymers were dissolved in deionized water (1 mg/mL) and measured at 600 nm with 1 °C/min ramp (measurement wait time of 30 s and measurement interval of 1 °C). The absorbance data were converted to transmittance by the following equation

$$\%T = 10^{-A} \quad (8)$$

where T is the transmittance and A is the absorbance. The resulting value was then plotted as $\%T$ versus temperature.

2.5. In Vitro Nasal Mucoadhesion Studies. **2.5.1. Preparation of Polymer/Fluorescein Sodium Mixtures and Artificial Nasal Fluid.** Artificial nasal fluid (ANF) was prepared using the established protocols^{25,51} by dissolving 7.45 g of NaCl, 1.29 g of KCl, and 0.32 g of $\text{CaCl}_2 \cdot 2\text{H}_2\text{O}$ in 1 L of deionized water. The artificial nasal fluid was kept at 37 °C throughout the experiments.

Solutions of sodium fluorescein (0.05 mg/mL) were prepared in deionized water into which polymer samples were dissolved; 10 mg of either PEOZ, $\text{MA}_{10}\text{PEOZ}$, $\text{MA}_{25}\text{PEOZ}$, $\text{MA}_{35}\text{PEOZ}$, or glycol chitosan was dispersed in 10 mL of the sodium fluorescein solution and the pH was adjusted to 5.70. These mixtures were stirred for 24 h at room temperature until complete dissolution and were protected from light with an aluminum foil.

2.5.2. Retention Studies on Nasal Mucosa. Sheep heads were received from P.C. Turner Abattoir (Farnborough, U.K.) and used within 24 h after animal slaughter. The nasal septum mucosal tissue ($1.5 \times 1 \text{ cm}^2$) was dissected with scissors and washed with 1 mL of ANF.

All experiments assessing retention of formulations on nasal mucosal tissues were conducted at 37 °C in an incubator. Images of mucosal surfaces were taken using a fluorescence microscope (MZ10F, Leica Microsystems, U.K.) equipped with an “ET GFP” filter and a Zeiss Imager A1/AxioCam MRm camera. All images were at 0.8× magnification with a 211 ms exposure time. Initially, the fluorescence images of mucosal tissues were recorded for each sample to collect the background fluorescence intensity. Then, 20 μL solution of either 1 mg/mL PEOZ, $\text{MA}_{10}\text{PEOZ}$, $\text{MA}_{25}\text{PEOZ}$, $\text{MA}_{35}\text{PEOZ}$, or glycol chitosan containing 0.05 mg/mL sodium fluorescein was placed on the mucosal surface and fluorescence images were recorded again. After 3 min of dosing, the mucosal tissues were transferred to the incubator and washed with ANF using a syringe pump at 0.43 mL/min. Fluorescence images of the mucosal tissue were collected periodically and analyzed using ImageJ software to measure the pixel intensity after each wash. The results are presented as fluorescence intensity as a function of the time of irrigation after subtracting the background fluorescence from each wash image. Sodium fluorescein solution in deionized water (0.05 mg/mL) was used as a negative control, and glycol chitosan solution (1 mg/mL) was used as a positive control. The experiments were conducted in triplicate.

2.6. Toxicology. **2.6.1. Cell Toxicity Studies.** HEK293 was cultured in DMEM high glucose supplemented with 10% fetal calf serum and 1% penicillin/streptomycin. The cells were incubated at 37 °C in a humidified atmosphere of 5% CO_2 . Cell viability was assessed using the CellTiter 96 Aqueous Non-Radioactive Cell Proliferation Assay (MTS assay). The cells were seeded in a 96-well plate at 3×10^3 cells/well and incubated overnight for cell attachment. The cells were then treated with various concentrations of the polymers (25, 50,

75, 100, 125, and 150 $\mu\text{g}/\text{mL}$) for 72 h. The negative control group consisted of untreated cells and was considered as 100% of viable cells. After 72 h, treatment media were replaced with new growth media and 20 μL of MTS solution (prepared in phosphate-buffered saline) containing 2 mg/mL CellTiter 96 Aqueous MTS Reagent Powder and 0.92 mg/mL phenazine methosulfate. The cells were incubated for another 4 h before the absorbance (Abs) was measured at 490 nm using an Infinite 200 PRO microplate reader (Tecan Group Ltd., Switzerland). The results are expressed as a percentage of cell viability compared to the negative control group based on the following equation

$$\text{cell viability (\%)} = \frac{(\text{Abs}_{\text{treatment}} - \text{Abs}_{\text{blank}})}{(\text{Abs}_{\text{control}} - \text{Abs}_{\text{blank}})} \times 100 \quad (9)$$

2.6.2. Slug Mucosal Irritation Assay. The slug mucosal irritation (SMI) assay was performed according to our previous reports.^{52–54} *A. lusitanicus* slugs were collected in Harris Garden (Reading, U.K.). Slugs weighing between 6 and 18 g were individually placed in 2 L glass beakers lined with a paper towel moistened with 20 mL of phosphate-buffered saline (PBS; pH 7.40) and left for 48 h prior to experiments. All beakers were covered with a pierced cling film. Each slug was individually weighed and then placed in 90 mm plastic Petri dishes lined with Whatman filter paper moistened with either 2 mL of positive/negative controls (1% BAC prepared in PBS and PBS solution) or 2 mL of each test material (PEOZ, $\text{MA}_{10}\text{PEOZ}$, $\text{MA}_{25}\text{PEOZ}$, and $\text{MA}_{35}\text{PEOZ}$) prepared in PBS. The concentration of test materials (1 mg/mL) was chosen to correlate with nasal mucosal retention studies. Slugs were kept in contact with the test samples for 60 min and then removed, rinsed with 10 mL of PBS, gently wiped, and then reweighed. Mucus production (MP) was calculated using the following equation

$$\text{MP} = \frac{(m_b - m_a)}{m_b} \times 100\% \quad (10)$$

where m_b and m_a are the weights of a slug before and after the experiment, respectively. Each experiment was repeated five times with different slugs, and the results were presented as mean \pm standard deviation.

2.7. Statistical Analysis. All experiments were conducted in triplicate, and data were expressed as mean \pm standard deviation with a probability of $p < 0.05$ was considered as significant. GraphPad Prism statistical analysis software (version 9.0) was used to analyze data using a one-way analysis of variance (ANOVA) and paired t -tests.

3. RESULTS AND DISCUSSION

3.1. P(EOZ-co-EI) Synthesis and ^1H NMR Characterization. Complete hydrolysis of PEOZ to prepare pure linear PEI was reported by our group recently⁵⁵ and previously by Hoogenboom et al.^{56,57} Here, we prepared partially hydrolyzed PEOZ with some ethylene imine units remaining available for further functionalization by reaction with methacrylic anhydride (Figure 1).

To investigate the hydrolysis kinetics of PEOZ at 100 °C, the reaction was terminated at different times (0.5, 1, 1.5, 2,

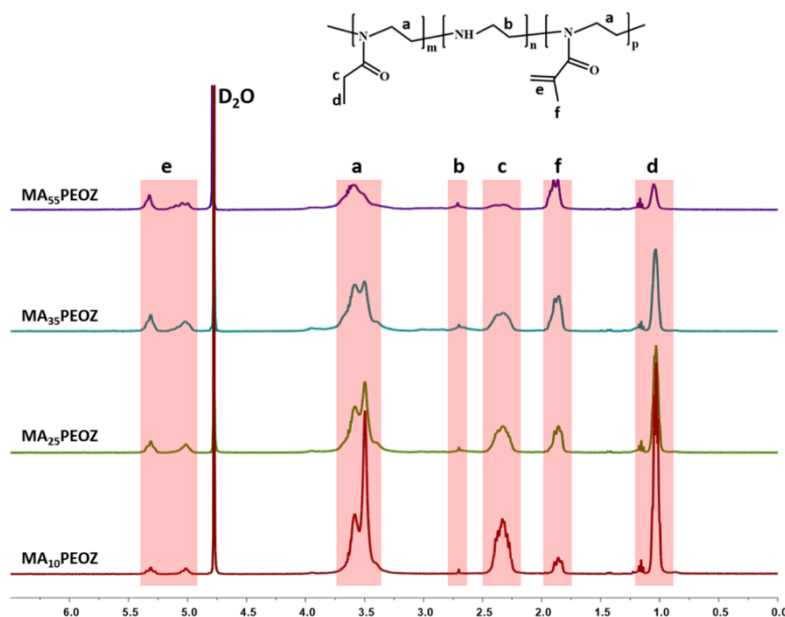


Figure 2. ^1H NMR spectra of MAPEOZ recorded in D_2O .

2.5, and 3 h). The ^1H NMR spectra of these copolymers showed signals corresponding to the PEOZ backbone at 3.5 ppm (peak a, Figure S1) with signals 2.44 ppm (peak c) and 1.13 ppm (peak d) attributed to PEOZ side chains. Partial hydrolysis of PEOZ was confirmed not only by both reduced signals from PEOZ side chains and reduced and broadened signals from the PEOZ backbone but also by a reaction time-dependent increasing signal at 3.34 ppm (peak b, Figure S1), which was attributed to the backbone of PEI moieties. The degree of conversion from PEOZ to P(EOZ-co-EI) was calculated using eq 1 and was plotted versus time (Figure S2). Under our reaction conditions, hydrolysis of PEOZ follows first-order kinetics, which is slightly different from a previous report⁴⁹ where pseudo-first-order kinetics was reported when using a microwave synthesizer with closed reactors and a lower HCl concentration. Taken from Figure S2, conversion from PEOZ to P(EOZ-co-EI) at 0.5, 1, 2, and 3 h was 15, 28, 53, and 78% of EI, respectively (Table S1).

3.2. Synthesis and Characterization of Methacrylated PEOZ. The secondary amines present in P(EOZ-co-EI) offer reactive sites for further methacrylation by reaction with methacrylic anhydride in the presence of TEA as a basic catalyst. P(EOZ-co-EI) copolymers prepared following 0.5, 1, 2, and 3 h of partial hydrolysis were selected for further methacrylation. The resultant MAPEOZ polymers were characterized using ^1H NMR, FTIR, and DSC.

The ^1H NMR spectra of MAPEOZ polymers showed signals corresponding to the backbone of EOZ repeating units as well as the backbone of methacrylated units at 3.5 ppm (peak a, Figure 2); the signals labeled as c (2.44 ppm) and d (1.13 ppm) are attributed to the methylene and methyl groups of EOZ units, respectively. The signal characteristic for the backbone of unreacted EI units shifted from 3.10 ppm (peak b, Figure S1) to 2.71 ppm (peak b, Figure 2) upon modification.

The signals labeled e (5.0–5.5 ppm) and f (1.86 ppm) are attributed to the protons of the double bond and methyl of the methacryloyl group, respectively. Increasing methacrylation or decreasing EOZ units, in other words, led to a significant weakening of peaks c and d and strengthening of peaks e and f. It should be noted that the ^1H NMR spectrum of MA₅₅PEOZ was recorded both in $\text{DMSO}-d_6$ and in D_2O since this sample exhibited limited solubility in D_2O (discussed below). The chemical shifts of protons of MA₃₅PEOZ in $\text{DMSO}-d_6$ were consistent with the spectra of other samples recorded in D_2O , with some expected minor shifts related to the switch of solvent (Figure S3).

The compositions of MAPEOZ polymers were calculated using eqs 5–7 and are presented in Table 1. As expected,

Table 1. Composition of MAPEOZ Calculated from the ^1H NMR Spectra

sources	products	EOZ (%)	EI (%)	MA (%)
P(EOZ-co-EI ₁₅)	MA ₁₀ PEOZ	89	1	10
P(EOZ-co-EI ₂₈)	MA ₂₅ PEOZ	70	5	25
P(EOZ-co-EI ₅₃)	MA ₃₅ PEOZ	52	13	35
P(EOZ-co-EI ₇₈)	MA ₅₅ PEOZ (D_2O)	27	18	55
	MA ₅₅ PEOZ ($\text{DMSO}-d_6$)	26	19	55

methacrylation increased with PEOZ hydrolysis, and for clarity, the methacrylated polymers are annotated with their MA content (i.e., MA₁₀PEOZ contains 10% MA groups and was synthesized from the PEOZ sample that had hydrolyzed for 0.5 h). It can be seen that the secondary amines were not completely substituted by methacryloyl groups due to steric hindrance with 1, 5, 13, and 18% residual EI units remaining in the four MAPEOZ products. The proportion of EOZ units (89, 70, 52, and 27%, Table 1) in the four MAPEOZ samples

shows good agreement with the PEOZ to P(EOZ-co-EI) hydrolysis study (85, 72, 47, and 22%, Table S1). The composition of MA₅₅PEOZ calculated from ¹H NMR spectra recorded in D₂O (27% EOZ, 18% EI, and 55% MA) was in good agreement with the composition determined in DMSO-*d*₆ (26% EOZ, 19% EI, and 55% MA).

Infrared analysis of PEOZ provided peaks at 2977 and 2940 cm⁻¹ (CH₂ stretch) (Figure S4), 1626 cm⁻¹ (C=O stretch), 1470 cm⁻¹ (C–H bending), 1420 cm⁻¹ (C–H bending), and 1240 cm⁻¹ (C–N stretch). New peaks at 1719 and 916 cm⁻¹ (Figure 3), assigned to the stretching mode and bending

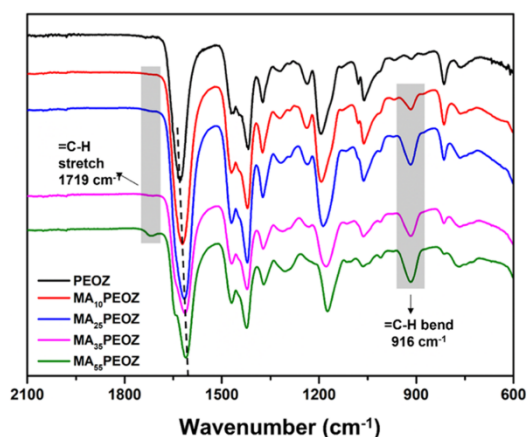


Figure 3. FTIR spectra of PEOZ and MAPEOZ in the range of 2100–600 cm⁻¹.

modes of =C–H, became evident with increasing methacrylation, which further confirmed its successful modification. In addition, it is notable that the peak attributed to the carbonyl group of MAPEOZ gradually shifted to lower wavenumbers (1622 cm⁻¹ for MA₁₀PEOZ, 1617 cm⁻¹ for MA₂₅PEOZ, 1614 cm⁻¹ for MA₃₅PEOZ, and 1611 cm⁻¹ for MA₅₅PEOZ) with increasing methacrylation. It is problematic to detect EI moieties in these FTIR spectra because the characteristic N–H bending mode of EI at 1474 cm⁻¹^{55,55} overlaps with the C–H bending mode of EOZ moieties at 1470 cm⁻¹.

PEOZ and MAPEOZ samples were also analyzed using differential scanning calorimetry (Figure 4). PEOZ, MA₁₀PEOZ, MA₂₅PEOZ, MA₃₅PEOZ, and MA₅₅PEOZ showed glass-transition temperatures (*T*_g) at 60.7, 62.5, 64.4, 65.2, and 68.7 °C, respectively. The increase in *T*_g with an increasing degree of methacrylation in MAPEOZ can be explained by the lower flexibility of the macromolecules with bulky groups, which decreases the overall chain mobility.

The thermal properties of the new polymers were also studied in aqueous solutions. To this end, PEOZ and MAPEOZ samples (1 mg/mL) were dissolved in deionized water, and their phase behavior was studied by measuring solution turbidity between 5 and 95 °C (Figure 5a). The literature describes various methods to determine the cloud point (*T*_{cp}), including the onset of the fall in transmittance, or the temperature where transmittance is 80 or 50%, or by taking the inflection point of the turbidity curve.⁵⁸ Here, the onset of the fall in transmittance was used as this value was accessible

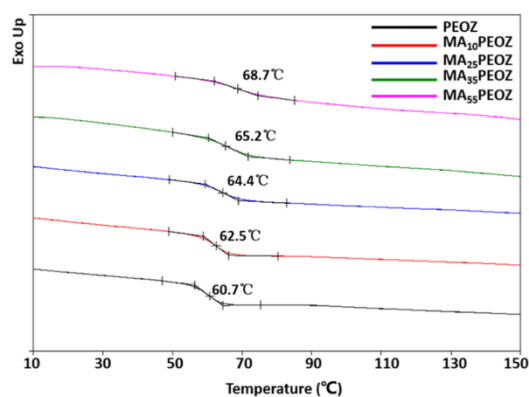


Figure 4. DSC thermograms (second scan) of PEOZ and MAPEOZ samples showing increasing glass-transition temperatures with increasing methacrylation.

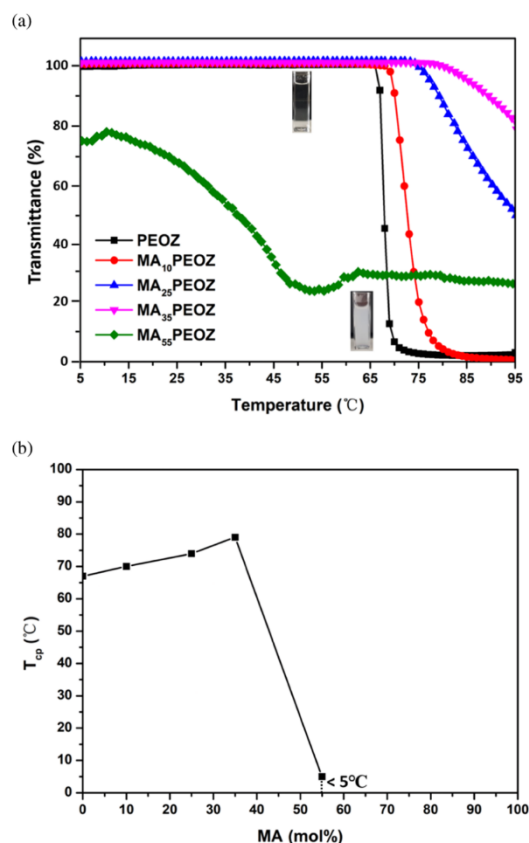


Figure 5. (a) Turbidity measurements of aqueous solutions of PEOZ and MAPEOZ samples (1 mg/mL). (b) *T*_{cp} as a function of MA mol % in MAPEOZ polymers.

for all MAPEOZ samples. PEOZ exhibited a cloud point of 67 °C, in agreement with the literature where PEOZ undergoes

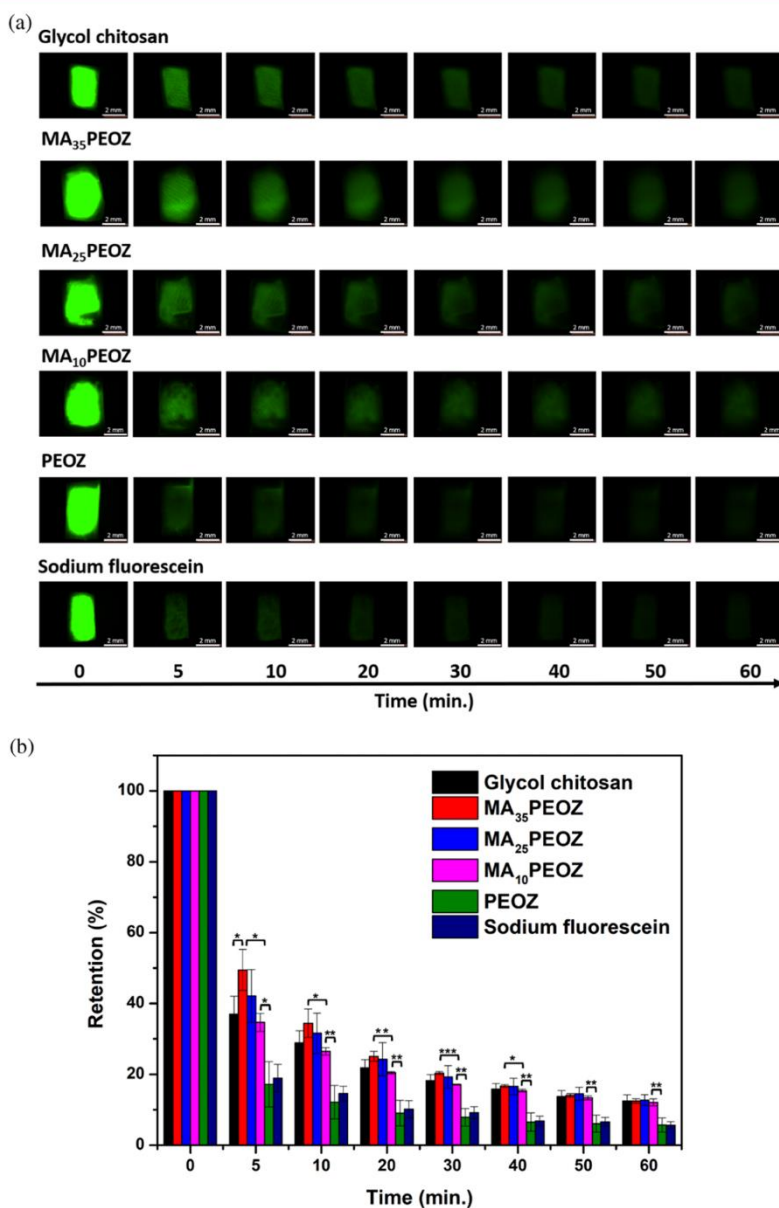


Figure 6. (a) Fluorescence images showing retention of 1 mg/mL glycol chitosan, PEOZ, MA₁₀PEOZ, MA₂₅PEOZ, and MA₃₅PEOZ solutions using 0.05 mg/mL sodium fluorescein as the solvent and pure 0.05 mg/mL sodium fluorescein solution on sheep nasal mucosa and washed with ANF. Scale bars are 2 mm. (b) Retention of 1 mg/mL glycol chitosan, PEOZ, MA₁₀PEOZ, MA₂₅PEOZ, and MA₃₅PEOZ solutions using 0.05 mg/mL sodium fluorescein as the solvent and pure 0.05 mg/mL sodium fluorescein solution on sheep nasal mucosa as washed with different volumes of ANF (pH = 5.70; $n = 3$, mean \pm SD, “*” represents $p < 0.05$; “**” represents $p < 0.01$; “***” represents $p < 0.001$).

phase separation between 61 and 70 °C, depending on the molecular weight and the solution concentration.^{59,60}

Methacrylate groups of MAPEOZ make the macromolecules more hydrophobic.⁶¹ Therefore, increasing the proportion of MA was expected to lower T_{cp} . However, the results showed the opposite trend with T_{cp} increasing with increasing

methacrylation; T_{cp} values for MA₁₀PEOZ, MA₂₅PEOZ, and MA₃₅PEOZ were 70, 74, and 79 °C, respectively (Figure 5). The unexpected increase in T_{cp} may be explained by the increasing proportion of hydrophilic EI units that accompanies the increase in methacrylation (Table 1), and indeed, these may be positively charged upon protonation⁶² such that the

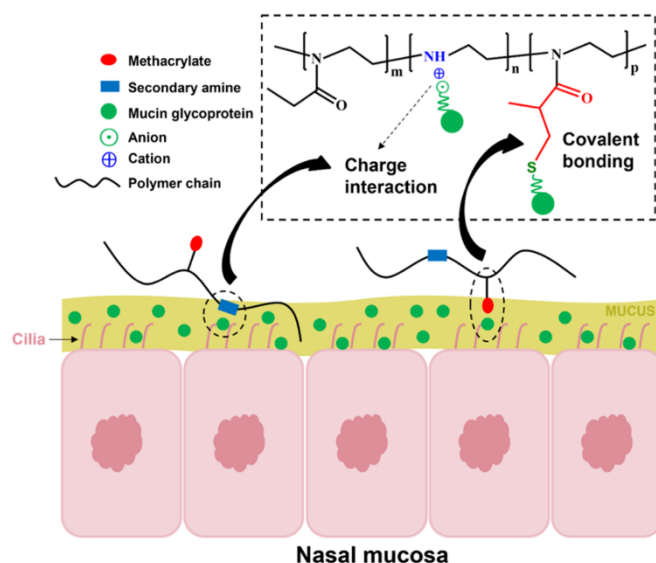


Figure 7. Proposed mechanism of interaction between MAPEOZ polymers and mucosal surfaces.

hydrophilicity of the whole macromolecule was improved. Interestingly, increasing the MA from 35 to 55% decreased the T_{cp} to a temperature below 5 °C (Figure 5b); the aqueous solution of MA₅₅PEOZ was already cloudy at 5 °C. It is feasible that the high hydrophobic MA content in MA₅₅PEOZ (MA% 55%) dominates the hydrophilic contribution of the EI groups and makes the macromolecules more hydrophobic than the parent PEOZ. The variability of T_{cp} with both MA and EI content suggests that systems can be tuned to provide a cloud point for desired applications.

3.3. In Vitro Nasal Mucoadhesion Studies. Given the limited water solubility of MA₃₅PEOZ at 37 °C, this polymer was not used in subsequent studies.

The retention of PEOZ, MA₁₀PEOZ, MA₂₅PEOZ, and MA₃₅PEOZ solutions with sodium fluorescein was evaluated on sheep nasal mucosa and washed with ANF. Glycol chitosan was used as a positive control with strong mucoadhesive properties,¹⁹ whereas sodium fluorescein was used as a negative control. Figure 6 shows the retention of sodium fluorescein mediated with glycol chitosan, PEOZ, MA₁₀PEOZ, MA₂₅PEOZ, and MA₃₅PEOZ on sheep nasal mucosa. Numerical values from these experiments are summarized in Table S2.

As expected, the water-soluble dye sodium fluorescein was poorly retained when dosed from a simple aqueous solution and was rapidly washed from the nasal mucosa surface with only ~5.7% of the initial fluorescence detected after 60 min of washing (Figure 6b). This residual fluorescence results from the penetration of sodium fluorescein into the biological tissue rather than its adhesion to the surface. Retention of sodium fluorescein was not improved in the presence of unmodified PEOZ, confirming the poor mucoadhesive properties of PEOZ shown in our previous studies⁴⁴ and attributed to the nonionic nature of this polymer.³⁰ PEOZ samples chemically modified through hydrolysis and subsequent methacrylation significantly improved sodium fluorescein retention on the mucosal surface. Particularly notable at shorter irrigation times (5, 10 min),

increasing methacrylation led to a greater retention of the fluorescent dye. For example, after 5 min of washing, ~50% of the dye was retained when administered with MA₃₅PEOZ compared with 42% retention when using MA₂₅PEOZ and 35% of the dye was retained when deposited with MA₁₀PEOZ. Indeed, after 5 min of irrigation, MA₃₅PEOZ retained significantly more sodium fluorescein than the positive control (cationic glycol chitosan) ($p < 0.05$).

As expected, retention declines with irrigation time, but the trend remains that mucoadhesion/mucoadhesion of the polymers is in the order MA₃₅PEOZ > glycol chitosan > MA₂₅PEOZ > MA₁₀PEOZ > PEOZ. It can be hypothesized that MAPEOZ polymers interact with mucosal surfaces through two mechanisms as shown in Figure 7: (1) the methacrylate groups could potentially form covalent bonds with the thiol groups present in mucins at the mucosal surface; (2) electrostatic interaction between cationic secondary amines within the polymer and negatively charged mucins due to the presence of carboxylate groups and ester sulfates in their structure.³² It is likely that the strong mucoadhesive properties of the MAPEOZ result from the synergistic positive effects from both the MA groups and residual secondary amines being available to interact with the mucosal surface.

3.4. Cell Toxicity Studies. The HEK293 cell line, consisting of immortalized human embryonic kidney cells, has been used for *in vitro* toxicity testing with varied toxicological endpoints.⁶³ The effects of the polymers on HEK293 cell viability were studied over 72 h using the MTS assay (Figure 8); numerical values as mean ± standard deviation are summarized in Table S3. Poly(2-oxazolines) have demonstrated excellent biocompatibility in a number of studies and are proposed as a versatile platform for biomedical applications,^{39,64} but here, PEOZ was found to moderately affect HEK293 cells, notably at >100 μg/mL where cell viability fell to below 90%, consistent with a previous study.⁶⁵ Hydrolyzed PEOZ with 15 mol % EI units (P(EOZ-co-EI₁₅)) showed a similar cell viability trend to PEOZ, suggesting that

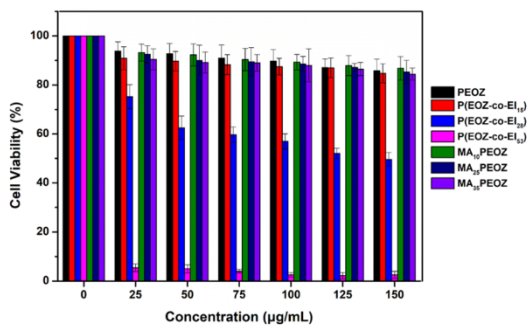


Figure 8. Viability of HEK293 cells determined after treatment with PEOZ, P(EOZ-co-EI₁₅), P(EOZ-co-EI₂₈), P(EOZ-co-EI₅₃), MA₁₀PEOZ, MA₂₅PEOZ, and MA₃₅PEOZ for 72 h. The untreated cells served as the control. Values are expressed as means \pm SD ($n = 3$).

15% EI did not alter the biocompatibility of the copolymer. However, poly(ethylenimine) (PEI), a widely used transfection agent, is known to be toxic, and so it is unsurprising that as the EI content in our hydrolyzed PEOZ increases, the cell viability declines. For example, when applied at 100 $\mu\text{g}/\text{mL}$, P(EOZ-co-EI₁₅) with 15 mol % EI units retained $>87\%$ cell viability, but this fell to 57% when treated with the polymer containing 28 mol % EI units and less than 3% of cells remained viable when treated with the polymer containing 53 mol % EI units at the same concentration. It is known that the positive charges of EI can induce cell death and apoptosis and cause toxicity both *in vitro* and *in vivo*.⁶⁶

Although the MAPEOZ polymers formed from the P(EOZ-co-EI) retain some EI units (Table 1), methacrylation essentially reverses or “blocks” the toxicity of the intermediate polymer and cell viability returns to the same levels seen with the parent PEOZ with $>90\%$ cell viability for PEOZ and all MAPEOZ samples when dosed at 25 $\mu\text{g}/\text{mL}$ and 88–90% viability for all when dosed at 100 $\mu\text{g}/\text{mL}$. The introduction of MA groups clearly reduced the cellular toxicity of hydrolyzed PEOZ, suggesting the equivalent biocompatibility of our modified MAPEOZ with the parent poly(2-ethyl-2-oxazoline).

3.5. Mucosal Irritancy. The slug mucosal irritation (SMI) *in vivo* assay, developed by Adriaens and co-workers,^{67,68} was used to evaluate the toxicological properties of PEOZ and its methacrylated derivatives. This test has been validated as a reliable method and is useful as a prescreen assay for evaluating the irritation potential of chemicals, formulations, and active ingredients to different mucosal membranes, including evaluation of nasal irritation.^{69–73} The slug’s mucosal layer is located at the outer surface of the body and, for this reason, it is easily observable by the investigator. In this test, colorless mucus, secreted by slugs after contact with a test substance, is a good initial indicator of biocompatibility. The total amount of mucus production serves as the main criterion to test the biocompatibility of formulations since this increases on exposure to stronger irritants.^{54,67,74} These assessments provide quantifiable data for test materials to be classified as nonirritating, mild, moderate, or severely irritating.^{72,73}

Figure 9 shows the data on mucus production by slugs exposed to filter paper surfaces soaked in PEOZ and its modified derivatives solutions at 1 mg/mL prepared in PBS, as well as positive and negative controls. On exposure to 1% BAC

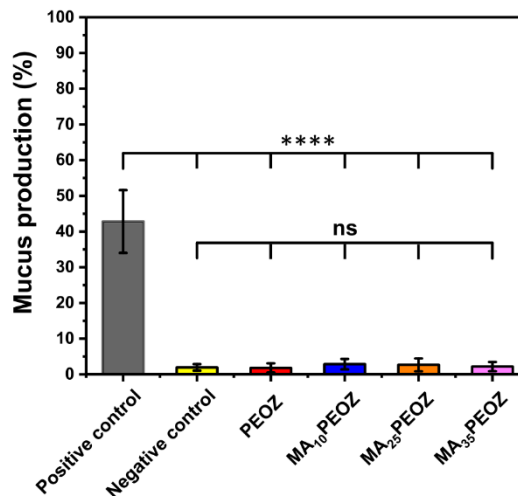


Figure 9. Mucus production by *Arion lusitanicus* slugs in response to 60 min exposure to PEOZ and its methacrylated derivatives as well as positive (BAC) and negative (PBS) controls. Statistically significant differences are given as follows: **** $p < 0.0001$; ns: no significance.

in PBS (positive control; pH 7.37), slugs experienced severe irritation ($p < 0.0001$), producing $\sim 43 \pm 8\%$ of yellow mucus, compared to slugs exposed to PBS (negative control; pH 7.40) with a very low level of mucus production ($2 \pm 1\%$). These data are in good agreement with our previous reports.^{53,54} Mucus production recorded for the slugs exposed to the solutions of PEOZ, MA₁₀PEOZ, MA₂₅PEOZ, and MA₃₅PEOZ (pH 7.47) was 2 ± 1 , 3 ± 1 , 3 ± 1 , and $2 \pm 1\%$ of colorless mucus, respectively. No significant differences ($p \gg 0.05$) in mucus production were seen between values recorded for the negative control and test materials, indicating the nonirritating nature of both PEOZ and modified PEOZs (Figure S5 provides the images with *A. lusitanicus* slugs exposed to various test materials).

4. CONCLUSIONS

This study demonstrated successful methacrylation of poly(2-ethyl-2-oxazoline) through a reaction between hydrolyzed poly(2-ethyl-2-oxazoline) bearing secondary amino groups and methacrylic anhydride. The structure and physicochemical behavior of these polymers were studied using ¹H NMR, FTIR, and UV/vis spectroscopies and differential scanning calorimetry. Methacrylated PEOZ showed temperature-dependent phase separation in aqueous solutions, and the cloud point temperature values were dependent on the degree of polymer modification. Cell toxicity studies demonstrated equivalent biocompatibility of the methacrylated polymers with the parent poly(2-ethyl-2-oxazoline), although the intermediate hydrolyzed product was toxic. Slug mucosal irritation tests demonstrated the nonirritating nature of methacrylated PEOZ. Methacrylation significantly increased mucoadhesion on the nasal mucosa tissue compared to parent poly(2-ethyl-2-oxazoline) attributed to the synergistic binding of methacrylate groups as well as residual secondary amines being available to interact with the mucosal surface. Methacrylated PEOZ can potentially be used as a mucoadhesive material in dosage forms for transmucosal drug delivery.

To the best of our knowledge, this is the first study reporting the chemical modification of the PEOZ backbone to enhance the mucoadhesive properties of this emerging class of polymers.

■ ASSOCIATED CONTENT

SI Supporting Information

The Supporting Information is available free of charge at <https://pubs.acs.org/doi/10.1021/acsapm.1c01097>.

(Figure S1) ^1H NMR spectra of PEOZ and hydrolyzed PEOZ in D_2O ; (Figure S2) first-order kinetic plot for the hydrolysis of PEOZ 500 kDa at $100\text{ }^\circ\text{C}$, $[\text{HCl}] = 18\text{ wt } \%$; (Table S1) composition of P(EOZ-co-EI) calculated from the standard curve in Figure S2; (Figure S3) ^1H NMR spectrum of $\text{MA}_{55}\text{PEOZ}$ in $\text{DMSO-}d_6$; (Figure S4) FTIR full spectra of PEOZ and MAPEOZ; (Table S2) retention values of 1 mg/mL glycol chitosan, PEOZ, $\text{MA}_{10}\text{PEOZ}$, $\text{MA}_{25}\text{PEOZ}$, and $\text{MA}_{35}\text{PEOZ}$ solutions using 0.05 mg/mL sodium fluorescein as the solvent and pure 0.05 mg/mL sodium fluorescein solution on sheep nasal mucosa as washed with different volumes of ANF ($\text{pH} = 5.70$); (Table S3) values of viability of HEK293 cells determined after treatment with different concentrations (25, 50, 75, 100, 125, and $150\text{ }\mu\text{g/mL}$) of PEOZ, P(EOZ-co-EI₁₅), P(EOZ-co-EI₂₈), P(EOZ-co-EI₃₃), $\text{MA}_{10}\text{PEOZ}$, $\text{MA}_{25}\text{PEOZ}$, and $\text{MA}_{35}\text{PEOZ}$ for 72 h; and (Figure S5) photographs of mucus production by *Arion lusitanicus* slugs in contact with positive (1% solution of BAC in PBS) and negative (PBS solution) controls as well as PEOZ and its methacrylated derivatives (1 mg/mL each) after 60 min of exposure (PDF)

■ AUTHOR INFORMATION

Corresponding Author

Vitaliy V. Khutoryanskiy – Reading School of Pharmacy, University of Reading, Reading RG6 6DX, United Kingdom; orcid.org/0000-0002-7221-2630; Phone: +44(0) 118 378 6119; Email: v.khutoryanskiy@reading.ac.uk

Authors

Xiaoning Shan – Reading School of Pharmacy, University of Reading, Reading RG6 6DX, United Kingdom

Sam Aspinall – Reading School of Pharmacy, University of Reading, Reading RG6 6DX, United Kingdom

Daulet B. Kaldybekov – Reading School of Pharmacy, University of Reading, Reading RG6 6DX, United Kingdom; Department of Chemistry and Chemical Technology, Al-Farabi Kazakh National University, 050040 Almaty, Kazakhstan

Fhataheya Buang – Reading School of Pharmacy, University of Reading, Reading RG6 6DX, United Kingdom; Centre for Drug Delivery Research, Faculty of Pharmacy, Universiti Kebangsaan Malaysia, 50300 Kuala Lumpur, Malaysia

Adrian C. Williams – Reading School of Pharmacy, University of Reading, Reading RG6 6DX, United Kingdom

Complete contact information is available at: <https://pubs.acs.org/doi/10.1021/acsapm.1c01097>

Author Contributions

The manuscript was written by X.S. and through contributions of all authors. All authors have given approval to the final version of the manuscript.

Notes

The authors declare no competing financial interest.

■ ACKNOWLEDGMENTS

The authors acknowledge the University of Reading and the China Scholarship Council (201707040071) for funding the Ph.D. studentship of X.S. The authors also thank the staff in the Chemical Analysis Facility (CAF, University of Reading) for assistance with thermal analysis. The authors thank Amnani Aminuddin for her technical help with cell culture experiments and the Faculty of Pharmacy UKM for providing the cell culture research facilities.

■ ABBREVIATIONS

PEOZ, poly(2-ethyl-2-oxazoline); P(EOZ-co-EI), poly[(2-ethyl-2-oxazoline)-co-ethylenimine]; MAPEOZ, methacrylated PEOZ

■ REFERENCES

- Grassin-Delyle, S.; Buenestado, A.; Naline, E.; Faisy, C.; Blouquit-Laye, S.; Couderc, L. J.; Le Guen, M.; Fischler, M.; Devillier, P. Intranasal drug delivery: an efficient and non-invasive route for systemic administration: focus on opioids. *Pharmacol. Ther.* **2012**, *134*, 366–379.
- Türker, S.; Onur, E.; Özer, Y. Nasal route and drug delivery systems. *Pharm. World Sci.* **2004**, *26*, 137–142.
- Wattanakumtornkul, S.; Pinto, A. B.; Williams, D. B. Intranasal hormone replacement therapy. *Menopause* **2003**, *10*, 88–98.
- Fazil, M.; Hassan, M. Q.; Baboota, S.; Ali, J. Biodegradable intranasal nanoparticulate drug delivery system of risedronate sodium for osteoporosis. *Drug Delivery* **2016**, *23*, 2428–2438.
- Rapoport, A. M.; Bigal, M. E.; Tepper, S. J.; Sheffell, F. D. Intranasal Medications for the Treatment of Migraine and Cluster Headache. *CNS Drugs* **2004**, *18*, 671–685.
- Pires, A.; Fortuna, A.; Alves, G.; Falcão, A. Intranasal Drug Delivery: How, Why and What for? *J. Pharm. Pharm. Sci.* **2009**, *12*, 288–311.
- Bruinsmann, F. A.; Richter Vaz, G.; de Cristo Soares Alves, A.; Aguirre, T.; Raffin Pohlmann, A.; Staniscuaski Guterres, S.; Sonvico, F. Nasal Drug Delivery of Anticancer Drugs for the Treatment of Glioblastoma: Preclinical and Clinical Trials. *Molecules* **2019**, *24*, No. 4312.
- Poovaiah, N.; Davoudi, Z.; Peng, H.; Schlichtmann, B.; Mallapragada, S.; Narasimhan, B.; Wang, Q. Treatment of neurodegenerative disorders through the blood-brain barrier using nanocarriers. *Nanoscale* **2018**, *10*, 16962–16983.
- Illum, L.; Jorgensen, H.; Bisgaard, H.; Krogsgaard, O.; Rossing, N. Bioadhesive microspheres as a potential nasal drug delivery system. *Int. J. Pharm.* **1987**, *39*, 189–199.
- Pereswetoff-Morath, L. Microspheres as nasal drug delivery systems. *Adv. Drug Delivery Rev.* **1998**, *29*, 185–194.
- Björk, E.; Edman, P. Characterization of degradable starch microspheres as a nasal delivery system for drugs. *Int. J. Pharm.* **1990**, *62*, 187–192.
- Muramatsu, K.; Maitani, Y.; Takayama, K.; Nagai, T. The Relationship Between the Rigidity of the Liposomal Membrane and the Absorption of Insulin After Nasal Administration of Liposomes Modified with an Enhancer Containing Insulin in Rabbits. *Drug Dev. Ind. Pharm.* **1999**, *25*, 1099–1105.
- Law, S. L.; Huang, K. J.; Chou, H. Y. Preparation of desmopressin-containing liposomes for intranasal delivery. *J. Controlled Release* **2001**, *70*, 375–382.

- (14) Iwanaga, K.; Matsumoto, S.; Morimoto, K.; Kakemi, M.; Yamashita, S.; Kimura, T. Usefulness of liposomes as an intranasal dosage formulation for topical drug application. *Biol. Pharm. Bull.* **2000**, *23*, 323–326.
- (15) Witschi, C.; J. M. R. In Vitro Evaluation of Microparticles and Polymer Gels for Use as Nasal Platforms for Protein Delivery. *Pharm. Res.* **1999**, *16*, 382–390.
- (16) Zhou, M.; D. Donovan, M. Intranasal mucociliary clearance of putative bioadhesive polymer gels. *Int. J. Pharm.* **1996**, *135*, 115–125.
- (17) Sogias, I. A.; Williams, A. C.; Khutoryanskiy, V. V. Why is Chitosan Mucoadhesive? *Biomacromolecules* **2008**, *9*, 1837–1842.
- (18) Tyagi, P.; Tyagi, S.; Kaufman, J.; Huang, L.; de Miguel, F. Local drug delivery to bladder using technology innovations. *Urol. Clin. North Am.* **2006**, *33*, 519–530.
- (19) Ways, T. M. M.; Lau, W.; Khutoryanskiy, V. Chitosan and Its Derivatives for Application in Mucoadhesive Drug Delivery Systems. *Polymers* **2018**, *10*, No. 267.
- (20) Davoudi, Z.; Peroutka-Bigus, N.; Bellaire, B.; Jergens, A.; Wannemuehler, M.; Wang, Q. Gut Organoid as a New Platform to Study Alginate and Chitosan Mediated PLGA Nanoparticles for Drug Delivery. *Mar. Drugs* **2021**, *19*, No. 282.
- (21) Shi, L.; Zhang, J.; Zhao, M.; Tang, S.; Cheng, X.; Zhang, W.; Li, W.; Liu, X.; Peng, H.; Wang, Q. Effects of polyethylene glycol on the surface of nanoparticles for targeted drug delivery. *Nanoscale* **2021**, *13*, 10748–10764.
- (22) Kolawole, O. M.; Lau, W. M.; Khutoryanskiy, V. V. Methacrylated chitosan as a polymer with enhanced mucoadhesive properties for transmucosal drug delivery. *Int. J. Pharm.* **2018**, *550*, 123–129.
- (23) Shitrit, Y.; Bianco-Peled, H. Acrylated chitosan for mucoadhesive drug delivery systems. *Int. J. Pharm.* **2017**, *517*, 247–255.
- (24) Davidovich-Pinhas, M.; Bianco-Peled, H. Alginate-PEGAc: a new mucoadhesive polymer. *Acta Biomater.* **2011**, *7*, 625–633.
- (25) Porfiruyeva, N. N.; Nasibullin, S. F.; Abdullina, S. G.; Tukhbatullina, I. K.; Moustafine, R. I.; Khutoryanskiy, V. V. Acrylated Eudragit E PO as a novel polymeric excipient with enhanced mucoadhesive properties for application in nasal drug delivery. *Int. J. Pharm.* **2019**, *562*, 241–248.
- (26) Brannigan, R. P.; Khutoryanskiy, V. V. Synthesis and evaluation of mucoadhesive acryloyl-quaternized PDMAEMA nanogels for ocular drug delivery. *Colloids Surf, B* **2017**, *155*, 538–543.
- (27) Tonglairoum, P.; Brannigan, R. P.; Opanasopit, P.; Khutoryanskiy, V. V. Maleimide-bearing nanogels as novel mucoadhesive materials for drug delivery. *J. Mater. Chem. B* **2016**, *4*, 6581–6587.
- (28) Shtenberg, Y.; Goldfeder, M.; Schroeder, A.; Bianco-Peled, H. Alginate modified with maleimide-terminated PEG as drug carriers with enhanced mucoadhesion. *Carbohydr. Polym.* **2017**, *175*, 337–346.
- (29) Sahatsapan, N.; Rojanarata, T.; Ngawhirunpat, T.; Opanasopit, P.; Tonglairoum, P. 6-Maleimidohexanoic acid-grafted chitosan: A new generation mucoadhesive polymer. *Carbohydr. Polym.* **2018**, *202*, 258–264.
- (30) Davidovich-Pinhas, M.; Bianco-Peled, H. Novel mucoadhesive system based on sulfhydryl-acrylate interactions. *J. Mater. Sci.: Mater. Med.* **2010**, *21*, 2027–2034.
- (31) Kim, K.; Kim, K.; Ryu, J. H.; Lee, H. Chitosan-catechol: a polymer with long-lasting mucoadhesive properties. *Biomaterials* **2015**, *52*, 161–170.
- (32) Khutoryanskiy, V. V. Advances in mucoadhesion and mucoadhesive polymers. *Macromol. Biosci.* **2011**, *11*, 748–764.
- (33) Grabovac, V.; Guggi, D.; Bernkop-Schnurch, A. Comparison of the mucoadhesive properties of various polymers. *Adv. Drug Delivery Rev.* **2005**, *57*, 1713–1723.
- (34) Bernkop-Schnurch, A. Thiomers: a new generation of mucoadhesive polymers. *Adv. Drug Delivery Rev.* **2005**, *57*, 1569–1582.
- (35) Matsumoto, A.; Cabral, H.; Sato, N.; Kataoka, K.; Miyahara, Y. Assessment of Tumor Metastasis by the Direct Determination of Cell-Membrane Sialic Acid Expression. *Angew. Chem., Int. Ed.* **2010**, *49*, 5494–5497.
- (36) Liu, A.; Peng, S.; Soo, J. C.; Kuang, M.; Chen, P.; Duan, H. Quantum dots with phenylboronic acid tags for specific labeling of sialic acids on living cells. *Anal. Chem.* **2011**, *83*, 1124–1130.
- (37) Tong, T.; Qi, Y.; Bussiere, L. D.; Wannemuehler, M.; Miller, C. L.; Wang, Q.; Yu, C. Transport of artificial virus-like nanocarriers through intestinal monolayers via microfold cells. *Nanoscale* **2020**, *12*, 16339–16347.
- (38) Kolawole, O. M.; Lau, W. M.; Khutoryanskiy, V. V. Synthesis and Evaluation of Boronated Chitosan as a Mucoadhesive Polymer for Intravesical Drug Delivery. *J. Pharm. Sci.* **2019**, *108*, 3046–3053.
- (39) de la Rosa, V. R. Poly(2-oxazoline)s as materials for biomedical applications. *J. Mater. Sci.: Mater. Med.* **2014**, *25*, 1211–1225.
- (40) Hoogenboom, R. Poly(2-oxazoline)s: a polymer class with numerous potential applications. *Angew. Chem., Int. Ed.* **2009**, *48*, 7978–7994.
- (41) Lorson, T.; Lubtow, M. M.; Wegener, E.; Haider, M. S.; Borova, S.; Nahm, D.; Jordan, R.; Sokolski-Papkov, M.; Kabanov, A. V.; Luxenhofer, R. Poly(2-oxazoline)s based biomaterials: A comprehensive and critical update. *Biomaterials* **2018**, *178*, 204–280.
- (42) Chen, W.; Zhou, S.; Ge, L.; Wu, W.; Jiang, X. Translatable High Drug Loading Drug Delivery Systems Based on Biocompatible Polymer Nanocarriers. *Biomacromolecules* **2018**, *19*, 1732–1745.
- (43) Glassner, M.; Vergaelen, M.; Hoogenboom, R. Poly(2-oxazoline)s: A comprehensive overview of polymer structures and their physical properties. *Polym. Int.* **2018**, *67*, 32–45.
- (44) Ways, T. M. M.; Lau, W. M.; Ng, K. W.; Khutoryanskiy, V. V. Synthesis of thiolated, PEGylated and POZylated silica nanoparticles and evaluation of their retention on rat intestinal mucosa in vitro. *Eur. J. Pharm. Sci.* **2018**, *122*, 230–238.
- (45) Mansfield, E. D.; de la Rosa, V. R.; Kowalczyk, R. M.; Grillo, I.; Hoogenboom, R.; Sillence, K.; Hole, P.; Williams, A. C.; Khutoryanskiy, V. V. Side chain variations radically alter the diffusion of poly(2-alkyl-2-oxazoline) functionalised nanoparticles through a mucosal barrier. *Biomater. Sci.* **2016**, *4*, 1318–1327.
- (46) Ruiz-Rubio, L.; Alonso, M. L.; Perez-Alvarez, L.; Alonso, R. M.; Vilas, J. L.; Khutoryanskiy, V. V. Formulation of Carbopol((R))/Poly(2-ethyl-2-oxazoline)s Mucoadhesive Tablets for Buccal Delivery of Hydrocortisone. *Polymers* **2018**, *10*, No. 175.
- (47) Abilova, G. K.; Kaldybekov, D. B.; Ozhmukhametova, E. K.; Saimova, A. Z.; Kazybayeva, D. S.; Irmukhametova, G. S.; Khutoryanskiy, V. V. Chitosan/poly(2-ethyl-2-oxazoline) films for ocular drug delivery: Formulation, miscibility, in vitro and in vivo studies. *Eur. Polym. J.* **2019**, *116*, 311–320.
- (48) Abilova, G. K.; Kaldybekov, D. B.; Irmukhametova, G. S.; Kazybayeva, D. S.; Iskakbayeva, Z. A.; Kudaibergenov, S. E.; Khutoryanskiy, V. V. Chitosan/Poly(2-ethyl-2-oxazoline) Films with Ciprofloxacin for Application in Vaginal Drug Delivery. *Materials* **2020**, *13*, No. 1709.
- (49) de la Rosa, V. R.; Bauwens, E.; Monnery, B. D.; De Geest, B. G.; Hoogenboom, R. Fast and accurate partial hydrolysis of poly(2-ethyl-2-oxazoline) into tailored linear polyethylenimine copolymers. *Polym. Chem.* **2014**, *5*, 4957–4964.
- (50) Sedlacek, O.; Janouskova, O.; Verbraken, B.; Hoogenboom, R. Straightforward Route to Superhydrophilic Poly(2-oxazoline)s via Acylation of Well-Defined Polyethylenimine. *Biomacromolecules* **2019**, *20*, 222–230.
- (51) Da Silva Barbi, M.; Carvalho, F. C.; Kiill, C. P.; Barud Hda, S.; Santagneli, S. H.; Ribeiro, S. J.; Gremiao, M. P. Preparation and Characterization of Chitosan Nanoparticles for Zidovudine Nasal Delivery. *J. Nanosci. Nanotechnol.* **2015**, *15*, 865–874.
- (52) Khutoryanskaya, O. V.; Mayeva, Z. A.; Mun, G. A.; Khutoryanskiy, V. V. Designing Temperature-Responsive Biocompatible Copolymers and Hydrogels Based on 2-Hydroxyethyl(meth)acrylates. *Biomacromolecules* **2008**, *9*, 3353–3361.

- (53) Kaldybekov, D. B.; Filippov, S. K.; Radulescu, A.; Khutoryanskiy, V. V. Maleimide-functionalised PLGA-PEG nanoparticles as mucoadhesive carriers for intravesical drug delivery. *Eur. J. Pharm. Biopharm.* **2019**, *143*, 24–34.
- (54) Khutoryanskaya, O. V.; Morrison, P. W.; Seilkhanov, S. K.; Mussin, M. N.; Ozhmukhametova, E. K.; Rakhypbekov, T. K.; Khutoryanskiy, V. V. Hydrogen-bonded complexes and blends of poly(acrylic acid) and methylcellulose: nanoparticles and mucoadhesive films for ocular delivery of riboflavin. *Macromol. Biosci.* **2014**, *14*, 225–234.
- (55) Shan, X.; Williams, A. C.; Khutoryanskiy, V. V. Polymer structure and property effects on solid dispersions with haloperidol: Poly(N-vinyl pyrrolidone) and poly(2-oxazolines) studies. *Int. J. Pharm.* **2020**, *590*, No. 119884.
- (56) Mees, M. A.; Hoogenboom, R. Full and partial hydrolysis of poly(2-oxazoline)s and the subsequent post-polymerization modification of the resulting polyethylenimine (co)polymers. *Polym. Chem.* **2018**, *9*, 4968–4978.
- (57) Sedlacek, O.; Monnery, B. D.; Hoogenboom, R. Synthesis of defined high molar mass poly(2-methyl-2-oxazoline). *Polym. Chem.* **2019**, *10*, 1286–1290.
- (58) Zhang, Q.; Weber, C.; Schubert, U. S.; Hoogenboom, R. Thermoresponsive polymers with lower critical solution temperature: from fundamental aspects and measuring techniques to recommended turbidimetry conditions. *Mater. Horiz.* **2017**, *4*, 109–116.
- (59) Chen, F. P.; Ames, A. E.; Taylor, L. D. Aqueous solutions of poly(ethylloxazoline) and its lower consolute phase transition. *Macromolecules* **1990**, *23*, 4688–4695.
- (60) Lin, P.; Clash, C.; Pearce, E. M.; Kwei, T. K.; et al. Solubility and miscibility of poly(ethyl oxazoline). *J. Polym. Sci., Part B: Polym. Phys.* **1988**, *26*, 603–619.
- (61) Ouellette, R. J.; Rawn, J. D. Alkanes and Cycloalkanes. In *Principles of Organic Chemistry*; Academic Press, 2015; Chapter 3, pp 65–94.
- (62) Lungu, C. N.; Diudea, M. V.; Putz, M. V.; Grudzinski, I. P. Linear and Branched PEIs (Polyethylenimines) and Their Property Space. *Int. J. Mol. Sci.* **2016**, *17*, No. 555.
- (63) Hu, J.; Han, J.; Li, H.; Zhang, X.; Liu, L.; Chen, F.; Zeng, B. Human Embryonic Kidney 293 Cells: A Vehicle for Biopharmaceutical Manufacturing, Structural Biology, and Electrophysiology. *Cells Tissues Organs* **2018**, *205*, 1–8.
- (64) Bauer, M.; Lautenschlaeger, C.; Kempe, K.; Tauhardt, L.; Schubert, U. S.; Fischer, D. Poly(2-ethyl-2-oxazoline) as alternative for the stealth polymer poly(ethylene glycol): comparison of in vitro cytotoxicity and hemocompatibility. *Macromol. Biosci.* **2012**, *12*, 986–998.
- (65) Wang, M.; Gustafsson, O. J. R.; Siddiqui, G.; Javed, I.; Kelly, H. G.; Blin, T.; Yin, H.; Kent, S. J.; Creek, D. J.; Kempe, K.; Ke, P. C.; Davis, T. P. Human plasma proteome association and cytotoxicity of nano-graphene oxide grafted with stealth polyethylene glycol and poly(2-ethyl-2-oxazoline). *Nanoscale* **2018**, *10*, 10863–10875.
- (66) Yuan, W.; Li, H. Polymer-Based Nanocarriers for Therapeutic Nucleic Acids Delivery. In *Nanostructures for Drug Delivery*; Academic Press, 2017; Chapter 14, pp 445–460.
- (67) Adriaens, E.; Remon, J. P. Gastropods as an evaluation tool for screening the irritating potency of absorption enhancers and drugs. *Pharm. Res.* **1999**, *16*, 1240–1244.
- (68) Adriaens, E.; Dierckens, K.; Bauters, T. G. M.; Nelis, H. J.; Goethem, F.v.; Vanparys, P.; Remon, J. P. The mucosal toxicity of different benzalkonium chloride analogues evaluated with an alternative test using slugs. *Pharm. Res.* **2001**, *18*, 937–942.
- (69) Callens, C.; Adriaens, E.; Dierckens, K.; Remon, J. P. Toxicological evaluation of a bioadhesive nasal powder containing a starch and carbopol 974 p on rabbit nasal mucosa and slug mucosa. *J. Controlled Release* **2001**, *76*, 81–91.
- (70) Ceulemans, J.; Vermeire, A.; Adriaens, E.; Remon, J. P.; Ludwig, A. Evaluation of a muco-adhesive tablet for ocular use. *J. Controlled Release* **2001**, *77*, 333–344.
- (71) Dhondt, M. M.; Adriaens, E.; Roey, J. V.; Remon, J. P. The evaluation of the local tolerance of vaginal formulations containing dapivirine using the Slug Mucosal Irritation test and the rabbit vaginal irritation test. *Eur. J. Pharm. Biopharm.* **2005**, *60*, 419–425.
- (72) Lenoir, J.; Adriaens, E.; Remon, J. P. New aspects of the Slug Mucosal Irritation assay: predicting nasal stinging, itching and burning sensations. *J. Appl. Toxicol.* **2011**, *31*, 640–648.
- (73) Lenoir, J.; Bachert, C.; Remon, J. P.; Adriaens, E. The Slug Mucosal Irritation (SMI) assay: a tool for the evaluation of nasal discomfort. *Toxicol. In Vitro* **2013**, *27*, 1954–1961.
- (74) Adriaens, E.; Remon, J. P. Evaluation of an alternative mucosal irritation test using slugs. *Toxicol. Appl. Pharmacol.* **2002**, *182*, 169–175.

Supporting Information

Synthesis and evaluation of methacrylated poly(2-ethyl-2-oxazoline) as a mucoadhesive polymer for nasal drug delivery

Xiaoning Shan¹, Sam Aspinall¹, Daulet B. Kaldybekov^{1,2}, Fhataheya Buang^{1,3}, Adrian C.

Williams¹, Vitaliy V. Khutoryanskiy^{1}*

¹Reading School of Pharmacy, University of Reading, Whiteknights, RG6 6DX Reading, United Kingdom, e-mail: v.khutoryanskiy@reading.ac.uk

²Department of Chemistry and Chemical Technology, Al-Farabi Kazakh National University, 050040 Almaty, Kazakhstan

³Centre for Drug Delivery Research, Faculty of Pharmacy, Universiti Kebangsaan Malaysia, Jalan Raja Muda Abdul Aziz, 50300 Kuala Lumpur, Malaysia

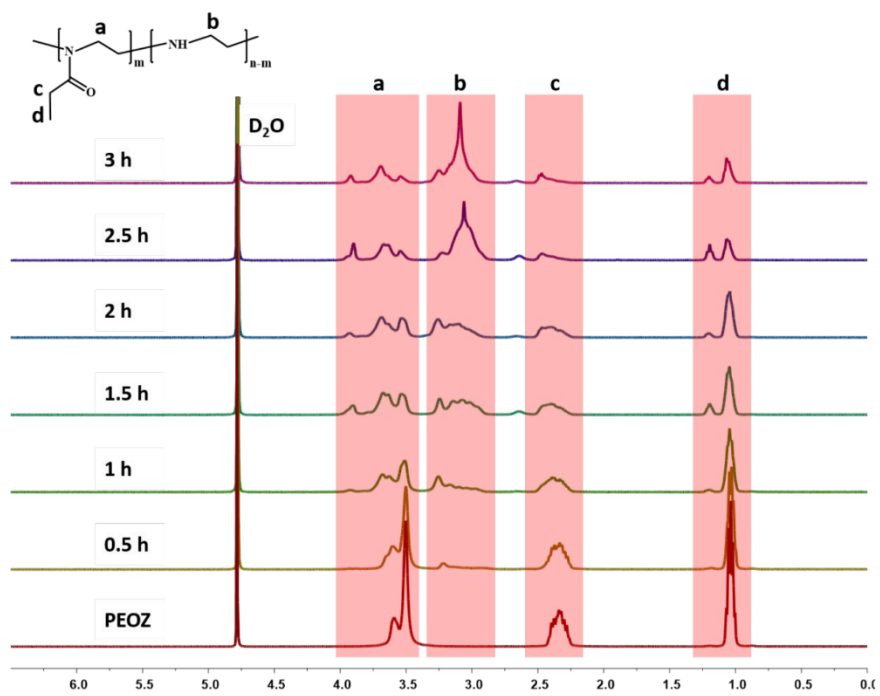


Figure S1. ¹H-NMR spectra of PEOZ and hydrolyzed PEOZ in D₂O.

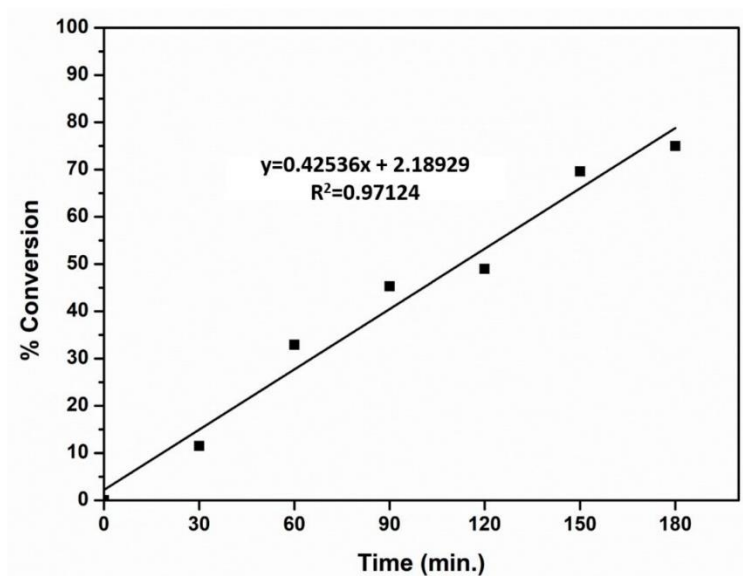


Figure S2. First order kinetic plot for the hydrolysis of PEOZ 500 kDa at 100 °C, [HCl] = 18 wt%.

Table S1. Composition of P(EOZ-co-EI) calculated from the standard curve in Figure S2

Hydrolysis time (hour)	Hydrolyzed PEOZ	EOZ (%)	EI (%)
0.5	P(EOZ-co-EI ₁₅)	85	15
1	P(EOZ-co-EI ₂₈)	72	28
2	P(EOZ-co-EI ₅₃)	47	53
3	P(EOZ-co-EI ₇₈)	22	78

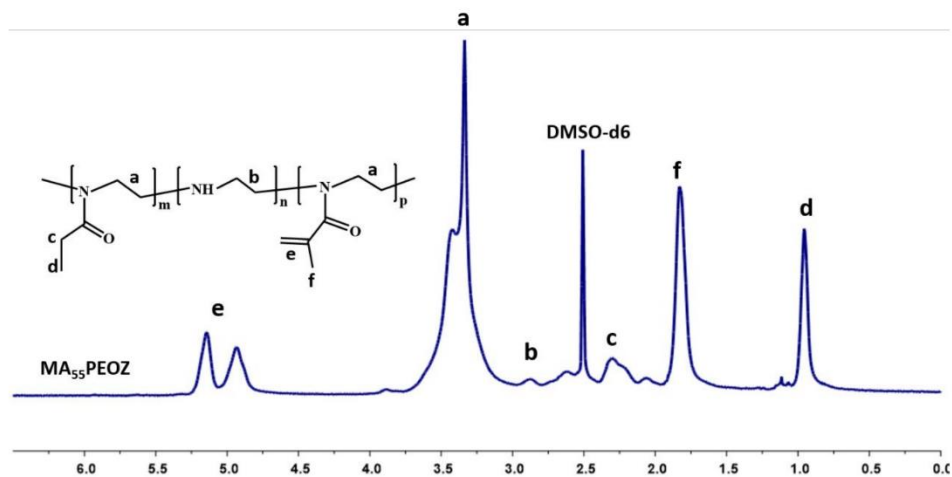


Figure S3. ¹H-NMR spectrum of MA₅₅PEOZ in DMSO-d₆.

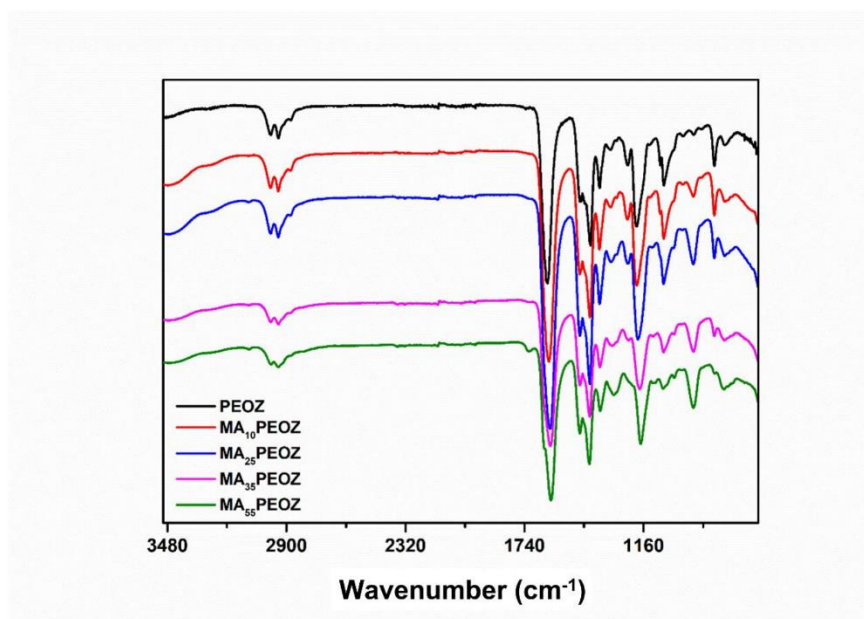


Figure S4. FTIR full spectra of PEOZ and MAPEOZ.

Table S2. Retention values of 1 mg/mL glycol chitosan; PEOZ; MA₁₀PEOZ; MA₂₅PEOZ and MA₃₅PEOZ solutions using 0.05 mg/mL sodium fluorescein as the solvent and pure 0.05 mg/mL sodium fluorescein solution on sheep nasal mucosa as washed with different volumes of ANF (pH = 5.70). Values were expressed as means (n = 3)

Retention (%)								
Time (min.) Sample	0	5	10	20	30	40	50	60
Glycol chitosan	100	37.22	28.91	21.92	18.33	15.94	13.81	12.52
MA ₃₅ PEOZ	100	49.53	34.45	25.12	20.41	16.74	14.11	12.54
MA ₂₅ PEOZ	100	42.13	31.63	24.34	19.32	16.63	14.53	12.75
MA ₁₀ PEOZ	100	34.71	26.52	20.53	17.15	15.41	13.41	12.13
PEOZ	100	17.22	12.22	9.11	7.93	6.58	6.15	5.75
Sodium fluorescein	100	19.05	14.62	10.21	9.24	6.92	6.62	5.73

Table S3. Values of viability of HEK 293 cells determined after treatment with different concentrations (25, 50, 75, 100, 125 and 150 $\mu\text{g/mL}$) of PEOZ; P(EOZ-co-EI₁₅); P(EOZ-co-EI₂₈); P(EOZ-co-EI₅₃); MA₁₀PEOZ; MA₂₅PEOZ and MA₃₅PEOZ for 72 h. The untreated cells served as the control. Values were expressed as means (n = 3)

Cell Viability (%)							
Concentration ($\mu\text{g/mL}$)	0	25	50	75	100	125	150
Sample							
PEOZ	100	93.81	92.72	90.93	89.65	87.05	85.75
P(EOZ-co-EI ₁₅)	100	90.87	89.68	88.27	87.45	86.93	84.75
P(EOZ-co-EI ₂₈)	100	75.23	62.51	59.65	56.92	52.05	49.62
P(EOZ-co-EI ₅₃)	100	5.45	5.07	4.08	2.58	2.25	2.56
MA ₁₀ PEOZ	100	93.21	92.25	90.34	89.29	87.86	86.75
MA ₂₅ PEOZ	100	92.54	90.07	89.41	88.56	87.14	85.27
MA ₃₅ PEOZ	100	90.42	89.12	88.97	87.95	86.43	84.38

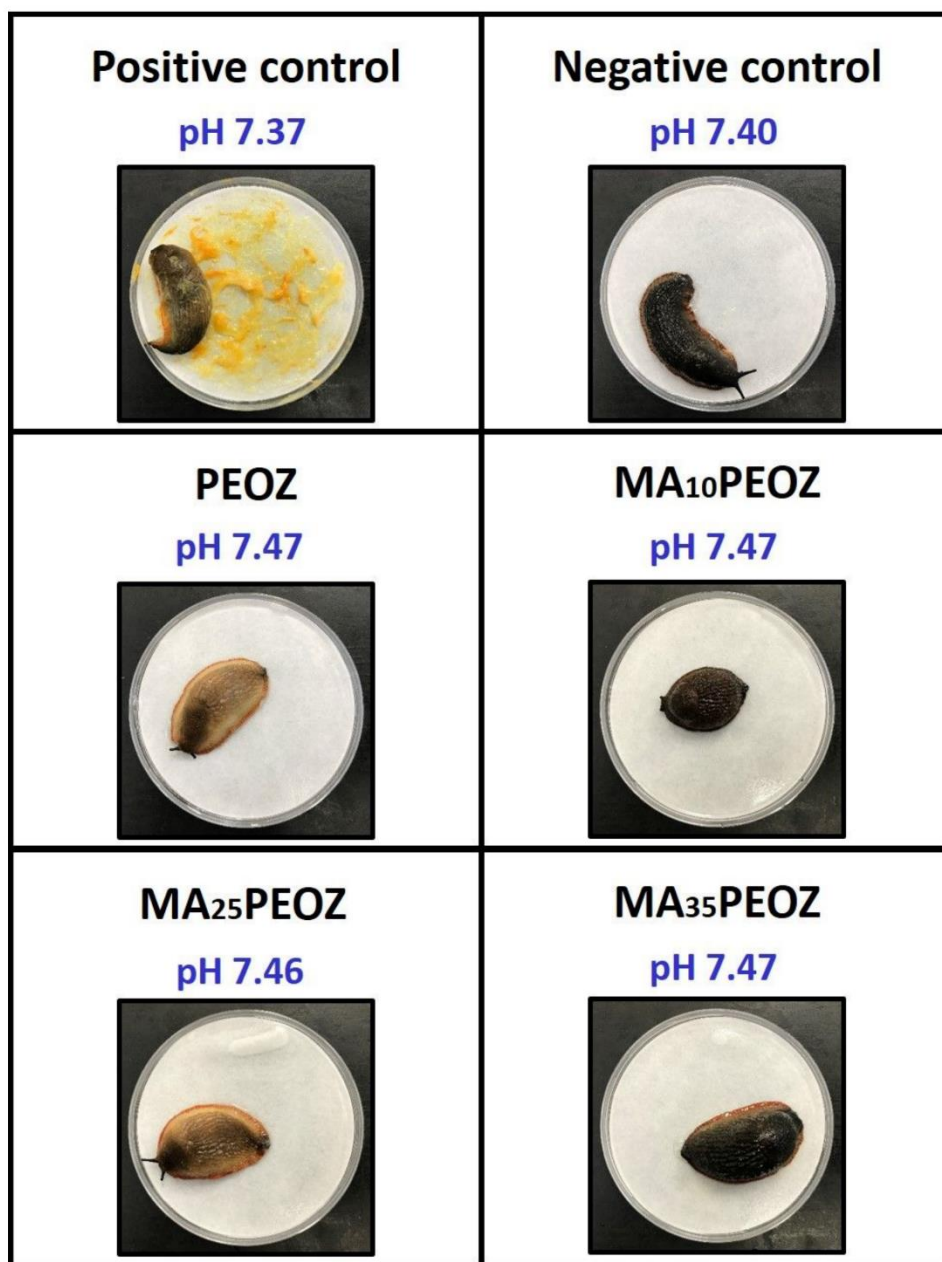


Figure S5. Photographs of mucus production by *Arion lusitanicus* slugs in contact with positive (1% solution of BAC in PBS) and negative (PBS solution) controls as well as PEOZ and its methacrylated derivatives (1 mg/mL each) after 60 min exposure.

Chapter 5

Mucoadhesive formulations with maleimide modified poly(*N*-(2-hydroxypropyl)methacrylamide) copolymer for nasal drug delivery

This manuscript is under review before submission.

Mucoadhesive formulations with maleimide modified poly(*N*-(2-hydroxypropyl)methacrylamide) copolymer for nasal drug delivery

*Xiaoning Shan*¹, *Robert Pola*², *Daulet B. Kaldybekov*¹, *Sam Aspinall*¹, *Fhataheya Buang*^{1,3}, *Adrian C. Williams*¹, *Tomas Etrych*², *Vitaliy V. Khutoryanskiy*^{1*}

*Correspondence: v.khutoryanskiy@reading.ac.uk

¹Reading School of Pharmacy, University of Reading, Whiteknights, PO Box 224, Reading RG6 6AD, United Kingdom

²Institute of Macromolecular Chemistry of the Czech Academy of Sciences, Heyrovského nám. 2, Prague 6, Czech Republic

³Centre for Drug Delivery Research, Faculty of Pharmacy, Universiti Kebangsaan Malaysia, Jalan Raja Muda Abdul Aziz, 50300 Kuala Lumpur, Malaysia

Abstract:

Nasal drug administration represents one of the most investigated route for the systemic administration, which is unfortunately often affected by inadequate nasal drug absorption. Here, we have investigated novel mucoadhesive poly(*N*-(2-hydroxypropyl)methacrylamide) copolymer (PHPMA) enriched with maleimide moieties. PHPMA and its maleimide derivatives were investigated for their cytotoxicity and mucosal irritation. Importantly, copolymers with low maleimide content, which was nevertheless sufficient for the mucoadhesion, had no significant cytotoxicity against HEK293 cell line and no mucosal irritancy against slugs was also observed, respectively. The presence of maleimide groups had a remarkable positive effect on the mucoadhesive properties of PHPMA. These PHPMA derivatives have excellent potential as mucoadhesive materials for formulation of dosage forms for nasal drug delivery.

Keywords: poly(*N*-(2-hydroxypropyl)methacrylamide), mucoadhesion, maleimide, mucoadhesive materials, nasal drug delivery

1. Introduction

Nasal drug administration has been established as an alternative route for the systemic availability of drugs restricted to intravenous administration due to the large surface area, porous endothelial membrane, high total blood flow, the avoidance of first-pass metabolism, and ready accessibility [1]. However, the drug absorption through the nasal mucosa is generally affected by the physicochemical properties of the drug [2], nasal mucus layer and mucociliary clearance [3], and nasal absorption enhancers [4]. Therefore, one of the greatest limitations for nasal drug delivery is inadequate nasal drug absorption.

Several drug delivery systems (DDS), such as microspheres [5-7], liposomes [8-10] and gels [11, 12] have been demonstrated to have good bioadhesive characteristics and are able to control the rate of drug clearance from the nasal cavity as well as protect the drug from enzymatic degradation in nasal secretions. In addition, nasal DDS based on polymer materials exhibiting mucoadhesive properties have also been studied for increasing the residence time of drug formulations in the nasal cavity, resulting in improved nasal drug absorption. Of which, maleimide groups have been demonstrated to have a significant positive effect on the mucoadhesion performance of some hydrophilic polymers. For example, liposomes decorated with maleimide-functionalised PEG exhibited superior in vitro retention on the bladder tissue, which is related to their ability to form covalent bonds with thiols present in mucosal tissue [13]; maleimide-functionalised nanogels were found to exhibit excellent mucoadhesive properties on ex vivo conjunctival tissue when compared to the known mucoadhesive chitosan [14-16]; maleimide-functionalised chitosan demonstrated excellent mucoadhesive properties which is superior to chitosan itself [17].

(*N*-(2-hydroxypropyl)methacrylamide)-based copolymers (PHPMA) are a hydrophilic biocompatible copolymers that has been widely explored as carriers for chemotherapeutic agents, and at least six of PHPMA-based therapeutics have

progressed into phase I or phase II clinical trials or compassionate clinical trials [18-20]. In addition, PHPMA has been validated as a dissociable “mucus-inert” coating material to enhance mucus permeation of nanoparticles by assembling on the nanoparticle surface and separating in time from the surface of nanoparticles for subsequent epithelium absorption [21]. Liu et al. [22] developed PHPMA coated trimethyl chitosan-based nanoparticles and demonstrated that the PHPMA coating could enhance the diffusion of trimethyl chitosan nanoparticles through both human cervicovaginal mucus and epithelial layer while non-coated trimethyl chitosan nanoparticles were found to be less diffusive in both mucus and E12 cells. In another study [23], Liu et al. investigated the effect of M_w of PHPMA as a “mucus-inert” material for overcoming the intestinal absorption barrier and found that the trimethyl chitosan-based nanoparticles coated by lower M_w of PHPMA (M_w of 17 kDa) exhibited the highest stability and excellent permeability across mucus while a high M_w coating (M_w of 120 kDa) results in premature dissociation of the PHPMA shell and hindrance in mucus, and the best candidate for promoting cell uptake and transepithelium transportation is 26 kDa. Liu et al. [24] developed PHPMA-coated wheat germ agglutinin-modified lipid-polymer hybrid nanoparticles, co-loaded with silibinin and cryptotanshinone and revealed that PHPMA enhanced nanoparticle mucus penetration through the in vitro mucus diffusion study. Lu et al. [25] modified the surface of mesoporous carbon nanoparticles with chitosan concealed by PHPMA layer and concluded that the mucus-permeable nanocarrier could effectively overcome multiple gastrointestinal absorption barriers and the oral bioavailability of drug-loaded nanoparticles was 2.76-fold that of commercial preparation. However, studies into the mucoadhesive properties of PHPMA or its derivatives are currently lacking; most studies are about mucus penetration.

Here, we have employed novel strategy to increase the mucoadhesive properties of PHPMA by the introduction of the maleimide groups into the PHPMA side chains. Liquid formulations based on PHPMA and its maleimide derivatives with sodium fluorescein as a model compound were prepared and their retention on freshly

excised sheep nasal mucosa was evaluated using fluorescent microscopy. Tensile test was utilized as the other way to investigate the mucoadhesive properties of samples. The biocompatibility of parent PHPMA and its maleimide derivatives was studied in HEK293 cell line and slugs.

2. Materials and methods

2.1 Materials

The monomers *N*-(2-hydroxypropyl)methacrylamide (HPMA) and 3-(3-methacrylamidopropanoyl)thiazolidine-2-thione (Ma- β -Ala-TT) was prepared as described previously [26]. 2,2'-Azobis(4-methoxy-2,4-dimethylvaleronitrile) (V70) was from FUJIFILM Wako Pure Chemical Corporation (Japan). (1-cyano-1-methyl-ethyl) benzenecarbodithioate (CTA), tert-butyl alcohol, *N,N*-dimethylacetamide (DMA), dimethyl sulfoxide (DMSO), azobisisobutyronitrile (AIBN) and 2-aminoethyl maleimide trifluoroacetate (AEMI) were from Merck (Czech Republic). Acetone and diethyl ether were from Lach-Ner (Czech Republic). *N,N*-diisopropylethylamine (DIPEA) was from Iris Biotech, GmbH (Germany). Deuterium oxide (D₂O), sodium fluorescein, glycol chitosan, calcium chloride dehydrate, sodium chloride, potassium chloride and benzalkonium chloride (BAC) were from Sigma-Aldrich (UK). DMEM High Glucose was from Capricorn Scientific (Germany). 10 % fetal calf serum was from GE Healthcare Life Sciences (USA). 1 % penicillin/streptomycin was from Nacalai Tesque Inc. (Japan). CellTiter 96 aqueous MTS reagent powder was from Promega Corporation (USA). Phenazine methosulfate was from Thermo Fisher Scientific (USA). Phosphate buffered saline (PBS) was purchased from Fisher Scientific (UK).

2.2 Synthesis of PHPMA functionalised with maleimide groups (PHPMA-Mi)

At first, the copolymer poly(HPMA-*co*-Ma- β -Ala-TT) (PHPMA-TT) was prepared by reversible addition-fragmentation chain transfer (RAFT) copolymerization of

HPMA (2 g, 13.97 mmol, 87.5 mol %) and Ma- β -Ala-TT (515 mg, 2.0 mmol, 12.5 mol %) using V70 (0.013 mmol, 4.1 mg) as an azo initiator and CTA (0.027 mmol, 5.9 mg) as a chain transfer agent. The molar ratio of monomers/CTA/ initiator was 1200:2:1. The polymerization mixture was dissolved in tert-butyl alcohol with 15 % of DMA (22.8 mL, 0.7 M solution of monomers), transferred into a glass ampule, bubbled with Ar and sealed. After 16 h at 40 °C, the tough product was diluted with DMSO and isolated by precipitation in acetone/diethyl ether, then washed with diethyl ether and dried under vacuum. The resulting copolymer was reacted with AIBN (10 molar excess) in DMSO (15% w/w solution of polymer) under Ar for 3 h at 70 °C in a sealed ampule to remove dithiobenzoate (DTB) ω -end groups. The reaction mixture was isolated by precipitation with acetone/diethyl ether, the precipitate was washed with diethyl ether and dried under vacuum to yield copolymer PHPMA-TT-1. The copolymer PHPMA-TT-2 was prepared by the same way but with 25 mol% of Ma- β -Ala-TT and with the molar ratio of monomers/CTA/ initiator 1600:2:1.

The obtained reactive polymer precursors (PHPMA-TT) were dissolved in DMA and 1.1 molar amount of 2-aminoethyl maleimide trifluoroacetate (AEMI) to TT (thiazolidine-2-thione) groups was added to the solution using 1.1 molar amount of DIPEA as the base. The course of the reaction was analyzed using HPLC and after removing all TT groups from polymer, the reaction mixture was precipitated in acetone/diethyl ether, then washed with diethyl ether and dried under vacuum to form PHPMA-Mi conjugates.

2.3 Characterization of polymers

2.3.1 Proton nuclear magnetic resonance ($^1\text{H-NMR}$)

^1H NMR spectra of polymers were recorded with a Bruker spectrometer operating at 250 MHz using D_2O (15 mg/mL) as the solvent. All chemical shifts are given in ppm. MestReNova software was used for analysis of spectra.

2.3.2. Fourier transform infrared (FTIR) spectroscopy

FTIR spectra were recorded on a Nicolet iS5 spectrometer using a diamond ATR (Attenuated Total Reflection) accessory. After a background scan was collected, samples were placed on the crystal and scanned from between 4000 and 600 cm^{-1} at a resolution of 4 cm^{-1} and an average of 64 scans. The OMNIC software was used for spectral analysis.

2.3.3 Size exclusion chromatography (SEC)

The molecular weights and polydispersity of polymers were measured by size exclusion chromatography (SEC) on a HPLC system (Shimadzu, Japan) equipped with UV, differential refractive index and multi-angle light scattering detectors (Wyatt Technology Corp., USA) using TSKgel G4000 SWXL, (Tosoh Bioscience, Japan) (80% methanol, 20% 0.3 M acetate buffer pH 6.5) at a flow rate of 0.5 mL/min. The calculation of molecular weights from the light-scattering intensity was based on the known injected mass, assuming 100% mass recovery.

2.3.4 Calculation of maleimide modification

The modification of maleimide was calculated from ^1H NMR spectra of MPHPMA in D_2O based on the integrated areas (I) of -CH signals of HPMA monomer and -CH=CH- signals of maleimide moieties, as displayed in the following equations:

$$\frac{I_{[\text{CH}=\text{CH}]}}{2y} = \frac{I_{[\text{CH}]}}{x} \quad (1)$$

$$\text{Maleimide (\%)} = \frac{y}{x+y} \quad (2)$$

where $I_{[\text{CH}=\text{CH}]}$ is the integrated area of -CH=CH- of maleimide moieties, $I_{[\text{CH}]}$ is the integrated area of -CH of HPMA moieties, x is the number of repeating units of HPMA moieties, y is the number of repeating units of maleimide moieties.

then the equation (2) was modified to:

$$\text{Maleimide (\%)} = \frac{I_{[\text{CH}=\text{CH}]}}{2 \cdot I_{[\text{CH}]} + I_{[\text{CH}=\text{CH}]}} \quad (3)$$

2.4 In vitro nasal mucoadhesion studies

2.4.1 Preparation of polymer/fluorescein sodium mixtures and artificial nasal fluid

Artificial nasal fluid (ANF) was prepared according to the established protocol [27, 28] by dissolving 7.45 g NaCl, 1.29 g KCl and 0.32 g CaCl₂·2H₂O in 1000 mL deionised water. The solution was left stirring overnight at room temperature. The artificial nasal fluid was kept at 37 °C in a water bath throughout the experiments.

Sodium fluorescein solutions (0.05 mg/mL) were prepared in deionised water into which polymer samples were dissolved; 10 mg of either PHPMA, PHPMA-Mi, or glycol chitosan were dispersed in 10 mL of the sodium fluorescein solution and pH was adjusted to 5.7. The dispersions were left for 24 h at room temperature with stirring until complete dissolution and were protected from light by aluminium foil.

2.4.2 Fluorescence retention studies on nasal mucosa

Sheep heads were obtained from P.C. Turner Abattoir (Farnborough, UK) and transported to the laboratory in a cold box (3–4 °C). The nasal septum tissue containing mucosal lining (1.5×1 cm) was carefully dissected and extracted from each head with scissors, washed with 1 mL of ANF and placed on a microscope slide. All tissues were used within 24 h after animal slaughter.

All experiments assessing retention of formulations on nasal mucosa were conducted at 37 °C in an incubator. Images of mucosal surfaces were taken using a fluorescence microscope (MZ10F, Leica Microsystems, UK), equipped with an “ET GFP” filter and a Zeiss Imager A1/AxioCam MRm camera. All images were at 0.8× magnification with a 211 ms exposure time. Initially, fluorescence images of mucosal tissues were recorded for each sample to collect background fluorescence intensity. Then, 20 µL solution of 1 mg/mL PHPMA, PHPMA-Mi or glycol chitosan containing 0.05 mg/mL sodium fluorescein was placed on the mucosal surface and

fluorescence images were again recorded. After 3 min of dosing, the mucosal tissues were transferred to the incubator and irrigated with ANF using a syringe pump at 0.43 mL/min. Fluorescence images of the mucosal tissue were collected periodically and analyzed using ImageJ software to measure pixel intensity after each wash. Results are presented as fluorescence intensity versus the time of irrigation after subtracting the background fluorescence from each wash image. Sodium fluorescein solution in deionised water was used as a negative control and glycol chitosan solution (1 mg/mL) was used as a positive control. The experiments were conducted in triplicate.

2.4.3 Mucoadhesive properties studies using tensile test

Tensile test was performed on a TA XT plus texture analyser (Stable Mirco systems) where nasal tissue 4 cm² was incubated to 37 °C before being placed on a platform (24 mm opening) that was surrounded by water at 37 °C to maintain the tissue temperature during the test. Each sample was prepared by soaking a filter paper (diameter =15 mm) in polymer solution (3 mg/mL) using ANF as the solvent for 30 s before drying in a vacuum oven at 25 °C for 20 mins and this process was repeated once to obtain a dry polymer coated filter paper, which was then attached to the probe via a carbon tab (12 mm). The contact time between the probe and the tissue was 30 s with 100 g of force before pulling apart with a removal speed of 1 mm/s. All samples were tested in triplicate. T.A. Exponent software was used to record the area under the force versus distance curves (work of adhesion) as well as the force of adhesion/adhesive strength which is the maximum force needed to detach tissue from the polymer coated filter paper.

2.5 Biocompatibility studies

2.5.1 Cytotoxicity studies

HEK293 was cultured in DMEM High Glucose supplemented with 10 % fetal calf serum and 1 % penicillin/streptomycin. The cells were incubated at 37 °C in a

humidified atmosphere of 5 % CO₂. Cell viability was assessed using CellTiter 96 AQueous Non-Radioactive Cell Proliferation Assay (MTS assay). Cells were seeded in 96-well plate at 3×10^3 cells/well and incubated overnight at 37 °C in 5 % CO₂ humidified air for cell attachment. The cells were then treated with various concentrations of the polymers (25, 50, 75, 100, 125 and 150 µg/mL) for 72 h. The negative control group consisted of untreated cells and was considered as 100 % of viable cells. After 72 h, treatment media were replaced with new growth media and 20 µL MTS solution (prepared in phosphate buffered saline) containing 2 mg/mL of CellTiter 96 Aqueous MTS reagent powder and 0.92 mg/mL of phenazine methosulfate. The cells were incubated for a further 4 h before absorbance (Abs) was measured at 490 nm using an Infinite 200 PRO microplate reader (Tecan Group Ltd., Switzerland). The results are expressed as percentage of cell viability compared to the negative control group based on the following equation:

$$\text{Cell viability (\%)} = \frac{(\text{Abs}_{\text{Treatment}} - \text{Abs}_{\text{Blank}})}{(\text{Abs}_{\text{Control}} - \text{Abs}_{\text{Blank}})} \times 100 \quad (4)$$

2.5.2 Slug mucosal irritation assay

The slug mucosal irritation (SMI) assay was performed according to our previously published reports [29, 30]. *Arion lusitanicus* slugs were collected locally in Harris Garden (Reading, UK) and were housed in plastic containers and fed with lettuce, cabbage, and cucumber. Each slug's body lining was carefully inspected and only slugs showing no evidence of macroscopic injuries with clear tubercles and a foot surface were used for testing purposes. Slugs weighing between 6 and 20 g were isolated from the culture and were placed individually in 1 L glass beakers lined with a paper towel moistened with 20 mL of phosphate buffered saline (PBS, pH 7.40) and left at room temperature for 48 h before the start of an experiment. All beakers were covered with cling film pierced with tiny holes to allow air exchange. Each slug was individually weighed before the experiment and then placed in 90

mm plastic Petri dishes lined with Whatman™ filter paper moistened with either positive/negative controls (2 mL of 1% BAC in PBS and 2 mL of PBS solution, respectively) or 2 mL of each test materials (PHPMA, PHPMA-Mi) prepared in PBS with different 1, 2 and 3 mg/mL concentrations. After 60 min contact period slugs were taken out, rinsed with 10 mL of PBS, gently wiped with the paper towel, and then reweighed. The mucus production (MP) was estimated as a slug body weight loss and calculated using the following equation:

$$MP = \frac{(m_b - m_a)}{m_b} \times 100\% \quad (5)$$

where m_b and m_a are the weights of a slug before and after experiment, respectively. Each experiment was repeated 5 times using different slugs and the results were evaluated statistically, calculating the mean \pm standard deviation values.

2.6 Statistical analysis

All experiments were conducted in triplicate and data expressed as mean \pm standard deviation with the probability of $p < 0.05$ considered as significant. GraphPad Prism statistical analysis software (version 7.0) was used to analyze data using one-way analysis of variance ANOVA and paired t-tests.

3. Results and Discussion

3.1. Synthesis and characterization of PHPMA-Mi conjugates

PHPMA-Mi conjugates were synthesized by two-step procedure, first, the RAFT copolymerization of HPMA and Ma- β -Ala-TT was employed for the preparation of PHPMA-TT copolymers, which were used for subsequent reaction with AEMI to substitute the TT groups with maleimide groups (**Fig. 1**). The resultant PHPMA-Mi copolymers were characterized using ^1H NMR, FTIR and SEC.

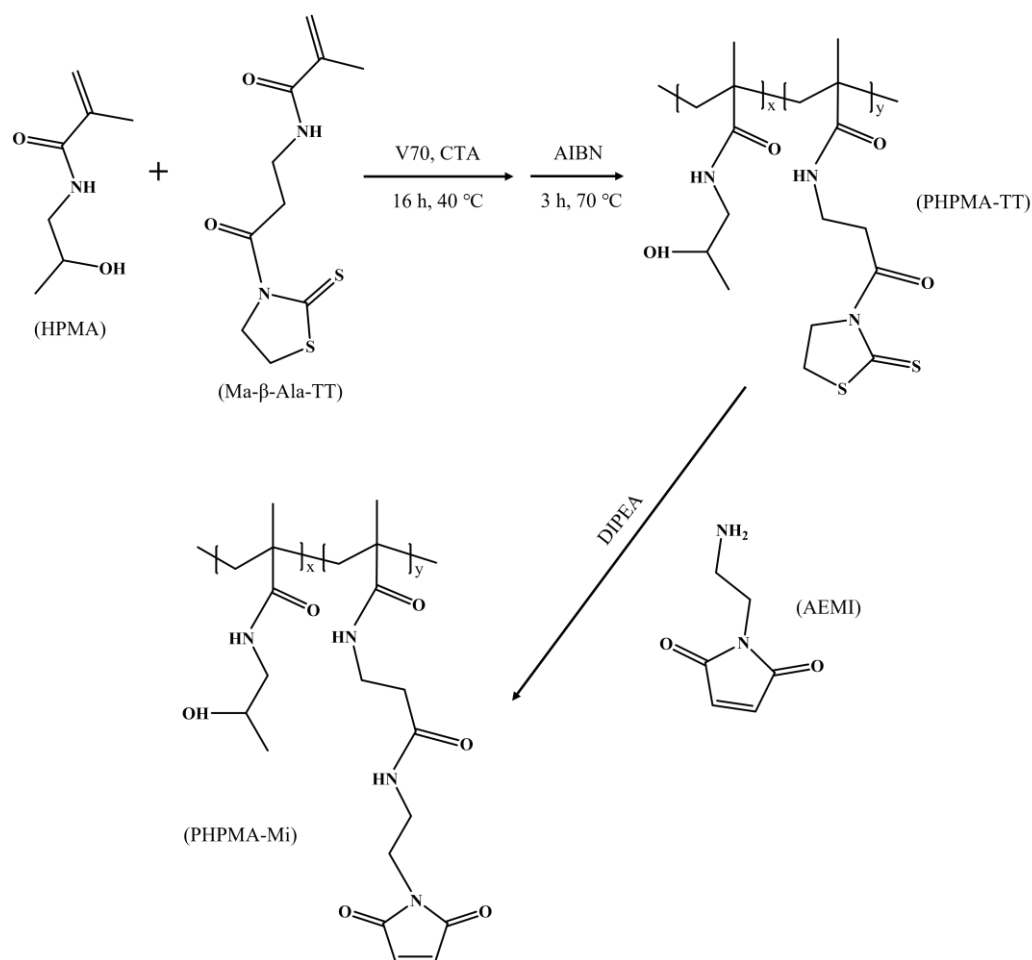


Fig. 1. Synthesis of PHPMA-Mi conjugates.

The ^1H NMR spectrum of PHPMA showed signals which were in agreement with the published literature [31]: δ (ppm) 3.82 (peak *d*, CH of PHPMA side chain), 3.19–2.90 (peak *c*, CH_2 of PHPMA side chain), 1.99–1.51 (peak *a*, CH_2 of PHPMA backbone), 1.17–0.74 (peak *b*, CH_3 of PHPMA backbone and CH_3 of PHPMA side chain). The introduction of maleimide groups led to the signals at δ (ppm) 3.70–3.18 (peak *e* and *g*), 2.30 (peak *f*) and 6.81 (peak *h*) characteristic for $-\text{CH}_2$ attached to the amines, $-\text{CH}_2$ attached to the carbonyl groups and $-\text{CH}=\text{CH}-$ of maleimide moieties, respectively. The signal at δ (ppm) 7.56 (peak *i*) was attributed to NH of the copolymer side chain (Fig. 2), but this signal for PHPMA itself was too weak to be characterized probably because of the less NH groups in PHPMA homopolymer than that in PHPMA-Mi copolymers. It also could be seen from the ^1H NMR spectra of PHPMA-Mi that there were no TT groups signals as the TT

groups were entirely substituted by maleimide groups which was tracked and analyzed by HPLC equipped with UV (**Fig. S1**). However, side reactions are possible via Michael addition which would be further investigated in the future.

The functionalization of maleimide was calculated from ^1H NMR spectra of PHPMA-Mi in D_2O based on the integral values (I) of $-\text{CH}$ signals of HPMA monomer and $-\text{CH}=\text{CH}-$ signals of maleimide moieties, as displayed in **Table 1** that the maleimide substitution was 11% and 25% after the reaction with the reactive polymer precursor PHPMA-TT-1 and PHPMA-TT-2, respectively. For clarity, the maleimide functionalized PHPMA are annotated with their Mi content (i.e. PHPMA-Mi₁₁ contains 11% maleimide groups and was synthesized from PHPMA-TT-1). The resulting good polymer dispersity (1.10 for PHPMA-Mi₁₁ and 1.14 for PHPMA-Mi₂₅) was demonstrated by SEC (**Fig. S2**).

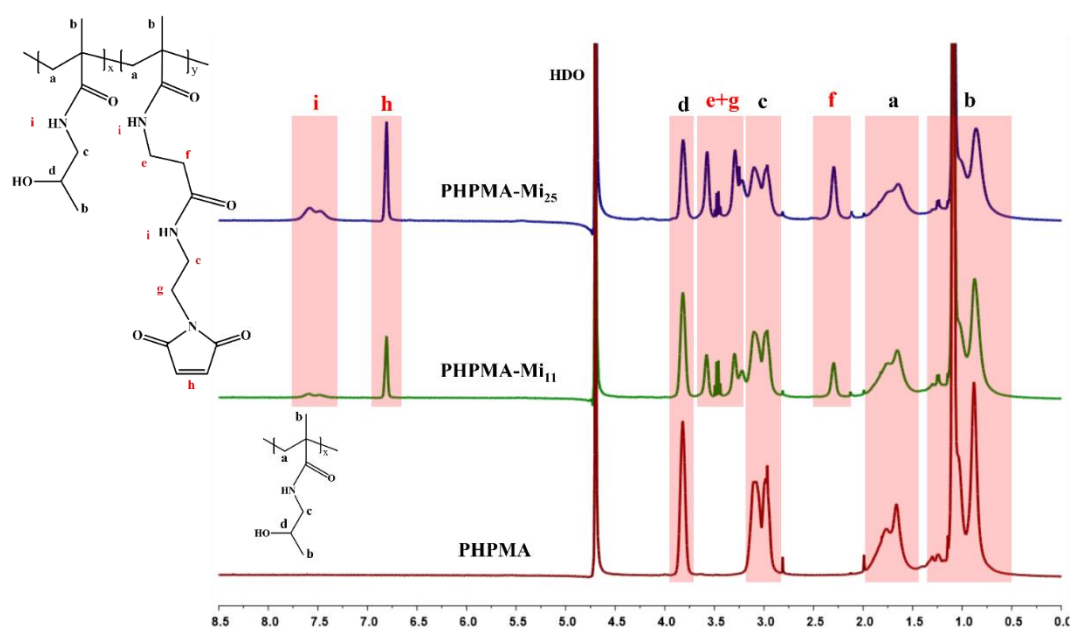


Fig. 2. ^1H NMR spectra of PHPMA and PHPMA-Mi in D_2O .

Table 1. Characterization of polymers.

Products	M_w^a	M_w/M_n^a	Content of maleimide group ^b (mol %)
PHPMA	74 700	1.08	0
PHPMA-Mi ₁₁	74 400	1.10	11
PHPMA-Mi ₂₅	72 000	1.14	25

^aMolecular weight and polydispersity were determined by SEC using RI and LS detection. ^bMaleimide content was determined by ¹H NMR.

The FTIR spectrum of PHPMA shows the following peaks: 3337 cm⁻¹ (N–H and O–H stretch); 2970 and 2923 cm⁻¹ (alkyl C–H stretch); 1640 cm⁻¹ (amide C=O stretch); 1528 cm⁻¹ (N–H bend); 1443 cm⁻¹ (alkane); 1200 cm⁻¹ (C–O stretch). Successful maleimide modification from PHPMA to PHPMA-Mi was shown not only through the N-H and C-H stretch enhancement but also by strong features appearing at 1705 cm⁻¹ (C=C stretch), 831 cm⁻¹ (=C-H bend) and 696 cm⁻¹ (=C-H bend), and the signals were significantly strengthened with the higher content of maleimide groups (**Fig. 3**).

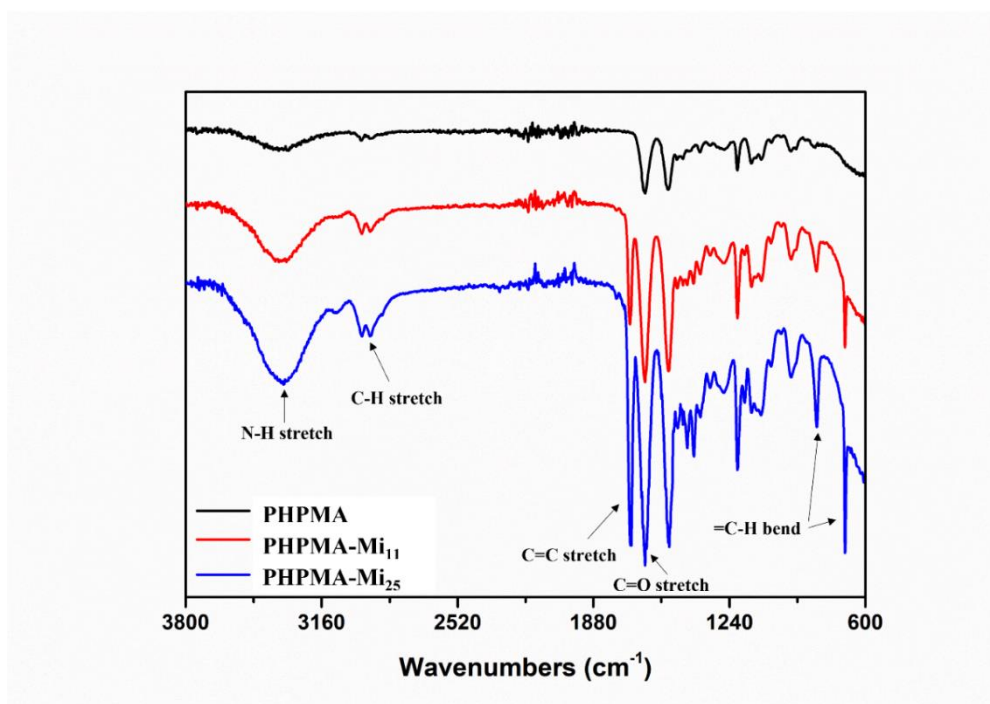


Fig. 3. FTIR spectra of PHPMA and PHPMA-Mi in the range of 3800-600 cm^{-1} .

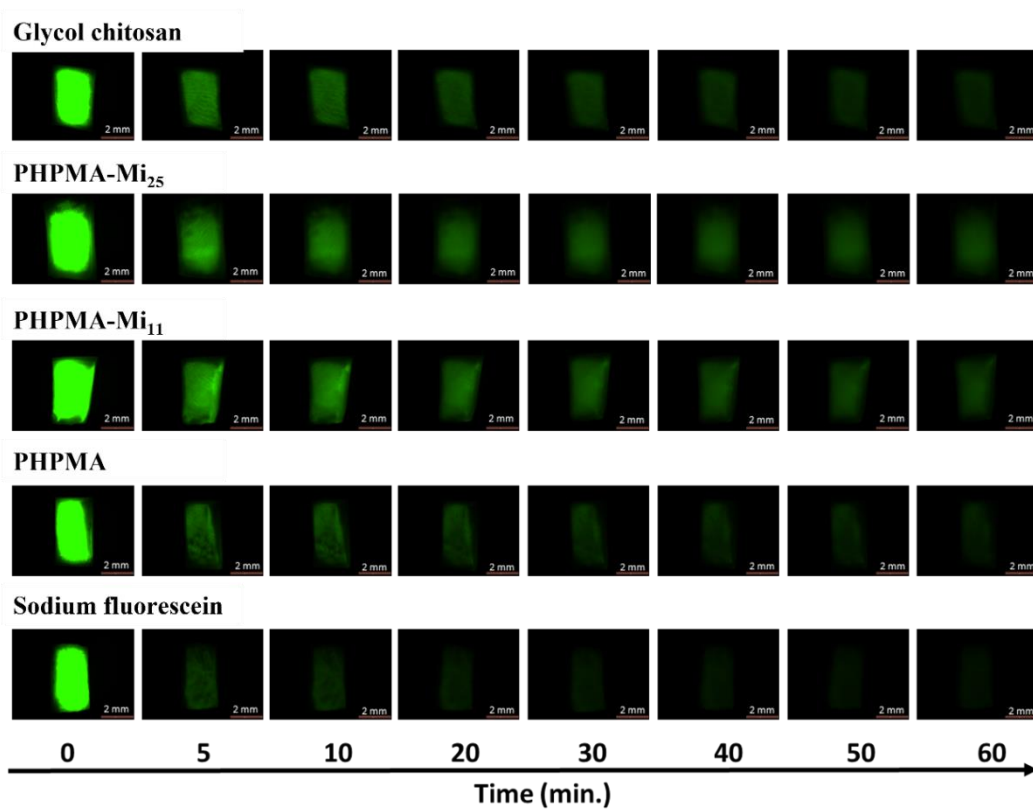
3.2. *In vitro* nasal mucoadhesion studies

The mucoadhesive properties of PHPMA, PHPMA-Mi₁₁ and PHPMA-Mi₂₅ solutions containing sodium fluorescein were studied on freshly excised sheep nasal mucosa, irrigated with ANF. The glycol chitosan served as the mucoadhesive positive control, whereas the negative control was sodium fluorescein. **Fig. 4** shows the retention of sodium fluorescein mediated with glycol chitosan, PHPMA, PHPMA-Mi₁₁ and PHPMA-Mi₂₅ on sheep nasal mucosa. Numerical values from these experiments are summarized in **Table S1**.

Parent PHPMA exhibited relatively poor mucoadhesive properties as only $\sim 7.1\%$ of fluorescence remained on nasal mucosa after 60 min washing which was similar to that for sodium fluorescein (**Fig. 4b**). PHPMA conjugation with higher amount of maleimide resulted in greater retention after each wash. For example, the retention values of PHPMA, PHPMA-Mi₁₁ and PHPMA-Mi₂₅ after 5 min washing were approximately 20.5%, 34.6% and 42.2%, respectively, calculated based on the fluorescence intensity after 5 min washing. It could be seen that there was no

significant retention difference between PHPMA-Mi₂₅ and glycol chitosan, indicating the potential mucoadhesive performance of PHPMA-Mi₂₅. In addition, PHPMA-Mi₁₁ showed significantly better mucoadhesive properties than parent PHPMA at all time points ($p < 0.005$). The superior mucoadhesive properties of PHPMA-Mi may be due to the high reactivity of maleimide towards thiol groups present in cysteine on the mucous membrane [17, 32].

(a)



(b)

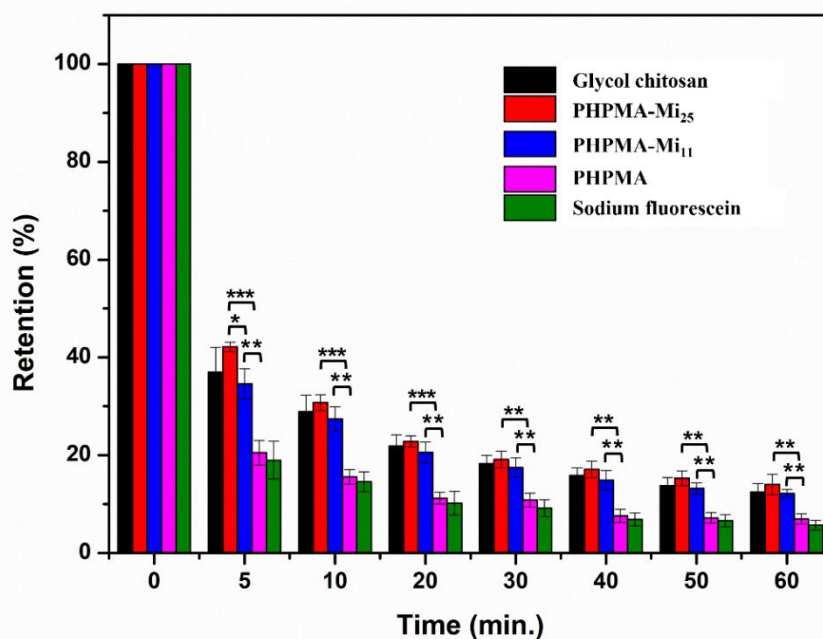


Fig. 4. (a) Fluorescence images showing retention of 1 mg/mL glycol chitosan, PHPMA, PHPMA-Mi₂₅, PHPMA-Mi₁₁ solutions using 0.05 mg/mL sodium fluorescein as the solvent, and pure 0.05 mg/mL sodium fluorescein solution on sheep nasal mucosa and washed with ANF. Scale bar is 2 mm. (b) Retention of 1 mg/mL glycol chitosan, PHPMA, PHPMA-Mi₁₁, PHPMA-Mi₂₅ solutions using 0.05 mg/mL sodium fluorescein as the solvent and pure 0.05 mg/mL sodium fluorescein solution on sheep nasal mucosa as washed with different volumes of ANF (pH=5.7, n=3, mean \pm SD, “*” represents $p < 0.05$).

Tensile test was utilized as the other way to investigate the mucoadhesive properties of samples. The force of detachment or adhesive strength indicates the force required to overcome the adhesive bonds between the sample and nasal mucosa, while the work of adhesion is the area under the force-distance curves. Dextran was used as a negative control [33]. The work of adhesion values showed that PHPMA-Mi₂₅ was statistically more mucoadhesive than PHPMA and PHPMA-Mi₁₁ (**Fig. 5b**), albeit PHPMA-Mi₁₁ and PHPMA-Mi₂₅ displayed similar force of detachment (**Fig. 5a**). Overall, the adhesive strength of the polymers correlated well with their

work of adhesion as PHPMA-Mi₂₅ exhibited greater force of detachment and work of adhesion relative to the parent PHPMA. This is in good agreement with the fluorescence retention studies on nasal mucosa.

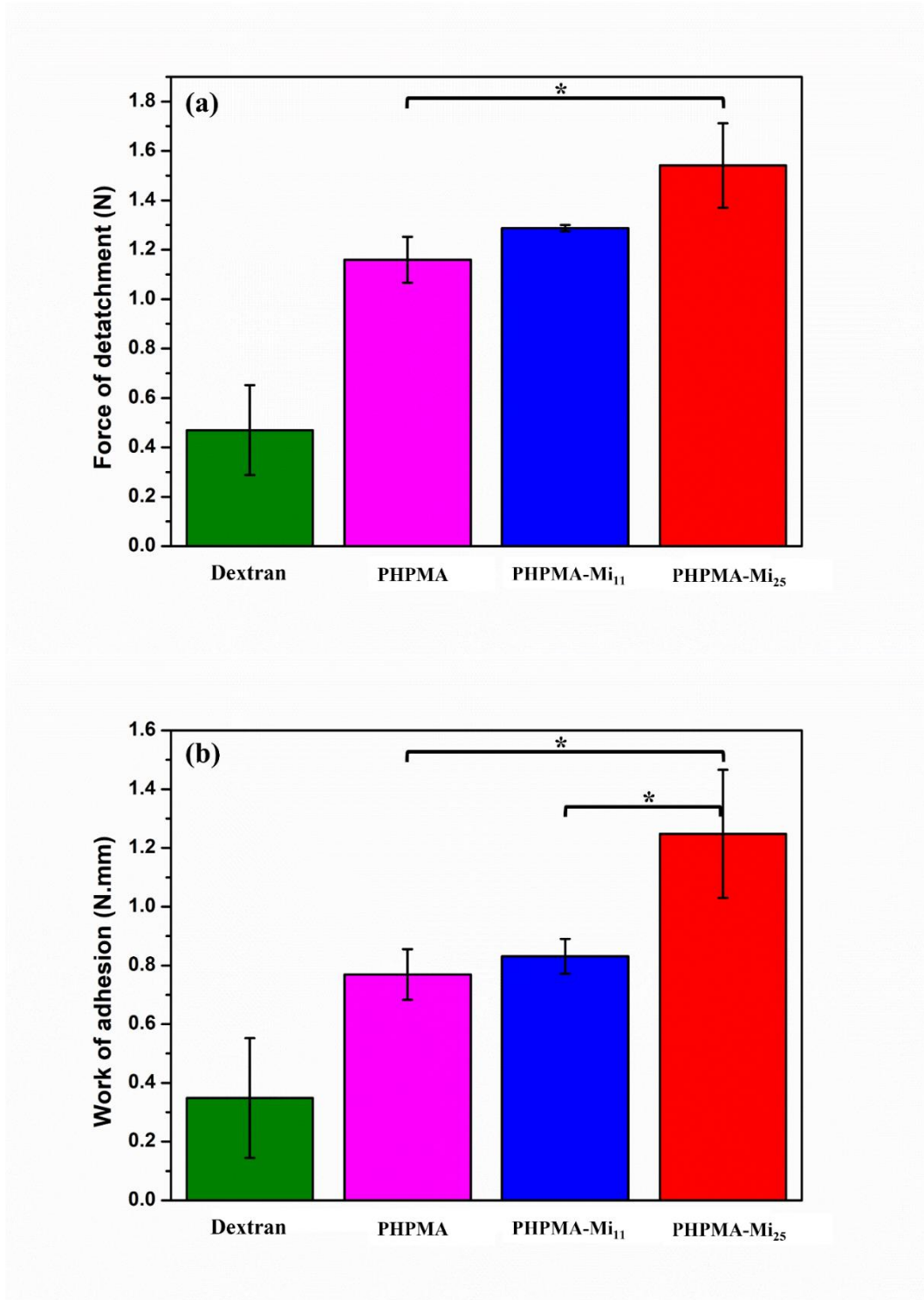


Fig. 5. (a) Force of detachment and (b) work of adhesion of dextran, PHPMA,

PHPMA-Mi₁₁ and PHPMA-Mi₂₅ to sheep nasal mucosa measured using tensile test (n=3, mean \pm SD, “*” represents $p < 0.05$).

3.3. Biocompatibility studies

The HEK293 cell growth inhibitory effect of the copolymers was studied over 72 h (**Fig. 6**). The cytotoxicity values were expressed as means and showed in **Table S2**. Recently, the toxicity of PHPMA has been tested in other cell lines such as HeLa, L-cells and WI-38, and none of the tested cell lines showed any cytotoxicity [34]. Similarly, in this study, PHPMA was proven to have no cytotoxic effect on the viability of HEK293 cells even at high concentrations ($> 100 \mu\text{g/mL}$). It could be seen that 11 mol% maleimide functionalized copolymer (PHPMA-Mi₁₁) showed no significant toxicity even at very high concentration (150 $\mu\text{g/mL}$). By contrast, 25 mol% maleimide functionalized copolymer (PHPMA-Mi₂₅) was relatively toxic compared to parent PHPMA, what could be escribed to the maleimide groups acting as a reactive oxygen species (ROS)-scavenging inhibitor. The maleimide groups are able to deactivate intracellular glutathione and cysteine, thus increasing cytotoxicity [35, 36]. Therefore, it is important to be aware of the maleimide content when selecting maleimide modified polymers as the mucoadhesive materials.

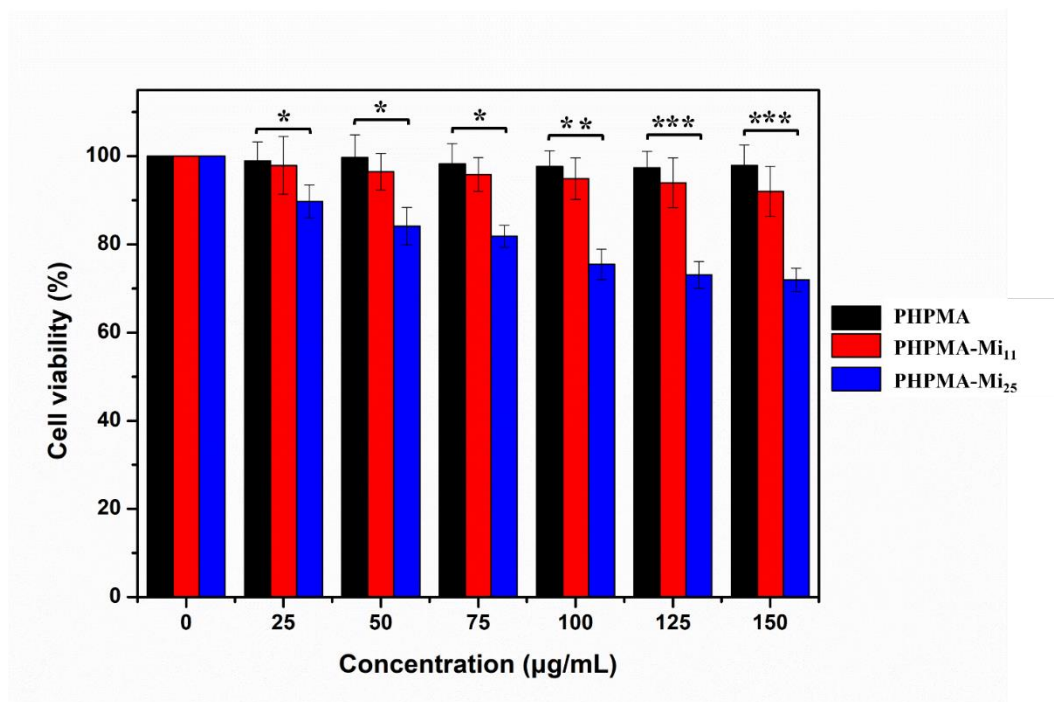


Fig. 6. Viability of HEK 293 cells determined after treatment with different concentrations (25, 50, 75, 100, 125 and 150 µg/mL) of PHPMA, PHPMA-Mi₁₁ and PHPMA-Mi₂₅ for 72 h. The untreated cells served as the control. Values were expressed as means ± SD (n = 3), “*” represents p < 0.05, “**” represents p < 0.005, “***” represents p < 0.001.

The mucosal irritancy of PHPMA and PHPMA-Mi conjugates was tested in *Arion lusitanicus* slugs. **Fig. 7** presents the results on mucus production by slugs exposed to filter paper moistened with PHPMA and PHPMA-Mi conjugates of various amount prepared in PBS as well as positive and negative controls. In experiments with 1% solution of BAC in PBS (pH 7.35), used as a positive control, slugs experienced a severe discomfort, producing approximately $36 \pm 5\%$ of yellow mucus, whereas slugs exposed to PBS (used as a negative control, pH 7.40) did show a low level of mucus production of $4 \pm 1\%$ (**Fig. S3** in Supporting information for the images of slugs exposed to various test materials). A significant variability of the data obtained from experiments with positive control is explained by slugs’ increased activity and tendency to escape a contact with an irritant chemical. In all experiments with negative control and PHPMA-based biomaterials slugs secreted

colorless mucus, which is the first sign of their reasonably good biocompatibility.

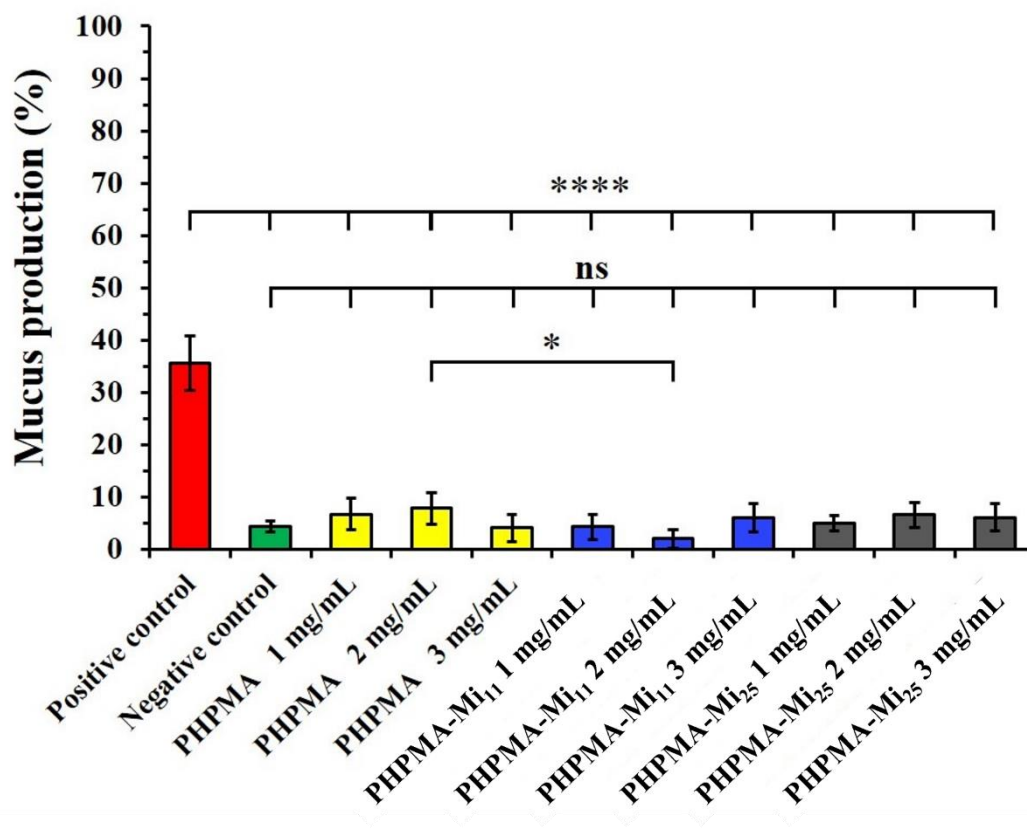


Fig. 7. Mucus production by *Arion lusitanicus* slugs in response to 60 min exposure to PHPMA, PHPMA-Mi₁₁ and PHPMA-Mi₂₅ as well as positive and negative controls. Statistically significant differences are given as: “****” represents $p < 0.0001$; “*” represents $p < 0.05$; “ns” represents no significance.

4. Conclusions

Within the present study we have successfully synthesized and tested maleimide functionalized PHPMA copolymers as suitable mucoadhesive excipients. Using the cytotoxicity studies and slug mucosal irritation assay we were able to demonstrate good biocompatibility of maleimide containing polymers, thus proving their applicability within the nasal delivery route. *In vitro* nasal mucoadhesion studies demonstrated that PHPMA-Mi copolymers exhibited superior mucoadhesive

properties on nasal mucosa tissue compared to parent PHPMA owing to the binding of maleimide groups being available to interact with the mucosal surface. To sum up, maleimide functionalized PHPMA can potentially be used as a mucoadhesive material in dosage forms for nasal drug delivery.

Declaration of Competing Interest

The authors declare that they have no known competing financial interests or personal relationships that could have appeared to influence the work reported in this paper.

Acknowledgements

The authors are grateful to the University of Reading and the China Scholarship Council (201707040071) for funding the PhD studentship of Xiaoning Shan. The authors are grateful to Czech Science Foundation for funding (grant number 21-11688S) experiments on synthesis of these polymers. The authors would like to thank Ms. Amnani Aminuddin for her technical help with cell culture experiments and Faculty of Pharmacy UKM for providing the cell culture research facilities.

Abbreviations

PHPMA, poly(*N*-(2-hydroxypropyl)methacrylamide); PHPMA-TT, poly(HPMA-*co*-Ma- β -Ala-TT); PHPMA-Mi, maleimide functionalised PHPMA.

References

- [1] S. Türker., E. Onur., Y. Özer., Nasal route and drug delivery systems., Pharm World Sci., 26 (2004) 137-142.
- [2] A.N. Fisher., K. Brown., S.S. Davis., G.D. Parr., D.A. Smith., The effect of molecular size on the nasal absorption of water-soluble compounds in the albino rat., J Pharm Pharmacol., 39 (1987) 357-362.
- [3] S. NGM., V. JC., M. HM., The nasal mucociliary clearance: relevance to nasal drug delivery., Pharm Res., 8 (1991) 807-814.

- [4] C.R. Behl., H.K. Pimplaskar., A.P. Sileno., W.J. Xia., W.J. Gries., J.C. deMeireles., V.D. Romeo., Optimization of systemic nasal drug delivery with pharmaceutical excipients., *Adv Drug Del Rev.*, 29 (1998) 117-133.
- [5] E. Bjsrk, P. Edman, Characterization of degradable starch microspheres as a nasal delivery system for drugs., *Int. J. Pharm.*, 62 (1990) 187-192.
- [6] L. Illum, H. Jorgensen, H. Bisgaard, O. Krogsgaard, N. Rossing, Bioadhesive microspheres as a potential nasal drug delivery system., *Int. J. Pharm.*, 39 (1987) 189-199.
- [7] L. Pereswetoff-Morath, Microspheres as nasal drug delivery systems., *Adv. Drug Delivery Rev.*, 29 (1998) 185-194.
- [8] K. Iwanaga, S. Matsumoto, K. Morimoto, M. Kakemi, S. Yamashita, T. Kimura, Usefulness of liposomes as an intranasal dosage formulation for topical drug application., *Biol Pharm Bull.*, 23 (2000) 323-326.
- [9] S.L. Law, K.J. Huang, H.Y. Chou, Preparation of desmopressin-containing liposomes for intranasal delivery., *J. Controlled Release*, 70 (2001) 375-382.
- [10] K. Muramatsu, Y. Maitani, K. Takayama, T. Nagai, The Relationship Between the Rigidity of the Liposomal Membrane and the Absorption of Insulin After Nasal Administration of Liposomes Modified with an Enhancer Containing Insulin in Rabbits., *Drug Dev. Ind. Pharm.*, 25 (1999) 1099-1105.
- [11] C. Witschi, R. J. Mrsny, In Vitro Evaluation of Microparticles and Polymer Gels for Use as Nasal Platforms for Protein Delivery., *Pharm. Res.*, 16 (1999) 382-390.
- [12] M. Zhou, M. D. Donovan, Intranasal mucociliary clearance of putative bioadhesive polymer gels., *Int. J. Pharm.*, 135 (1996) 115-125.
- [13] D.B. Kaldybekov, P. Tonglairoum, P. Opanasopit, V.V. Khutoryanskiy, Mucoadhesive maleimide-functionalised liposomes for drug delivery to urinary

bladder, *Eur. J. Pharm. Sci.*, 111 (2018) 83-90.

[14] T. M. Ways, W. Lau, V. Khutoryanskiy, Chitosan and Its Derivatives for Application in Mucoadhesive Drug Delivery Systems, *Polymers*, 10 (2018) 267.

[15] I.A. Sogias., A.C. Williams., V.V. Khutoryanskiy., Why is Chitosan Mucoadhesive?, *Biomacromolecules.*, 9 (2008) 1837-1842.

[16] P. Tonglairoum, R.P. Brannigan, P. Opanasopit, V.V. Khutoryanskiy, Maleimide-bearing nanogels as novel mucoadhesive materials for drug delivery, *J. Mater. Chem. B*, 4 (2016) 6581-6587.

[17] N. Sahatsapan, T. Rojanarata, T. Ngawhirunpat, P. Opanasopit, P. Tonglairoum, 6-Maleimidohexanoic acid-grafted chitosan: A new generation mucoadhesive polymer, *Carbohydr. Polym.*, 202 (2018) 258-264.

[18] D. Bissett, J. Cassidy, J.S. de Bono, F. Muirhead, M. Main, L. Robson, D. Fraier, M.L. Magne, C. Pellizzoni, M.G. Porro, R. Spinelli, W. Speed, C. Twelves, Phase I and pharmacokinetic (PK) study of MAG-CPT (PNU 166148): a polymeric derivative of camptothecin (CPT), *Br. J. Cancer*, 91 (2004) 50-55.

[19] L.W. Seymour, D.R. Ferry, D.J. Kerr, D. Rea, M. Whitlock, R. Poyner, C. Boivin, S. Hesslewood, C. Twelves, R. Blackie, A. Schatzlein, D. Jodrell, D. Bissett, H. Calvert, M. Lind, A. Robbins, S. Burtles, R. Duncan, J. Cassidy, Phase II studies of polymer-doxorubicin (PK1, FCE28068) in the treatment of breast, lung and colorectal cancer, *Int. J. Oncol.*, 34 (2009) 1629-1636.

[20] W. Shan., X. Zhu., M. Liu., L. Li., J. Zhong., W. Sun., Z. Zhang., Y. Huang., Overcoming the diffusion barrier of mucus and absorption barrier of epithelium by self-assembled nanoparticles for oral delivery of insulin., *ACS Nano.*, 9 (2015) 2345-2356.

[21] M. Liu, J. Zhang, X. Zhu, W. Shan, L. Li, J. Zhong, Z. Zhang, Y. Huang, Efficient mucus permeation and tight junction opening by dissociable "mucus-

inert" agent coated trimethyl chitosan nanoparticles for oral insulin delivery, *J. Control. Release*, 222 (2016) 67-77.

[22] M. Liu, L. Wu, X. Zhu, W. Shan, L. Li, Y. Cui, Y. Huang, Core-shell stability of nanoparticles plays an important role for overcoming the intestinal mucus and epithelium barrier, *J. Mater. Chem. B*, 4 (2016) 5831-5841.

[23] Y. Liu, X. Xie, X. Hou, J. Shen, J. Shi, H. Chen, Y. He, Z. Wang, N. Feng, Functional oral nanoparticles for delivering silibinin and cryptotanshinone against breast cancer lung metastasis, *J. Nanobiotechnology*, 18 (2020) 83.

[24] H. Lu, G. Yang, F. Ran, T. Gao, C. Sun, Q. Zhao, S. Wang, Polymer-functionalized mesoporous carbon nanoparticles on overcoming multiple barriers and improving oral bioavailability of Probuco, *Carbohydr. Polym.*, 229 (2020) 115508.

[25] R. Pola, J. Parnica, K. Zuska, E. Böhmová, M. Filipová, M. Pechar, J. Pankrác, J. Mucksová, J. Kalina, P. Trefil, L. Šefc, D. Větvička, P. Poučková, J. Bouček, O. Janoušková, T. Etrych, Oligopeptide-targeted polymer nanoprobe for fluorescence-guided endoscopic surgery, *Multifunct. mater.*, 2 (2019) 024004.

[26] S. Barbi Mda, F.C. Carvalho, C.P. Kiill, S. Barud Hda, S.H. Santagneli, S.J. Ribeiro, M.P. Gremiao, Preparation and Characterization of Chitosan Nanoparticles for Zidovudine Nasal Delivery, *J. Nanosci. Nanotechnol*, 15 (2015) 865-874.

[27] N.N. Porfiryeva, S.F. Nasibullin, S.G. Abdullina, I.K. Tukhbatullina, R.I. Moustafine, V.V. Khutoryanskiy, Acrylated Eudragit(R) E PO as a novel polymeric excipient with enhanced mucoadhesive properties for application in nasal drug delivery, *Int. J. Pharm.*, 562 (2019) 241-248.

[28] D.B. Kaldybekov, S.K. Filippov, A. Radulescu, V.V. Khutoryanskiy, Maleimide-functionalised PLGA-PEG nanoparticles as mucoadhesive carriers for intravesical drug delivery, *Eur. J. Pharm. Biopharm.*, 143 (2019) 24-34.

- [29] O.V. Khutoryanskaya, P.W. Morrison, S.K. Seilkhanov, M.N. Mussin, E.K. Ozhmukhametova, T.K. Rakhypbekov, V.V. Khutoryanskiy, Hydrogen-bonded complexes and blends of poly(acrylic acid) and methylcellulose: nanoparticles and mucoadhesive films for ocular delivery of riboflavin, *Macromol. Biosci.*, 14 (2014) 225-234.
- [30] P.G. Georgiou, A.N. Baker, S.J. Richards, A. Laezza, M. Walker, M.I. Gibson, "Tuning aggregative versus non-aggregative lectin binding with glycosylated nanoparticles by the nature of the polymer ligand", *J. Mater. Chem. B*, 8 (2020) 136-145.
- [31] A.B. Lowe., Thiol-ene "click" reactions and recent applications in polymer and materials synthesis., *Polym. Chem.*, 1 (2010) 17-36.
- [32] O.M. Kolawole, W.M. Lau, V.V. Khutoryanskiy, Chitosan/beta-glycerophosphate in situ gelling mucoadhesive systems for intravesical delivery of mitomycin-C, *Int. J. Pharm.: X*, 1 (2019) 100007.
- [33] P. Bojarova, M.R. Tavares, D. Laaf, L. Bumba, L. Petraskova, R. Konefal, M. Blahova, H. Pelantova, L. Elling, T. Etrych, P. Chytil, V. Kren, Biocompatible glyconanomaterials based on HPMA-copolymer for specific targeting of galectin-3, *J. Nanobiotechnology*, 16 (2018) 73.
- [34] B. Ali, L.D. Kanda Kupa, C.S. Heluany, C.C. Drewes, S.N.S. Vasconcelos, S.H.P. Farsky, H.A. Stefani, Cytotoxic effects of a novel maleimide derivative on epithelial and tumor cells, *Bioorg. Chem.*, 72 (2017) 199-207.
- [35] X. Guo, L. Wang, S. Wang, Y. Li, F. Zhang, B. Song, W. Zhao, Syntheses of new chlorin derivatives containing maleimide functional group and their photodynamic activity evaluation, *Bioorg. Med. Chem. Lett.*, 25 (2015) 4078-4081.

Supporting information to the paper

Mucoadhesive formulations with maleimide modified poly(*N*-(2-hydroxypropyl)methacrylamide) copolymer for nasal drug delivery

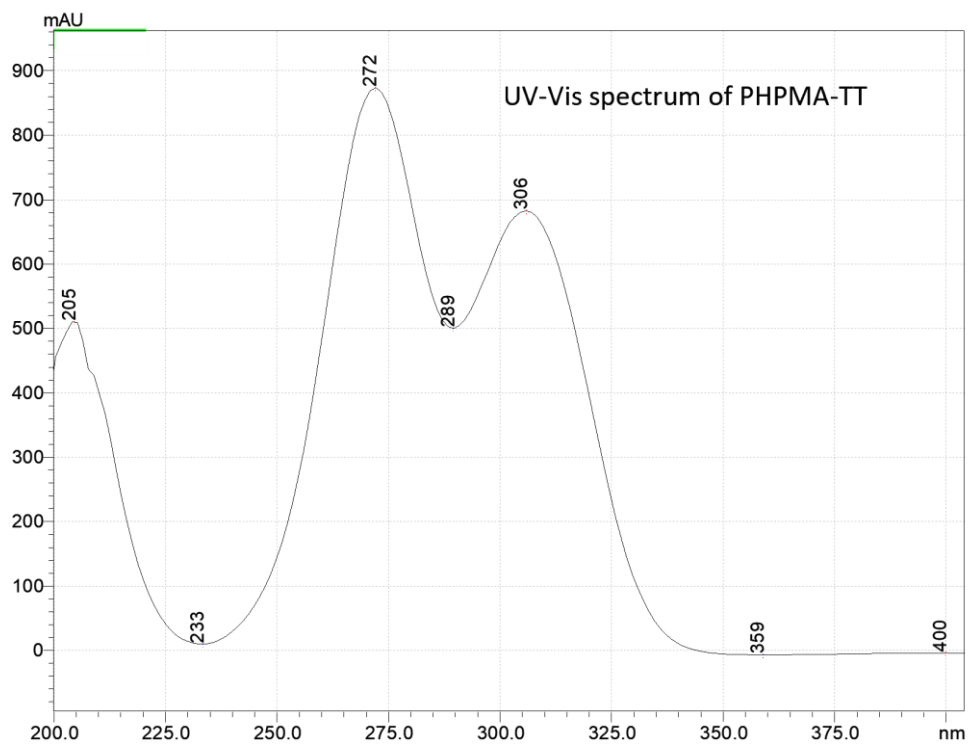
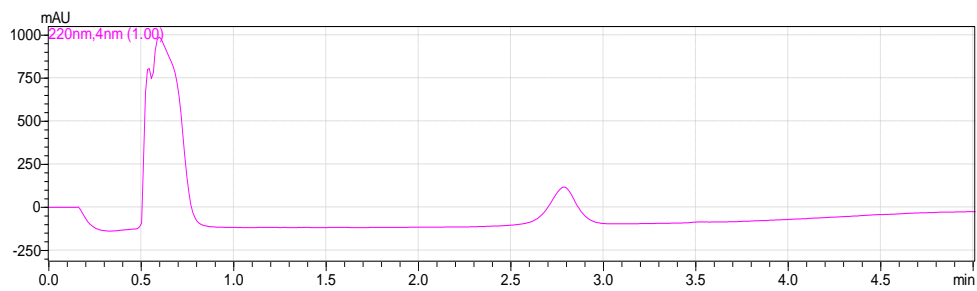
*Xiaoning Shan*¹, *Robert Pola*², *Daulet B. Kaldybekov*¹, *Sam Aspinall*¹, *Fhataheya Buang*^{1,3}, *Adrian C. Williams*¹, *Tomas Etrych*², *Vitaliy V. Khutoryanskiy*^{1*}

¹Reading School of Pharmacy, University of Reading, Whiteknights, PO Box 224, Reading RG6 6AD, United Kingdom

²Institute of Macromolecular Chemistry of the Czech Academy of Sciences, Heyrovského nám. 2, Prague 6, Czech Republic

³Centre for Drug Delivery Research, Faculty of Pharmacy, Universiti Kebangsaan Malaysia, Jalan Raja Muda Abdul Aziz, 50300 Kuala Lumpur, Malaysia

(a)



(b)

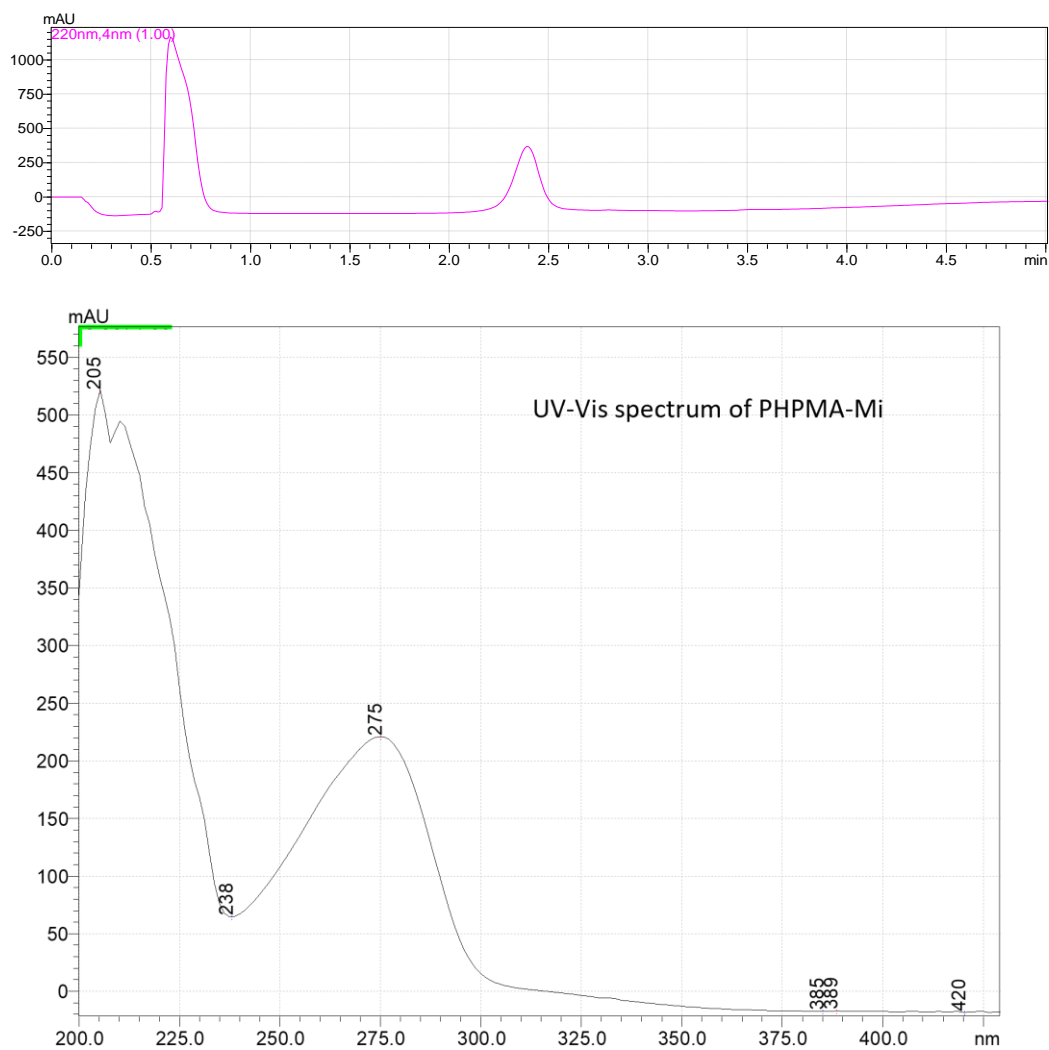


Fig. S1. (a) at 0 h (UV detector at 220 nm), the first peak was attributed to DMA, the second peak (2.8 min) was attributed to PHPMA-TT which showed two UV maximum absorption wavelength at 272 nm and 306 nm; (b) at 3 h (UV detector at 220 nm), the first peak was attributed to DMA and released TT groups, the second peak (2.4 min) was attributed to PHPMA-Mi which showed one UV maximum absorption wavelength at 275 nm.

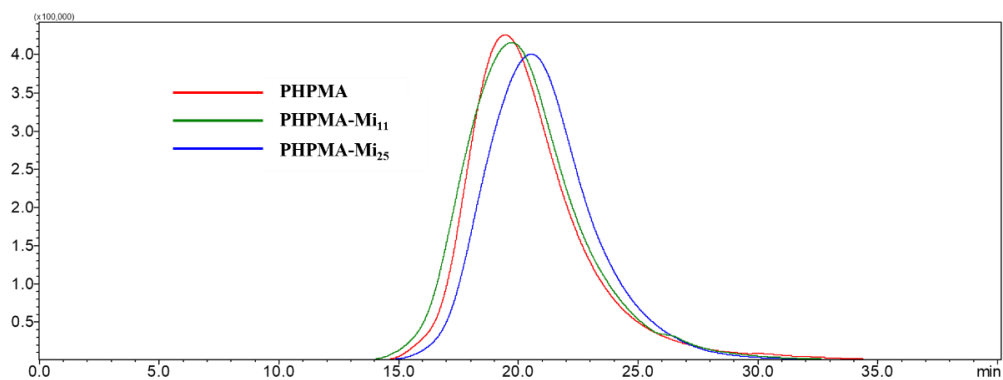


Fig. S2. SEC profiles of polymers (UV detector at 220 nm).

Table S1. Retention values of 1 mg/mL glycol chitosan, PHPMA, PHPMA-Mi₁₁ and PHPMA-Mi₂₅ solutions using 0.05 mg/mL sodium fluorescein as the solvent and pure 0.05 mg/mL sodium fluorescein solution on sheep nasal mucosa as washed with different volumes of ANF (pH=5.7). Values were expressed as means (n = 3).

		Retention (%)							
Sample	Time (min.)	0	5	10	20	30	40	50	60
		Glycol chitosan	100	37.22	28.91	21.92	18.33	15.94	13.81
	PHPMA-Mi ₁₁	100	34.64	27.42	20.62	17.51	14.94	13.23	12.24
	PHPMA-Mi ₂₅	100	42.17	30.77	22.83	19.13	17.12	15.31	14.03
	PHPMA	100	20.52	15.61	11.22	10.84	7.63	7.23	7.05
	Sodium fluorescein	100	19.05	14.62	10.21	9.24	6.92	6.62	5.73

Table S2. Values of viability of HEK 293 cells determined after treatment with different concentrations (25, 50, 75, 100, 125 and 150 $\mu\text{g/mL}$) of PHPMA, PHPMA-Mi₁₁ and PHPMA-Mi₂₅ for 72 h. The untreated cells served as the control. Values were expressed as means (n = 3).

		Cell Viability (%)						
Sample	Concentration ($\mu\text{g/mL}$)	0	25	50	75	100	125	150
	PHPMA	100	98.95	99.72	98.28	97.69	97.42	97.87
	PHPMA-Mi ₁₁	100	97.91	96.44	95.85	94.94	93.98	92.03
	PHPMA-Mi ₂₅	100	89.77	84.14	81.85	75.46	73.09	71.94

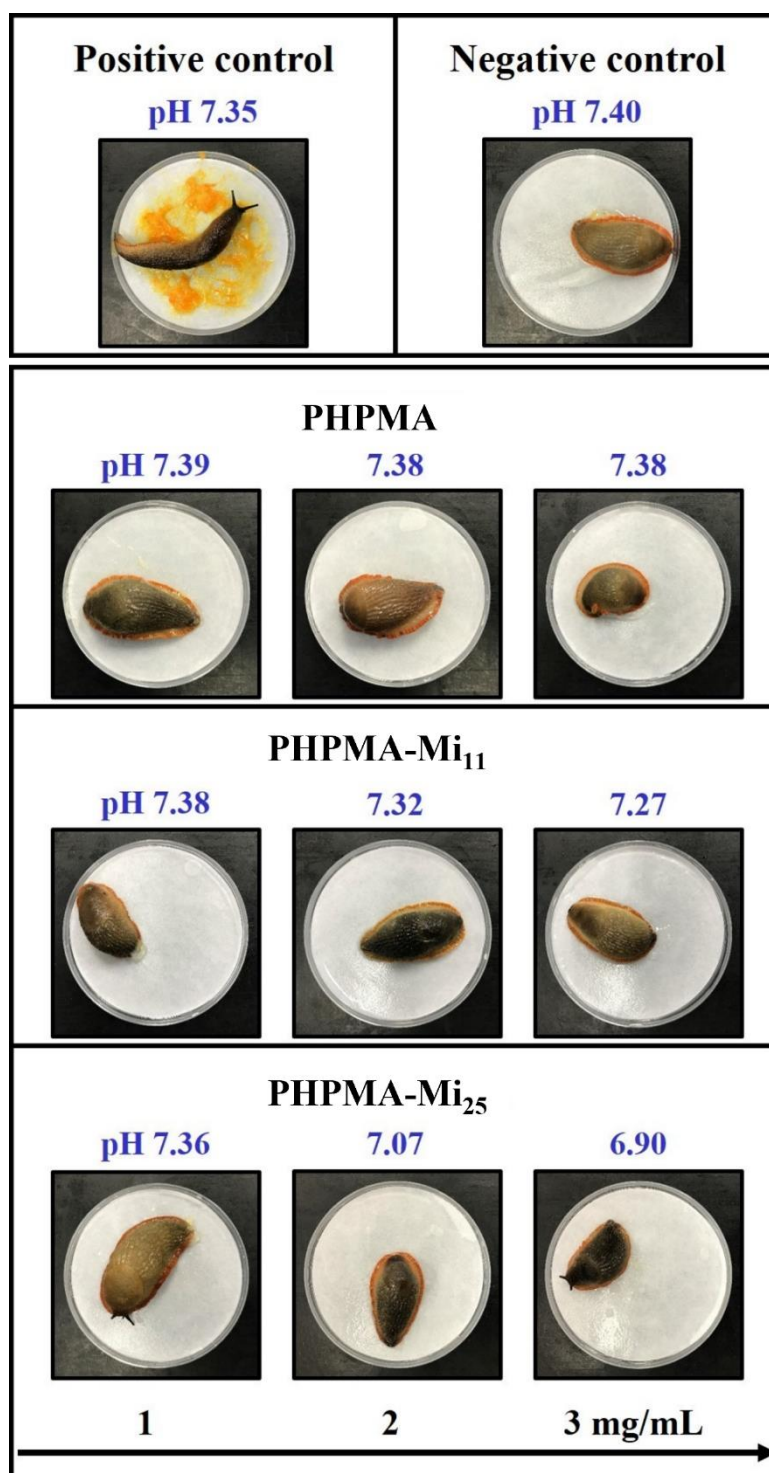


Fig. S3. Mucus production by *Arion lusitanicus* slugs in contact with positive (1% solution of BAC in PBS) and negative (PBS solution) controls as well as test materials after 60 min exposure.

Chapter 6

General discussion and future work

General discussion

Poly(2-oxazolines) (POZ) are an emerging polymer class with useful properties and are proposed as a versatile platform for different drug delivery systems such as nanoparticles [1], micelles [2], hydrogels [3], polymer-drug conjugates [4] and polymer-protein conjugates [5]. However, to date applications of POZ in solid dispersions as well as a mucoadhesive carrier are lacking. Here, we not only developed a series of poly(2-oxazolines)-based solid dispersions (second chapter and third chapter), but also modified poly(2-ethyl-2-oxazoline) with methacrylate groups which significantly improved its mucoadhesive performance (fourth chapter). In addition, PHPMA and its maleimide derivatives were studied in terms of their mucoadhesive properties and demonstrated that maleimide groups also resulted in enhanced mucoadhesion (fifth chapter), which could act as a parallel work to methacrylate groups modified poly(2-ethyl-2-oxazoline).

The first chapter provided an overview on intermolecular interactions in solid dispersions of amide-containing nonionic water-soluble polymers including PVP, PVP/VA, Soluplus and poly(2-oxazolines). The amide group could act as hydrogen bonding acceptors in intermolecular interactions between carriers and drugs. Apart from hydrogen bonding, dipole-dipole interactions, hydrophobic effects and Van der Waals forces were also discussed. However, hydrogen bonding between drug molecules and carriers remain most widely reported and are responsible for drug crystallinity reduction, and improvements in drug stability and dissolution rate. The influence of hydrogen bonding between drug molecules and polymer carriers (PVP, PVP/VA, Soluplus and poly(2-oxazolines)) on solid dispersion properties provides the rationale to select other nonionic water-soluble polymer carriers containing amide groups such as poly(N-vinyl acetamide) and polyacrylamide, which have not yet been studied as solid dispersion carriers.

The second chapter focused on the synthesis of a series of water-soluble poly(2-oxazolines) with equivalent degrees of polymerization and subsequent applications

in solid dispersions. The polymer structure and property effects on solid dispersions with haloperidol were investigated. Poly(N-vinyl pyrrolidone) (PVP) was superior in its ability to reduce crystallinity of haloperidol and gave rapid drug release from solid dispersions which is related to its ability to form hydrogen bonds with the drug molecules. Increasing the number of hydrophobic groups (-CH₂-and -CH₃) in poly(2-oxazolines) resulted in greater inhibition of crystallinity of haloperidol. However, poly(2-isopropyl-2-oxazoline) had very poor ability to reduce crystallinity of haloperidol, which is related to the semi-crystalline nature of this polymer. Dissolution studies indicated good agreement with the levels of drug crystallinity measured in the solid dispersions. However, solid dispersions with poly(n-propyl-2-oxazoline) were found to release drug very slowly due to its lower critical solution temperature and hence insolubility of this polymer in the dissolution medium.

Given the hydrogen bonding between haloperidol and poly(2-oxazolines) was almost absent due to the poor hydrogen bond donating ability of the haloperidol hydroxy group, the third chapter utilized ibuprofen as another model drug to explore the impacts of both polymer hydrophobicity and drug-polymer hydrogen bonding considering ibuprofen's strong hydrogen bond donating ability (because of its carboxylic group). Poly(2-methyl-2-oxazoline), the most hydrophilic polymer, showed the poorest ability to reduce or inhibit the crystallinity of ibuprofen. In contrast, more hydrophobic polymers PVP, poly(2-ethyl-2-oxazoline), poly(n-propyl-2-oxazoline) and poly(2-isopropyl-2-oxazoline) provided greater but similar abilities to reduce ibuprofen crystallinity, despite the different polymer hydrophobicity and that poly(2-isopropyl-2-oxazoline) is semi-crystalline. These results indicate that crystallinity disruption is predominantly due to hydrogen bonding between the drug molecules and the polymer. However, carrier properties affected drug dissolution, where poly(n-propyl-2-oxazoline) exhibited lower critical solution temperature that inhibited the release of ibuprofen, which is consistent with the haloperidol dissolution study. Drug release from other systems

was consistent with the degree of ibuprofen crystallinity within the dispersions.

The fourth chapter demonstrated successful methacrylation of poly(2-ethyl-2-oxazoline) through reaction between partially hydrolysed poly(2-ethyl-2-oxazoline) bearing secondary amino-groups and methacrylic anhydride. Cell toxicity studies demonstrated equivalent biocompatibility of the methacrylated polymers with the parent poly(2-ethyl-2-oxazoline). Methacrylation significantly increased mucoadhesion to nasal mucosal tissue compared to the parent poly(2-ethyl-2-oxazoline), attributed to the synergistic binding of methacrylate groups as well as residual secondary amines being available to interact with the mucosal surface.

The fifth chapter demonstrated successful maleimide functionalization of PHPMA through reaction between copolymer poly(HPMA-co-Ma- β -Ala-TT) bearing TT groups and 2-aminoethyl maleimide trifluoroacetate. The cytotoxicity studies and slug mucosal irritation assay indicated good biocompatibility of maleimide functionalized PHPMA. In vitro nasal mucoadhesion studies demonstrated that PHPMA-Mi copolymers exhibited superior mucoadhesive properties on nasal mucosa tissue compared to its parent PHPMA owing to the covalent bonding of maleimide groups being available to interact with the mucosal surface.

In summary, the solid dispersion studies provide guidelines through which it is possible to rationally select polymer carriers for a given drug structure in solid dispersion preparation. For example, when selecting a carrier for solid dispersions, it is important to consider not only the hydrogen bonding capabilities of the polymer but also its broader properties such as hydrophobicity, semi-crystallinity and lower critical solution temperatures. The mucoadhesion studies based on poly(2-ethyl-2-oxazoline) and PHPMA proved that they can potentially be used as mucoadhesive materials in dosage forms for nasal drug delivery.

The work described in this thesis has demonstrated potential future uses and benefits of poly(2-oxazolines) as a pharmaceutical excipient. Polymers can be prepared to span a broad range of hydrophilicities – from water soluble to highly

hydrophobic. The polymers can be easily functionalized to provide excipients with tailored properties such as mucoadhesion, and indeed to control the degree of mucoadhesion. The poly(2-oxazolines) and functionalized derivatives appear to offer good biocompatibility- similar to that of other pharmaceutical polymeric excipients as assessed in cell cytotoxicity and mucosal irritation studies. Clearly further work is merited on this novel class of polymers to fully exploit and maximize their potential.

Future work

The solid dispersion work demonstrated the value of POZ's as drug carriers and stability studies and long-term storage (or accelerated stability) studies could be performed in the future. For example, after preparation of the physical mixtures and solid dispersions, the samples could be stored for 8 weeks at 25 °C and 45 °C under an RH of 70%, respectively. Every week during this time, drug crystallinity within the dispersions could be measured alongside drug dissolution rates to assess not only stability but potentially identify moisture uptake effects on the dispersion (shown in literature studies to potentially led to phase separation). Further, the effect of humidity on the dissolution rates of solid dispersions would be beneficial; obtained powders could be kept under varying RHs for 4 weeks, with dissolution tests and drug crystallinity monitored throughout [6].

A natural extension to the solid dispersion studies is to undertake an *in vivo* pharmacokinetic study. For example, haloperidol or ibuprofen could be administered orally to one group of animals (rats, which have been used for haloperidol pharmacodynamic studies) while their solid dispersions will be administered orally to another group. Then blood samples from these animals could be analyzed [7] periodically and related to the pharmacodynamic actions (of haloperidol or ibuprofen).

Mocoadhesion studies could also be extended to *in vivo* studies. For example, haloperidol could be used as a model drug and formulated with MAPEOZ or PHPMA-Mi and tested in rats by nasal administration against haloperidol alone as a control. The catalepsy test would demonstrate whether the polymers could prevent unwanted central side effects of nasally administered haloperidol [8].

Advanced imaging techniques would also be useful to demonstrate the biodistribution and potential accumulation of the polymers *in vivo*. For example, *in vivo* optical imaging could be conducted [9]; polymers would be labeled with a near-infrared fluorescence (NIRF) dye such as DiR and mice given nasal administration of free DiR and DiR/polymer. Additionally, DiR/polymer could be injected at the same dose into the tail vein as the control group. The major organs (heart, liver, spleen, lung and kidney) would then be collected and imaged to demonstrate biodistribution of the polymers from either nasal or iv administration.

References

- [1] P. Wilson, P.C. Ke, T.P. Davis, K. Kempe, Poly(2-oxazoline)-based micro- and nanoparticles: A review, *Eur. Polym. J.*, 88 (2017) 486-515.
- [2] K. Xu, X. Liu, L. Bu, H. Zhang, C. Zhu, Y. Li, Stimuli-Responsive Micelles with Detachable Poly(2-ethyl-2-oxazoline) Shell Based on Amphiphilic Polyurethane for Improved Intracellular Delivery of Doxorubicin, *Polymers*, 12 (2020).
- [3] T.R. Dargaville, J.R. Park, R. Hoogenboom, Poly(2-oxazoline) Hydrogels: State-of-the-Art and Emerging Applications, *Macromol. Biosci.*, 18 (2018) e1800070.
- [4] O. Sedlacek, B.D. Monnery, J. Mattova, J. Kucka, J. Panek, O. Janouskova, A. Hocherl, B. Verbraeken, M. Vergaelen, M. Zadinova, R. Hoogenboom, M. Hraby, Poly(2-ethyl-2-oxazoline) conjugates with doxorubicin for cancer therapy: In vitro

and in vivo evaluation and direct comparison to poly[N-(2-hydroxypropyl)methacrylamide] analogues, *Biomaterials*, 146 (2017) 1-12.

[5] O. Sedlacek, V.R. de la Rosa, R. Hoogenboom, Poly(2-oxazoline)-protein conjugates, *Eur. Polym. J.*, 120 (2019) 109246.

[6] E. Khodaverdi., N. Khalili., F. Zangiabadi., A. Homayouni., Preparation, characterization and stability Studies of glassy Solid Dispersions of indomethacin using PVP and isomalt as carriers, *Iran. J. Basic Med. Sci.*, 15 (2012) 820-832.

[7] L.F. Yin, S.J. Huang, C.L. Zhu, S.H. Zhang, Q. Zhang, X.J. Chen, Q.W. Liu, In vitro and in vivo studies on a novel solid dispersion of repaglinide using polyvinylpyrrolidone as the carrier, *Drug Dev. Ind. Pharm.*, 38 (2012) 1371-1380.

[8] A.A. Natfji, D.O. Nikitin, Semina, II, R.I. Moustafine, V.V. Khutoryanskiy, H. Lin, G.J. Stephens, K.A. Watson, H.M.I. Osborn, F. Greco, Conjugation of haloperidol to PEG allows peripheral localisation of haloperidol and eliminates CNS extrapyramidal effects, *Journal of controlled release: official journal of the Controlled Release Society*, 322 (2020) 227-235.

[9] L. Hou, X. Shan, L. Hao, Q. Feng, Z. Zhang, Copper sulfide nanoparticle-based localized drug delivery system as an effective cancer synergistic treatment and theranostic platform, *Acta biomaterialia*, 54 (2017) 307-320.

Appendix

Synthesis of poly(2-ethyl-2-oxazoline) hydrogels

Synthesis of macromonomers

Acrylated poly(2-ethyl-2-oxazoline) (APEOZ) macromonomer was synthesized by two synthetic strategies as depicted in Figure 1. The first method was based on the esterification of the hydroxy group ended poly(2-ethyl-2-oxazoline) with acryloyl chloride. The second method consists of two steps, namely the living cationic ring opening polymerization of 2-ethyl-2-oxazoline and the subsequent termination by acrylic acid. The bis-APEOZ macromonomer was obtained by the second method and terminated by 1,4- dibromo 2-butene. APEOZ and bis-APEOZ were characterized by ^1H NMR and gel permeation chromatography (GPC) and shown in Figure 2 and Table 1.

Synthesis of hydrogels by thermal free radical polymerization

Triethylene glycol dimethacrylate (TEGDMA) and 2,2-Azobis (2-methylpropionitrile) (AIBN) was used as the crosslinker and thermal initiator, respectively. Nitrogen was bubbled through the well-mixed solutions for 5 min to remove dissolved oxygen. The reaction vessels were placed in a water bath at 70 °C.

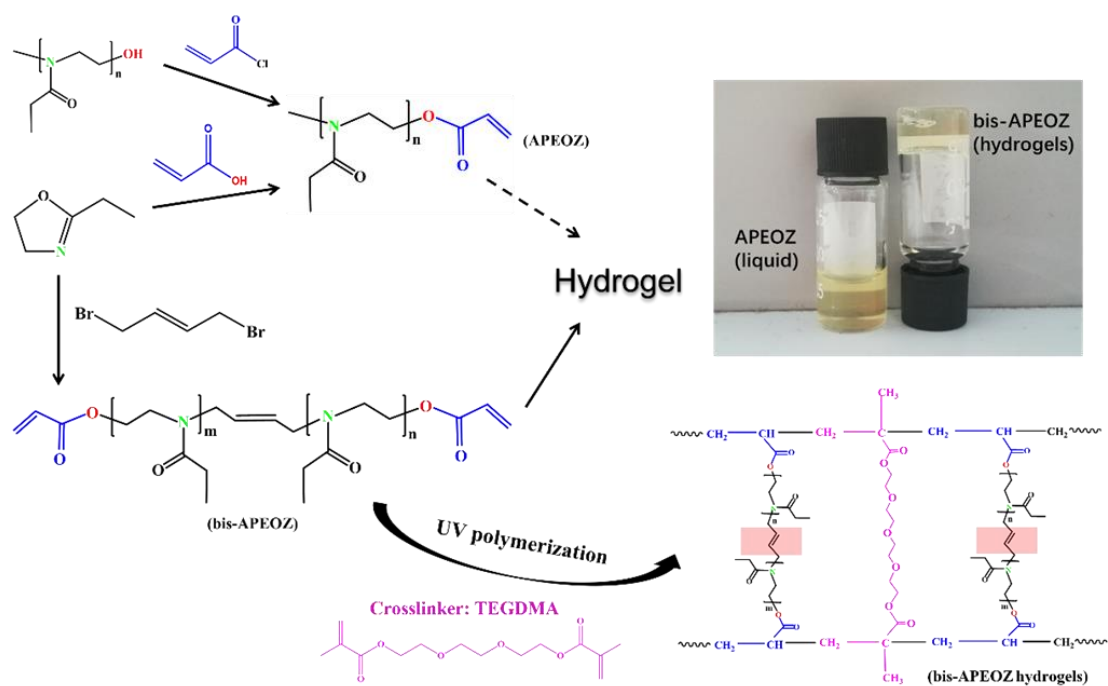


Figure 1. Synthesis of poly(2-ethyl-2-oxazoline) macromonomers and hydrogels.

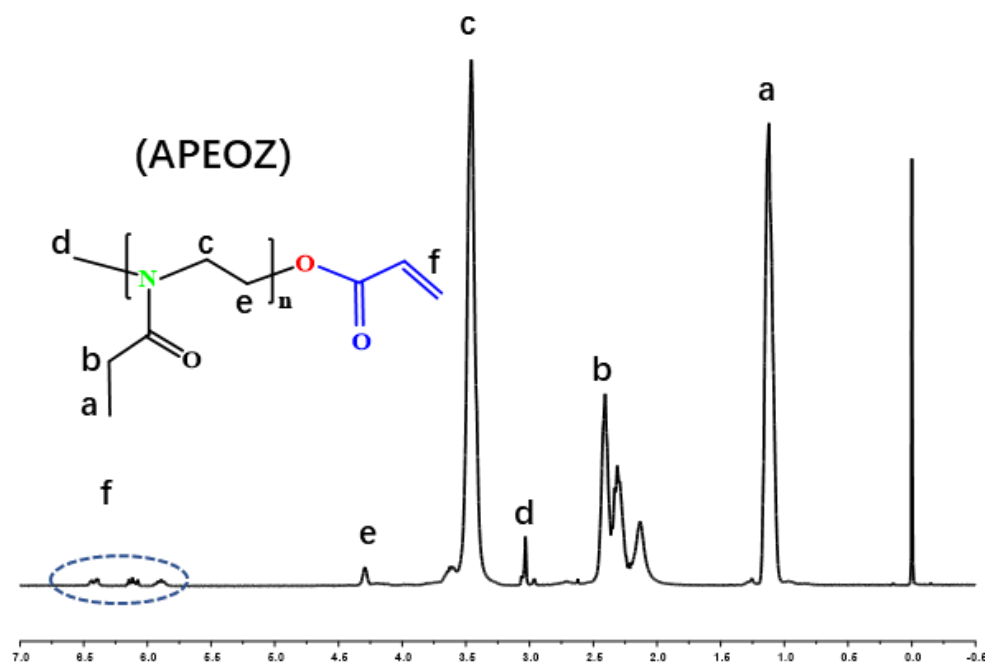


Figure 2. ^1H NMR spectra of APEOZ and bis-APEOZ. The degree of functionality was calculated from the integrals of the peaks of the vinylic protons of the acrylate (labeled as f) in comparison with the end methyl protons of the polymer backbone (labeled as a).

Table 1. Characterization of polymers.

Product	M _w ^a	PDI ^a	Functionality of acrylates ^b
APEOZ	1554	1.115	52.0%
bis-APEOZ	1624	1.182	53.6%

^aMolecular weight and polydispersity (PDI) were determined by GPC. Maleimide
^bfunctionality was determined by ¹H NMR.

Results and discussion

The acrylate functionality for APEOZ and bis-APEOZ is 52.0% and 53.6%, respectively. It could be seen from scheme 1 that APEOZ macromonomer could not be made into hydrogels, but bis-APEOZ could form hydrogels, which might be related to the low functionalization of APEOZ due to the chain transfer reaction resulted from the water traces involved in the living cationic ring opening polymerization. Double vinyl end groups in bis-APEOZ makes it act as the other type of crosslinker to accelerate the free radical polymerization.

Future work on this project will be purification of the reagents used in the synthesis of macromonomer to remove the water traces and accordingly improve the acrylate functionality.